

ลักษณะเฉพาะของกลุ่มรอยเลื่อนเมย-แมปิง จังหวัดตาก  
ภาคตะวันตกเฉียงเหนือของประเทศไทย



นายปรีชา สายทอง

## สถาบันวิทยบริการ จุฬาลงกรณ์มหาวิทยาลัย

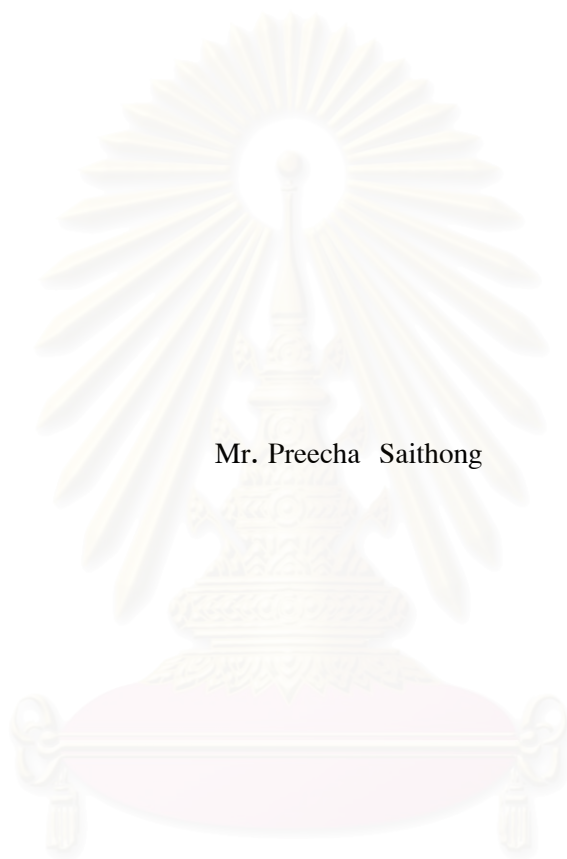
วิทยานิพนธ์นี้เป็นส่วนหนึ่งของการศึกษาตามหลักสูตรปริญญาวิทยาศาสตรมหาบัณฑิต

สาขาวิชาธรณีวิทยา      ภาควิชาธรณีวิทยา  
คณะวิทยาศาสตร์      จุฬาลงกรณ์มหาวิทยาลัย

ปีการศึกษา 2549

ลิขสิทธิ์ของจุฬาลงกรณ์มหาวิทยาลัย

CHARACTERISTICS OF THE MOEI-MAE PING FAULT ZONE,  
CHANGWAT TAK, NORTHWESTERN THAILAND



Mr. Preecha Saithong

สถาบันวิทยบริการ  
จุฬาลงกรณ์มหาวิทยาลัย

A Thesis Submitted in Partial Fulfillment of the Requirements  
for the Degree of Master of Science Program in Geology

Department of Geology

Faculty of Science

Chulalongkorn University

Academic Year 2006

Thesis Title                      Characteristics of the Moei–Mae Ping Fault Zone,  
Changwat Tak, Northwestern Thailand.  
By                                      Mr. Preecha Saithong  
Field of Study                      Geology  
Thesis Advisor                      Associate Professor Punya Charusiri, Ph.D.  
Thesis Co–Advisor                Mr. Suwith Kosuwan, M.Sc.

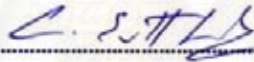
---

Accepted by the Faculty of Science, Chulalongkorn University in Partial  
Fulfillment of the Requirements for the Master’s Degree



..... Dean of the Faculty of Science  
(Professor Piamsak Menasveta, Ph.D.)

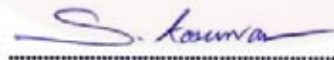
THESIS COMMITTEE



..... Chaiman  
(Assistant Professor Chakkaphan Sutthirat, Ph.D.)



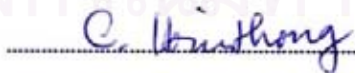
..... Thesis Advisor  
(Associate Professor Punya Charusiri, Ph.D.)



..... Thesis Co–Advisor  
(Suwith Kosuwan, M.Sc.)



..... Member  
(Assistant Professor Somchai Nakapadungrat, Ph.D.)



..... Member  
(Chaiyan Hinthong, M.Sc.)

นายปรีชา สายทอง : ลักษณะเฉพาะของกลุ่มรอยเลื่อนเมย-แม่ปิง จังหวัดตาก ภาคตะวันตกเฉียงเหนือของประเทศไทย (CHARACTERISTICS OF THE MOEI-MAE PING FAULT ZONE, CHANGWAT TAK, NORTHWESTERN THAILAND)  
อ.ที่ปรึกษา : รศ. ดร. ปัญญา จารุศิริ, อ.ที่ปรึกษาร่วม : นายสุวิทย์ โคสุวรรณ, 218 หน้า.

การวิจัยฉบับนี้เป็นการสำรวจธรณีวิทยาแผ่นดินไหวในพื้นที่จังหวัดตาก โดยการประยุกต์ใช้ข้อมูลโทรสัมผัสในการประเมินอันตรายจากแผ่นดินไหว ของกลุ่มรอยเลื่อนเมย-แม่ปิง จังหวัดตาก มีวัตถุประสงค์เพื่อกำหนดตำแหน่งแนวรอยเลื่อนมีพลัง ทิศทางการวางตัวและลักษณะการเคลื่อนตัวของรอยเลื่อนมีพลัง ตลอดจนช่วงเวลาของการเคลื่อนตัวของกลุ่มรอยเลื่อนดังกล่าว

ผลจากการศึกษาวิจัยพบว่า กลุ่มรอยเลื่อนเมย-แม่ปิง วางตัวในแนวทิศตะวันตกเฉียงเหนือ-ตะวันออกเฉียงใต้ แสดงการเคลื่อนตัวแบบเหลื่อมด้านข้าง มีความยาวรวมทั้งสิ้นประมาณ 230 กิโลเมตร ต่อเนื่องมาจากสภาพพม่าถึงที่ราบภาคกลางของประเทศไทย สามารถแบ่งออกเป็น 10 รอยเลื่อนย่อย มีความยาวตั้งแต่ 8 ถึง 43 กิโลเมตร ได้แก่ รอยเลื่อนย่อยสบเมย รอยเลื่อนย่อยห้วยแม่ล้อ รอยเลื่อนย่อยบ้านท่าสองยาง รอยเลื่อนย่อยเขาแม่สอง รอยเลื่อนย่อยห้วยแม่ลา รอยเลื่อนย่อยดอยกะลา รอยเลื่อนย่อยดอยขุนแม่ท้อ รอยเลื่อนย่อยดอยหลวง รอยเลื่อนย่อยเขายาว และรอยเลื่อนย่อยคลองโพธิ์ ส่วนใหญ่วางตัวในแนวทิศตะวันตกเฉียงเหนือ-ตะวันออกเฉียงใต้ นอกจากรอยเลื่อนย่อยดอยกะลาที่วางตัวในแนวเกือบทิศเหนือ-ใต้ รอยเลื่อนเหล่านี้หลายแนวตัดผ่านแอ่งตะกอนยุคซีโนโซอิกด้วย ผลการตรวจสอบภาคสนามในพื้นที่ 3 คือ บริเวณบ้านแม่อุสุ ตำบลแม่ต๋าน อำเภอท่าสองยาง จังหวัดตาก พบว่ารอยเลื่อนย่อยเขาแม่สองมีความยาว 25 กิโลเมตร ปรากฏหลักฐานซึ่งแสดงลักษณะธรณีสัณฐานที่สำคัญและชัดเจนอันได้แก่ ผารอยเลื่อน ผาสามเหลี่ยม ทางน้ำหักงอและสันเขาปิดกั้น ได้ทำการสำรวจธรณีวิทยาแผ่นดินไหวชั้นรายละเอียดในพื้นที่ 3 ซึ่งพบแนวรอยเลื่อนย่อยเขาแม่สอง วางตัวในแนวทิศตะวันตกเฉียงเหนือ-ตะวันออกเฉียงใต้ จากหลักฐานแสดงว่าในอดีตมีการเคลื่อนตัวตามอิทธิพลของรอยเลื่อนในแนวเฉียง กล่าวคือมีการเคลื่อนตัวแบบเหลื่อมขวาและเลื่อนขึ้นในแนวตั้งด้วย เนื่องจากมีลักษณะธรณีสัณฐานที่สำคัญคือผาสามเหลี่ยมรวมทั้งทางน้ำที่มีการหักงอไปทางขวาด้วย ทั้งนี้รอยแตกที่ปรากฏบนพื้นผิวมีความยาวถึง 20 กิโลเมตร บ่งชี้ว่าสามารถก่อให้เกิดแผ่นดินไหวในอดีตได้สูงสุด 6.70 ริกเตอร์ และมีอัตราการเคลื่อนตัวที่ 0.17-0.73 มิลลิเมตรต่อปี จัดเป็นรอยเลื่อนที่มีพลัง สำหรับในกลุ่มรอยเลื่อนเมย-แม่ปิง ในอดีตเคยเกิดเหตุการณ์แผ่นดินไหว ขนาด 5.6 ตามมาตราริกเตอร์ เมื่อวันที่ 17 กุมภาพันธ์ 2518 จากรอยเลื่อนย่อยบ้านท่าสองยางใกล้กับบ้านท่าสองยางและบ้านสบเมย

ภาควิชา.....ธรณีวิทยา..... สายมือชื่อนิสิต.....  
สาขาวิชา.....ธรณีวิทยา..... สายมือชื่ออาจารย์ที่ปรึกษา.....  
ปีการศึกษา.....2549..... สายมือชื่ออาจารย์ที่ปรึกษาร่วม.....

##4672328423: MAJOR GEOLOGY

KEYWORD: MOEI-MAE PING FAULT ZONE (MPFZ)/  
MORPHOTECTONICS/ THERMOLUMINESCENCE DATING/ PALEOEARTHQUAKE  
PREECHA SAITHONG: CHARACTERISTICS OF THE MOEI-MAE PING  
FAULT ZONE, CHANGWAT TAK, NORTHWESTERN, THAILAND. THESIS  
ADVISOR: ASSOCIATE PROFESSOR PUNYA CHARUSIRI, Ph.D. THESIS  
COADVISOR: Mr. SUWITH KOSUWAN, M.Sc. 218 pp.

The Moei-Mae Ping Fault Zone (MPFZ) in Changwat Tak was selected for identifying its detailed characteristics and locating active faults. The application of remote-sensing data was conducted toward the present study. Events of earthquake faultings, paleomagnitudes, and slip-rates of these fault movements constitute the main tasks.

Results from remote-sensing interpretation indicate that the MPFZ is the northwest-southeast trending, oblique-slip fault with a total length of about 230 km. The MPFZ can be traced from eastern Myanmar through the border zone of northwestern Thailand to the northern part of central Thailand. A number of ten fault segments, ranging in length from 8 to 43 km, are recognized and some of which run and pass through Cenozoic basins. Based on the reconnaissance surveys, several kinds of morphotectonic landforms along the Khao Mae Song segment (25 km, in total length) including fault scarps, triangular facets, shutter ridges, and offset streams, are clearly shown in northern part of the study area (Ban Mae Ou Su). A detailed topographic map at a scale of 1:750 covering this fault segment was conducted. The detailed map together with the results on two excavated paleoseismic trenches were performed for determining of its paleoseismic age dating. Estimation from the surface rupture length, the Khao Mae Song segment indicates that earthquake may have occurred in this 20 km rupture length with the maximum paleoearthquake of Mw 6.70. The slip rate of this fault segment is estimated as 0.17-0.73 mm/yr. Consequently, various evidences indicate that the MPFZ is still active till present. The Ban Tha Song Yang fault segment is regarded as the most active and was responsible for the 5.6 on the Richter scale, 1975 earthquake. The dextral movement along the fault controls Cenozoic fault-tip basins in the study area.

Department.....Geology..... Student's signature..... P. Saithong  
Field of study....Geology..... Advisor's signature..... Tunya  
Academic year.....2006..... Co-advisor's signature..... Kosuwat

## ACKNOWLEDGMENTS

The author wishes to express his profound and sincere appreciation to his advisor, Associate Professor Punya Charusiri, and the thesis co-advisor, Mr. Suwith Kosuwan, for their enthusiastic support, continuous guidance and invaluable advice throughout the period of this study.

Sincere thanks and appreciation are extended to the Research Institute of Materials and Resources, Akita University, Professor Isao Takashima, Dr. Krit Won-in for their assistance and support all the facilities such as thermoluminescence and their hospitality during his visit in Japan.

I would like to thank the executive director of The Geo-Informatics and Space Technology Department Agency (Public Organization), for the grants and accessibility to the satellites images from the Landsat 5 TM and Radarsat.

A special thank to the Secretary and staff of Office of Atoms for Peace (OAEP), especially Mr. Pisarn Tungpitayakul for his help in sample analysis with NAA method. I also would like to express my sincerely gratitude to Mr. Arag Vitittheeranon for his help in working in gamma ray issues.

Thanks are also extended to Mr. Somsak Potisat, the Director General of Department of Mineral Resources (DMR), Mr. Worawoot Tantiwanit, the director of Environmental Geology Division, DMR and Mr. Wisut Chotikasathien the head of Geohazard Section, for providing permission and suggestions in my graduate study.

Special thanks extend to Mr. Saroth Surakotra, Mr. Rattakorn Songmuang, Mr. Rachata Meetuwong, Mr. Thitisorn Thipattanakul for their helping at the fieldwork and manage collecting all samples, and I would like to sincerely thank to all of the faculty and staff at the Department of Geology, Chulalongkorn University for all their help and support.

This research was supported by several agencies including the Thailand Research Fund (TRF) and Thailand Research Fund-Master Research Grants (TRF-MRG), Chulalongkorn University, and the Department of Mineral Resources.

Finally, a very special thank to my family, my parents for continuous financial and emotional supports throughout the program. No amount of my gratitude to them would be sufficient. Last, but not least, my dearest sister, Sadee Saithong, thank you for being a proofreader. Your responses make my work a better one. Thank you very much.

## CONTENTS

	PAGE
ABSTRACT IN THAI.....	iv
ABSTRACT IN ENGLISH.....	v
ACKNOWLEDGMENTS.....	vi
CONTENTS.....	vii
LIST OF FIGURES.....	xi
LIST OF TABLES.....	xxiv
CHAPTER I INTRODUCTION .....	1
1.1 General Information.....	1
1.2 Objectives.....	3
1.3 The Study Area.....	7
1.4 Study Methodology.....	7
1.4.1 Planning and Preparation.....	7
1.4.2 Field Reconnaissance.....	7
1.4.3 Remote-Sensing and Aerial Photographic Interpretations.....	10
1.4.4 Field Investigation.....	10
1.4.5 Laboratory Analyses.....	10
1.4.6 Result Integration.....	10
1.5 Active Fault Studies in Thailand.....	10
CHAPTER II LITERATURE REVIEWS.....	32
2.1 Plate Tectonics.....	32
2.2 Geological Evolution during Cenozoic in the Sunda Shelf and Northern Thailand.....	37
2.3 Major Tectonic Elements.....	43
2.4 Active Faults.....	48
2.4.1 Definition of Active Faults.....	48
2.4.2 Active Faults in Thailand.....	50
2.4.3 Moei – Mae Ping Fault Zone.....	51
CHAPTER III REMOTE-SENSING INTERPRETATION.....	55
3.1 Lineaments Interpretation.....	55
3.1.1 Result from Landsat 5 TM Image Interpretation.....	58

	PAGE
3.1.2 Result from Radarsat Image Interpretation.....	58
3.1.3 Result from JERS SAR Image Interpretation.....	65
3.2 Fault Segmentation.....	65
3.2.1 General.....	65
3.2.2 Results of Fault Segmentation.....	68
3.3 Tectonic Geomorphology.....	71
3.3.1 General.....	71
3.3.2 Results of Tectonic Geomorphological Study.....	79
3.3.2.1 Area A, Ban Sop Moei, Amphoe Sop Moei, Changwat Mae Hong Son .....	79
3.3.2.2 Area B, Ban Tha Song Yang, Amphoe Tha Song Yang, Changwat Tak .....	79
3.3.2.3 Area C, Ban Mae Ou Su, Amphoe Tha Song Yang, Changwat Tak .....	84
3.3.2.4 Area D, Ban Mae Ramat, Amphoe Mae Ramat, Changwat Tak .....	84
3.3.2.5 Area E, Doi Krathing, Taksin Maharat National Park, Changwat Tak .....	88
3.3.2.6 Area F, Ban Tha Lay, Tambon Lan Sang, Amphoe Muang, Changwat Tak .....	92
3.3.2.7 Area G, Ban Tha Thong Daeng, King Amphoe Na Bot, Changwat Tak .....	92
3.3.2.8 Area H, Ban Pang Khanun, Amphoe Muang, Changwat Kamphaeng Phet .....	92
CHAPTER IV FIELD INVESTIGATIONS.....	97
4.1 Field Evidences of Morphotectonic Features.....	97
4.1.1 Area A, Ban Sop Moei, Amphoe Sop Moei, Changwat Mae Hong Son.....	97
4.1.1.1 General Geology.....	97
4.1.1.2 Field Investigations.....	99
4.1.1.3 Evaluation of Morphotectonic study.....	99
4.1.2 Area B, Ban Tha Song Yang, Amphoe Tha Song Yang, Changwat Tak.....	99



	PAGE
4.1.2.1 General Geology.....	99
4.1.2.2 Field Investigations.....	102
4.1.2.3 Evaluation of Morphotectonic study.....	102
4.1.3 Area C, Ban Mae Ou Su, Amphoe Tha Song Yang, Changwat Tak	104
4.1.3.1 General Geology.....	104
4.1.3.2 Field Investigations.....	104
4.1.3.3 Evaluation of Morphotectonic study.....	108
4.1.4 Area D, Ban Mae Ramat, Amphoe Mae Ramat, Changwat Tak.....	108
4.1.4.1 General Geology.....	108
4.1.4.2 Field Investigations.....	108
4.1.4.3 Evaluation of Morphotectonic study.....	112
4.1.5 Area E, Doi Krathing, Taksin Maharat National Park, Changwat Tak.....	112
4.1.5.1 General Geology.....	112
4.1.5.2 Field Investigations.....	112
4.1.5.3 Evaluation of Morphotectonic study.....	114
4.1.6 Area F, Ban Tha Lay, Tambon Lan Sang, Amphoe Muang, Changwat Tak.....	114
4.1.6.1 General Geology.....	114
4.1.6.2 Field Investigations.....	116
4.1.6.3 Evaluation of Morphotectonic study.....	116
4.1.7 Area G, Ban Tha Thong Daeng, King Amphoe Na Bot, Changwat Tak.....	116
4.1.7.1 General Geology.....	116
4.1.7.2 Field Investigations.....	119
4.1.7.3 Evaluation of Morphotectonic study.....	119
4.1.8 Area H, Ban Pang Khanun, Amphoe Muang, Changwat Kamphaeng Phet.....	119
4.1.8.1 General Geology.....	119
4.1.8.2 Field Investigations.....	122
4.1.8.3 Evaluation of Morphotectonic study.....	122
4.2 Detail Field Investigation.....	122

	PAGE
4.2.1 Selection of the Detailed Investigated Area.....	122
4.2.2 Result of Detailed Investigation.....	125
4.3 Field Investigations of Ban Mae Ou Su Trench.....	125
4.3.1 Trenching Locations.....	125
4.3.2 Stratigraphic Description.....	130
4.3.3 Collected Dating Samples Locations.....	139
4.3.3.1 Ban Mae Ou Su trench no.1.....	139
4.3.3.2 Ban Mae Ou Su trench no.2 .....	139
CHAPTER V THERMOLUMINESCENCE DATING.....	144
5.1 Basic Concept.....	144
5.2 Paleodose and Annual Dose Evaluation.....	146
5.2.1 Laboratory Analysis .....	147
5.2.1.1 Crushing and Sieving.....	147
5.2.1.2 Paleodose or Equivalent Dose Evaluation.....	149
5.2.2 Regeneration Technique.....	151
5.2.3 Residual Test.....	152
5.2.4 Plateau Test.....	152
5.2.5 Annual Dose Evaluation .....	153
5.2.6 Error Determination.....	158
5.3 Result from Thermoluminescence Dating.....	158
CHAPTER V IDISCUSSIONS.....	167
6.1 Characteristics of the Studied Fault .....	167
6.2 Slip rate and Paleoequake Magnitude.....	170
6.3 The Linkage of Neotectonic Evolution.....	176
CHAPTER VII CONCLUSIONS.....	183
REFERENCES.....	185
APPENDICES.....	199
BIOGEAPHY.....	218

## LIST OF FIGURES

PAGE

Figure 1.1	Present-day tectonic of South and Southeast Asia showing major active structure, direction of the plate movement (arrows) and some important tectonic blocks of Southeast Asia. Note that WBB = Western Burma Block, SCB = South China Block, SMB = Simao Block, STB = Shan-Thai Block, ICB = Indochina Block, LCB = Lampang-Chiang Rai Block, NTB = Nakhon Thai Block, SGF = Sagaing Fault, MPF = Mae Ping Fault, RNF = Ranong Fault, KMF = Klong Marui Fault, SMF = Sumatra Fault, NUF = Nan Uttaradit Fault, TPF = Three Pagodas Fault, RRF = Red River Fault (Modified after Polachan and Sattayarak, 1989).....	4
Figure 1.2	Map of mainland Southeast Asia showing epicenter distribution from 1912 to 2006 (Data from Nutalaya et al., 1985, Thailand Meteorological Department, 2002 <a href="http://neic.usgs.gov/neis/epic/epic_global.html">http://neic.usgs.gov/neis/epic/epic_global.html</a> .).....	5
Figure 1.3	Map of eastern Myanmar and western to northwestern Thailand showing active and associated faults and their relative movements (Modified after Nutalaya et al., 1985). Note that the present study area is shown in box which covers part of the so-called Moei-Uthai-Thani Fault Zone or Moei-Mae Ping Fault Zone of the present study.....	6
Figure 1.4	Map of western Thailand and eastern Myanmar showing the location of the study area (After <a href="http://map-project.doh.go.th/ZoomRaster.asp?Region=3&amp;Zoom=1">http://map-project.doh.go.th/ZoomRaster.asp?Region=3&amp;Zoom=1</a> ).....	8
Figure 1.5	Steps of work in the method of study for this thesis research.....	9
Figure 1.6	Seismic source zones of Burma, Thailand and Indochina (Modified after Nutalaya et al., 1985).....	12
Figure 1.7	Intensity map of Tak earthquake of 17 February 1975 (Modified from Nutalaya et al., 1985).....	13
Figure 1.8	Map showing the elevations of the Lower Central Plain of Thailand generally 2 to 3 m above MSL and in the eastern margin of the plain, the elevation at Ban Khok Pib lies 17-18 m above MSL (After Thiramonkol, 1986).....	14

Figure 1.9	Cross-section along Nong Chok, Bang Nam Prieo and Khok Pib (After Thiramonkol, 1986).....	14
Figure 1.10	Active and suspected active faults in Thailand (Modified after Woodward-Clyde Federal Services, 1996).....	16
Figure 1.11	Active and suspected active faults in Thailand (Modified after Hinthong, 1997).....	18
Figure 1.12	Late Cenozoic faults and historical seismicity (1362 to 1996) of the northern Basin and Range seismotectonic province. (After Bott et al., 1997).....	19
Figure 1.13	Combined magnetic- radiometric - gravity data interpretation showing structural map of Central Plain with magnetic and radiometric lineaments underlain. Note that 1 = Phitsanulok Basin, 2 = Nong Bua Basin, 3 = Na Khon Sawan Basin, 4 = Lop Buri Basin, 5 = Supanburi Basin, 6 = Kamphaeng Saen Basin, 7 = Thon Buri Basin, 8 = Ayuthaya Basin (After Tulyatid, 1997).....	20
Figure 1.14	Location of Ban Hat Chom Phu trench site, southern part of Mae Ai segment of Mae Chan Fault, Chiang Mai, Northern Thailand (After Kosuwan et al., 1999).....	22
Figure 1.15	Trench stratigraphy of the east wall side of the Ban Hat Chom Phu trench showing reverse fault movement and locations of samples for TL dating and their dates (After Kosuwan et al., 1999).....	23
Figure 1.16	Map of the Three Pagodas Fault showing the fault segments (After Won-In, 1999).....	24
Figure 1.17	Major active faults in Thailand showing preliminary TL dating results on earthquake events, location of hot spring and epicenter distribution (After Charusiri et al., 2001).....	25
Figure 1.18	Geologic map along the trace of the Mae Kuang fault. P, undifferentiated Permian rocks; Cmt, Mae Tha Formation; SD, Silurian and Devonian Rocks; Pzph, Paleozoic phyllite; Pzv, Paleozoic metabasalt; Mzg, granitic rocks of the Fang-Mae Suai batholith. (After Rhodes et al., 2002).....	26

Figure 1.19	Topographic map of a portion of the Mae Kuang Valley, showing the mapped trace of the Mae Kuang Fault. A, B, and C point to shutter ridges that have diverted northwest-flowing tributaries (After Rhodes et al., 2002).....	26
Figure 1.20	Fault segments of the Phrae fault system based on Landsat TM5 image data (After Udchachon, 2002).....	27
Figure 1.21	Landsat 5 TM satellite image showing orientation of three major faults, the Mae Ping Fault, the Sri Sawat, Fault and the Three Pagodas Fault. The Sri Sawat fault are separated into three segments, namely northern, central, and southern segments (After Nutee, 2002).....	29
Figure 1.22	Seismotectonic provinces in Thailand (Modified after Woodward-Clyde Federal Services, 1996).....	30
Figure 1.23	Potentially active fault map of the area covering the Salaween Power Plant Project (After Charusiri et al., 2004).....	31
Figure 2.1	Map of the major tectonic plates with arrows showing directions of movement .Amounts of movement are shown in centimeters per year (After Abbott, 2004).....	33
Figure 2.2	Model of the earth's interior. Summary of the physical model of the earth's crust. Left, representation of major subdivisions of the earth's interior. Right, the variation of seismic wave (P and S) velocity plotted against depth (After <a href="http://dept.kent.edu/geology/ehlab/tectonics/tectonics.htm">http://dept.kent.edu/geology/ehlab/tectonics/tectonics.htm</a> ).....	35
Figure 2.3	The outermost layer of the Earth is the lithosphere. This layer makes up the topmost 100 km of the Earth, and includes the very upper part of the mantle and all the whole of the crust ( <a href="http://www.physicalgeography.net/fundamentals/images/lithosphere.gif">http://www.physicalgeography.net/fundamentals/images/lithosphere.gif</a> ).....	35
Figure 2.4	An idealized cross-section illustrating to relationship between the lithosphere and the underlying asthenosphere and the three principal types of plate boundaries (After <a href="http://dept.kent.edu/geology/tectonics/tectonics.htm">http://dept.kent.edu/geology/tectonics/tectonics.htm</a> ).....	36

Figure 2.5	Divergent plate boundaries on the ocean floor After <a href="http://www.ac.wvu.edu/~debari/406/lec1.html">www.ac.wvu.edu/~debari/406/lec1.html</a> ).....	38
Figure 2.6	Zone of plate convergent, A = oceanic–continental, B = oceanic–oceanic, and C = continental–continental (After <a href="http://dept.kent.edu/geology/ehlab/tectonics/tectonics.htm">http://dept.kent.edu/geology/ehlab/tectonics/tectonics.htm</a> ).....	38
Figure 2.7	The Blanco, Mendocino, Murray, and Molokai fracture zones are some of the many fracture zones (transform faults) that scar the ocean floor and offset ridges. The San Andreas is one of the few transform faults exposed on land (After <a href="http://dept.kent.edu/geology/ehlab/tectonics/tectonics.htm">http://dept.kent.edu/geology/ehlab/tectonics/tectonics.htm</a> ).....	39
Figure 2.8	Tectonic map of central–east Asia illustrating ‘extension’ model and its relationship with Cenozoic structures in the region. Numbers in white arrows indicate the relative order in which certain continental blocks were extruded toward the southeast (After Tapponnier et al., 1982).....	40
Figure 2.9	Three successive stages (I to III and IV to VI are in interpretation) of extrusional model experiment with plasticine (plain view). In unilaterally confined experiment, two major faults (F1 and F2) guide successive extrusion of two blocks. In stage VI, blocks 1 and 2 can be compared to Indochina and southern China, and open gap 1, 1+2, 2 to South China Sea, Andaman sea, and northeastern China, respectively (After Tapponnier et al., 1982).....	41
Figure 2.10	Tectonic map of Southeast Asia showing major structural elements in relation to direction of present maximum horizontal stress (After Srisuwon, 2002).....	44
Figure 2.11	Faults systems of Southeast Asia illustrating sequential Cainozoic deformation. The map displays plate fragmentation, north–west–south–east shears, and north–east by south–west expansion (Modified from Hutchison, 1989).....	45
Figure 2.12	Map of Thailand showing distributions of major classified active faults and fault zones in Thailand (After Hinthong, 1995).....	47
Figure 2.13	Map of Thailand showing major fault zones with TL–age dating data (After Charusiri et al., 2001).....	54

Figure 3.1	Enhanced Landsat 5 TM taken on June 25, 1997 showing physiographic features of the western part of the study area (Interpreted result is shown in Figure 3.6).....	56
Figure 3.2	Enhanced Landsat 5 TM taken on June 25, 1997 showing physiographic features of the eastern part of the study area (Interpreted result is shown in Figure 3.7).....	57
Figure 3.3	Enhanced Radarsat image taken on June 7, 2004 showing physiographic features of the northern and central parts of the study area (Interpreted result is shown in Figure 3.8).....	59
Figure 3.4	Enhanced Radarsat image taken on June 14, 2004 showing physiographic features of the central and southern parts of the study area (Interpreted result is shown in Figure 3.9).....	60
Figure 3.5	Enhanced JERS SAR taken on June 25, 1997 showing physiographic features of the central and southern parts of the study area (Interpreted result is shown in Figure 3.10).....	61
Figure 3.6	Lineaments interpreted using the enhanced Landsat 5 TM image in figure 3.1 and distribution of Cenozoic basins.....	62
Figure 3.7	Lineaments interpreted using the enhanced Landsat 5 TM image in figure 3.2.....	63
Figure 3.8	Lineament map of the northern area (Mae Ramat-Sop Moei) showing lineament patterns and distribution of Cenozoic basins interpreted using enhanced Radarsat image (from figure 3.3). A = Mae Saraing basin, B = Mae Tun basin, C = Muaywadee1 basin, D = Mae Ramat-Mae Sot basin, E = Muawadee2 basin.....	64
Figure 3.9	Lineament map of the southern area (Mae Sot-Tak) showing lineament patterns and distribution of Cenozoic basins interpreted, using the enhanced Radarsat image (from figure 3.4). C = Muaywadee1 basin, D = Mae Ramat-Mae Sot basin, E = Muaywadee2 basin, G = Mae Lamao basin.....	66
Figure 3.10	Lineaments and distribution of Cenozoic basins in central and southern parts of the study area interpreted using the enhanced JERS SAR image (from figure 3.5).....	67

Figure 3.11	Map of the study area displaying locations of the NW-trending Moei-Mae Ping Fault Zone (red line), its major inferred active fault segments, and the 17 February 1975 epicenter.....	72
Figure 3.12	Plan view of structure associated with an idealized strike-slip fault (After Christie-Blick and Biddle, 1985).....	73
Figure 3.13	Simple shear models associated with strike-slip fault (a) and producing contractional and extensional features (b) (After Christie-Blick and Biddle, 1985).....	73
Figure 3.14	Sags and pressure ridges associated with bends and steps along strike-slip faults (After Keller and Pinter, 1996).....	75
Figure 3.15	Assemblage of landform associated with active tectonic strike-slip faulting (After Burbank and Anderson, 2001).....	75
Figure 3.16	Idealized cross-section of extension tectonic environments (After Burbank and Anderson, 2001).....	76
Figure 3.17	Basic slope elements that may be present on a fault scarp (After McCalpin, 1996).....	76
Figure 3.18	Development of triangular facets produced by episodic vertical tectonic movement (After Fenton et al., 1997).....	77
Figure 3.19	Types of reverse fault scarps. (A) Simple reverse (or thrust) scarp. (B) Hanging-wall collapse scarp. (C) Simple pressure ridge. (D) Dextral pressure ridge. (E) Back-thrust pressure ridge. (F) Low-angle ridge. (G) En-echelon pressure ridge. 1, bed rock; 2, soft Quaternary sediments; 3, turf (After Phillip et al., 1992).....	78
Figure 3.20	Map showing locations of the Moei-Mae Ping Fault Zone (MPFZ, red line) and its major inferred active fault segments. Boxes with numbers indicate selected areas for remote-sensing and aerial photographic interpretations, and detailed paleoseismic studies.....	80
Figure 3.21	Symbols used as guidelines for descriptions appearing in the interpreted morphotectonic maps (in figures 3.22-3.32).....	81
Figure 3.22	Aerial photograph and interpreted morphotectonic landforms along the Sop Moei fault segment, in Area A, Ban Sop Moei, Amphoe Sop Moei, Changwat Mae Hong Son. ....	82



Figure 3.23	Aerial photograph and interpreted morphotectonic landforms along the Ban Tha Song Yang fault segment in Area B, Ban Tha Song Yang, Amphoe Tha Song Yang, Changwat Tak. ....	83
Figure 3.24	Aerial photograph and interpreted morphotectonic landforms along the Khao Mae Song fault segment, in Area C, Ban Mae Ou Su, Amphoe Tha Song Yang, Changwat Tak. ....	85
Figure 3.25	Aerial photograph and interpreted morphotectonic landforms along the Khao Mae Song fault segment, in Area C, Ban Mae Ou Su, Amphoe Tha Song Yang, Changwat Tak. ....	86
Figure 3.26	Aerial photograph and interpreted morphotectonic landforms along the Doi Kala fault segment, in Area D, Ban Mae Ramat, Amphoe Mae Ramat, Changwat Tak.....	87
Figure 3.27	Aerial photograph and interpreted morphotectonic landforms along the Doi Kala fault segment, in Area D, Ban Mae Ramat, Amphoe Mae Ramat, Changwat Tak.....	89
Figure 3.28	Aerial photograph and interpreted morphotectonic landforms in Area E, the Doi Krathing fault segment, Taksin Maharat National Park, Changwat Tak.....	90
Figure 3.29	Aerial photograph and interpreted morphotectonic landforms in Area E, the Doi Krathing fault segment, Taksin Maharat National Park, Changwat Tak.....	91
Figure 3.30	Aerial photograph and interpreted morphotectonic landforms in Area F, Ban Tha Lay, Tambon Lan Sang, Amphoe Mueang, Changwat Tak.....	93
Figure 3.31	Aerial photograph and interpreted morphotectonic landforms in Area G covering the Khao Yao fault segment, Ban Tha Thong Daeng, King Amphoe Na Bot, Changwat Tak.....	94
Figure 3.32	Aerial photograph and interpreted morphotectonic landforms in Area H covering the Khlong Phri fault segment, Ban Pang Khanun, Amphoe Muang, Changwat Kamphaeng Phet.....	96

Figure 4.1	Topographic map of Ban Bun Loe, Sheet 4544 IV, showing locations of the Sop Moei fault segment. Note that the box represents the area of aerial photographic interpretation in investigated area A (Royal Thai Survey Department, 1976).....	98
Figure 4.2	A set of triangular facets of the Sop Moei fault segment, and panoramic view of its NE-trending. (0361935E/1972014N, 4544 IV).....	100
Figure 4.3	A set of triangular facets of the Sop Moei fault segment, and panoramic view of its NE-trending around Ban Sop Moei area, Amphoe Sop Moei, Changwat Mae Hong Son.....	100
Figure 4.4	Topographic map of Ban Tha Song Yang, Sheet 4544 II, showing locations of the Ban Tha Song Yang fault segment. Note that the box represents the area of aerial photographic interpretation in area B. (Royal Thai Survey Department, 1969).....	101
Figure 4.5	Photograph showing the NE-trending offset stream observed along the Ban Tha Song Yang fault segment (no.3 in Figure 3.11) in Ban Mae Tun area, Amphoe Tha Song Yang, Changwat Tak (view looking at 0384194E/1945584N to NE).....	103
Figure 4.6	Photograph showing the NE-trending fault acarp observed along the Ban Tha Song Yang fault segment (no.3 in Figure 3.11) in Ban Tha Song Yang area, Amphoe Tha Song Yang, Changwat Tak (view looking at 0385685E/1941726N to NE).....	103
Figure 4.7	Topographic map of Amphoe Tha Song Yang, Sheet 4643 IV, showing location of the Khao Mae Song fault segment. Note that the boxes represent the areas of aerial photographic interpretations in area C (Royal Thai Survey Department, 1969).....	105
Figure 4.8	The faults cutting into Tertiary semi-consolidated sediments observed along Amphoe Mae Ramat-Amphoe Tha Song Yang road, Changwat Tak.....	106
Figure 4.9	Photograph showing the NE-trending triangular facet and bench observed along the Khao Mae Song fault segment (no. 4 Figure 3.11) in Amphoe Tha Song Yang area, Changwat Tak.....	106

Figure 4.10	Photograph shows the NE trending triangular facet and shutter ridge observed along the Khao Mae Song fault segment (no. 4 Figure 3.11) in Ban Mae Ou Su area, Amphoe Tha Song Yang, Changwat Tak (view looking to NW).....	107
Figure 4.11	Photograph shows the NE trending triangular facet observed along the Khao Mae Song fault segment (no. 4 Figure 3.11) in Ban Mae Ou Su area, Amphoe Tha Song Yang, Changwat Tak (view looking to SW).....	107
Figure 4.12	Topographic map of Amphoe Mae Ramat Noi, Sheet 4743 III, showing location of the Doi Kala fault segment. Note that the box represents the area of aerial photographic interpretation in area D (Royal Thai Survey Department, 1969).....	109
Figure 4.13	Topographic map of Amphoe Mae Ramat, Sheet 4742 IV, showing location of the Doi Kala fault segment. Note that the box represents the area of aerial photographic interpretation in area D (Royal Thai Survey Department, 1979).....	110
Figure 4.14	Photograph showing the northern trending facet spurs of Ban Mae Ramat area, Amphoe Mae Ramat, Changwat Tak along the Doi Kala fault segment (no.6 in Figure 3.20).....	111
Figure 4.15	Fault scarp observed at eastern side of limestone mountain, indicating youthfulness of the fault in area D.....	111
Figure 4.16	Topographic map of Ban Pang San, Sheet 4742 I, showing locations of the Doi Luang fault segment. Note that the boxes represent the areas of aerial photographic interpretations in area E and F (Royal Thai Survey Department, 1995).....	113
Figure 4.17	Topographic map of Changwat Tak, Sheet 4842 IV, showing locations of the Doi Luang fault segment. Note that the boxes represent the areas of aerial photographic interpretations in area F (Royal Thai Survey Department, 1995).....	115
Figure 4.18	Photograph showing the NE trending triangular facets along the Khao Yao fault segment (no. 9 in Figure 3.11) in Ban Tha Lay area, Amphoe Muang Tak, Changwat Tak.....	117

Figure 4.19	Topographic map of Ban Na Bot, Sheet 4842 III, showing locations of the Khao Yao fault segment. Note that the box represents the area of aerial photographic interpretation in area G (Royal Thai Survey Department, 1989).....	118
Figure 4.20	Photograph showing the NE trending triangular facets along the Khao Yao fault segment (no. 9 in Figure 3.11) in Ban Tha Thong Daeng area, King Amphoe Na Bot, Changwat Tak.....	120
Figure 4.21	Topographic map of Ban Na Bo Kham, Sheet 4841 I, showing locations of the Klong Phri fault segment. Note that the box represents the area of aerial photographic interpretation in area H (Royal Thai Survey Department, 1986).....	121
Figure 4.22	Photograph showing the NE trending fault scarp in Ban Pang Khanun, Amphoe Muang, Changwat Kamphaeng Phet along the Khlong Phri fault segment (no. 10 in Figure 3.11).....	123
Figure 4.23	Detailed survey map covering offset stream and shutter ridge along the fault segment no. 4 (Figure 3.11) of the Ban Mae Ou Su area, Amphoe Tha Song Yang, Changwat Tak.....	131
Figure 4.24	Topographic features of area C, Ban Mae Ou Su, Amphoe Tha Song Yang, Changwat Tak. Detailed survey map covering offset stream and shutter ridge of the Ban Mae Ou Su area. Note that in box A is late fault movement, box B is past fault movement, and box C is present fault movement.....	132
Figure 4.25	The southeastern wall of Ban Mae Ou Su Trench No.1 (MOS1) showing principle stratigraphy.....	133
Figure 4.26	Trench-log at the southeastern wall of MOS trench showing principal stratigraphy. Note: Boxes showing the closed-up structures found at SE wall of MSO1 trench (in Figures 4.29 and 4.30).....	134
Figure 4.27	The southeastern wall of Ban Mae Ou Su Trench No.2 (MOS2) showing principle stratigraphy.....	135

Figure 4.28	Trench-log at the southeastern wall of MOS2 trench showing principal stratigraphy. Note: Boxes showing the closed-up structures found at SE wall of MSO2 trench (in Figures 4.31 and 4.32).....	136
Figure 4.29	Close-up of the southeast wall, MOS1, the fault cuts the Unit E and Unit D.....	137
Figure 4.30	Close-up of the southeast wall, MOS1, the fault cuts the Unit E, strike of S65°W and dip of 80° westward.....	138
Figure 4.31	Close-up of the southeast wall, MOS2, the fault cuts the Unit E and Unit D.....	140
Figure 4.32	Close-up of the southeast wall, MOS2, the fault cuts the Unit E, Unit D, and unit C in the reverse sense of movement.....	141
Figure 4.33	The southeastern wall of MOS2 trench and showing locations of collected TL dating samples.....	142
Figure 4.34	The southeastern wall of MOS1 trench showing locations of collected TL and C-14 dating samples.....	143
Figure 5.1	A simplified model of lattice structure of an ionic crystal showing three simple types of defect which are negative-ion vacancy on the left, negative-ion interstitial at the center, and substitution impurity center on the bottom right (After Aitken, 1985).....	145
Figure 5.2	Thermoluminescence-process diagram showing energy-level related to three processes; (i) irradiation process, caused by crystal exposed to nuclear radiation, ionized electrons are trapped at hole (T). (ii) Storage stage in which electrons have been trapped, need hole deep enough for electrons (E) during geological time period of sample. (iii) Heating process, at optimum level of temperature, electrons are released and re-combined at luminescence center (L), and then light (TL) is released (After Aitken, 1985).....	145
Figure 5.3	Diagram of thermoluminescence instrument (After Aitken, 1985).	147
Figure 5.4	A glow curve graph shows relationship between TL intensity versus temperature.....	147

Figure 5.5	Simplified flow chart illustrating laboratory analysis use in this research study. The red dash line is the annual dose procedure and the blue dash line is the equivalent dose procedure (Modified from Takashima and Honda, 1989).....	148
Figure 5.6	Graph showing relationship between TL ratio (artificial glow curves/natural glow curve) versus temperature ( $^{\circ}\text{C}$ ). N is natural signal, H is heated sample at $320^{\circ}\text{C}$ for 5 hours, and (is known dosage that irradiated sample).....	151
Figure 5.7	Schematic charts of regeneration technique (Takashima et al., 1989). Note that several portions are used for measurement of the TL intensity; N is natural sample, $I_0$ is residual intensity from sample, H is $350^{\circ}\text{C}$ heated sample and (is known dosage that irradiated sample).....	153
Figure 5.8	Thermoluminescence remaining after bleaching by exposes to sunlight for various time of sample no. OS 1-17.....	154
Figure 5.9	Thermoluminescence remaining after bleaching by exposes to sunlight for various time of sample no. OS 2-7.....	155
Figure 5.10	Plateau-curve (dashed line) plotted with glow-curves (solid line). Plateau-curve is the ratio of the two glow-curves; N is represented the “natural” glow-curve and $N+\beta$ is the “natural + artificial” glow-curve (After Aitken, 1985).....	156
Figure 5.11	Summary of neutron activation analysis (NAA) procedures with sample preparation and annual dose determination.....	157
Figure 5.12	Trench-log in the southeastern wall of MOS2 trench and showing principal stratigraphy and locations of TL dating samples.....	159
Figure 5.13	Trench-log in the southeastern wall of MOS2 trench and showing principal stratigraphy and thermoluminescence (TL) dates of dating samples.....	160
Figure 5.14	Trench-log in the southeastern wall of MOS2 trench and showing principal stratigraphy and locations of TL and C-14 dating samples	164
Figure 5.15	Trench-log in the southeastern wall of MOS2 trench and showing principal stratigraphy and thermoluminescence (TL) and C-14 dates of dating samples.....	165

Figure 6.1	A) Photograph of trenching MOS1 logging B) the GPR interpretation profile from the first line survey (After Thitipattanakul 2005).....	169
Figure 6.2	A) Photograph of trenching MOS2 logging B) the GPR interpretation profile from the first line survey (After Thitipattanakul 2005).....	170
Figure 6.3	Map of Tak and adjacent areas showing epicentral distribution from 1912 to 2006 (Data from Nutalaya et al., 1985; Thai Metrological Department, 2002; and <a href="http://neic.usgs.gov/neis/epic/epic_global.html">http://neic.usgs.gov/neis/epic/epic_global.html</a> ).....	172
Figure 6.4	Map showing fault segments and their paleoearthquake magnitudes of the Moei-Mae Ping Fault Zone.....	173
Figure 6.5	Simplified distribution granite map of Northwestern Thailand, and offset of Triassic granites (Modified after DMR, 1999).....	177
Figure 6.6	Map of Thailand showing the tectonic units, 1 = Shan-Thai plate 2 = Lampang-Chiang Rai plate, 3 = and Nakhon Thai plate, 4 = Indochina plate (After Charusiri et al., 2002).....	178
Figure 6.7	A simplified tectonic model of Tertiary basin formation in the study area (Modified after Uttamo et al., 2003). A simplified tectonic model of Tertiary basin formation in the study area (Modified after Uttamo et al., 2003).....	180
Figure 6.8	Interpretation map showing the dextral movement along the NW-trending of Moei-Mae Ping Fault Zone and the development of fault-tip or fault-bend (This study and modified from Uttamo, 2003 and Morley, 2002).....	181

## LIST OF TABLES

	PAGE
Table 2.1 Active fault rank, criteria, and examples in Thailand (After Charusiri et al., 2001).....	52
Table 2.2 Activity of faults in Thailand based upon age-dating data (After Charusiri et al., 2001).....	53
Table 3.1 Type of fault segments and the characteristics used to define them (After McCalpin, 1996).....	69
Table 3.2 Fault segment lengths proposed for active fault by various authors (After McCalpin, 1996).....	70
Table 4.1 Rating Criteria and Priority for Selection of Detailed Investigation Area (Higher number indicates more weight).....	124
Table 4.2 Rating of Suitability for Selection of the Detailed Field Investigation.....	126
Table 5.1 Summarization of TL-dating results.....	167
Table 6.1 paleoearthquake magnitudes of the MPFZ in Tak area, estimation from Well and Coppersmith (1994).....	175



## CHAPTER I

### INTRODUCTION

#### 1.1 General Information

Basically, tectonics refers to the processes, structures and landforms associated with deformation of the Earth's crust (Keller and Pinter, 1996). In Thailand, the major tectonic evolution can be divided into four episodes, namely, archeotectonic, paleotectonic, mesotectonic, and neotectonic episodes (Charusiri et al., 2002). The archeotectonic episode is a tectonic event that occurred during pre-Paleozoic era, whereas paleotectonic, mesotectonic, and neotectonic episodes are limited in Paleozoic, Mesozoic, and Cenozoic times, respectively.

Tectonics occurring in Cenozoic times has played an important role in our ways of life since its time span covers Tertiary and Quaternary times. Neotectonic event in this study is a technical term referred to a new tectonic event, occurring in Tertiary in Thailand or the so-called neotectonic episode by Charusiri et al. (2002). Many scientists had tried to explain the definition of neotectonics for several decades since the effects of neotectonics, such as catastrophic earthquakes, are concerned to society. For example, Obruchev (1948) mentioned that neotectonics is referred to the study of the young and a recent movement taking places at the end of the Tertiary and the first half of the Quaternary. Neotectonic phase starts at different times in different places, depending on tectonic regime (Morner, 1990). Neotectonics can be broadly described as tectonic events and processes that have occurred in post Miocene time (Slemmons, 1991). Neotectonic structures develop in the current tectonic regime to embrace the prevailing state of deformation within an intraplate region (Muir et al., 1992). Neotectonics is, therefore, the branch of tectonics concerned with the past and is continuing at the present day (Stewart and Hancock, 1994).

Other disciplines related to neotectonic terminology consist of active tectonics, which referred to tectonic processes that produce the crust deformation on a time of scale of significances to human society (Wallace, 1986). Paleoseismology is the study of prehistoric earthquakes, especially their locations, timing, and sizes (Solonenko, 1973 and Wallace, 1981). Paleoseismic data can be used in neotectonic investigation and can supply

relatively short-term geological data for regional fault behaviors and deformation styles (Wesnousky, 1984). Seismotectonics is a branch of geosciences that are concerned with the relationships between the seismological characteristics of present-day earthquakes and tectonics. Seismogeology is the study of geological structures, such as, soft-sediment deformation, and fault scarp analysis, of contemporary seismicity. Archeoseismology can be referred to the study of archeological evidences for historical and pre-historical earthquakes. Morphotectonics is the study of all aspects of relationship between geological structures and landforms; others restrict it to relationships between neotectonic structures and landforms. Tectonic geomorphology is the study of the relations of vertical and horizontal ground movements to erosional and depositional processes and landforms (Stewart and Hancock, 1994).

According to tectonically active regions in the world, there are usually observed tectonic evidences around active margins and subduction zones of the major plates. The common evidence of this tectonism is characterized by large earthquakes. However, depending on historical and instrumental records, many of earthquakes had also found experiences within intraplate regions, even not frequent and large as compared to the former. In western basin and range province of the United States of America, it has long been recognized as earthquake regions (Wallace, 1990). Tectonism influence in this region is generated from two main sources; the San Andreas Fault system and the subduction zone in eastern pacific. Note that, only on the San Andreas Fault and its major branches have average recurrent intervals as short as 10-200 years (Wallace, 1990). In Turkey, conventional tectonic evidence in this region is expressed by the Anatolian fault. This fault is characterized by extensional tectonics associated with transcurrent displacement, which is the result of N-S relative convergence of Eurasia and Africa-Arabia (McKenzie, 1972). In New Zealand, the Awatere fault is a system of dextral strike-slip faults constituting the Australia-Pacific plate boundary. At least six ground-rupturing events, which were younger than 8,330-8,610 yrs., were generated by this fault (Benson, 2001). In China, several fault systems are located in the region of high historical seismicity. Good examples are the Altyn Tagh fault, the Nan Shan-Kansu Fault system, the Kun Lun fault, the Kang Ting fault, and the Red River fault. In addition, all of the recent tectonics of China is related to the convergence of India and Eurasia during the Cenozoic at a rate of about 5 cm/yr (Tapponnier and Molnar, 1977). In Japan, the 1995 Kobe earthquake with the magnitude of 6.4 on the Richter scale is believed to be related to right-lateral strike-slip on the Nojima fault. Net offset was found to be about 1.5 m with several vertical displacements.

The hypocenter was far from the tectonic plate boundary between the Philippine Sea plate and the Eurasia plate about 200 km (Bolt, 1999).

In Thailand and mainland Southeast Asia (SE Asia), present-day tectonics in this region is the result of the collision between Indian and Eurasian plates since middle Tertiary time (Fenton et al., 1997; Charusiri et al., 2002; Bunopas, 1994; and Hinthong, 1991). Although the majority of deformation at present occurred on the faults outside Thailand, (for example, the Kun Lun, the Red River, and the Altyn Tagh faults), a moderate earthquake activity throughout the mainland SE Asia indicates contemporary deformation in this region (Fenton et al., 2003). Progressive rotation of SE Asia results in an increasing strike-slip faults with the associated development of pull-apart basins in Thailand (Figure 1.1) (Polachan and Sattayarak, 1989).

Thailand, a country in mainland SE Asia, has not been considered to be a seismically active country due to the disappearance of the large earthquakes in the past. However, Thailand has been subjected to minor to moderate earthquake damages overtime. Stronger earthquakes frequently occurred in the neighboring countries, e.g. Myanmar, China, Laos, and Vietnam (Figure 1.2). Recent geologic and geochronological investigations reveal that late Quaternary faults appeared in northern Thailand to be characterized by long recurrent intervals of hundreds to tens of thousand of years (Bott et al., 1997; Kosuwan et al., 1999; and Fenton et al., 2003). The major faults in the Myanmar-Thailand border zone are the Taunggyi Fault, the Pan Laung Fault, the Mae Hong Song Fault, the Moei-Uthai Thani Fault Zone, the Si Sawat (or Sri Sawat) Fault, and the Three Pagoda (or Three Pagodas) Fault (Figure 1.3) (Nutalaya et al., 1985). The Moei-Mae Ping Fault Zone (MPFZ of this study), or the Moei-Uthai Thani Fault Zone of Charusiri et al. (1996), or the Lan Sang-Wang Chao Fault Zone of Bunopas (1981) or the Mae Ping Fault of Polachan and Sattayarak (1989), is characterized by narrow and complex fault zones of normal, thrust, and strike-slip natures. Two earthquakes along this fault zone occurred on September 23, 1933 and February 17, 1975 (Nutalaya et al., 1983 and Thailand Meteorological Department, 2002). The latter had a magnitude of 5.6 on the Richter scale and was felt throughout central Thailand, causing minor damage. Therefore it is important to understand landforms which were formed by earthquake activities.

## 1.2 Objectives

The purpose of this research is to characterize the Moei-Mae Ping Fault Zone (MPFZ) and to clarify the paleoearthquakes along its fault zone. Recent knowledges and

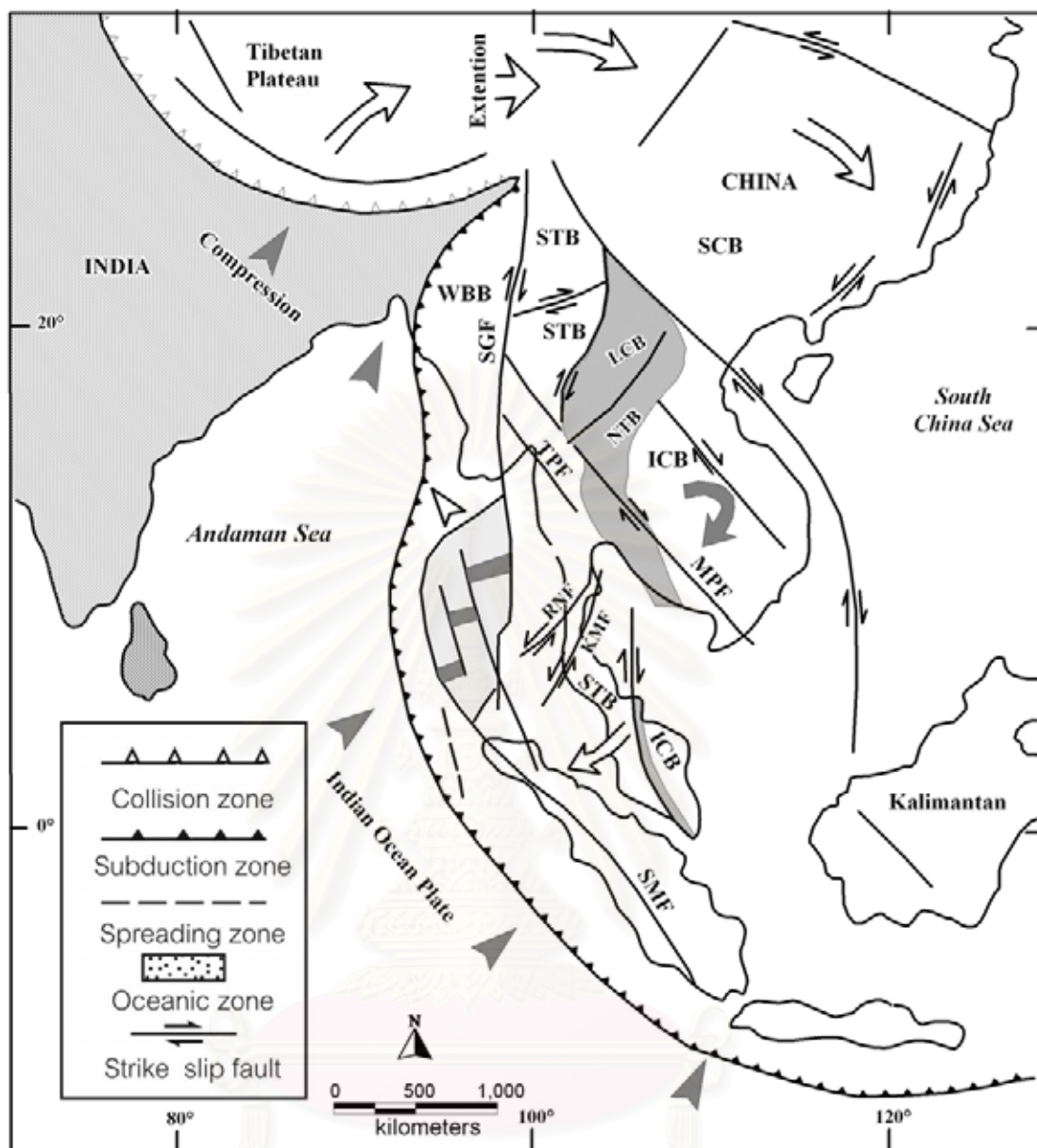


Figure 1.1 Present-day tectonic of South and Southeast Asia showing major active structure, direction of the plate movement (arrows) and some important tectonic blocks of Southeast Asia. Note that WBB = Western Burma Block, SCB = South China Block, SMB = Simao Block, STB = Shan-Thai Block, ICB = Indochina Block, LCB = Lampang-Chiang Rai Block, NTB = Nakhon Thai Block, SGF = Sagaing Fault, MPF = Mae Ping Fault, RNF = Ranong Fault, KMF = Klong Marui Fault, SMF = Sumatra Fault, NUF = Nan Uttaradit Fault, TPF = Three Pagodas Fault, RRF = Red River Fault (Modified after Polachan and Sattayarak, 1989).

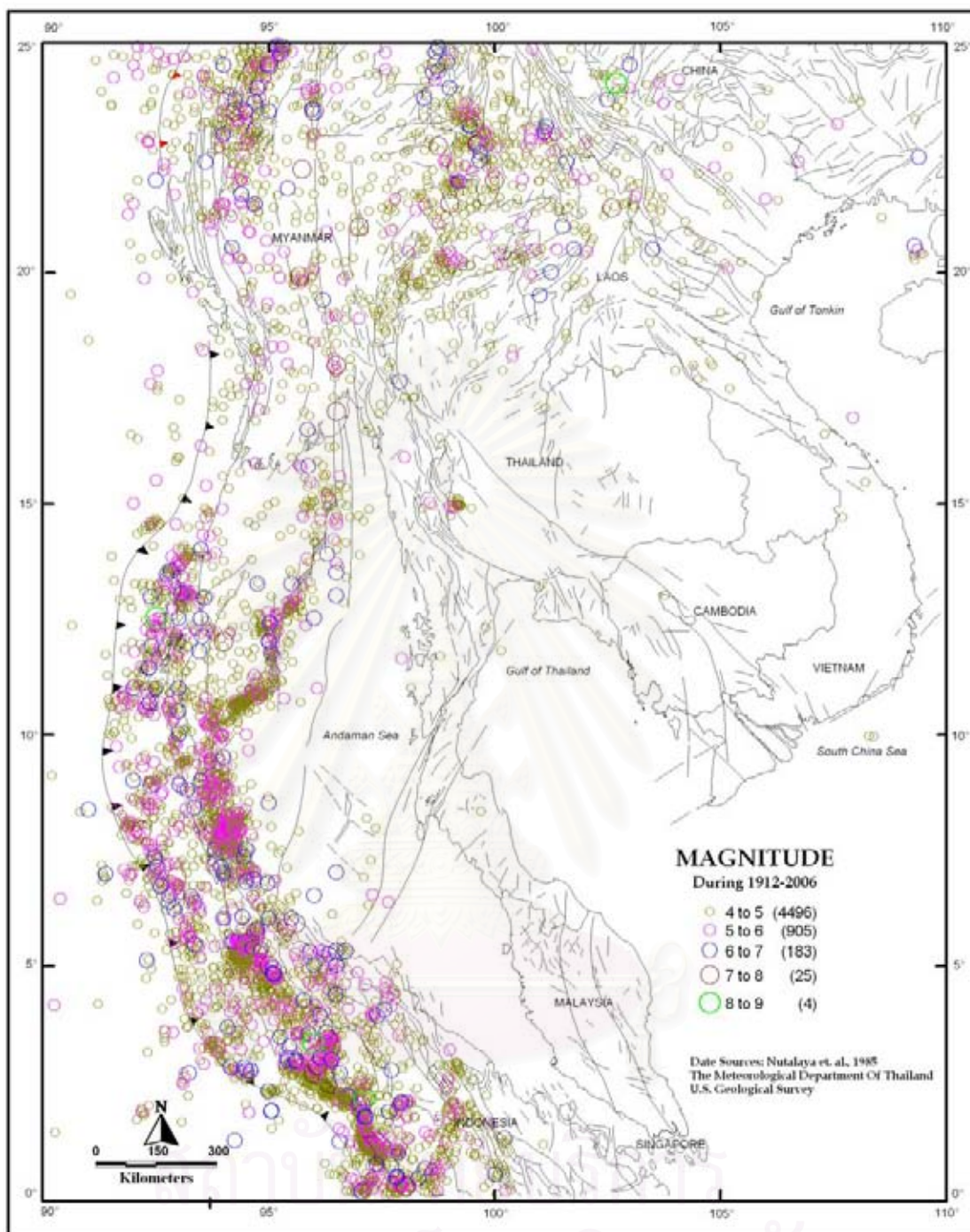


Figure 1.2 Map of mainland Southeast Asia showing epicentral distribution from 1912 to 2006 (Data from Nutalaya et al., 1985; Thai Meteorological Department, 2002; and [http://neic.usgs.gov/neis/epic/epic\\_global.html](http://neic.usgs.gov/neis/epic/epic_global.html)).

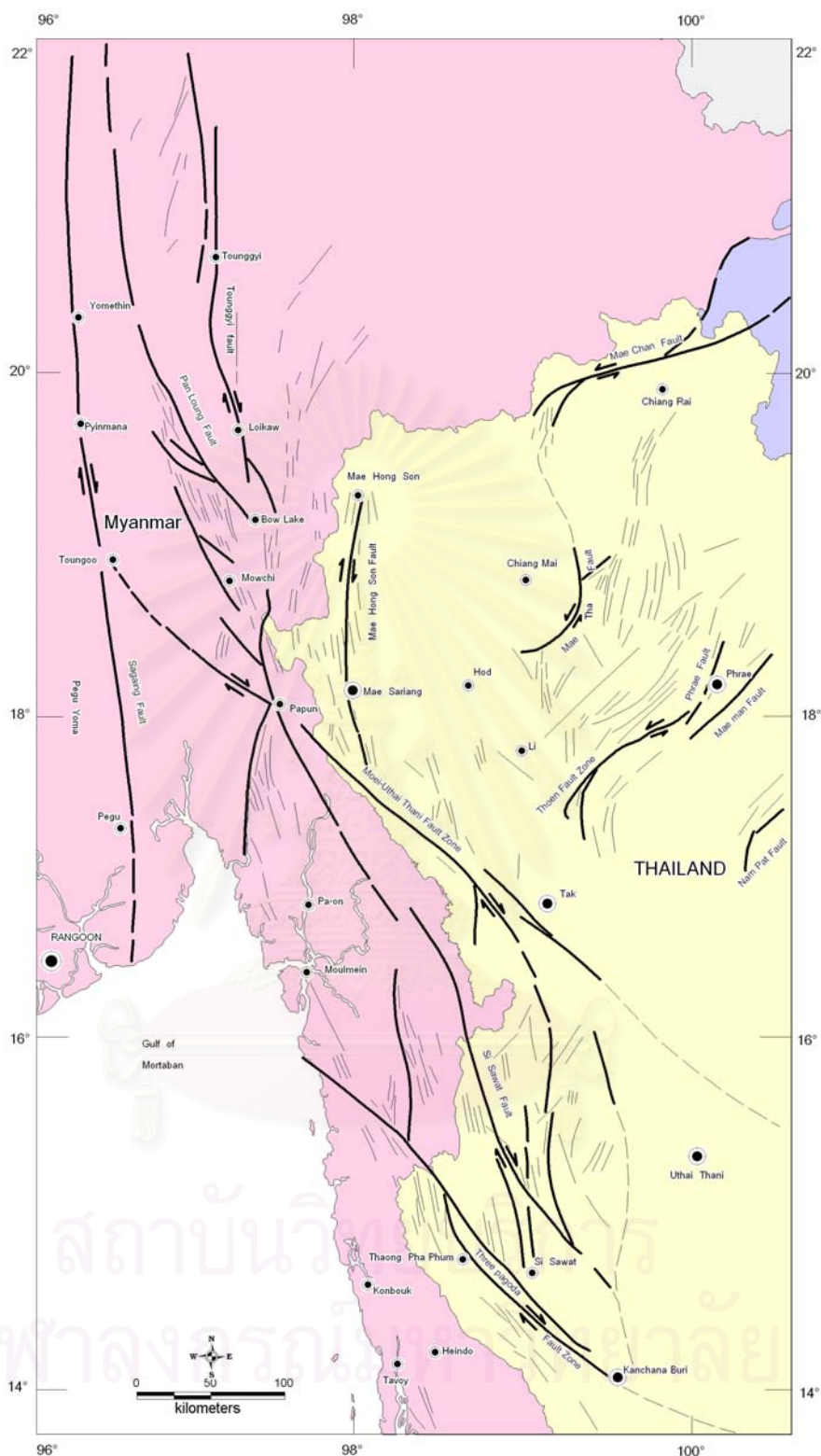


Figure 1.3 Map of eastern Myanmar and western to northwestern Thailand showing active and associated faults and their relative movements (Modified after Nutalaya et al., 1985). Note that the present study area is shown in box which covers parts of the so-called Moei-Uthai-Thani Fault Zone or Moei-Mae Ping Fault Zone of the present study.

techniques of paleoseismology are used for investigating the interesting faults along the zone and their associated paleoearthquakes. Results of the research lead towards characterizing the MPFZ, identifying each paleoearthquake, recognizing their behaviors, estimating magnitudes and ages of paleoearthquakes, and ultimately toward proving whether their fault segments are active or not, as well as their slip rates. Further study should be performed for the purpose of planning in order of preventing damages from earthquakes in the future.

Consequently, the main objectives of this study aim at the following four folds:

1. identifying characteristics of the Moei-Mae Ping Fault Zone;
2. locating active faults of the Moei-Mae Ping Fault Zone;
3. determining the ages of the Moei-Mae Ping Fault movements; and
4. estimating the magnitudes and slip-rates of these events.

### **1.3 The Study Area**

The study area selected for the present thesis research is located at the areas extent, bounded by latitudes  $16^{\circ}$  N to  $18^{\circ}$  N and longitudes  $97^{\circ} 30' E$  to  $99^{\circ} 30' E$ , to cover much of the Moei-Mae Ping Fault Zone (MPFZ) in the area of Changwat Tak, northwestern Thailand. The total study area ( $25,000 \text{ km}^2$ ) is approximately 440 km far from the capital city of Thailand, Bangkok (Figure 1.4).

### **1.4 Study Methodology**

The study methodology of this study is divided into six steps (Figure 1.5) including:

#### **1.4.1 Planning and Preparation**

The first step was conducted in order to contribute general data into a database for supporting further steps of study. This data is composed of relative previous works, enhanced remote-sensing images and digital files, aerial photographs, geologic maps, topographic maps, earthquake distribution information, and other related technical and nontechnical documents.

#### **1.4.2 Field Reconnaissance**

The second step, involving field reconnaissance in the study area, was launched in order to construct general guidelines for detailed investigations. Condition of transportation routes, accessibility to the area, method of collecting field data, duration, time and budget to spend for field work, etc., are examples of compilation for this step.

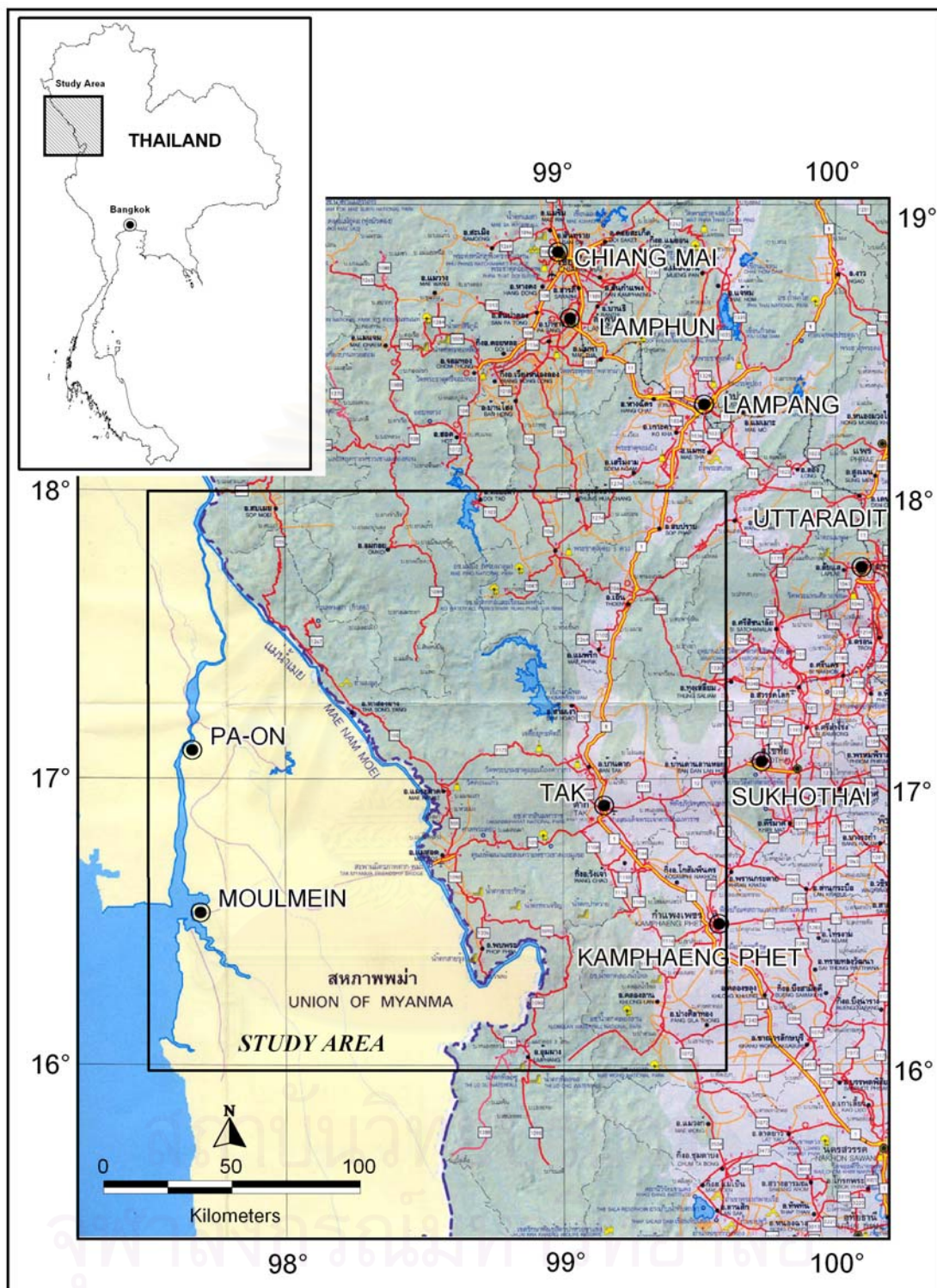


Figure 1.4 Map of western Thailand and eastern Myanmar showing the location of the study area (After <http://map-project.doh.go.th/ZoomRaster.asp?Region=3&Zoom=1>).



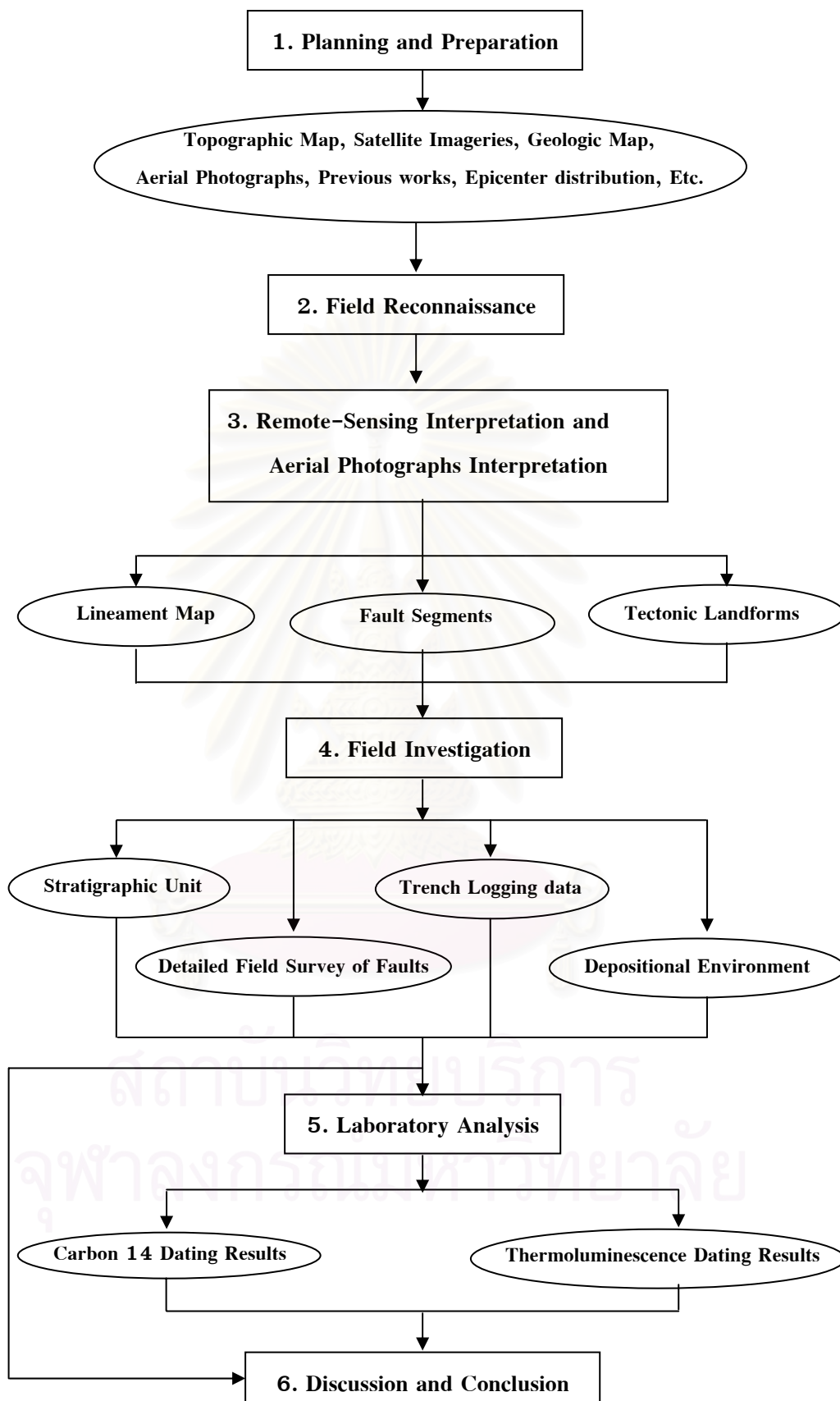


Figure 1.5 Steps of work in the method of study for this thesis research.

#### **1.4.3 Remote-Sensing and Aerial Photographic Interpretations**

The third step involves remote-sensing interpretation commencing on a small scale using digitally enhanced satellite imagery (1:250,000) and interpretation on a large scale with aerial photographs (1:50,000). Both approaches were derived from the basic data for lithological and structural interpretation, lineaments were then interpreted to locate their attitudes and orientations, and past movements of the fault zones. The detailed site investigation, including defining fault segments and their fault characteristics, was carried out with the utilization of stereoscopic aerial photographs.

#### **1.4.4 Field Investigation**

The fourth step commences with all morphotectonic landforms and interpretation of remote-sensing data were verified in the field. For this step, geomorphic mapping related to neotectonic evidence was conducted for evaluating locations and the nature of active faults, and identifying sequences of faulting in the focus area. Geological data were subsequently collected, particularly along the fault segments, for studying fault characteristics.

#### **1.4.5 Laboratory Analyses**

The fifth step includes sample collection, treatment of samples for datings, and further works. Emphasis is placed on splitting samples into two parts for datings, To facilitate the laboratory analysis, one part of samples was used for dating approach in Thermoluminescence geochronological method while the other used for the carbon 14 AMS method.

#### **1.4.6 Result Integration**

The sixth step coped with integrating all of the available investigated and surveyed results from various morphotectonic evidences toward the delineation of a lineament map, paleoearthquakes, estimation of paleomagnitudes from surface rupture lengths, and identification of active faults are also deduced.

### **1.5 Active Fault Studies in Thailand**

At present, no detailed study on morphotectonics has been performed in the study area. However, a few researches have been reported, more or less concerned with geological structures and the seismology of the Tak region.

Nutalaya et al. (1985) studied the characteristic earthquakes and described seismic source zones in the Myanmar, Thailand, and Indochina areas that consist of twelve zones.

They located Thailand within zone F and G on the west and the north, respectively (Figure 1.6). The Moei-Uthai-Thani Fault Zone in the zone F (Tenasserim Range) is characterized by narrow and complex fault zones of normal, thrust, and strike-slip nature. The horizontal displacement on outcrops gives a left-lateral appearance. Also, the study of Bunopas (1976) on the Lan Sang fault, which is one of the faults in this zone, shows the fault contact between Ordovician limestone and Tertiary lignite beds along its left-lateral displacement. The earthquake on February 17, 1975 with magnitude of 5.6 was felt throughout central Thailand and causing minor damage (see Figure 1.7). However, a focal plane solution by Nutalaya et al. (1985) shows a component of right lateral movement.

Siribhakdi (1986) investigated seismogenic zones in Thailand and its periphery and reported earthquakes in Thailand throughout her past 1,500 year's history. The foci and epicenters of the seismicity have been located both in Thailand and neighboring countries. These indicated seismic active areas. Many of the earthquakes found have closed relation with four major faults including the Three Pagoda, the Si Sawat, the Moei-Uthai-Thani, and the Mae Hong Son-Mae Sariang Faults. The seismicity in Thailand associated with tectonism is believed to be related to the subduction zone and spreading ridge in the Andaman Sea.

Thiramongkol (1986) observed the neotectonism and rate of uplift in the eastern margin of the lower central plain of Thailand. The evidence of neotectonic movement is found on the difference of elevation between foot-wall and hanging-wall of the Bang Pakong fault (Figures 1.8 and 1.9), which is 18 m. Uplift rate of 2.4 mm was reported annually, calculated from topographic difference and timing. C14-dating AMS (on a wood fragment) indicated  $7,300 \pm 35$  years B.P. for the brackish clay bed.

Hinthong (1991) emphasized the role of tectonic setting in earthquake events in Thailand. He also cited that earthquakes in Thailand are closely related to two seismic source zones, namely, the Tenasserim Range zone (zone F) and the Northern Thailand zone (zone G) of Nutalaya et al. (1985). The faults within zone F are believed to be active more than those of zone G which are inferred to be possibly potentially active faults.

Klaipongpan et al. (1991) studied geological and seismicity evaluation of Srinagarin dam based upon earthquake catalogs, focal mechanism solutions, earthquake relocation studies, aerial and ground geologic reconnaissance surveys, analysis of remote-sensing imagery, and review of the pre-instrumental and instrumental seismicity of Thailand. They claimed that the 26 April, 1983 earthquake at Srinagarin dam was triggered by water load.

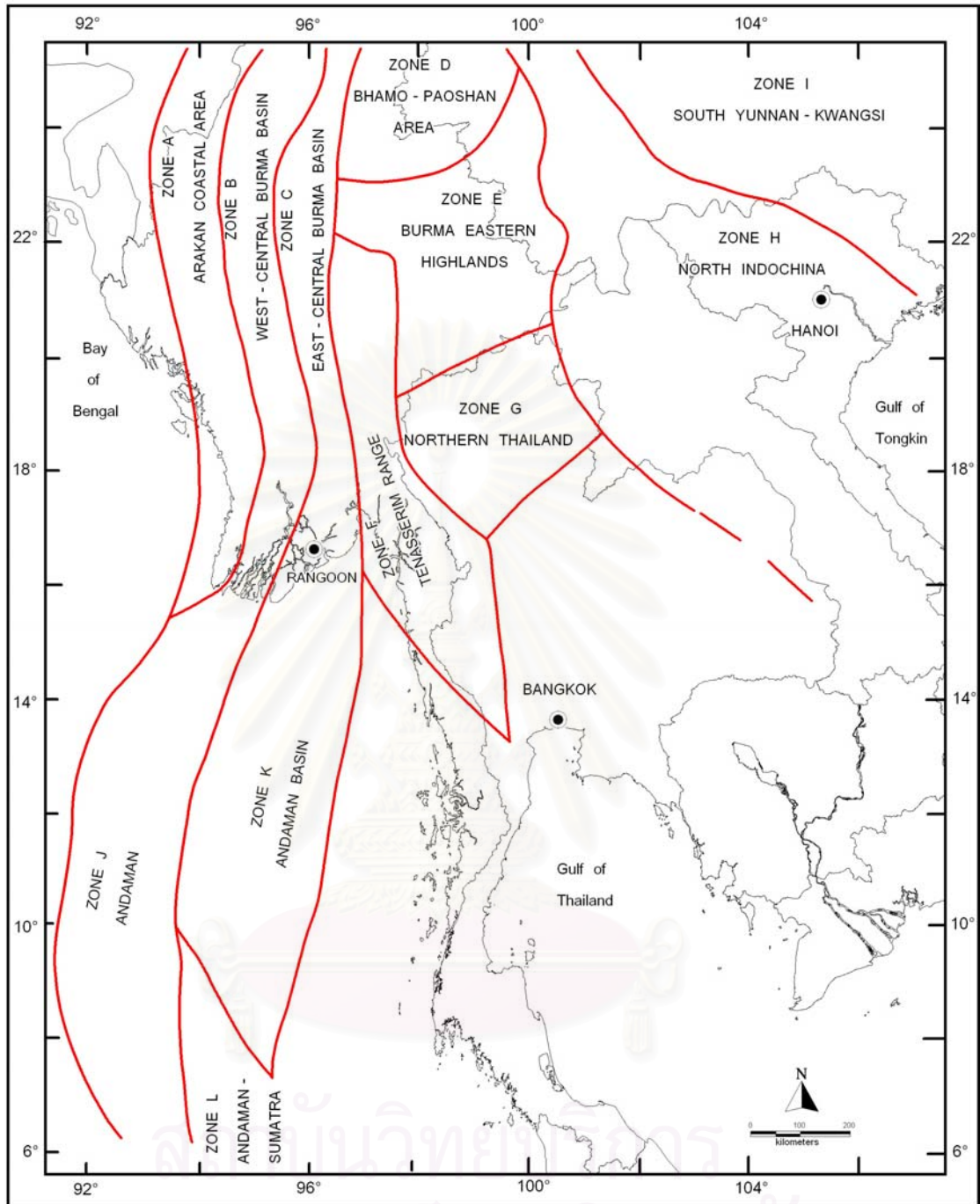


Figure 1.6 Seismic source zones of Burma, Thailand and Indochina (Modified after Nutalaya et al., 1985).

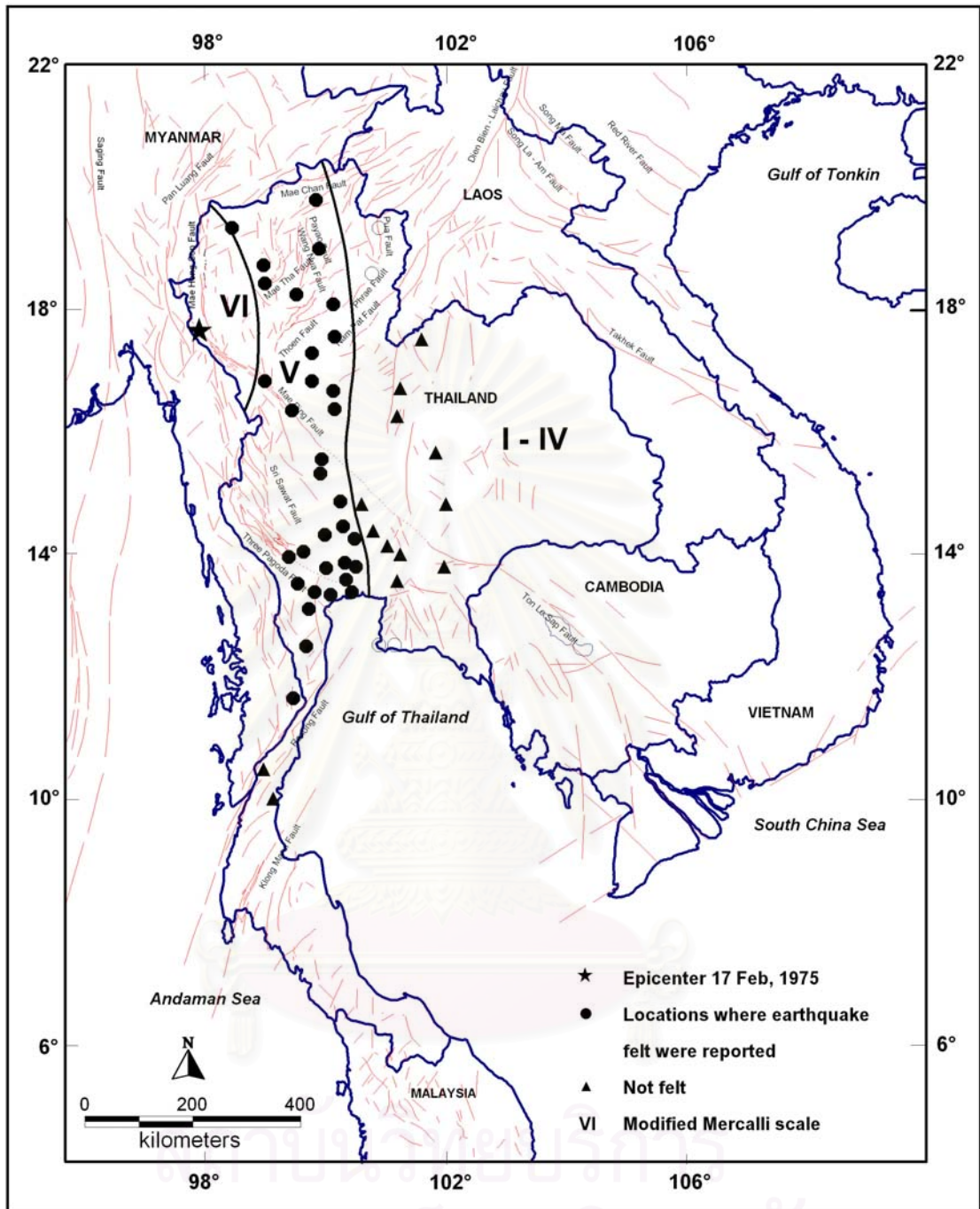


Figure 1.7 Intensity map of Tak earthquake of 17 February 1975 (Modified from Nutalaya et al., 1985).

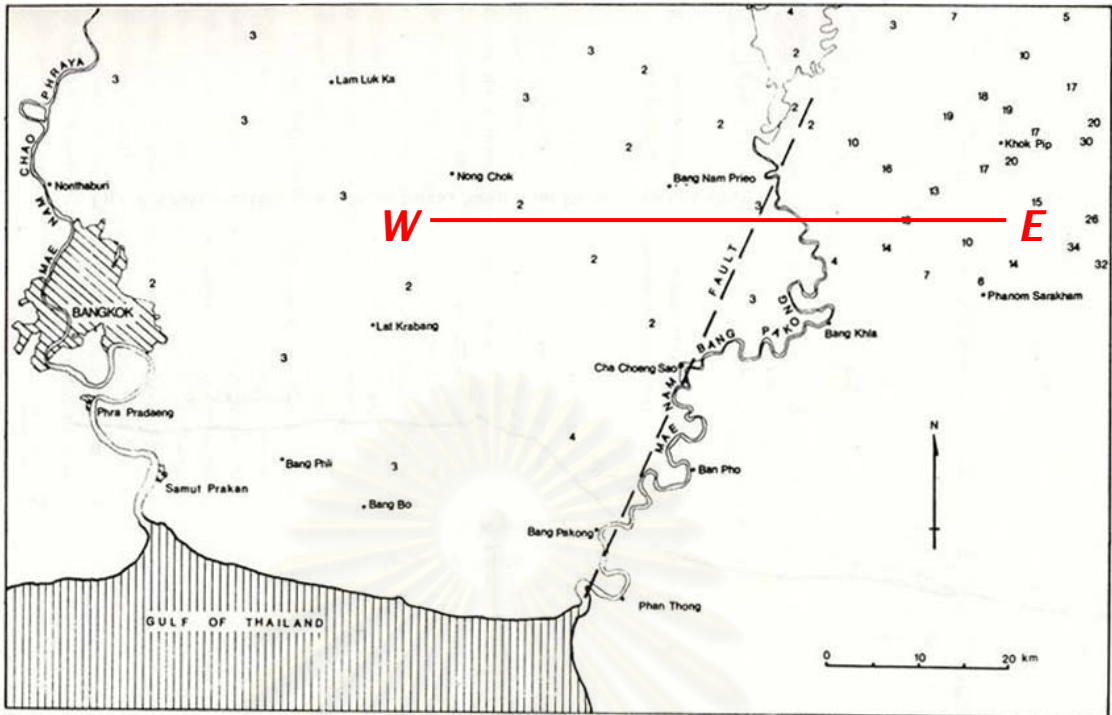


Figure 1.8 Map showing the elevations of the Lower Central Plain of Thailand generally 2 to 3 m above MSL and in the eastern margin of the plain, the elevation at Ban Khok Pib lies 17-18 m above MSL (After Thiramonkol, 1986).

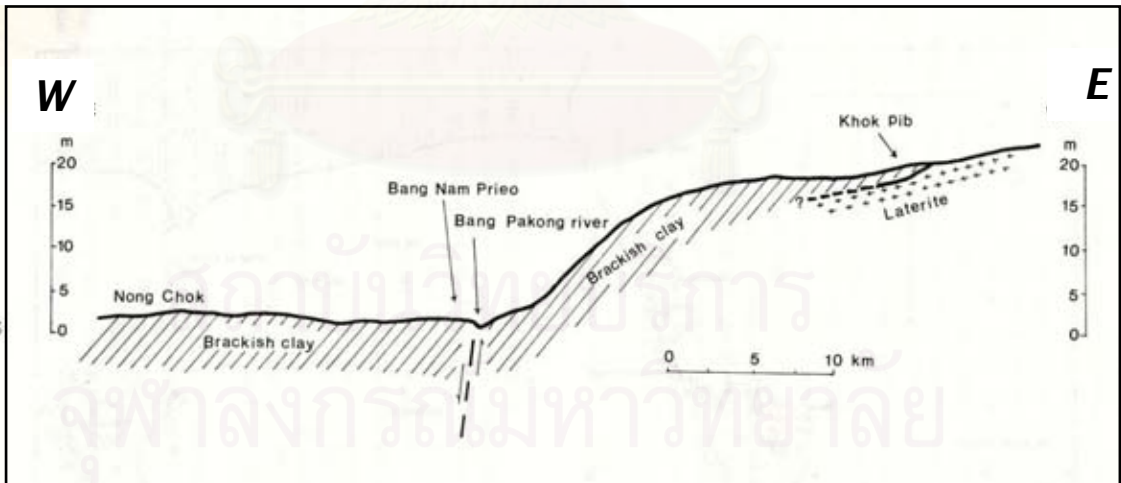


Figure 1.9 Cross-section along Nong Chok, Bang Nam Prieo and Khok Pib (After Thiramonkol, 1986).

Hinthong et al. (1992) studied on geology, earthquake, and mineral resources of the Nam Yuam River Basin project, Thailand. They considered that in the area there exist two major fault zones, namely, the NW–SE trending strike–slip Moei–Uthai–Thani fault zone or the so-called Moei–Lansang–Wang Chao Fault Zone (MLWF) and the N–S trending strike–slip Mae Saraing–Mae Hong Son fault zone (MMF). They stated that the results of Thermoluminescence dating associated with fault activities as 0.22, 0.21, 0.37, 0.16, 0.49, and 1.17 Ma on MLWF fault and 0.96, 4.81, 0.61 and 1.57 Ma with the MMF were examined. They also mentioned that the destructive earthquake with magnitude 5.6 occurring on February 17, 1975, closed to Ban Tha Song Yang, Changwat Tak was the instrument record.

Charusiri et al. (1994), based on enhanced Landsat 5 TM and SPOT images interpretation, indicated two major active faults including the north–trending Mae Hong Son and the northwest–trending Mae Ping Fault (MPF). They also noted that the MPF begins in eastern Myanmar to Thailand–Myanmar border, passes central Thailand and ends in Cambodia and southern Vietnam.

Sarapirome and Khundee (1994) investigated neotectonics in the Mae Hong Son–Khun Yuam valley using Landsat TM imageries and aerial photographs to interpret lineaments. The result had been analyzed together with statistic analysis of lineaments, epicentral distributions, hot spring locations, and Quaternary faulting data. The result of this study revealed that northwestern Thailand has been tectonically active from Late Paleozoic to Recent times.

Charusiri et al. (1996) applied several remote sensing techniques to study geological structures related to earthquakes in Thailand and neighboring countries. The results are useful in determining the seismic source zones to indicate the earthquake–prone areas. A new seismotectonic (or seismic–source) map is also proposed.

Hinthong (1995) divided active faults into four classes based on the degree of activeness as potentially active, historically and seismologically active, neotectonically active, and tentatively active. He regarded that the MPFZ is historically and seismologically active. Later, the study was referred by Woodward–Clyde Federal Services in 1996 (Figure 1.10).

Hinthong (1997) studied on the project “Study of Active Faults in Thailand”. According to various authors and researchers, three approaches to define active faults can be distinguished and applied. There are three definitions and characterized as general

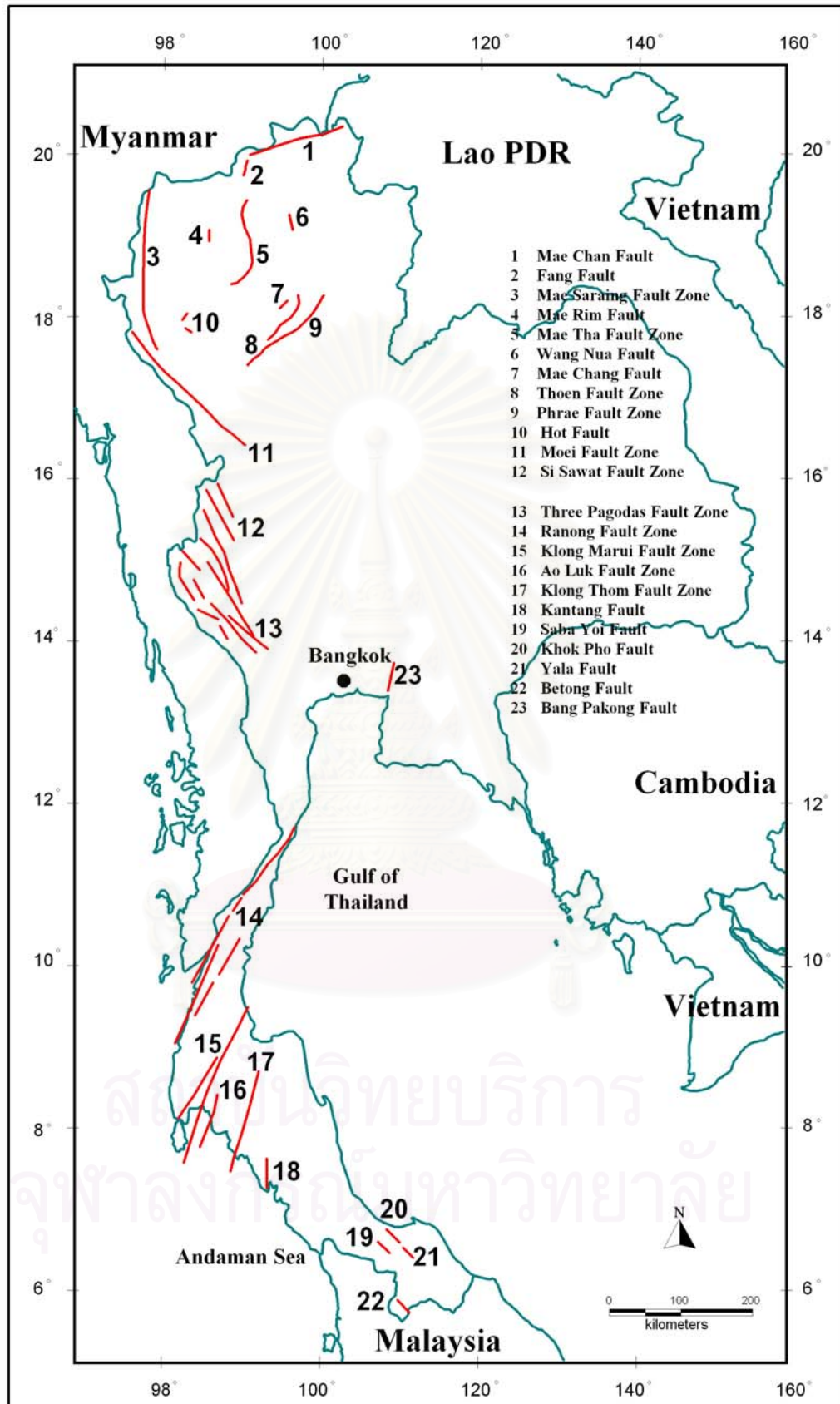


Figure 1.10 Active and suspected active faults in Thailand (Modified after Woodward-Clyde Federal Services, 1996).



definition, engineering definition, and regulatory definition. Those three applications of definitions were discussed, based primarily on its original definition which was proposed in the context of a two-fold classification of dead and alive or active faults, and with respect to their potential for future renewal or recurrence of displacement or offset. Based upon available data, and with the exclusion of the tentatively inactive and inactive classification, fault activity can be classified as three classes namely, active, potentially active, and tentatively active. Basically, there are three major criteria for recognition of active faults, namely, geologic, historic, and seismologic criteria. The study pointed out that the inventory of twenty-two preliminary active faults in Thailand, four classes have been proposed. They are potentially active (5 faults), historically and seismologically active (2 faults), neotectonically active (8 faults), and tentatively active (7 faults) (Figure 1.11).

Bott et al. (1997) mentioned that northern Thailand is similar to the Basin and Range province in the western United States of America in term of earthquake processes and tectonics. Lastly, Fenton et al., (2003) indicated their Late Cenozoic faults and historical seismicity within the northern Basin and Range seismotectonic province of Thailand as illustrated in Figure 1.12. The result based on focal mechanism revealed that northern Thailand has been formed by undergoing east-west extension.

Tulyatid (1997) used nationwide airborne geophysical data to interpret extensional tectonism in the Central Thailand based on geological structures and Cenozoic basins. The magnetic data help outline three NW-SE trending and NE-SW-trending major strike-slip fault zones of the Central Plain area. A new fault pattern (for the Chao Phraya Fault Zone) and a new fault path for the Three Pagoda Fault Zone were successfully delineated in his study using the magnetic data and its enhanced products. The data also outline the Uttaradit Fault Zone (UTFZ) by showing a shift of high magnetic bodies, indicating sinistral movement along the fault zone. The radiometric data, used in conjunction with river information, also helped in detecting the latest movement of the major NW-SE trending MPFZ as cut through the Kamphaengphet Fan, and providing a path way for the Mae Ping River to flow along to central plain of Thailand (Figure 1.13).

Saithong (1998) preliminarily studied geomorphology along the Mae Ping Fault nearby Tak township, and proposed 10 fault subsegments as potentially active fault, 12 sub-segments as tentatively active faults, following the work of Hinthong (1995).

Hongjaisee (1999) studied major faults and seismic hazard in northern Thailand. The characteristics of fault movement investigated using the morphology of fault, such as stream offsets, triangular facets, and canyon shapes, from which slip rates can be estimated.

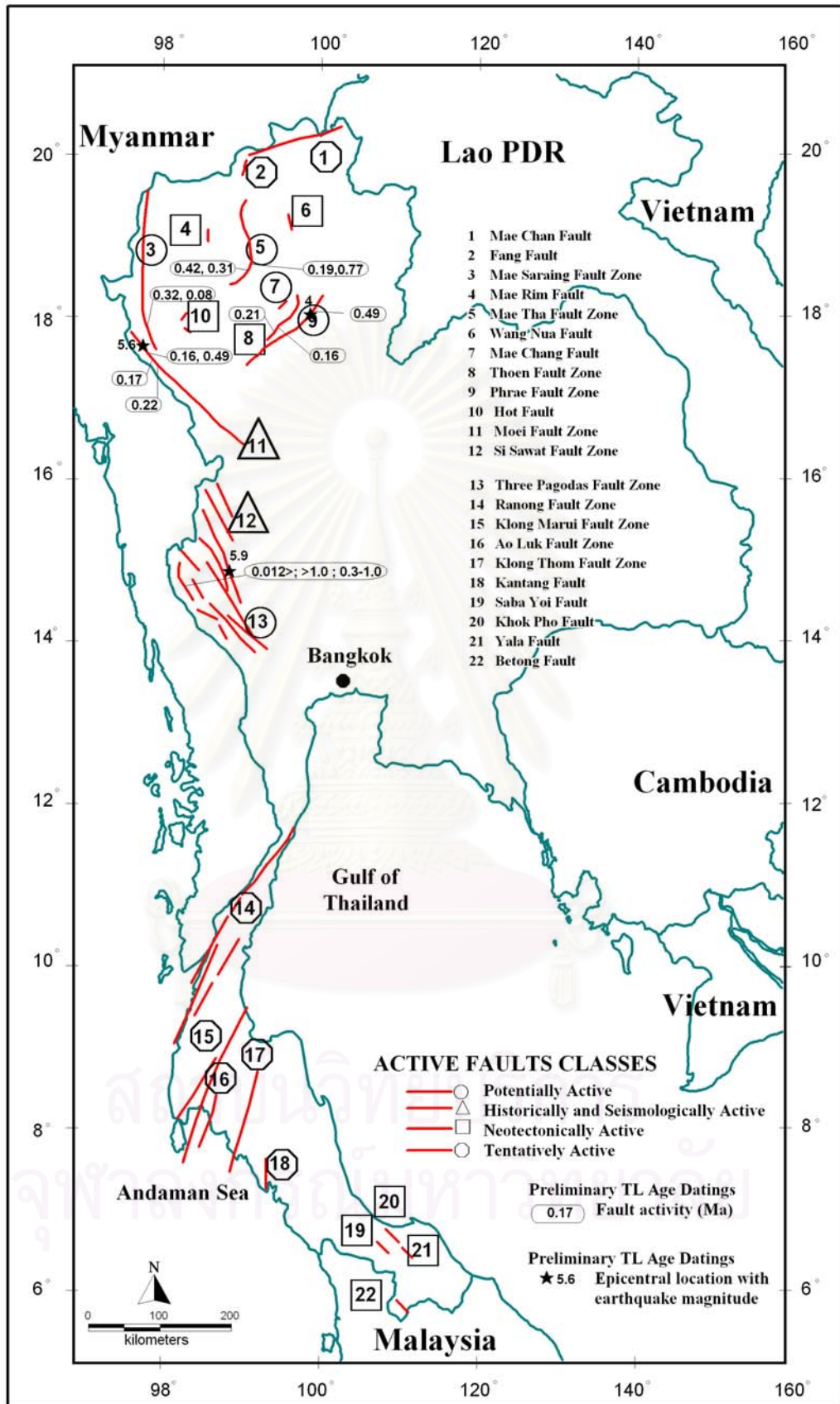


Figure 1.11 Active and suspected active faults in Thailand (Modified after Hinthong, 1997).

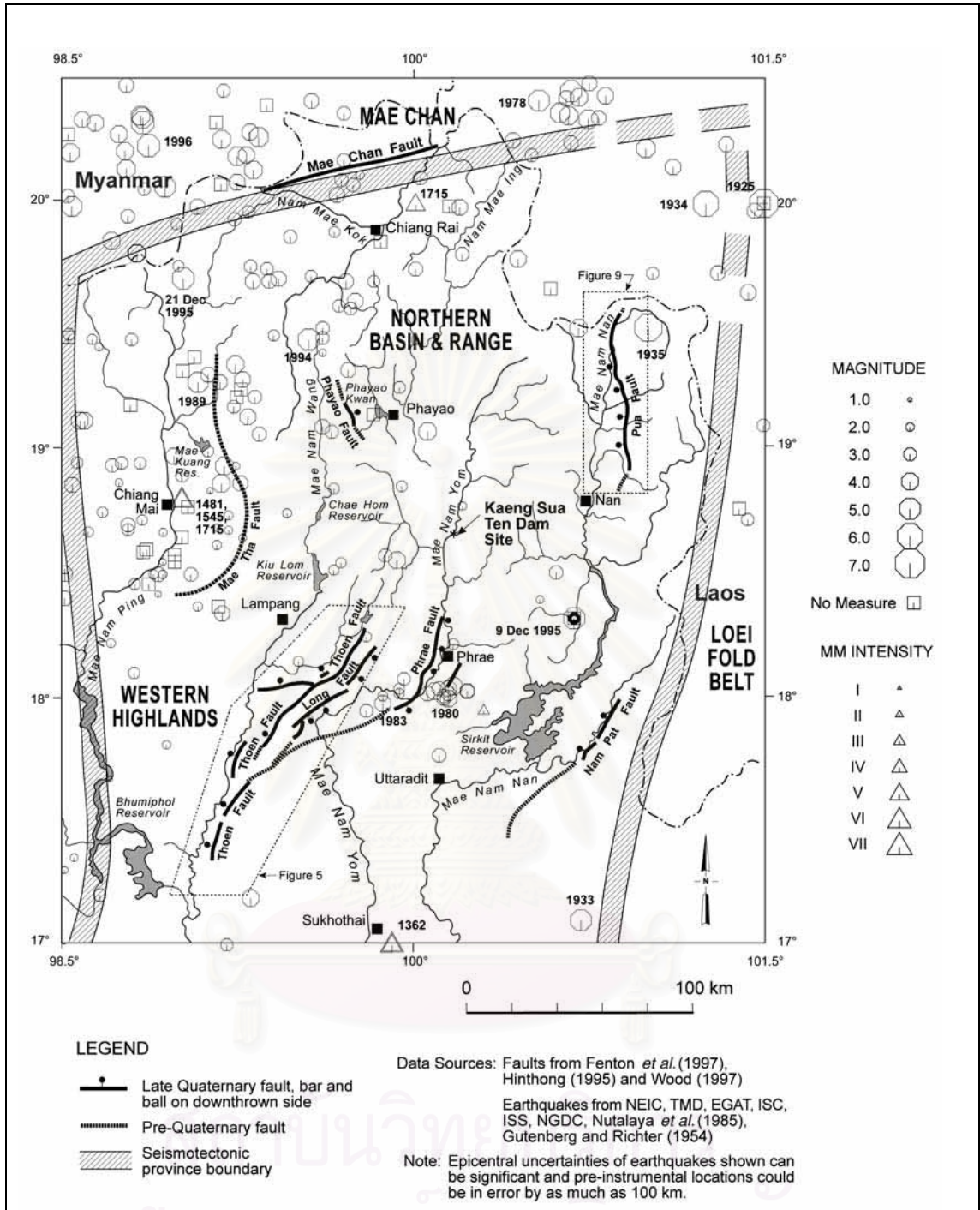


Figure 1.12 Late Cenozoic faults and historical seismicity (1362 to 1996) of the northern Basin and Range seismotectonic province (After Bott et al., 1997).

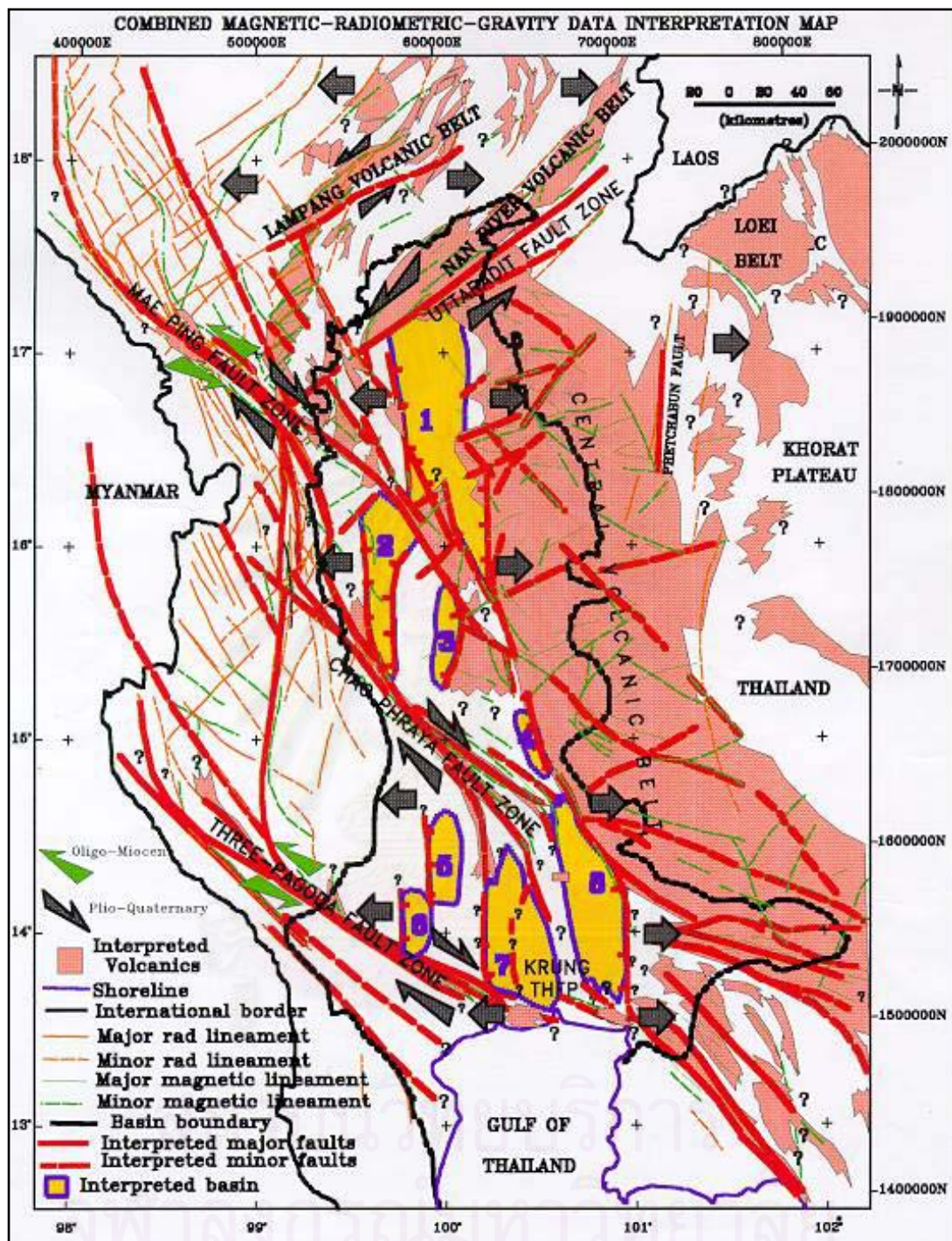


Figure 1.13 Combined magnetic- radiometric - gravity data interpretation showing structural map of Central Plain with magnetic and radiometric lineaments underlain. Note that 1 = Phitsanulok Basin, 2 = Nong Bua Basin, 3 = Nakhon Sawan Basin, 4 = Lop Buri Basin, 5 = Supanburi Basin, 6 = Kamphaeng Saen Basin, 7 = Thon Buri Basin, 8 = Ayuthaya Basin (After Tulyatid, 1997).

The high slip rates of the Mae Chan and the Wang Nua faults are 0.1–3.7 and 0.8–3.5 mm/yr, respectively. The Thoen and Phrae faults have the low slip rates, in the range of about 0.01–0.1 mm/yr.

Kosuwan et al. (1999) also applied remote-sensing, aerial photographs, field investigation, C-14, and TL-dating data to evaluate paleoseismology of the Mae Chan Fault in northern Thailand. The result concluded that fault movements gave rise to earthquake of about 92,000, 67,000, 48,000, 25,000 and 1,600 years of age. The 1,600 years ago event probably caused a characteristic earthquake with a magnitude greater than 7 Richter's scale (Figures 1.14 and 1.15).

Won-In (1999) showed neotectonic evidences along the Three Pagodas fault using remote-sensing and ground-truth surveys. The study revealed the Three Pagodas fault consisting of five segments based on geological and geomorphological analyses and indicating a main right lateral movement. Five events of earthquake faulting were reported based on geological evidence and dating results (Figure 1.16).

Charusiri et al. (2001) categorized the active faults in Thailand into five seismically active belts (SAB) using geologic, geotectonic, geochronological, and seismological criteria. These belts comprise Northern, Western-Northwestern, Central Peninsula, Southern Peninsula and Eastern-Northeastern SABs. The study area is inferred in the western-northern seismically active belt and hence the MPFZ is active based upon their study (Figure 1.17).

Rhodes et al. (2002) studied kinematics of the Mae Kuang Fault and evidences from satellite images and aerial photographs. The fault showed 30 km in length in northeast-trend between Chiang Mai basin and Wiang Pa Pao basin. They suggested that the Mae Kuang fault accommodates the transfer of extension between two basins. The fault is sinistral offset between 400 and 700 m and the rate of slip must be between 0.175 and 0.7 mm/yr, judging from the 3.5 km offset in 5 to 20 Ma (Figures 1.18 and 1.19).

Udchachon (2002) and Udchachon et al. (2005) studied the neotectonics of the Phrae basin based on remote-sensing interpretation, field investigation, seismic profiles, and focal mechanism data. He estimated that the southeastern segment of the Phrae fault system is a potentially active fault and maximum slip-rate of 0.06 mm/yr. This evidence is consistent with the study on contemporary stress axis orientation in this area which reveals a roughly east-west trend and north-south trend of extensional and compressional axes, respectively (Figure 1.20).

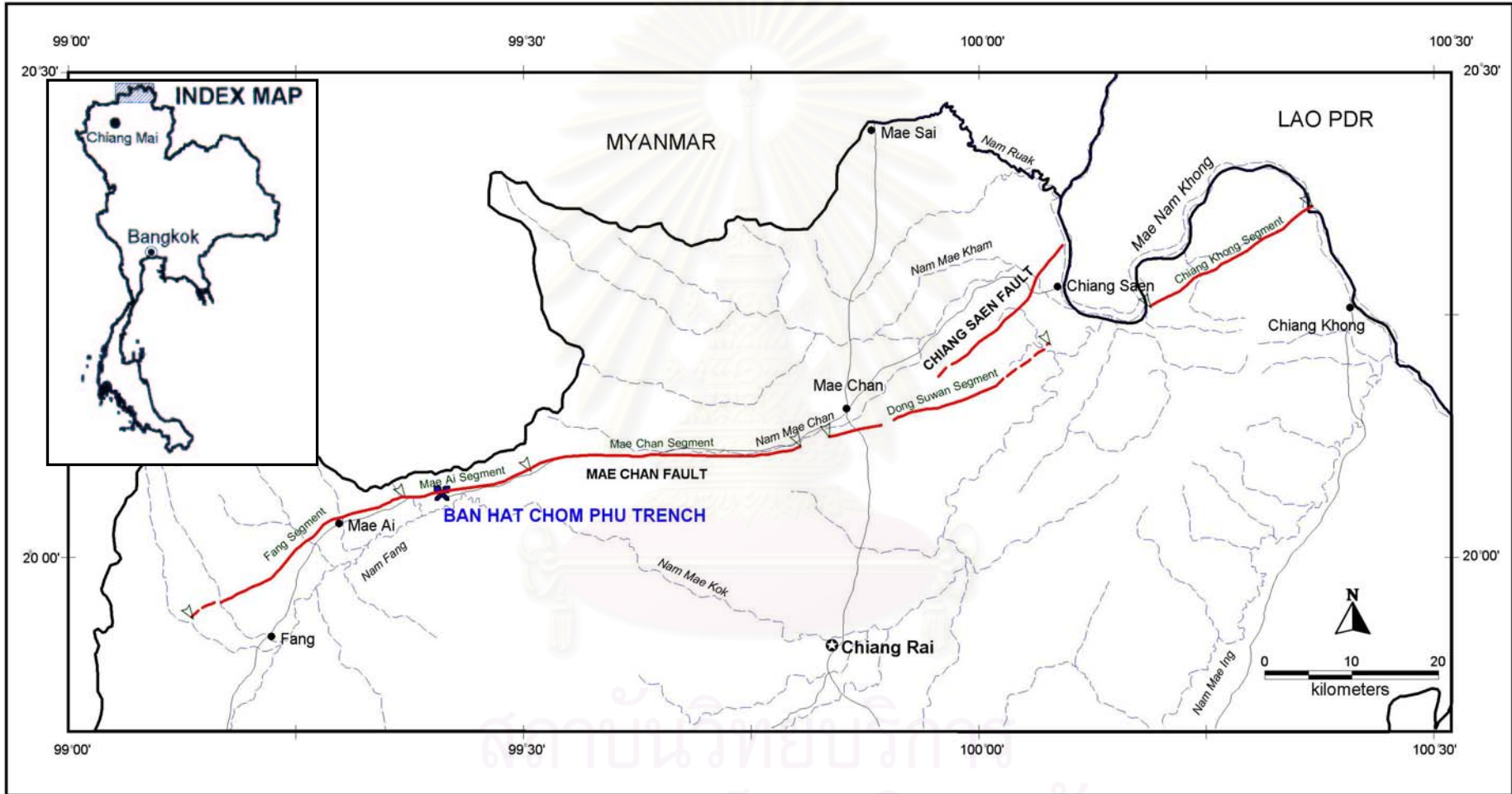


Figure 1.14 Location of Ban Hat Chom Phu trench site, southern part of Mae Ai segment of Mae Chan Fault, Chiang Mai, Northern Thailand (After Kosuwan et al.,1999).

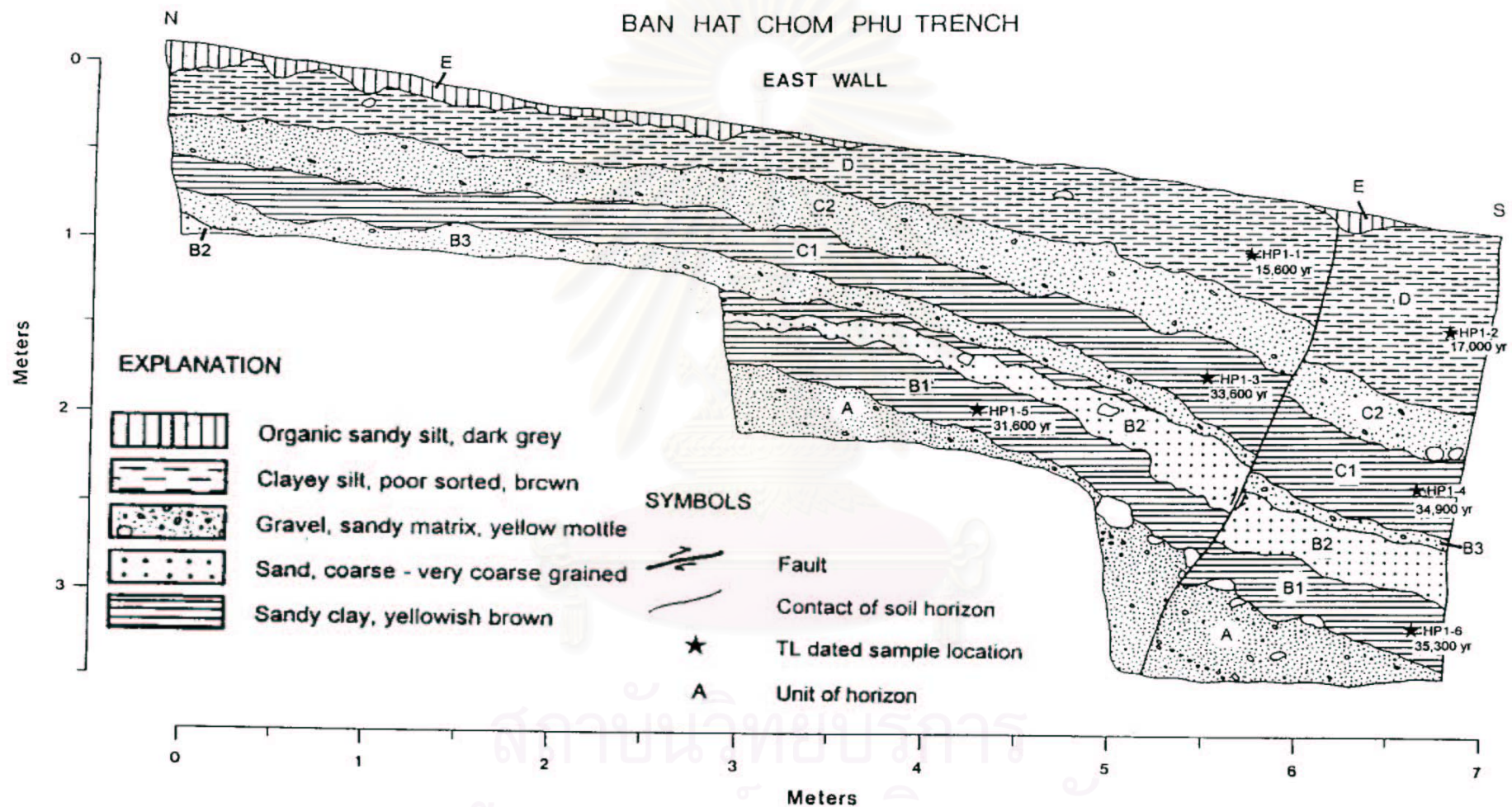


Figure 1.15 Trench stratigraphy of the east wall side of the Ban Hat Chom Phu trench showing reverse fault movement and locations of samples for TL dating and their dates (After Kosuwan et al., 1999).

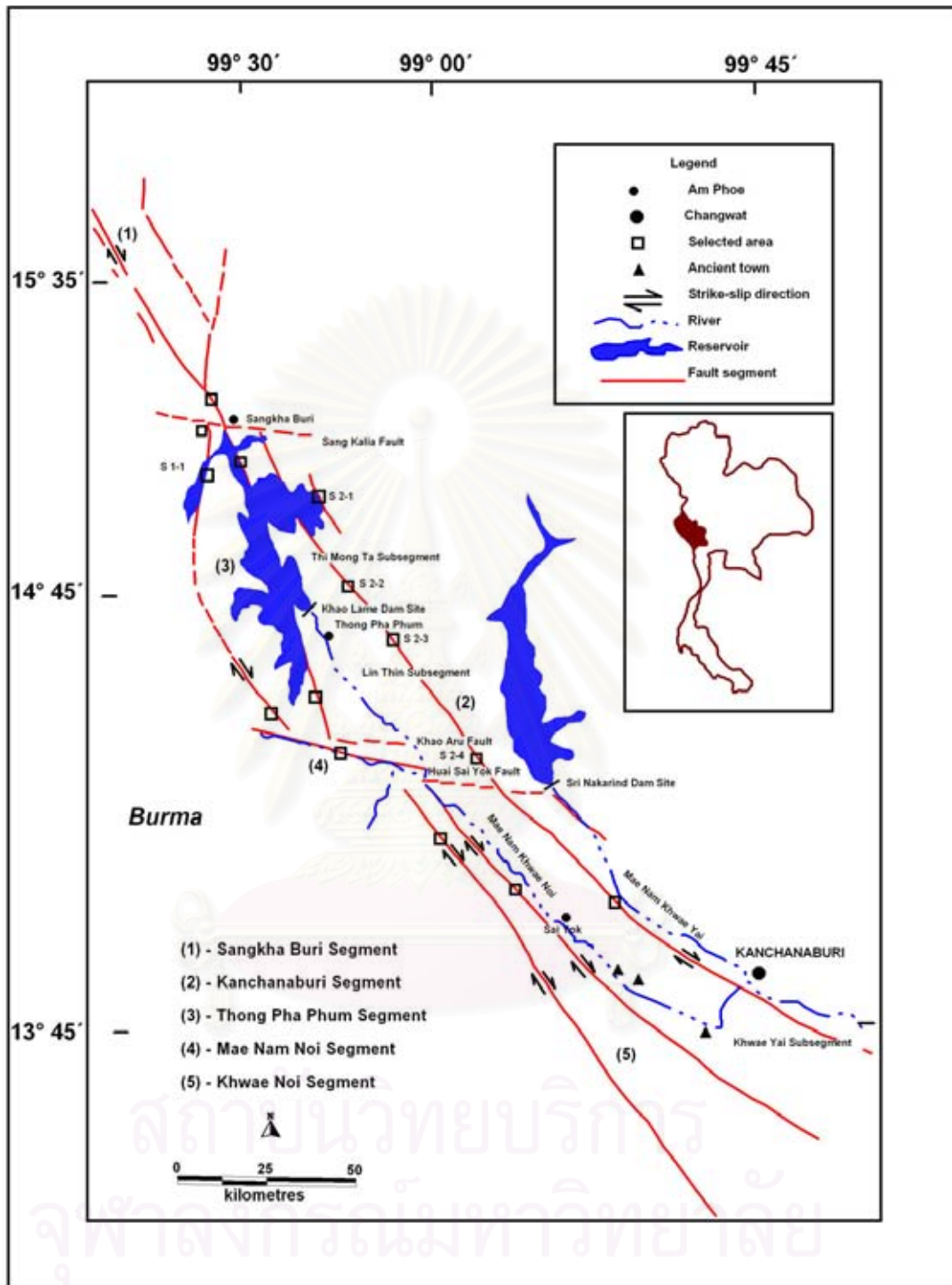


Figure 1.16 Map of the Three Pagodas Fault showing the fault segments (After Won-In, 1999).



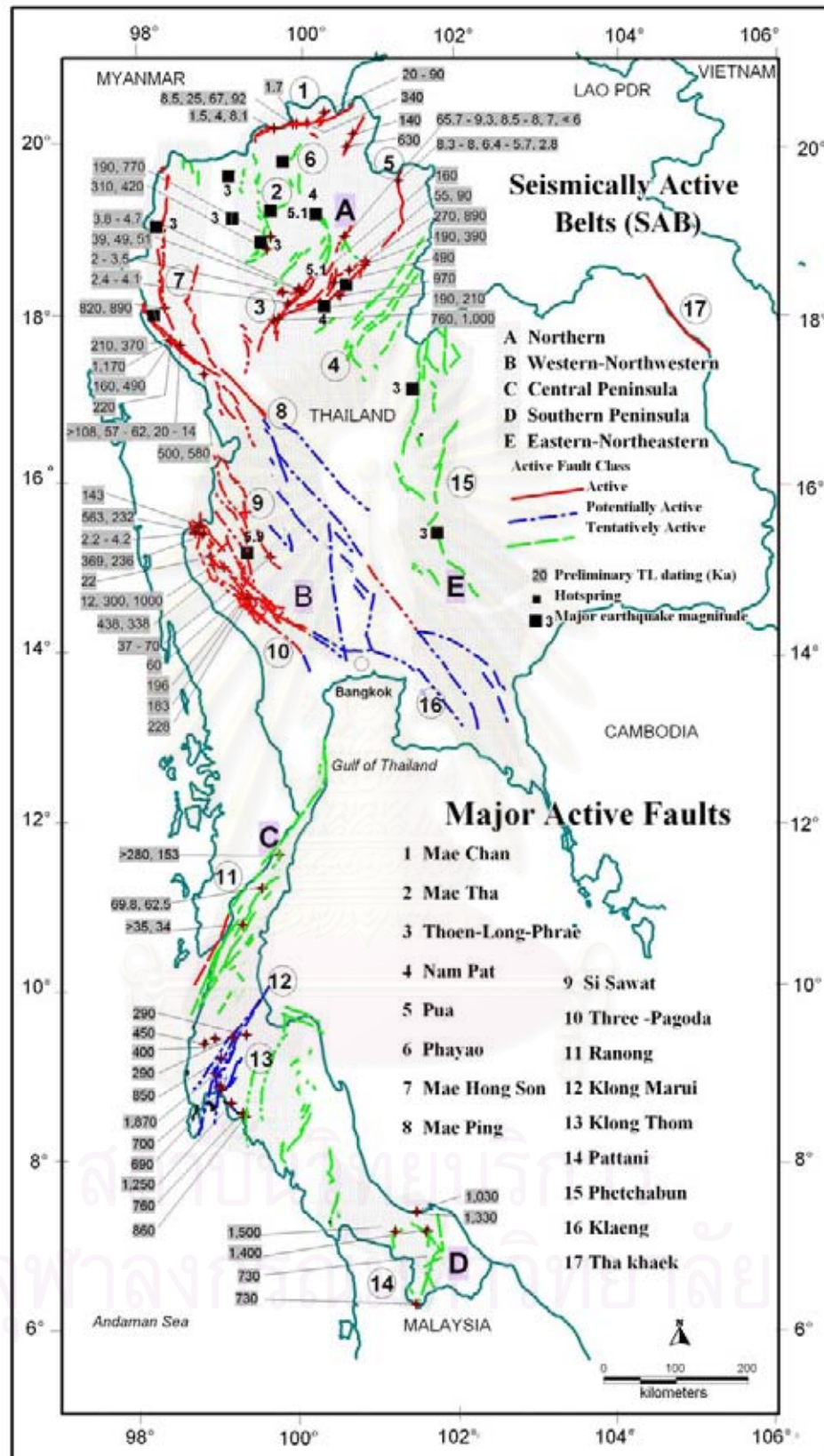


Figure 1.17 Major active faults in Thailand showing preliminary TL dating results on earthquake events, location of hot spring and epicenter distribution (After Charusiri et al., 2001).



Figure 1.18 Geologic map along the trace of the Mae Kuang fault. P, undifferentiated Permian rocks; Cmt, Mae Tha Formation; SD, Silurian and Devonian Rocks; Pzph, Paleozoic phyllite; Pzv, Paleozoic metabasalt; Mzg, granitic rocks of the Fang-Mae Suai batholith. (After Rhodes et al., 2002).

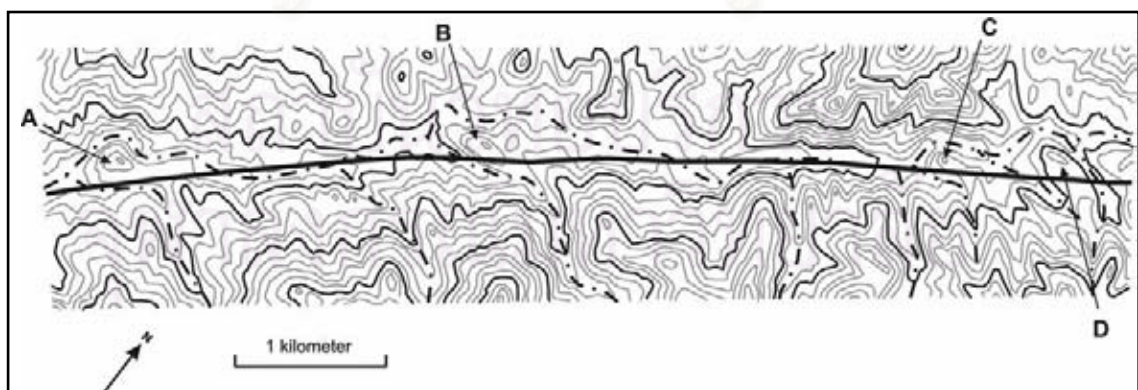


Figure 1.19 Topographic map of a portion of the Mae Kuang Valley, showing the mapped trace of the Mae Kuang Fault. A, B, and C point to shutter ridges that have diverted northwest-flowing tributaries (After Rhodes et al., 2002).

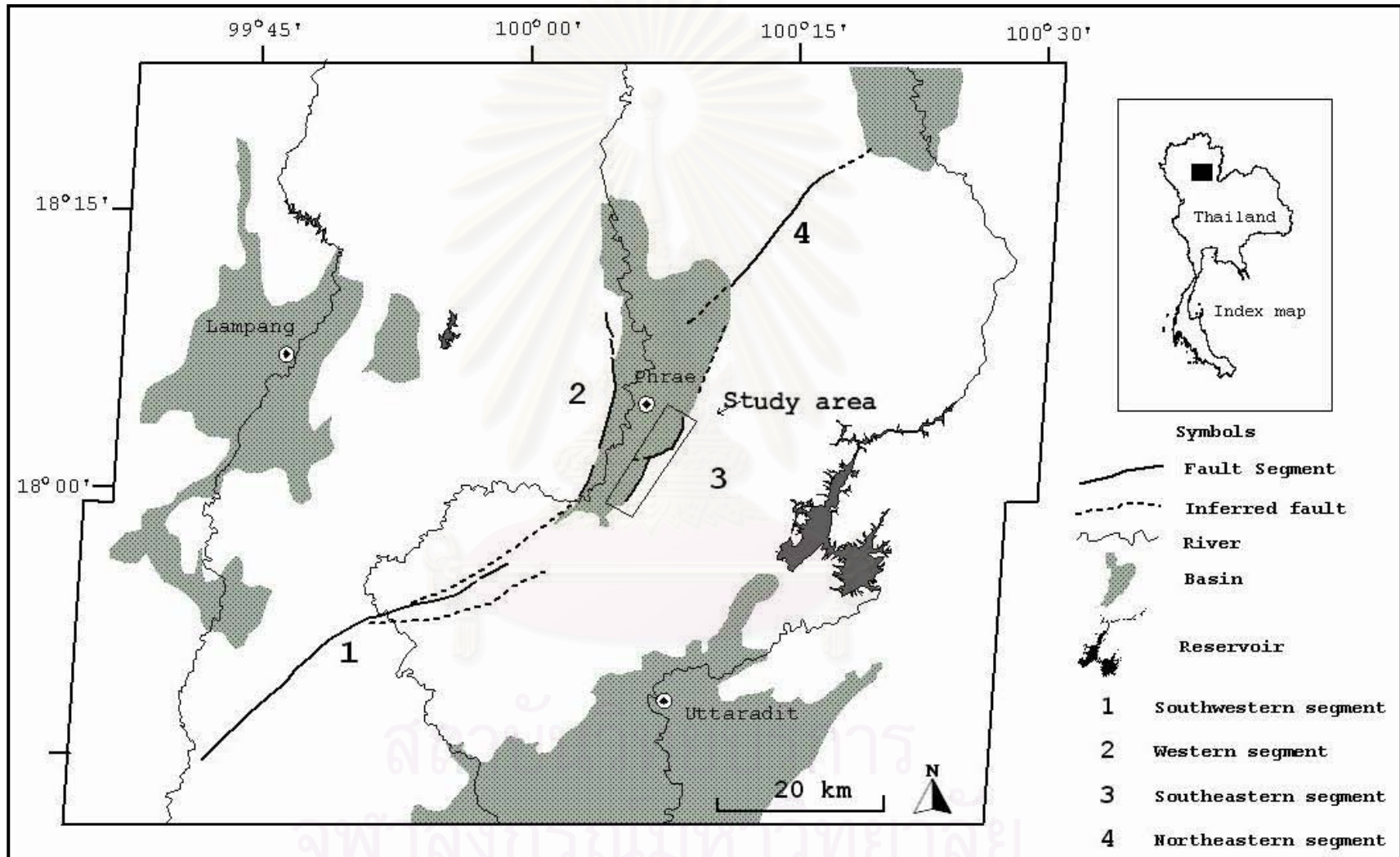


Figure 1.20 Fault segments of the Phrae fault system based on Landsat 5 TM image data (After Udchachon, 2002).

Nutthee (2002) and Nutthee et al. (2005) studied paleoearthquakes along the southern segment of the Sri Sawat fault. By means of remote-sensing interpretation, the appearances of sharp lineaments are well observed together with morphotectonic features. These indicated the oblique-right-lateral sense of movement. The slip-rate of movement is 0.68 mm/yr. and magnitude by using surface rupture length is 6.3 Mw (Figure 1.21).

Fenton et al. (2003) conducted recent paleoseismic investigations. They could identify a number of active faults in Northern and Western Thailand. They found out that the Mae Chan fault and the Three Pagodas fault zones are strike slip faults, with slip-rates between 0.1–0.3 mm/yr and damage earthquake of  $M=7.5$ . In the northern Thailand, six major faults showing sense of movement as slip-rates between 0.5–2.0 mm/yr in normal dip-slip, and damage earthquake about  $M=7.0$  on the Richter scale. Results of modification of the seismotectonic zone of Nutalaya et al. (1985) which were referred by Woodward-Clyde Federal Services in 1996 are shown in Figure 1.22.

Charusiri et al. (2004) performed a preliminary study on the active fault in the Salaween Project (usually, the “Salaween River” is spelled as “Salween River”). According to them, they suggested that based on the results of enhanced Landsat 7 ETM image and aerial photographic interpretation, the morphometric analysis, the epicentral distribution, and the present field investigation, linear structures in the study region can be grouped into thirteen fault zones. There are seven fault zones observed in Thailand side, namely, the Mae Hong Son Fault, the Ban Nam Peang Din Fault, the Khun Yuam Fault, the Mae Sariang Fault, the Mae Nam Ngao Fault, the Ban Tha Ta Fang Fault, and the Moei Fault. In Myanmar, there are six fault zones, including the Shan Boundary Fault, the Sagiang Fault, the Tounggyi Fault, the Pan Laung Fault, the Mawchi Fault, and the Papun Fault (Figure 1.23).

At present, no detailed studies on morphotectonics have been performed in the currently study area. However, a few researches have been reported, more or less concerned with geological structures and the seismology of the Tak region. Henceforward, the purpose of the research is to clarify paleoearthquakes along the MPFZ by enhance satellite-image and remote sensing interpretation, especially Radarsat and Landsat 5 TM. Recent knowledges and techniques of paleoseismology are used for investigating the interesting faults and their paleoearthquakes.

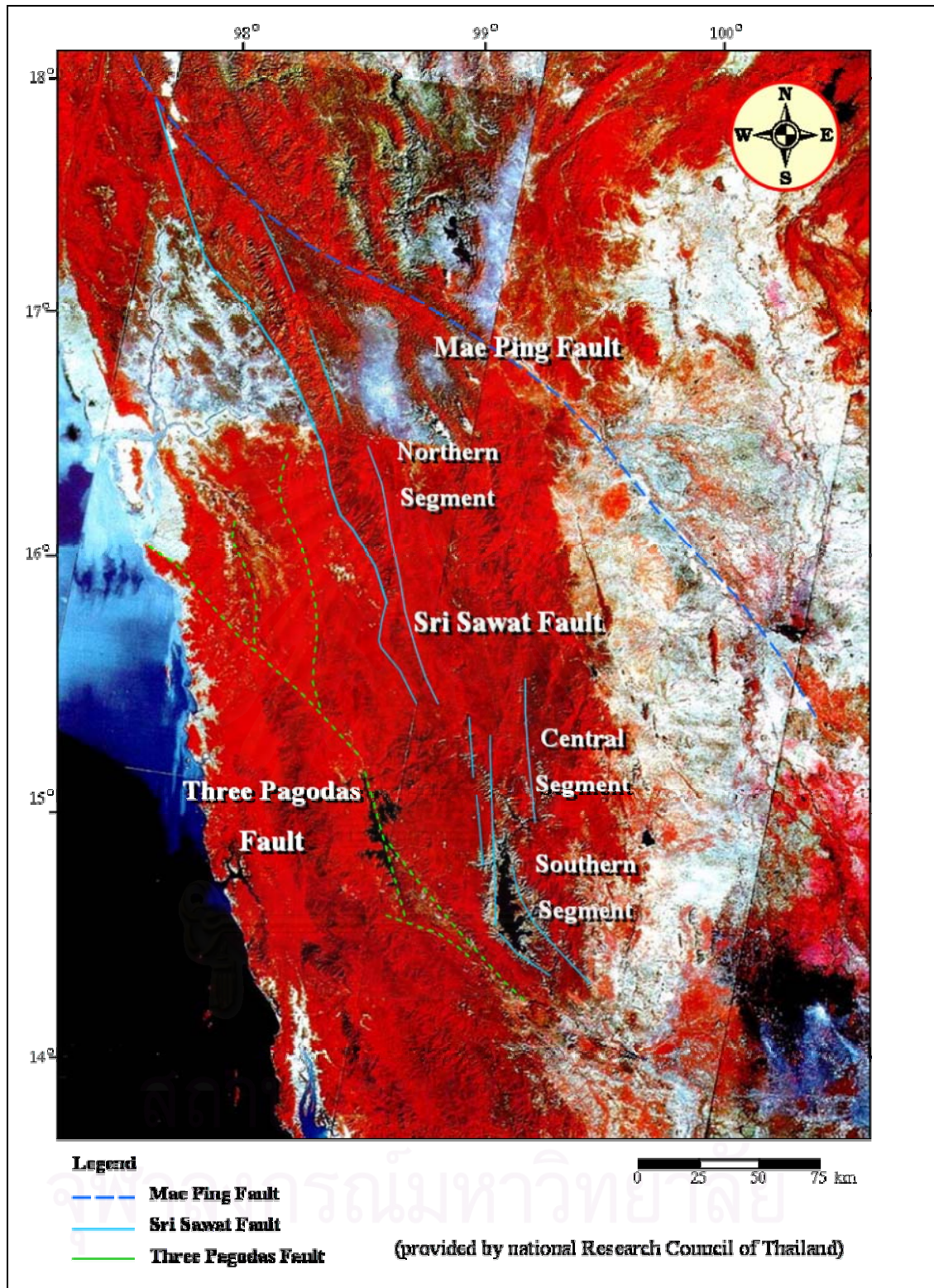


Figure 1.21 Landsat 5 TM satellite image showing orientation of three major faults, the Mae Ping Fault, the Sri Sawat Fault, and the Three Pagodas Fault. The Sri Sawat faults are separated into three segments, namely, northern, central, and southern segments (Nutthee, 2002).

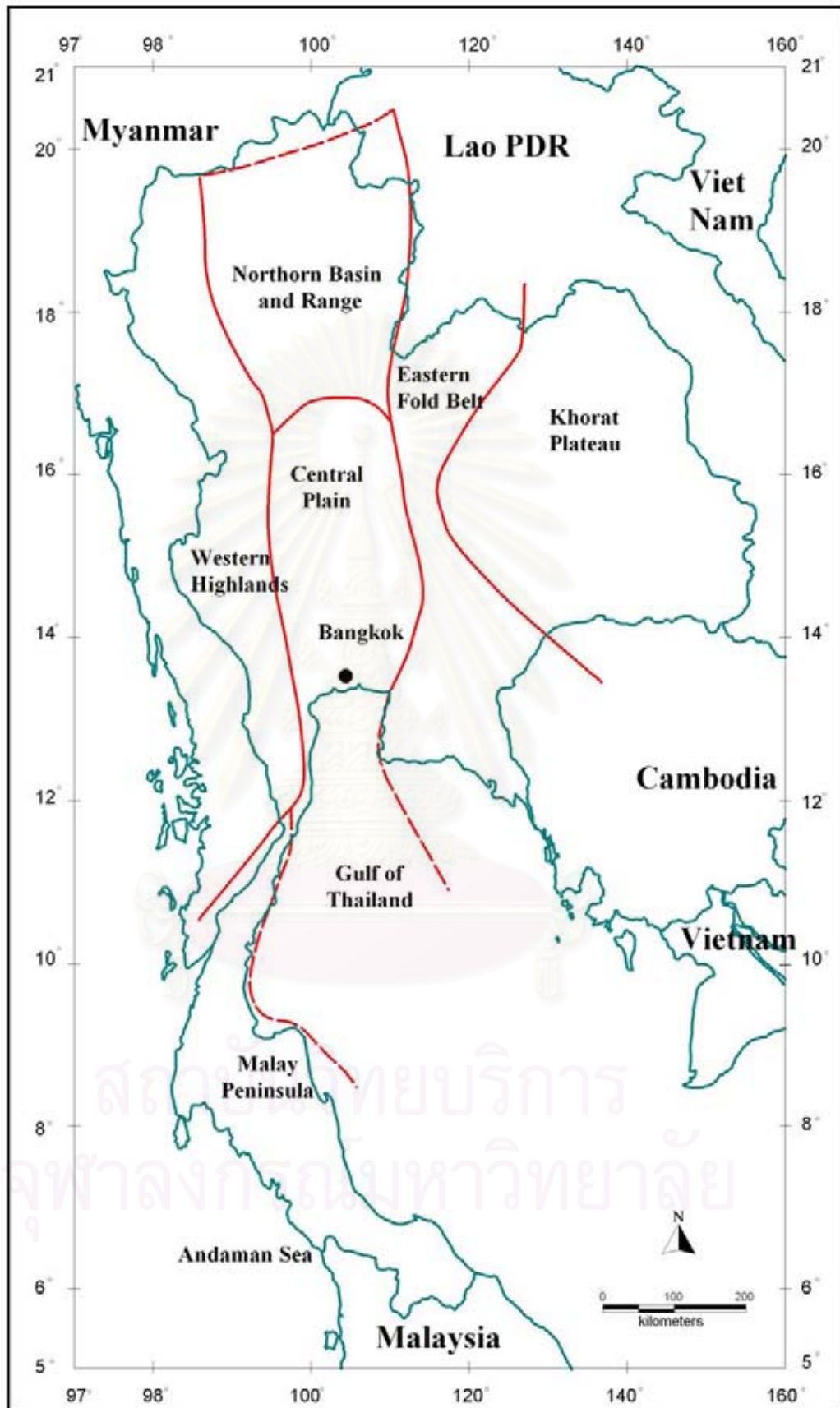


Figure 1.22 Seismotectonic provinces in Thailand (Modified after Woodward-Clyde Federal Services, 1996).

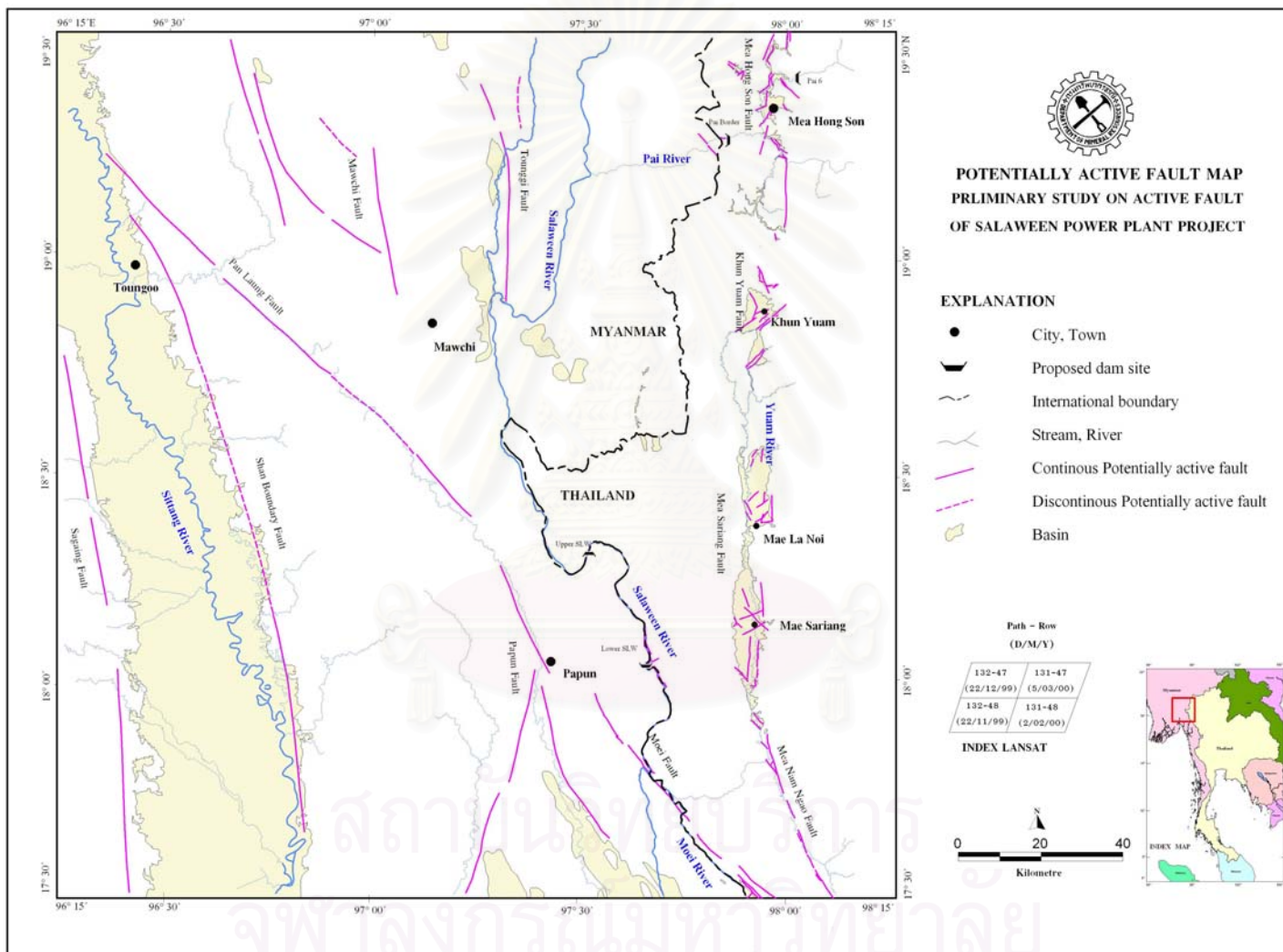


Figure 1.23 Potentially active fault map of the area covering the Salaween Power Plant Project (After Charusiri et al., 2004).

## CHAPTER II

### LITERATURE REVIEWS

#### 2.1 Plate Tectonics

The theory of plate tectonics proposes that the Earth's crust is broken up into eight major and about twenty smaller tectonic plates that move over the surface of the Earth (Figure 2.1). These tectonic plates are massive, irregularly shaped slabs of solid rocks. The smaller plates are only a few hundred km in diameter, while the major plates are thousands of km in diameter. Plate thickness is also highly variable, ranging from less than 15 km at the oceanic ridges to over 200 km beneath the Himalayan Mountains. With the exception of the dominantly oceanic Pacific Plate and some of the smaller plates, these plates consist of both oceanic and continental crust and upper mantle material. For example, the North American plate consists of the North American continental mass and the oceanic crust extending out from the eastern edge of the North American continent to the spreading ridge of the Mid-Atlantic ocean ridge.

Plate tectonics is the study of the structure of the Earth, and how the Earth's surface changes according to the movement of tectonic plates. Plate tectonics is responsible for the formation of the most spectacular natural features on Earth, such as mountain belts, volcanoes, rift valleys, hot springs, and mid-ocean ridges.

Earth is made of three compositional layers, the crust, mantle, and core. The latter of these is broken into two parts, the outer and inner cores (Figure 2.2).

The core has two layers: the inner core and the outer core. The inner core is a sphere composed mainly of iron and nickel—this is the densest of all the layers part of the Earth. Although the inner core is extremely hot (around 6,650°C), the huge pressures in the centre of the Earth mean that the inner core is solid. The inner core is surrounded by the outer one. The outer core has the same composition as the inner core does, but it exists as a liquid instead of a solid due to slightly lower pressure. Temperatures in the inner core are estimated to be around 4,700°C. Heat within the core is thought to be generated by decay of radioactive isotopes. It is this heat which generates convection currents on the mantle and drives plate tectonics.



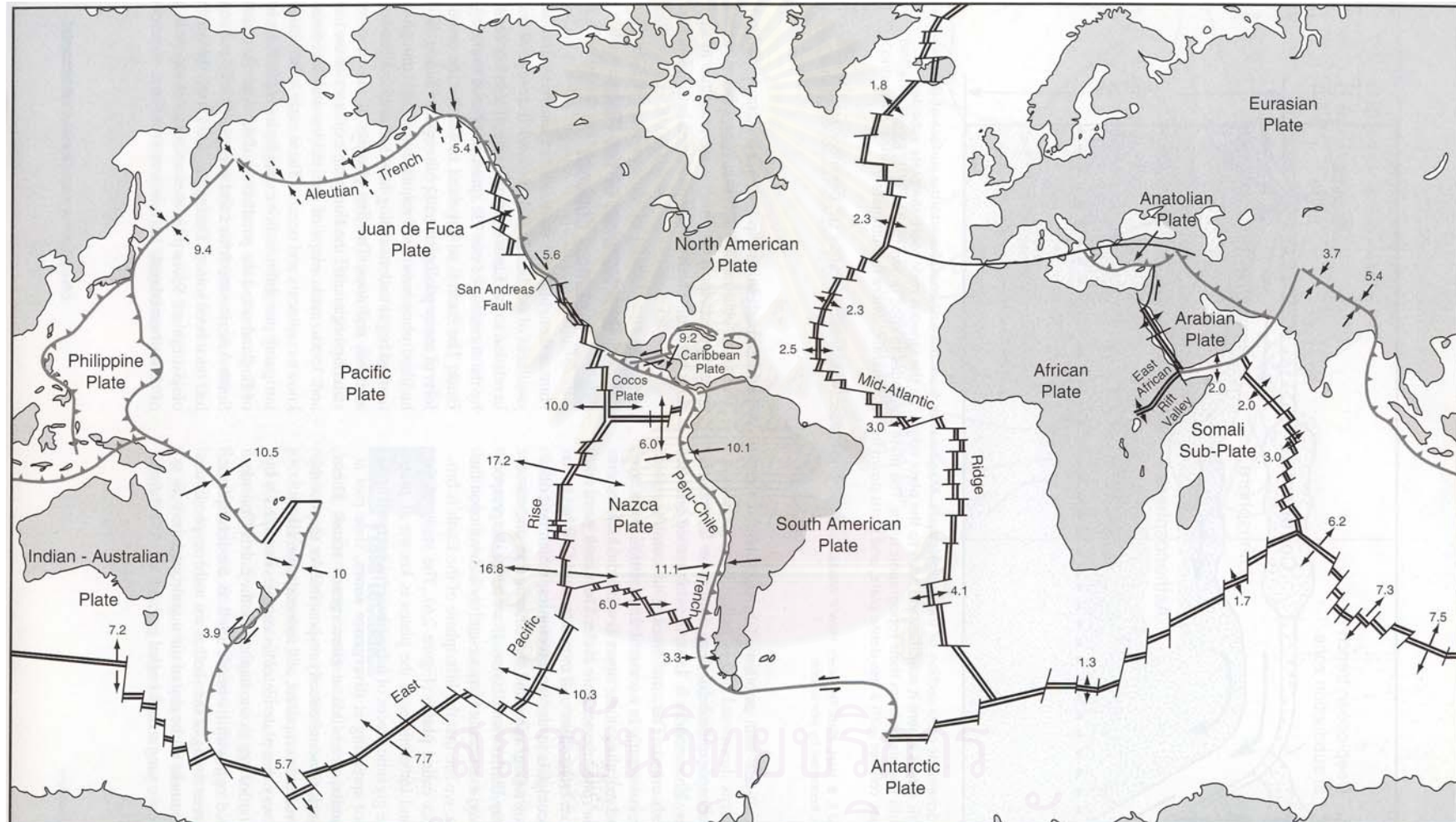


Figure 2.1 Map of the major tectonic plates with arrows showing directions of movement .Amounts of movement are shown in centimeters per year (After Abbott, 2004).

Surrounding the core lies a layer known as the mantle. The mantle is composed of dense, rocky material which ranges from being virtually solid near the lower boundary with the core, to more squiggly towards the boundary with the overlying layer, the crust. Mantle material is less dense than is the core, but still denser than the outer layers of the earth is.

The uppermost part of the mantle, up to about 100 km below the surface of the Earth, is known as the asthenosphere (Figure 2.3). This part of the mantle is much weaker and more flexible than is deeper parts of the mantle, but it is thought to have the same composition. The differences are controlled by temperature and pressure.

The outermost layer of the Earth is the lithosphere. This layer makes up the topmost 100 km of the Earth, and includes the very upper part of the mantle, and all the whole of the crust. The lithosphere, meaning sphere of rock, is much more rigid than the underlying asthenosphere, rather like a thick crust on a loaf of fresh bread, or ice on the surface of a lake.

On the very outside of the Earth is the crust. The crust is not a continuous layer, but is made up of a number of solid, curved tectonic plates. It is also known as lithospheric plates which fit together like pieces of a jigsaw. There are two types of crust: continental crust and oceanic crust. The differences between the continental crust and the oceanic crust are numerous, but in broad terms they have different compositions and thickness.

The Plate Tectonic Theory refers to the slow movement of plates (~cm/year as fast as hair grows), and large coterminous segments of continent and ocean around the surface of the Earth (Figure 2.4). There are three types of plate boundaries: divergent, convergent, and transform.

Divergent boundaries occur where two plates move away from one another. To avoid opening a gap, the mantle up wells and forms the new plate, thus transferring rock from deep in the mantle to the crust and uppermost mantle. These boundaries are almost always underwater since the new plate created is oceanic. Earthquakes are common here, and volcanism is also abundant (Figure 2.5). For example, divergent boundaries are seen in the Mid Atlantic ridge, Iceland, Gulf of California, and East African Rift.

Convergent boundaries occur where plates move toward one another. To avoid overlapping the plates on the surface, one plate must dive below the other into deep mantle. This occurs at subduction zones such as the ones rimming the Pacific Ocean. Here rocks of the upper mantle and crust are returned to the deep mantle. This is also the site of much volcanism and many earthquakes. Where continental land masses collide, mountains are

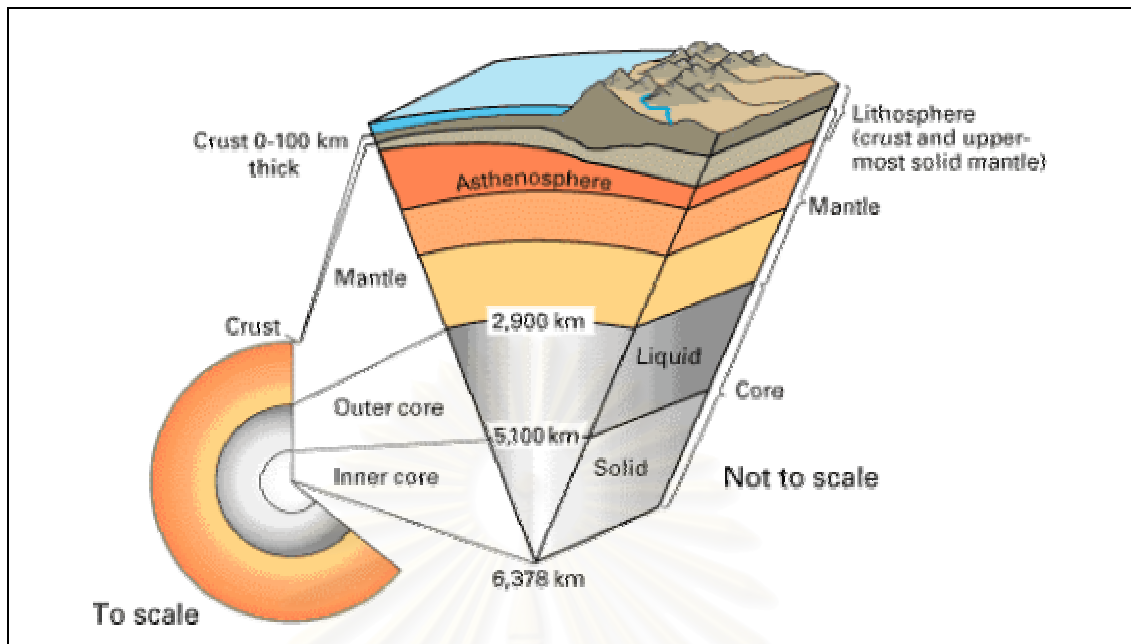


Figure 2.2 Model of the earth's interior. Summary of the physical model of the earth's crust. Left, representation of major subdivisions of the earth's interior. Right, the variation of seismic wave (P and S) velocity plotted against depth (After <http://dept.kent.edu/geology/ehlab/tectonics/tectonics.htm>).

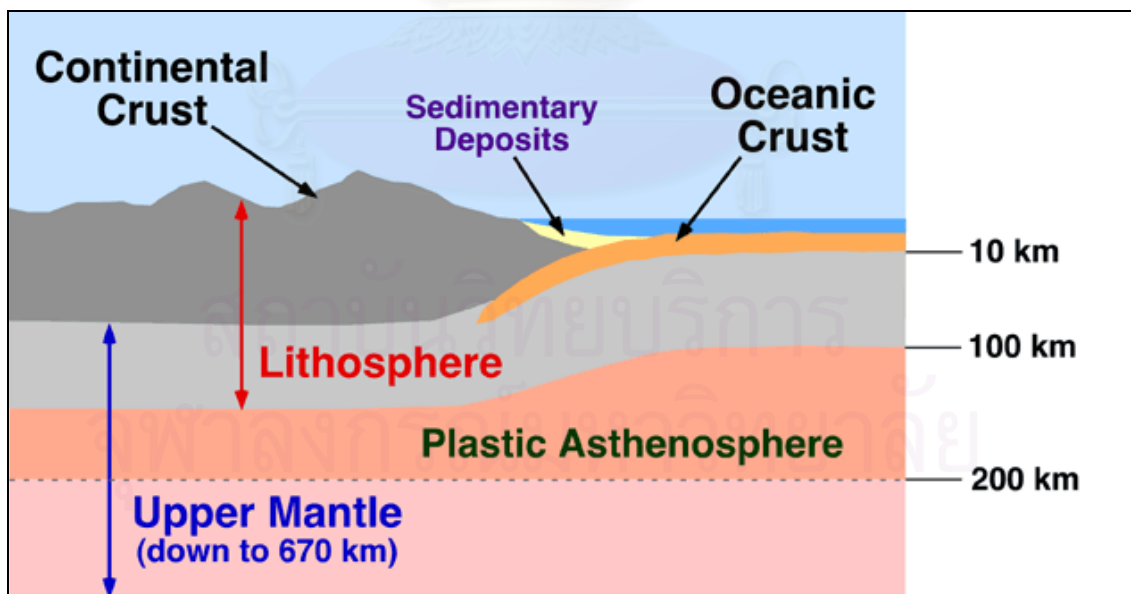


Figure 2.3 The outermost layer of the Earth is the lithosphere. This layer makes up the topmost 100 km of the Earth, and includes the very upper part of the mantle and all the whole of the crust (After <http://www.physicalgeography.net/fundamentals/images/lithosphere.gif>).

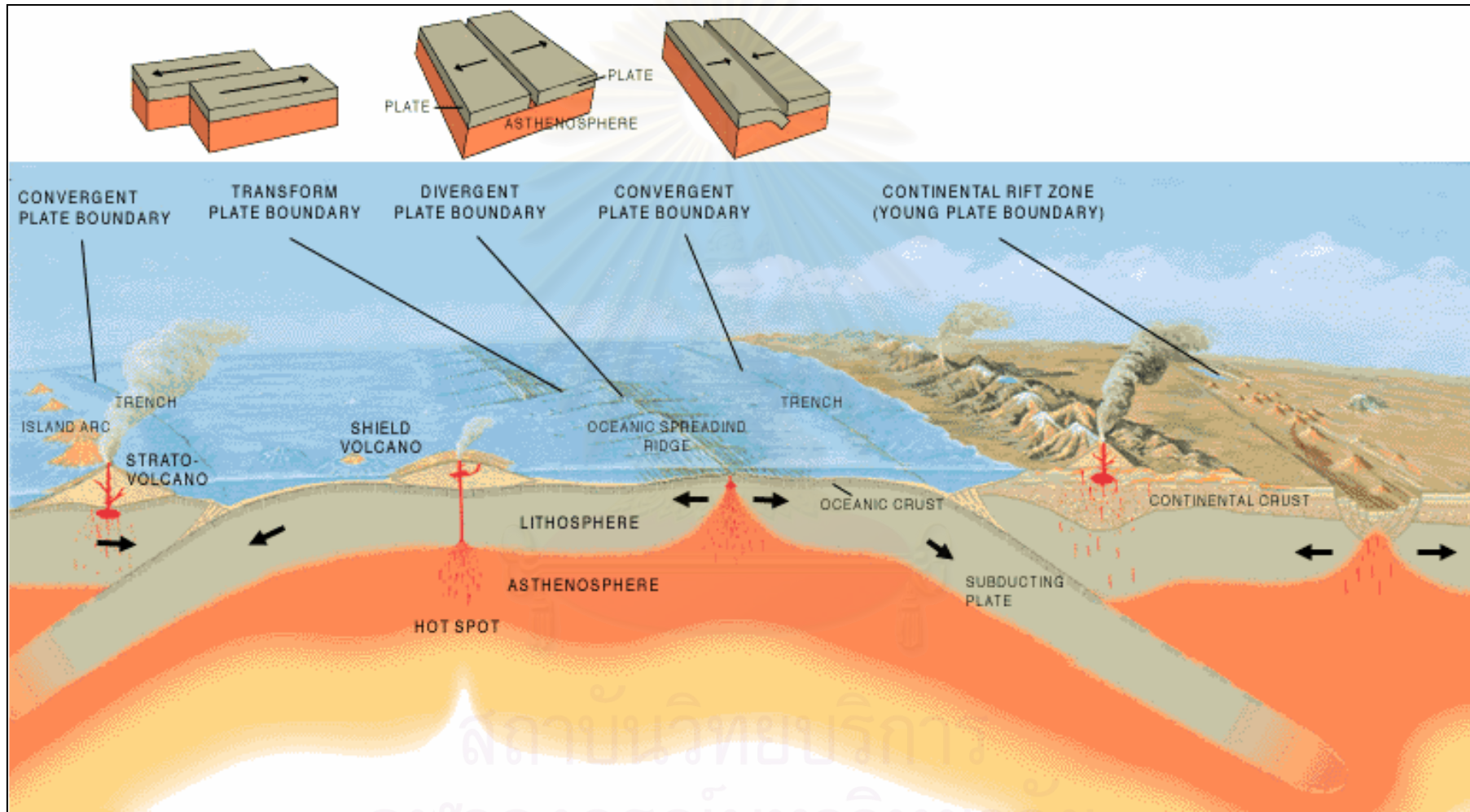


Figure 2.4 An idealized cross-section illustrating the relationship between the lithosphere and the underlying asthenosphere and the three principal types of plate boundaries (After <http://dept.kent.edu/geology/ehlab/tectonics/tectonics.htm>).

uplifted (Figure 2.6). These boundaries are seen within, for example, Pacific Northwest (Cascadia), Alaska/Aleutians, Japan, and Mexico.

Transform boundaries occur between plates that are sliding past one another, neither converging nor diverging. The San Andreas is a prime example (Figure 2.7). Here the North American and Pacific plates are in contact. The Pacific is moving NNW with respect to North America, parallel to the boundary among them. No plate is produced here, nor is any plate destroyed. For instance, those of San Andreas, Dead Sea, and Turkey

## 2.2 Geological Evolution during Cenozoic in the Sunda Shelf and Northern Thailand

Tertiary deformation of the South East Asia (SE Asia) has been accepted as the result of the collision of the Indian against Eurasian plates and mentioned by many researchers (Tapponnier et al., 1982, 1986; Daly et al., 1991; Dewey et al., 1989; Rangin et al., 1990; Lee and Lawver, 1995; Hall, 1996; Packham, 1996; and Matthews et al., 1997). The propagation extrusion model (Tapponnier et al., 1982) that has a free boundary to the south and east is widely accepted by many workers (Figure 2.8). However, there are other plate margins to be considered.

The experiments with plasticine of Tapponnier et al., (1982) are shown in Figure 2.9. They indicated many similarities between the results of their experiments and those of the geology of the Southeast Asia. For instance, they proposed that the F2 fault in the experiment corresponds to the Altyn Tagh Fault, and the F1 one corresponds to the Red River Fault. The tectonics of eastern Asia would thus reflect the succession in time of two major phases of the continental extrusion. The gap between block 2 and block 1, which are compared to the southern China and the Indochina respectively; (Figure 2.9), would be analogous to the South China Sea, whereas the gap A, between the rigid block and block 1, corresponds to the Andaman Sea. The principal tectonic units are shown in the Figure 2.9. According to Molnar and Tapponnier (1975), the Himalayan Thrust Fold belt was plane between the conjugate faults of the sinistral Quetta Chaman Fault in the west and the dextral Sittang Fault, Sagiang, in the east. These strike-slip faults mark the margins of the Indian plate indent which has been driven northward into the Eurasian plate. The action forced the N-S thrusting in the Himalayas (Molnar and Tapponnier, 1975; Ni and York, 1978).

A large number of NE-SW sinistral strike-slip faults and NW -SE dextral displacements can be observed (Ni and York, 1978). It also induced the Tibetan Plateau and developed various N-S trending basins since the Late Cenozoic (Molnar and Tapponnier, 1977; Ni and York, 1978). The outcome of N-S shortening by the

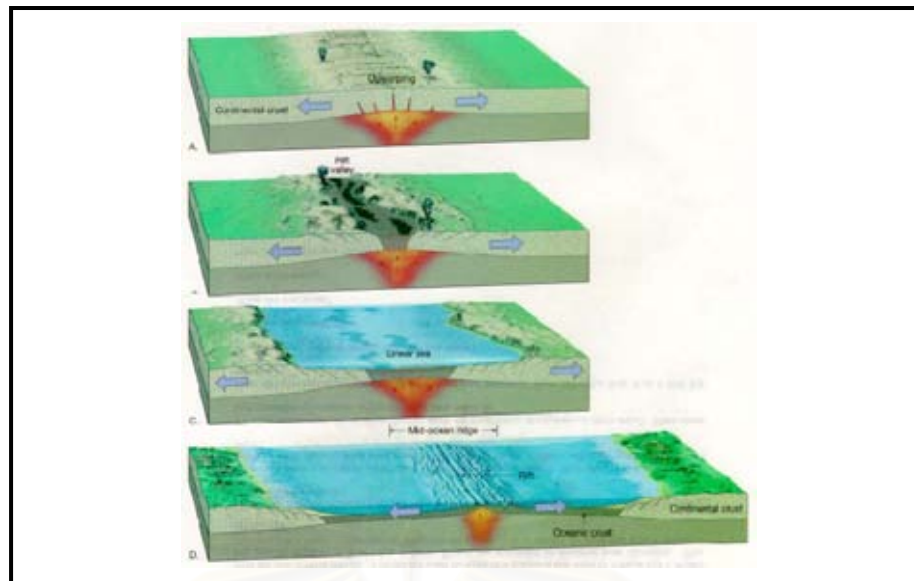


Figure 2.5 Divergent plate boundaries on the ocean floor (After [www.ac.wvu.edu/~debari/406/lec1.html](http://www.ac.wvu.edu/~debari/406/lec1.html)).

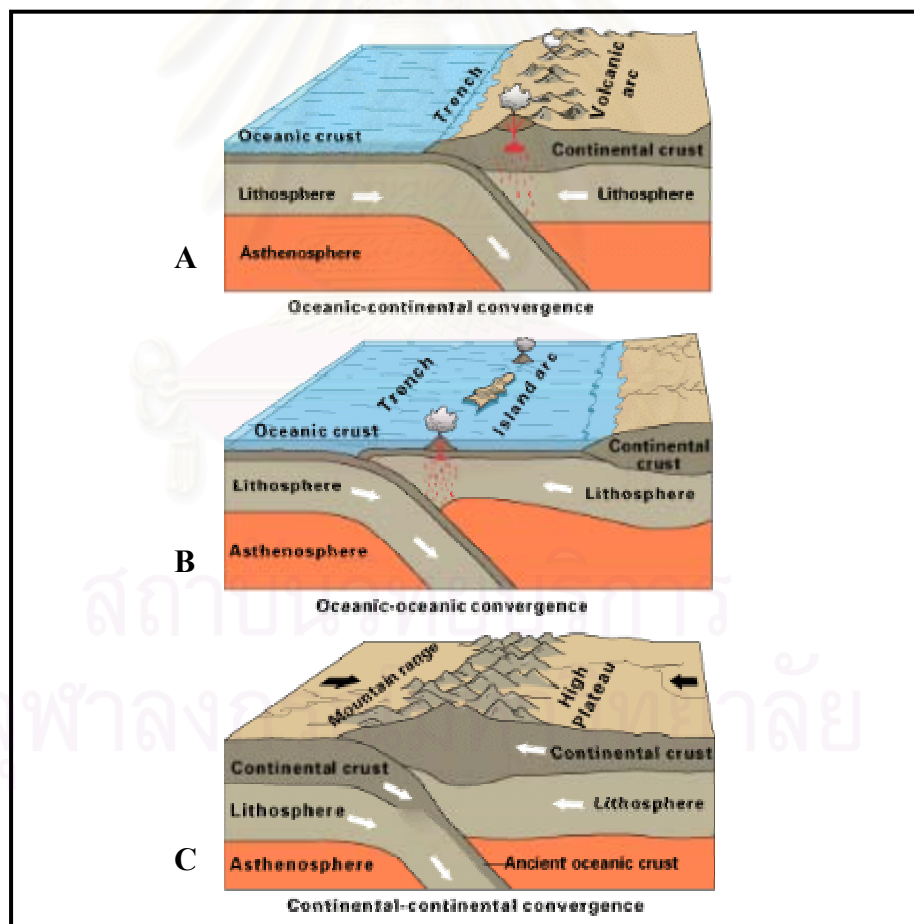


Figure 2.6 Zone of plate convergent, A = oceanic–continental, B = oceanic–oceanic, and C = continental–continental (After <http://dept.kent.edu/geology/ehlab/tectonics/tectonics.htm>).

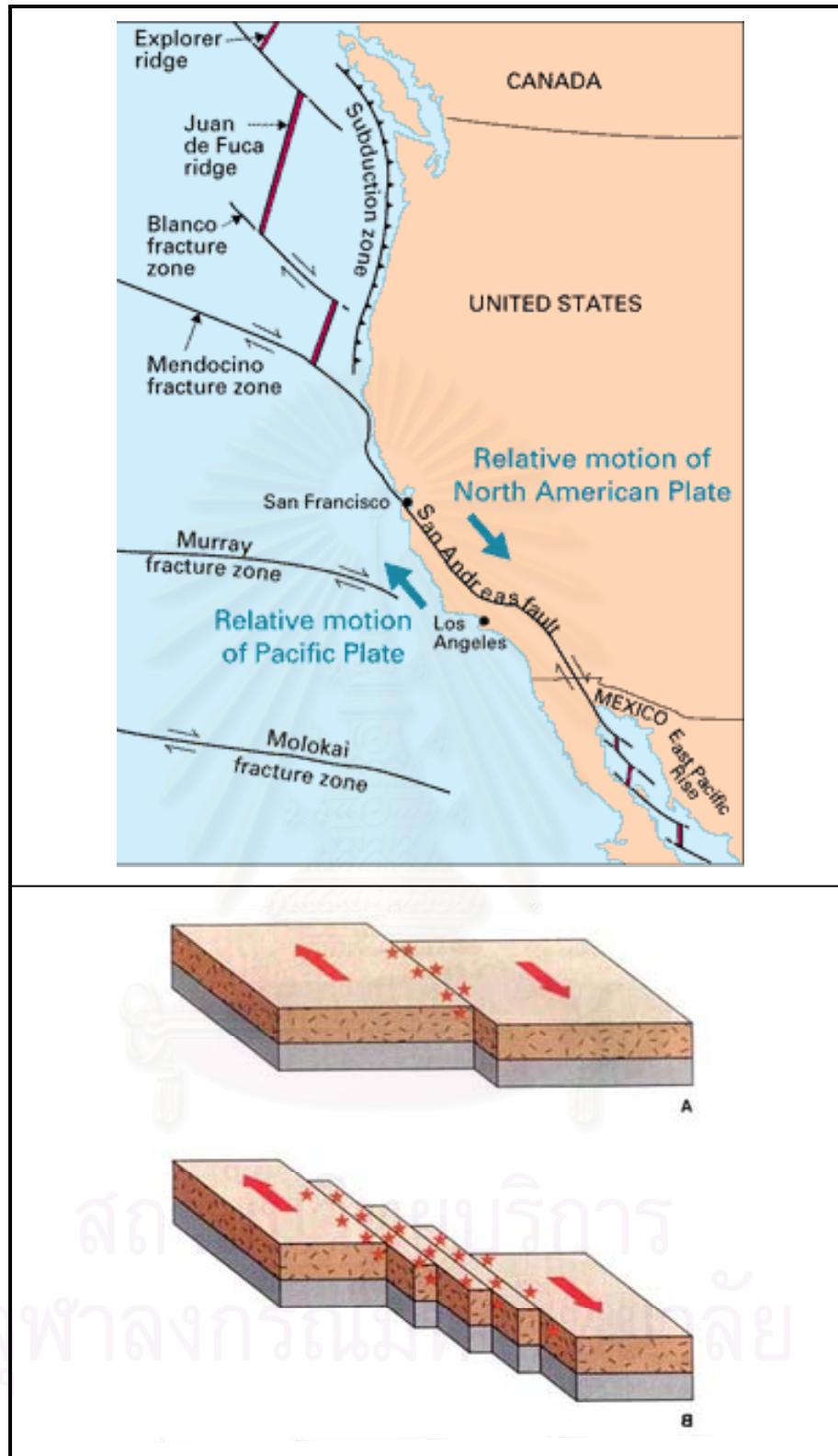


Figure 2.7 The Blanco, Mendocino, Murray, and Molokai fracture zones are some of the many fracture zones (transform faults) that scar the ocean floor and offset ridges. The San Andreas is one of the few transform faults exposed on land (After <http://dept.kent.edu/geology/ehlab/tectonics/tectonics.htm>).

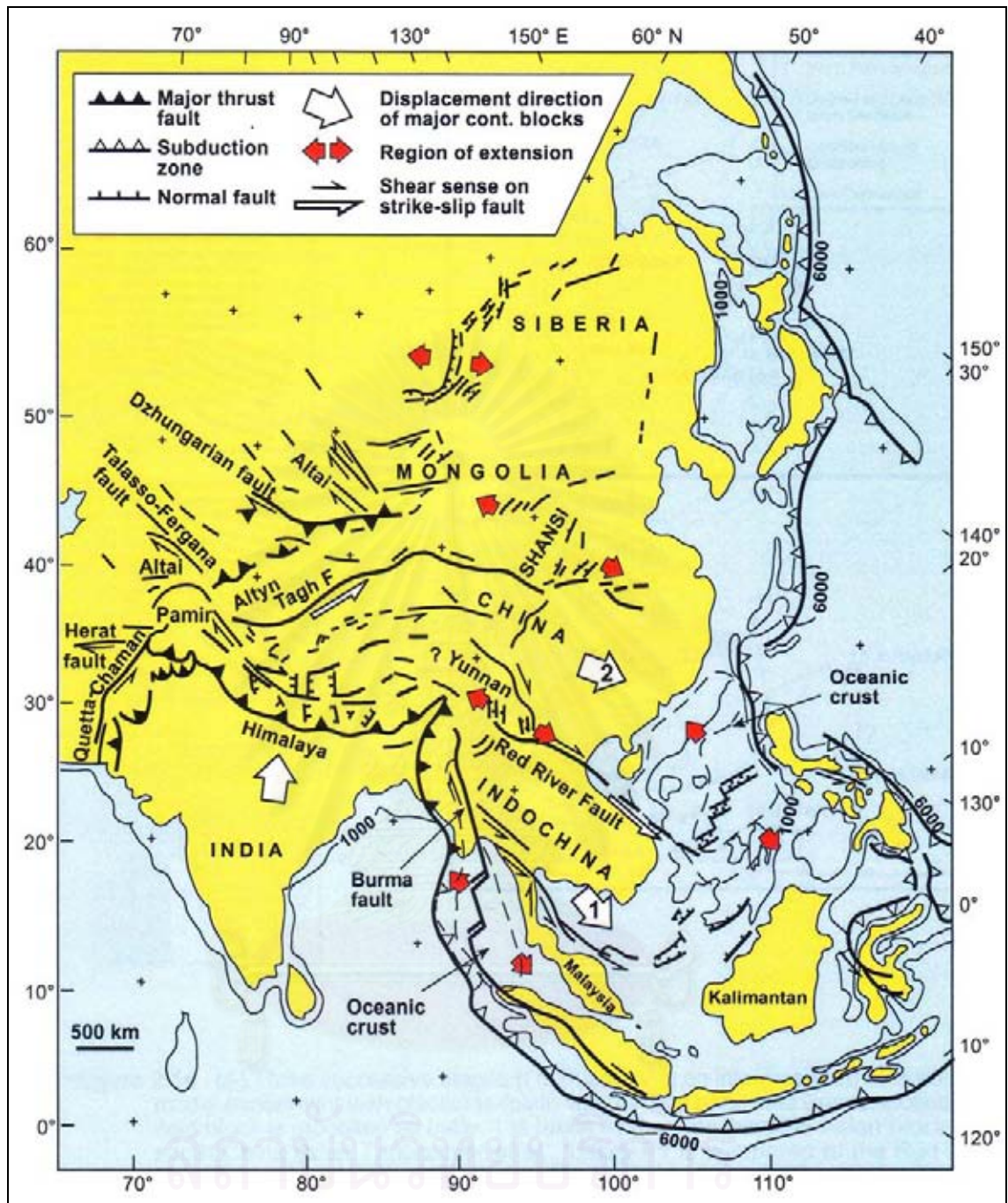


Figure 2.8 Tectonic map of central-east Asia illustrating 'extrusion' model and its relationship with Cenozoic structures in the region. Numbers in white arrows indicate the relative order in which certain continental blocks were extruded toward the southeast (After Tapponnier et al., 1982).



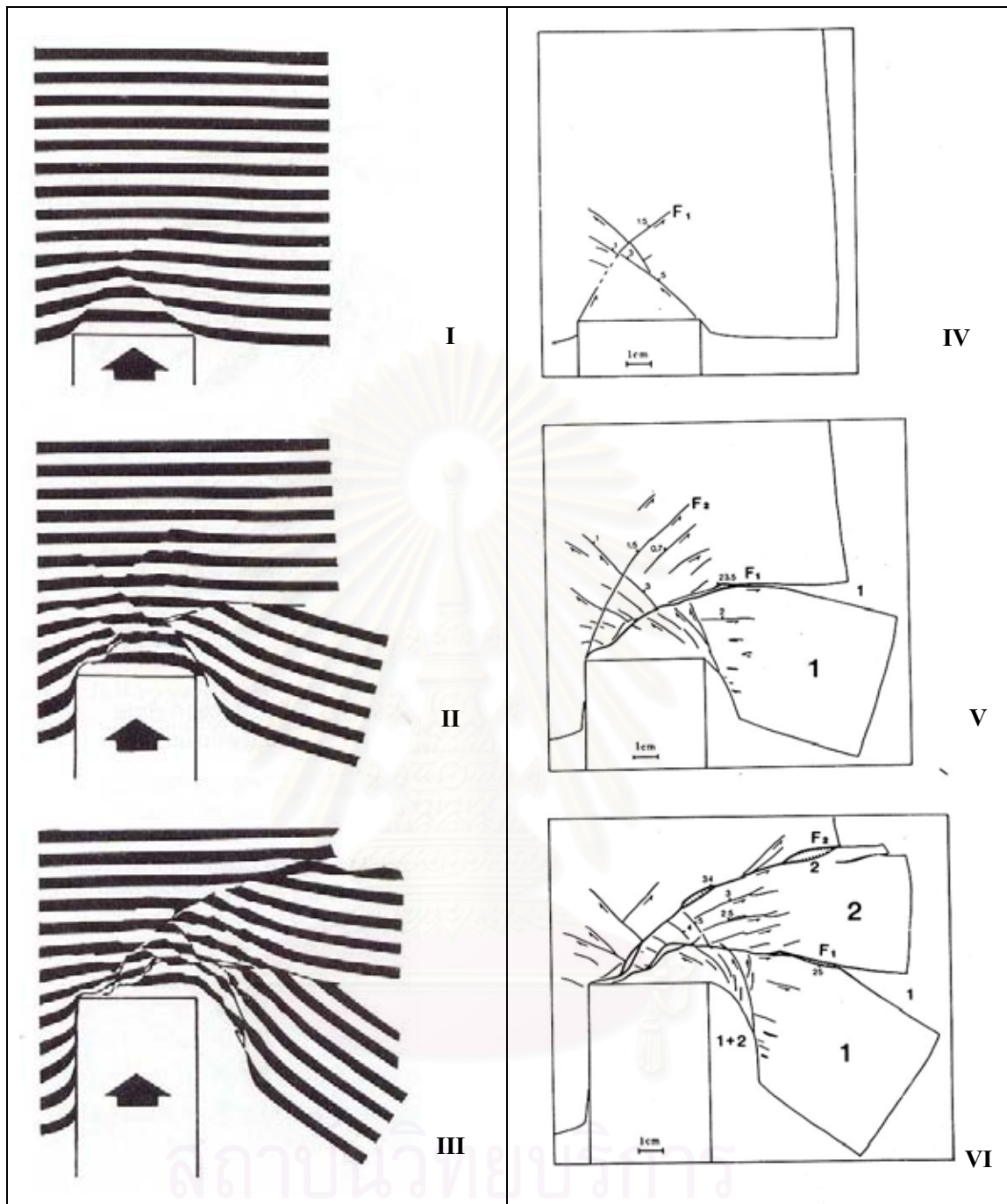


Figure 2.9 Three successive stages (I to III and IV to VI are in interpretation) of extrusional model experiment with plasticine (plain view). In unilaterally confined experiment, two major faults (F1 and F2) guide successive extrusion of two blocks. In stage VI, blocks 1 and 2 can be compared to Indochina and southern China, and open gap 1, 1+2, 2 to South China Sea, Andaman Sea, and northeastern China, respectively (After Tapponnier et al., 1982).

penetration of the Indian Plate into the Eurasian Plate yielded the E-W lateral flow of crustal materials from Tibet to South China which moved eastward away from the path of India (Molnar and Tapponnier, 1975). Molnar and Deng (1984) proposed that the at least half of the present-day northward convergence between India and Asia is accommodated by crustal thickening. These are the results of their studies of the seismic deformation in Central Asia.

The soft collision between Indian and Eurasian plates commenced during Late Palaeocene to Middle Eocene (58–44 Ma), whilst hard collision started in the Middle Eocene (44 Ma) (Lee and Lawver, 1995). The Cenozoic tectonic evolution of this region can be discussed in four stages, related to the northward movement of the Indian plate relative to the Eurasian plate. The eastern syntaxis, the right corner of the Indian plate (Lacassin et al., 1997), has penetrated through the Eurasian plate and has resulted in changing stress patterns of the region through time. The changing stress fields have controlled the opening of the sedimentary basins in this region and the South China Sea as well as the sense of movement of the major strike-slip faults (Huchon et al., 1994).

It is postulated by Srisuwan (2002) that the Cenozoic tectonic evolution of this region can be discussed in four stages, stages I: Early Eocene to Early Oligocene (50 to 32 Ma): the South China Sea margin extension commenced earlier than the collision of Indian–Eurasian and the supposed time of initiation of the Red River Fault. The more extensive rifting in the South China Sea is noted and the first time rifting in the West Natuna Basin area is also mentioned to commence at this stage. The Malay, Mekong Delta, and parts of Gulf of Thailand had been opening at 40–35 Ma.

Stages II: Early Oligocene to Early Miocene (32 to 23 Ma): end of left lateral Mae Ping Fault was approximately 30 Ma. Simultaneously, the onset of widespread extension in the Gulf of Thailand, Malay and West Natuna Sea Basins began during Late Oligocene. The Mergui Basin and Andaman Sea, are thought to be formed during Late Oligocene, and continued to Early Miocene. The northern Thailand basins probably developed at this stage. The Mae Ping and Three Pagodas Faults changed to dextral sense of movement whereas the Mae Chan, Uttaradit, and Phrae–Thoen Faults became sinistral.

Stages III: Early to Middle Miocene (23 to 15 Ma): clockwise rotation of the entire Greater Sunda Block and increasing in the convergence rate along the Sunda Arc. North Sumatra Basin and Central Thailand Basins were still undergoing extension. During 20 Ma to 15 Ma, clockwise rotation of Southern Thailand and counter-clockwise rotation of Malay Peninsula and Sumatra were reported. Inversion in the Malay and West Natuna

Basins, most Cenozoic basins in the Gulf of Thailand and onshore Thailand experienced uplift and erosion that corresponded to a pervasive Middle-Miocene unconformity.

Stages IV: Middle Miocene to Recent (15 to 0 Ma): the counter-clockwise rotation of Borneo still continued while rotation of the Thai-Malay Peninsula and Sumatra ceased, and continued northward moving of Australia. North Sumatra had rotated counter-clockwise with south Malaya and the rotation proceeded the orientation of the Sumatran margin became less oblique to the Indian plate motion vector. This caused the dextral Sumatran strike-slip system, and extension in the Andaman region. Extension occurred in the Gulf of Thailand and inversion in the Malay and West Natuna Basins, whereas the Andaman Sea continued opening toward its present extent. All NW trending strike-slip fault zones in the Sunda region were dextral. The inversion and uplift episode, the structural activity in the Cenozoic basins of the Sunda region slowed down toward quiescence around 10 to 5 Ma, during which period regional subsidence occurred and was probably induced by post-rift thermal re-equilibrium. This late-stage subsidence has continued to the recent time (Figure 2.10).

### 2.3 Major Tectonic Elements in Southeast Asia

Regarding the Southeast Asia region, the structural framework of Cenozoic basins in Thailand is governed by N-S trending extensional faults that are spatially related to the movement of the NW-SE and NE-SW trending strike-slip faults. The NW-SE trending Red River (RRF), Mae Ping (MPF), Three Pagodas (TPF), and Sumatra (SMF) Faults are the principal strike-slip faults, whereas the Mae Tha (MTF), Nan-Uttaradit (NUF), Ranong (RNF), and Klong Marui (KMF) Faults are the NE-SW trending conjugate strike-slip faults which are terminated by the major NW-SE strike-slip faults (Polachan, 1988).

Figure 2.11 shows present-day tectonics and major faults in the Sunda shelf area. The MPF and the TPF extend about 450 and 250 km, respectively. They probably continue to the southeastward under the Chao Phaya Central Plain and in the Gulf of Thailand (Bunopas, 1981; Tapponneir et al., 1986, and Lacassin et al., 1997). These two faults are roughly parallel to the Red River Fault Zones (RRF) and trend NW-SE. Both the MPF and the TPF are truncated by the Sagiang Fault Zone (SGF) in Myanmar. The splay of MPF probably extends farther southeastward to Chonburi province. The other splay also probably continues to the Tonle Sap depression of Cambodia and farther southeast to the west of Mekhong Basin (Tapponnier et al., 1986 and Lacassin et al., 1997). The Nan-Uttaradit Fault Zone (NUF) which is oriented NE-SW is bounded to the east by the Nakhon Thai Plate whereby a belt of ultramafic and mafic rocks, associated

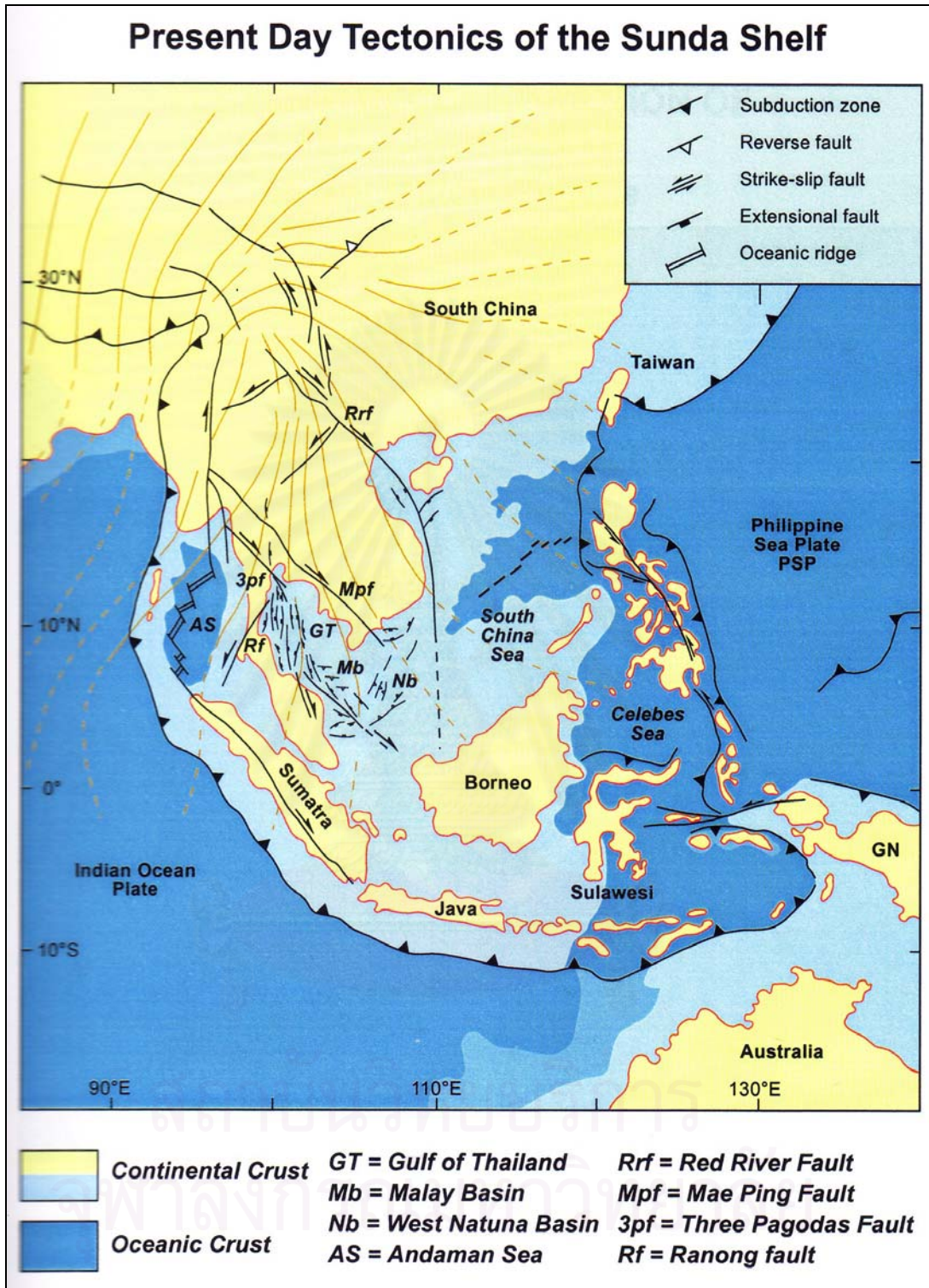


Figure 2.10 Tectonic map of Southeast Asia showing major structural elements in relation to direction of present maximum horizontal stress (After Srisuwon, 2002).

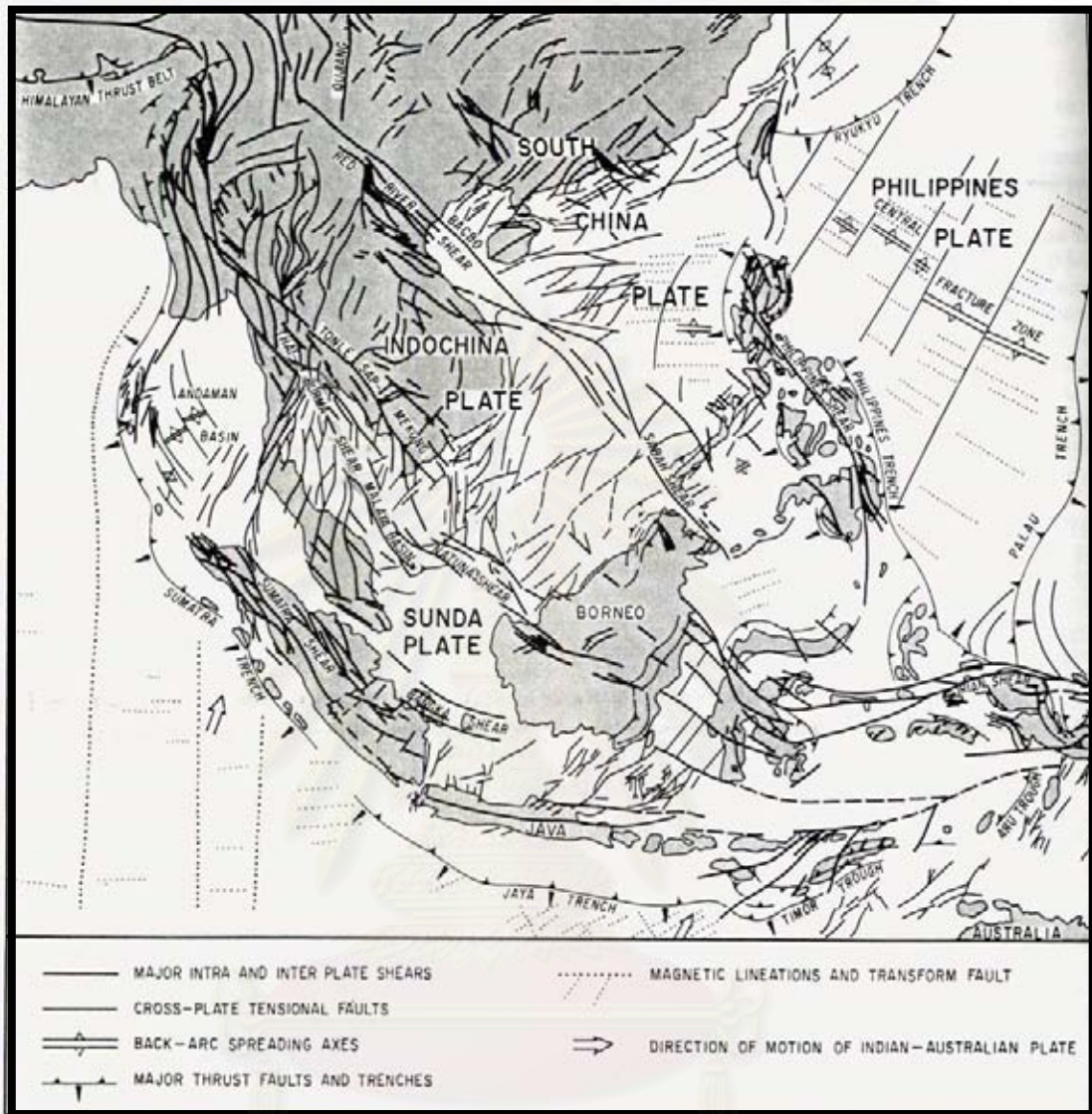


Figure 2.11 Faults systems of Southeast Asia illustrating sequential Cainozoic deformation. The map displays plate fragmentation, north-west-south-east shears, and north-east by south-west expansion (Modified from Hutchison, 1989).

with basaltic to andesitic metavolcanics, blueschists (Barr and MacDonald, 1987) and turbidites are situated. This belt with the NUF marks the suture zone of the Shan–Thai block, and the passive margin of the Kontum–Khorat block of the SE (Bunopas, 1981; Barr and MacDonald, 1987). Subduction and consequent collision probably occurred between the Upper Permian and Middle Triassic (Bunopas, 1981; Sengor and Hsu, 1984; Barr and MacDonald, 1987; and Hutchinson, 1989). The Mae Tha Fault Zone (MTF) is roughly parallel to the NUF, but it has a sigmoidal shape, swinging N–S through the central to southern part of Northern Thailand. This fault zone is made up of a series of anastomosing strike–slip and dip–slip faults (Strogen, 1994). Both the NUF and the MTF show sinistral movements based on earthquake fault plane solutions (Le Dain et al., 1984).

Hinthong (1997) studied active faults in Thailand and classified most of the faults in the Northern Thailand as potentially active faults. The hot springs can be observed along the trend of these faults (Figure 2.12). These comprise five fault zones in the northern and the western highlands geologic provinces, namely:

- 1) The N–S trending, Mae Sariang Fault Zone located in the west, which close to Thai–Myanmar border, having activity between 0.32 to 0.89 Ma;
- 2) The sigmoidal–shape, Mae Tha Fault Zone, which bounds the east part of the Chiang Mai Basin, having activity from 0.19 to 0.77 Ma;
- 3) The NE–trending Theon Fault Zone, which lies on the middle part of northern Thailand as a part of sigmoidal shape and occurred about 0.16 Ma;
- 4) The NE– trending Phrae Fault Zone, which bounds the eastern flank of Phrae Basin and has the shape similar to Theon Fault, shows fault activity of about 0.19 to 1.0 Ma; and
- 5) The NW– trending Three Pagodas Fault Zone, which has the activity range from 0.012 to > 1.0 Ma.

The age dating is only supported by some thermoluminescence dating mostly determined by Isao Takashima, Akita University (Hinthong, 1997).

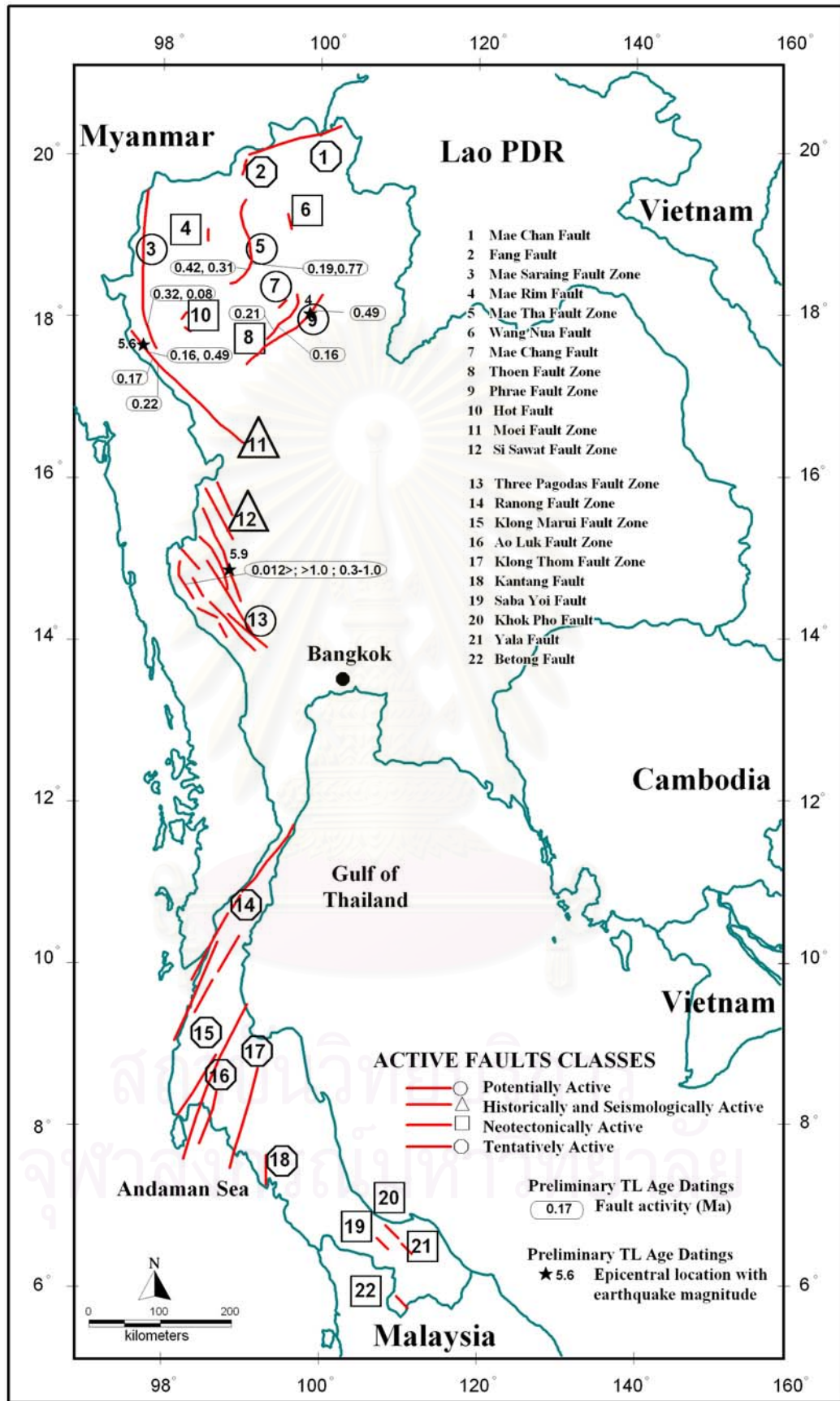


Figure 2.12 Map of Thailand showing distributions of major classified active faults and fault zones in Thailand (After Hinthong, 1995).

## 2.4 Active Faults

### 2.4.1 Definition of Active Faults

The definition of active faults varies widely. Willis (1923) defined an active fault as the one on which a slip is likely to occur and a dead fault as the one on which no movement may be expected.

Albee and Smith (1966) proposed a definition of an active fault in a geologic sense as a fault which has moved in the past and will eventually break again. The activeness of a fault is not just a single state that depends on the degree of activity.

An active fault in the definition of Wood (1915) refers to historic movement that shows evidence of recent surface movement known as the trace phenomena.

Cluff and Bolt (1969) said that a fault should be considered active if it has displaced recent alluvium or other recently formed deposits, whose surface effects have not been modified to an appreciable extent by erosion.

Allen et al. (1965) stated that faults that have had sufficiently recent movement to displace the ground surface are usually considered active by geologists simply because the ground surface is a very young and ephemeral feature. If stream offsets and scarps in alluvium are to be the criteria for activity of faults, then the term "active" must be applied to events dating back into the Pleistocene Epoch, perhaps as much as 100,000 years.

In engineering designation, fault activity is restricted to fault movement during the last 10,000 years, to the Holocene Epoch. This study adopted the definition proposed by the United States Bureau of Reclamation that an active fault is the fault that has a relative displacement within the past 100,000 years.

At present, methods for estimating future hazards of faults are deficient. The designation of a fault merely as active provides an inadequate indication of the attendant hazard. Restricting of the definition of active faults to those having had displacement within a defined past period of time, such as 10,000 or 100,000 years, provides little assessment of the hazard. In addition, the adoption of different restricted definitions by different agencies has caused confusion. An accurate expression of the probability of occurrence of future displacement, of earthquakes generated, and of the size of such events is needed in evaluating the hazards of active faults (Wallace, 1980).



The active fault, as used by U.S. Geological Survey, is a fault that is likely to have another earthquake some times in the future. Faults are commonly considered to be active if they have moved one or more times in the last 10,000 years.

The active fault based on International Committee on Large Dam (ICOLD, 1989), is a fault reasonably identified and located, known to have produced historical fault movements or showing geologic evidence of Holocene, around 11,000 years, displacements and which, because of its present tectonic setting, can undergo movement during the anticipated life of man-made structures

The Western States Seismic Policy Council (WSSPC, 1997) recommends that the following guidelines be used in defining active faults in the Basin and Range physiographic province. Active faults can be categorized into three types, recognizing that all degrees of fault activity exist and that it is the prerogative of the user to decide the degree of anticipated risk and what degree of fault activity is considered "dangerous". They are:

1. Holocene Active Fault – a fault that has moved within the last 10,000 years;
2. Late Quaternary Active Fault – a fault that has moved within the last 130,000 years; and
3. Quaternary Active Fault – a fault that has moved within the last 1,600,000 years.

It should be emphasized in this thesis that more than half of the historic magnitude 6.5 or greater earthquakes in the Basin and Range province have occurred on faults that did not have Holocene activity, furthermore, earthquakes in the province will occur on faults in all three categories.

Site investigations for foundations of nuclear power plants and research reactors (IAEA, 1988 and 1992; U.S. Nuclear Regulatory Commission, 1982.) states that a capable fault is a fault which has exhibited one or more of the following characteristics:

- (1) Movement at or near the ground surface at least once within the past 35,000 years or movement of a recurring nature within the past 500,000 years;
- (2) Macro-seismicity instrumentally was determined with records of sufficient precision to demonstrate a direct relationship with the fault; and
- (3) A structural relationship to a capable fault according to characteristics (1) or (2) such that movement on one could be reasonably expected to be accompanied by movement on the other.

#### 2.4.2 Active Faults in Thailand

Hinthong (1995) and Hinthong (1997) reviewed the present status of the study of active faults program in Thailand (Figure 2.12). Apart from the knowledge of the importance of understanding of active faults, the various basic concepts, principles or even the implications have been laid out for refining. Approaches towards refining their definitions and classifications, as well as their criteria for recognition of active faults have been compiled from various sources.

The importance of active fault evaluation to society is that it provides the basis for design, siting, zoning, communication, and response to earthquake hazards. It is necessary for all types of major engineering structures in order to reduce potential loss of life, injury, or damage.

According to various authors and researchers, three approaches to define active faults can be distinguished and applied. These three definitions are characterized as general technical definition, engineering definition, and regulatory definition. Those three applications of definitions were discussed, based primarily on its original definition which was proposed in the context of a two-fold classification of "dead" and "alive" or "active" faults, and with respect to their potential for future renewal or recurrence of displacement or offset.

In consideration that based upon available data, and with the exclusion of the tentatively inactive and inactive classifications, fault activity can be classified as three classes: active, potentially active, and tentatively active. Basically, there are three major criteria for recognition of active faults, namely, geologic, historic, and seismologic criteria.

In order to cope with the problem of the study of active faults in Thailand, the adoption of active fault classifications, specifically for the benefit of the utilization only in Thailand, four classes have been proposed, namely, potentially active, historically and seismologically active, neotectonically active, and tentatively active faults and fault zones.

Consequently, with the restriction, deficiency of necessary data, and the lack of various seismologic, geodetic, geophysical, and other subsurface methods of analysis, but only supported by some thermoluminescence age datings, the inventory of twenty-two preliminary active faults in Thailand have been outlined. The related purpose was to lay out major faults/fault zones for the preparation of preliminary active faults map of Thailand, scale 1:1,000,000.

Charusiri et al. (2001), therefore, ranked the active faults, based upon historic, geologic, and seismologic data (Table 2.1). Since Thailand is not the main site for present-day large earthquakes as compared with those of the nearby countries, the best definition used herein is from the combination and modification of those above-mentioned definitions. Additionally, the age of the fault is also essential in their justification, it is proposed (Table 2.2) that the fault becomes “active” if it displays a slip movement in the ground at least once in the past 35,000 years or a series of quakes within 100,000 years. If the fault shows only one movement within 100,000 years, it would be defined as “potentially active”. Furthermore, if only once in the past 500,000 years, it would be become “tentatively active”. All of these faults are expected to occur within a future time span of concern to society. The fault becomes “neotectonic” if it occurred in Pleiocene or Late Tertiary, and it is regarded as “(paleo-) tectonic” or “inactive” if it occurred before Pleiocene.

#### **2.4.3 Moei-Mae Ping Fault Zone (MPFZ)**

Hinthong (1995 and 1997) divided active faults into four classes based on the degree of activeness as potentially active, historically and seismologically active, neotectonically active, and tentatively active. He regarded that the MPFZ is historically and seismologically active.

According to Charusiri et al. (2001), Thailand active faults were classified into five seismic active belts (SABs) which were defined as linear or elongate zones of seismicity. These SABs were commonly classified based upon neotectonic movements and coincident with major tectonic structures (Figure 2.13). They are Northern, Western-Northwestern, Central Peninsula, Southern Peninsula, and Eastern-Northeastern SABs. The Western-Northwestern SAB, Mae Ping Fault zone was considered as the potentially active fault.

Table 2.1 Active fault rank, criteria, and examples in Thailand (After Charusiri et al., 2001)

<b>Rank</b>	<b>Historic</b>	<b>Geologic</b>	<b>Seismologic</b>	<b>Examples</b>
<b>Active (AF):</b>				
<b><i>Tectonic fault which displays a history of strong earthquake or surface faulting in the past 35,000 yrs, or a series of quakes during 100,000 yrs, and is expected to occur within a future time span of concern to human society.</i></b>				
Surface faulting and assoc. strong quakes, also with geodetic evidence.				
<b><i>Young Quaternary deposits cut by fault, distinct youthful geomorphic features.</i></b>				
Epicenters along that fault.				
<i>MaeChan,Phrae,Thoen,Pua.</i>				
<b>Potentially Active (PAF):</b>				
<b><i>A tectonic fault without historic surface offset, but with a recurrence interval sufficient to human concern, and with an earthquake within 100,000 yrs.</i></b>				
Surface faulting unclear.				
<b><i>Subdued &amp; eroded geomorphic features, faults not known to cut young alluviums, but offset older Quaternary deposits.</i></b>				
Alignment of epicenters but with low confidence of assigned locations.				
<i>Mae Tha, Mae Hong Son, Srisawat, Three - Pagoda.</i>				
<b>Tentatively Active (TAF):</b>				
<b><i>A fault with insufficient data to define past activity and its recurrence interval is relatively very long or poorly defined, or displaying an earthquake within 500,000 yrs.</i></b>				
Data indicate fault evidences, but evidences may not be definitive.				
<b><i>Traced clearly by remote-sensing data with some hot springs.</i></b>				
Scarce and low seismicity.				
<i>Payao, Nam Pat,</i>				
<i>Ranong, Klong Marui,</i>				
<i>Klong Thom, Southern Peninsula.</i>				

Table 2.2 Activity of faults in Thailand based upon age-dating data (after Charusiri et al., 2001).

Era	Period	Epoch	Yrs before	Fault activity
C E N O Z O I C	Quaternary		0	<b>Active fault</b> is categorized within one of these events: 1) <b>Active-</b> if one quake within 35,000 yrs, or several within 100,000 yrs. 2) <b>Potentially active-</b> if one quake within 100,000 yrs 3) <b>Tentatively active</b> – if one quake within 500,000 yrs Neotectonic fault (difficult to determine-active or inactive)
		Holocene	11,000	
		Pleistocene		
	Tertiary	Pliocene	160,000	
		Pre-Pleiocene	350,000	
		650,000,00	(Paleo-)Tectonic fault (or inactive)	
Pre-Cenozoic				

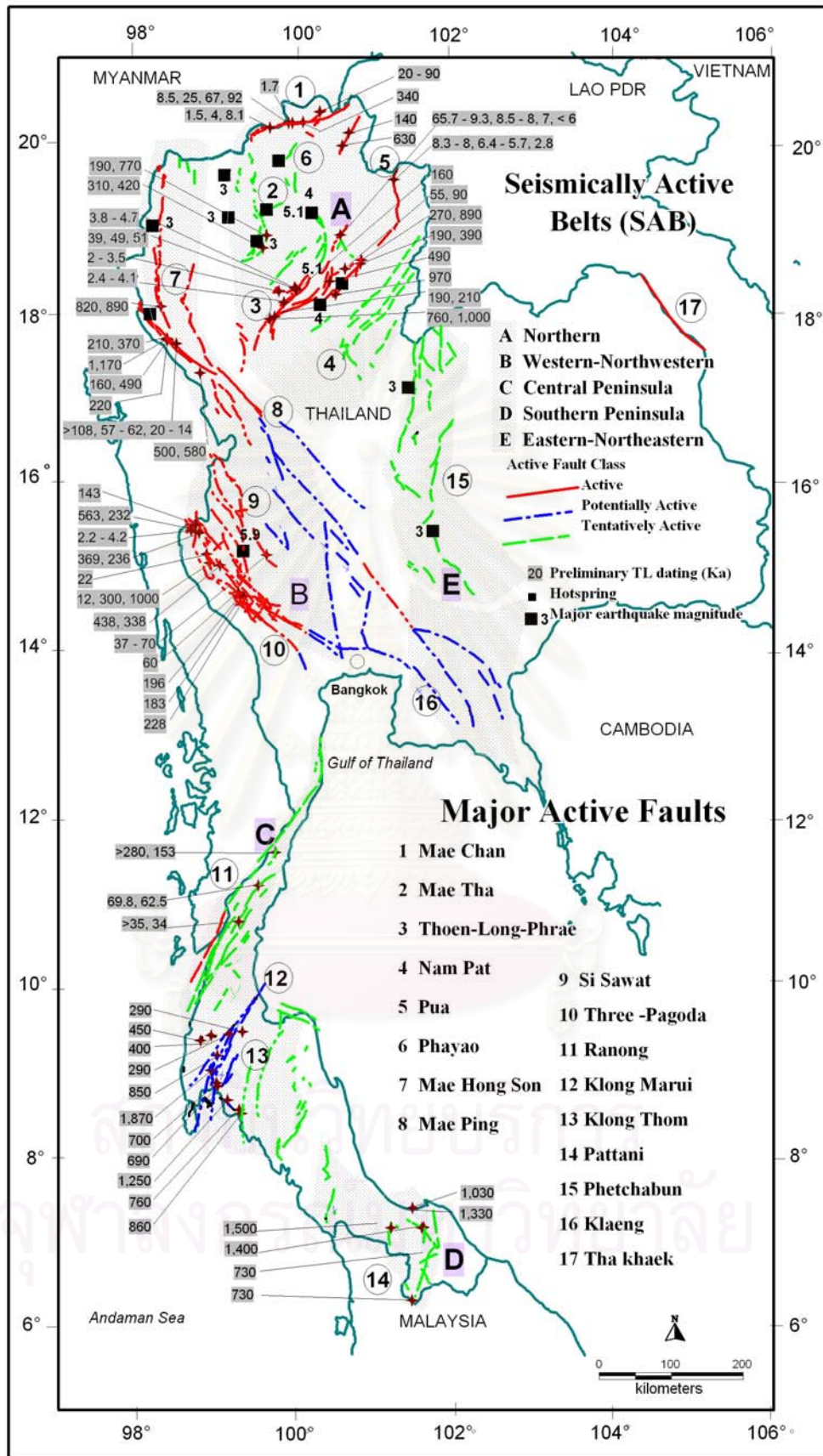


Figure 2.13 Map of Thailand showing major fault zones with TL-age dating data (After Charusiri et al., 2001).

## CHAPTER III

### REMOTE-SENSING INTERPRETATION

In this chapter, description is divided into three sections. The first section focuses on geological lineament interpretation in a regional scale. The Landsat 5 TM, the Radarsat, and the JERS SAR imageries are significant information applied for this interpretation. The second section describes fault segmentation of the MPFZ system. The last section emphasizes on morphotectonic interpretation using aerial photographs. In addition, morphotectonic maps, which include fault branches and geomorphic evidences of fault movements, are also shown in this section.

#### **3.1 Lineaments Interpretation**

Lineaments are referred to linear features found in the earth's surface. This feature can be delineated on maps or on aerial or satellite images, and is at least a few kilometers long (O' Leary et al., 1976). Various lines of disruption, which separate areas of different weathering and erosion, and morphologic and geologic features, are also referred to lineaments (O'Leary and Simpson, 1977). Normally, lineaments have been found influence with straight or curvilinear streams and valleys, topographic alignments, boundaries between areas and morphology or slopes, and linear trends due to both lithologic changes and breaks. These surface break lines are often observed related to tectonic activity (Strandberg, 1967). Geomorphologically, lineaments have also referred to significant lines of landscape which reveal the hidden architecture of the rock basement (Hobbs, 1972). Tectonically, real lineaments are surface expression of faults or fault zones, together with associated structures (Park et al., 1994). Satellite remote sensing imagery, which provides raw data in both regional and local scales, plays an important role in lineament analysis of structural and geotectonic investigations related to earthquake studies. Remote-Sensing data is a useful tool to understand geological framework of the region due to inexpensive, time-effective, and relatively accurate information (Charusiri et al., 1996).

In an attempt to understand regional characteristic and pattern of geological lineaments in the study area and nearby, Landsat 5 TM, Radarsat and JERS SAR imageries were conducted for lineament interpretation approach. The Landsat 5 TM image taken on June 25, 1997 (Figures 3.1 and 3.2) is a false-coloured composite, bands 4, 5, and 7 represented in red, green, and blue, respectively, and the Radarsat image taken on June 7,

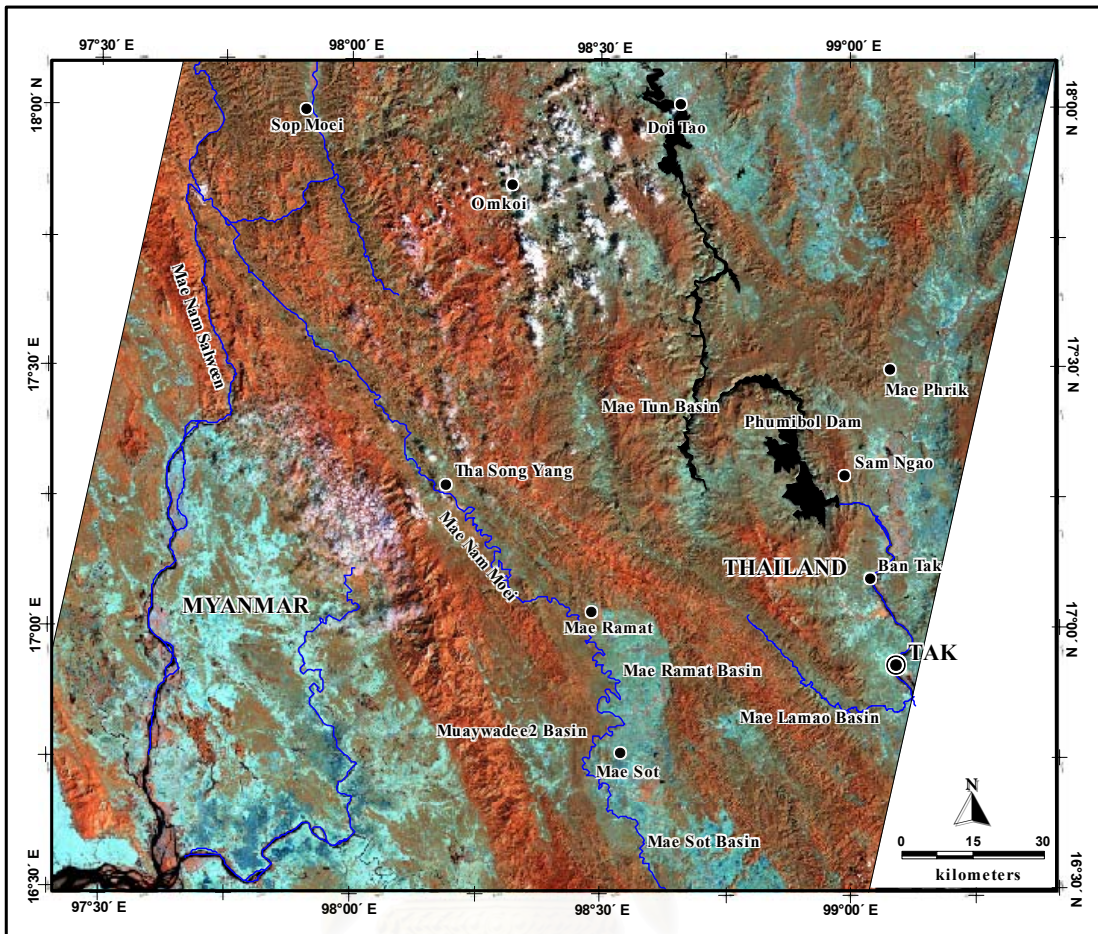


Figure 3.1 Enhanced Landsat 5 TM taken on June 25, 1997 showing physiographic features of the western part of the study area (Interpreted result is shown in Figure 3.6).



สถาบันวิทยบริการ  
จุฬาลงกรณ์มหาวิทยาลัย



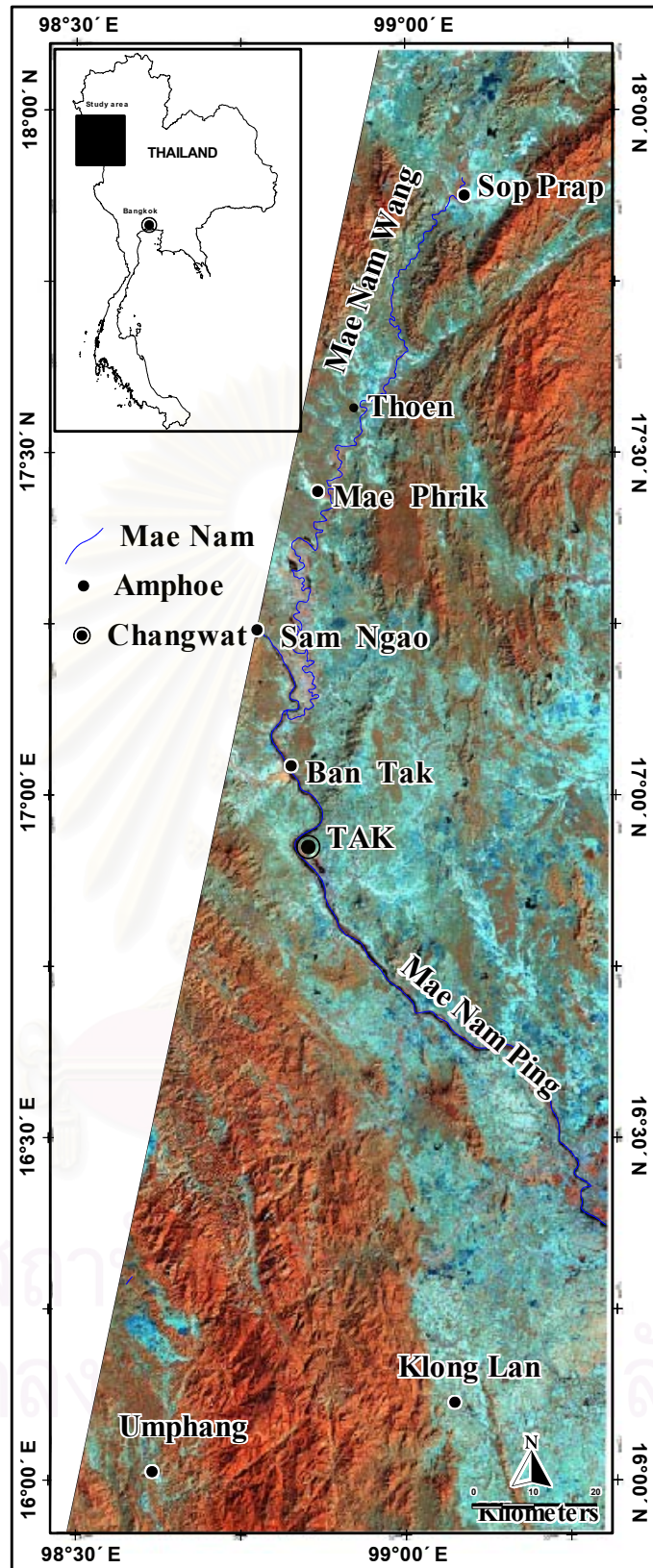


Figure 3.2 Enhanced Landsat 5 TM taken on June 25, 1997 showing physiographic features of the eastern part of the study area (Interpreted result is shown in Figure 3.7).

2004, and June 14, 2004 (Figures 3.3 and 3.4) at scale 1:250,000 to cover much of the MPFZ in Changwat Tak, northwestern Thailand. In addition, the JERS SAR image taken on June 25, 1997 at scale 1: 500,000, and covering the MPFZ and nearby areas, were applied for analysis as well (Figure 3.5). Identification of lineaments was performed by visual justification. Traceable lines are layout on a hard copy prior to digitally modify version using Map Info program.

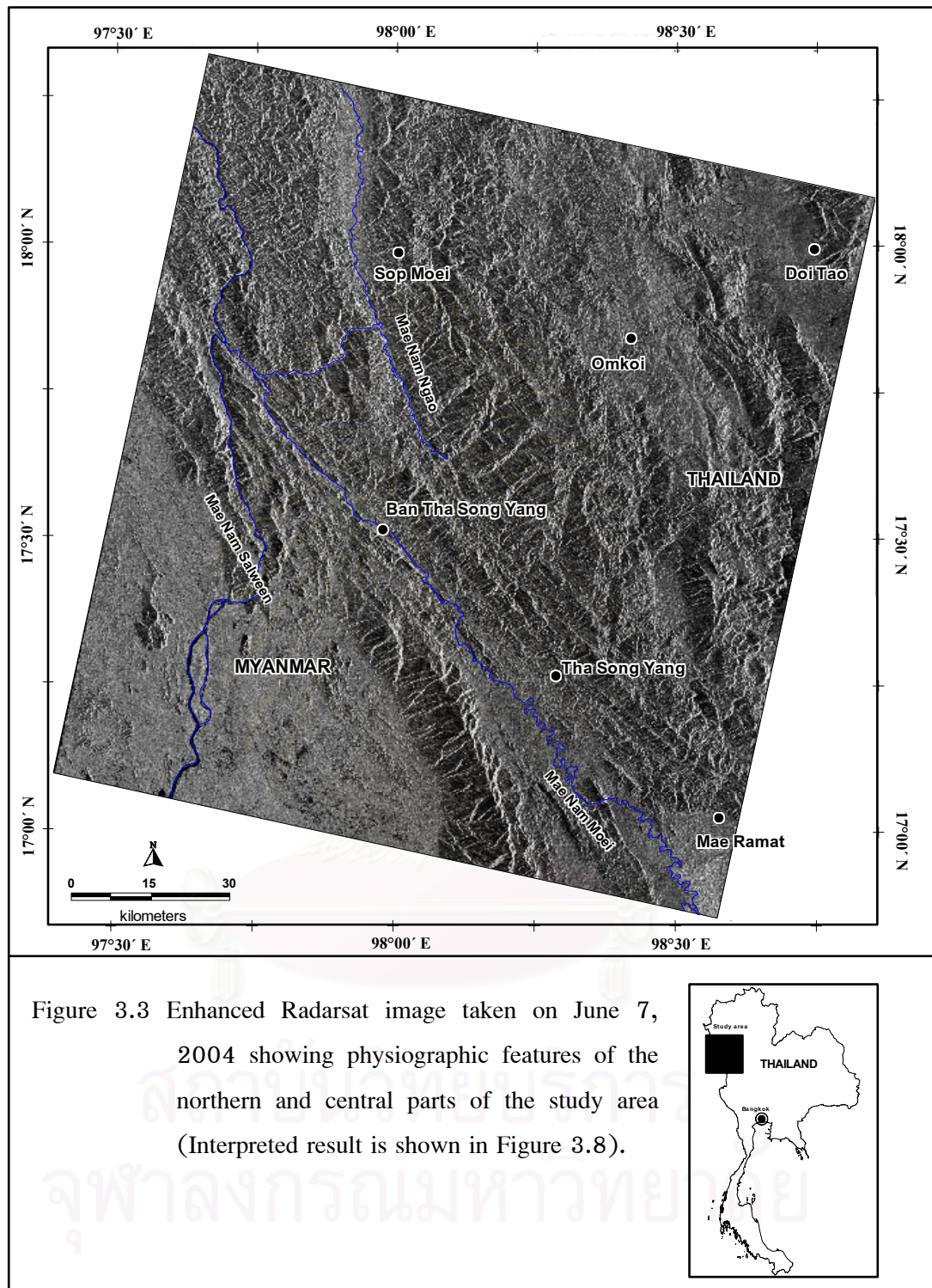
### 3.1.1 Result from Landsat 5 TM Image Interpretation

The result from enhanced Landsat 5 TM images for neotectonic evidence along the MPFZ is displayed in Figures 3.6 and 3.7. The false-colored composite (red, green, and blue) are digitally added to the image data of bands 4, 5, and 7, respectively. Practically, visual interpretation is used to assist in delineating large scale neotectonic features and to define orientations and directions of the investigated fault segments. The result shows the appearance of several neotectonic features including fault scarps, triangular facets, offset streams, and shutter ridges. Lineaments and faults can be traced from easternmost Myanmar to the border zone of northwestern Thailand (Figures 3.6 and 3.7). The result from remote-sensing interpretation indicates the major trend of lineaments and faults along the MPFZ in the northwest-southeast direction, and its branches may extend northward to the Mae Hong Son area. Three other minor trends of lineaments and faults lie in northeast-southwest, east-west, and north-south directions.

### 3.1.2 Result from Radarsat Image Interpretation

The study area covers much of the Thailand and Myanmar border by the Mae Nam Moei. The Mae Nam Moei has its flow direction from southeastward to northwestward before joining the Mae Nam Salween that has flow direction from northward to southward in Ban Sop Moei (Figure 3.3). Results from RADARSAT images enhanced by ENVI 3.6, indicate that most major lineaments are in the northwest-southeast trend with the length of 2-30 km. In the southern part of the Mae Sariang basin, the north-south and northnorthwest-southsoutheast lineaments are found along the Mae Nam Ngao (arrow head in box a in Figure 3.8). Additionally, the pronounced northwest-southeast lineaments are observed, one is near the Mae Nam Salween with the offset slip to the right at about 2 km (arrow head in box b, Figure 3.8), the other one is almost parallel to the Mae Nam Moei (box c in Figure 3.8). In box d, the straight and distinct lineaments are observed as segments continuously in the Amphoe Tha Song Yang (Figure 3.8).

In the Mae Ramat basin, (Figure 3.4) there exists the lineaments lying in the northwest-southeast and north-south directions, which indicate the normal movement (box



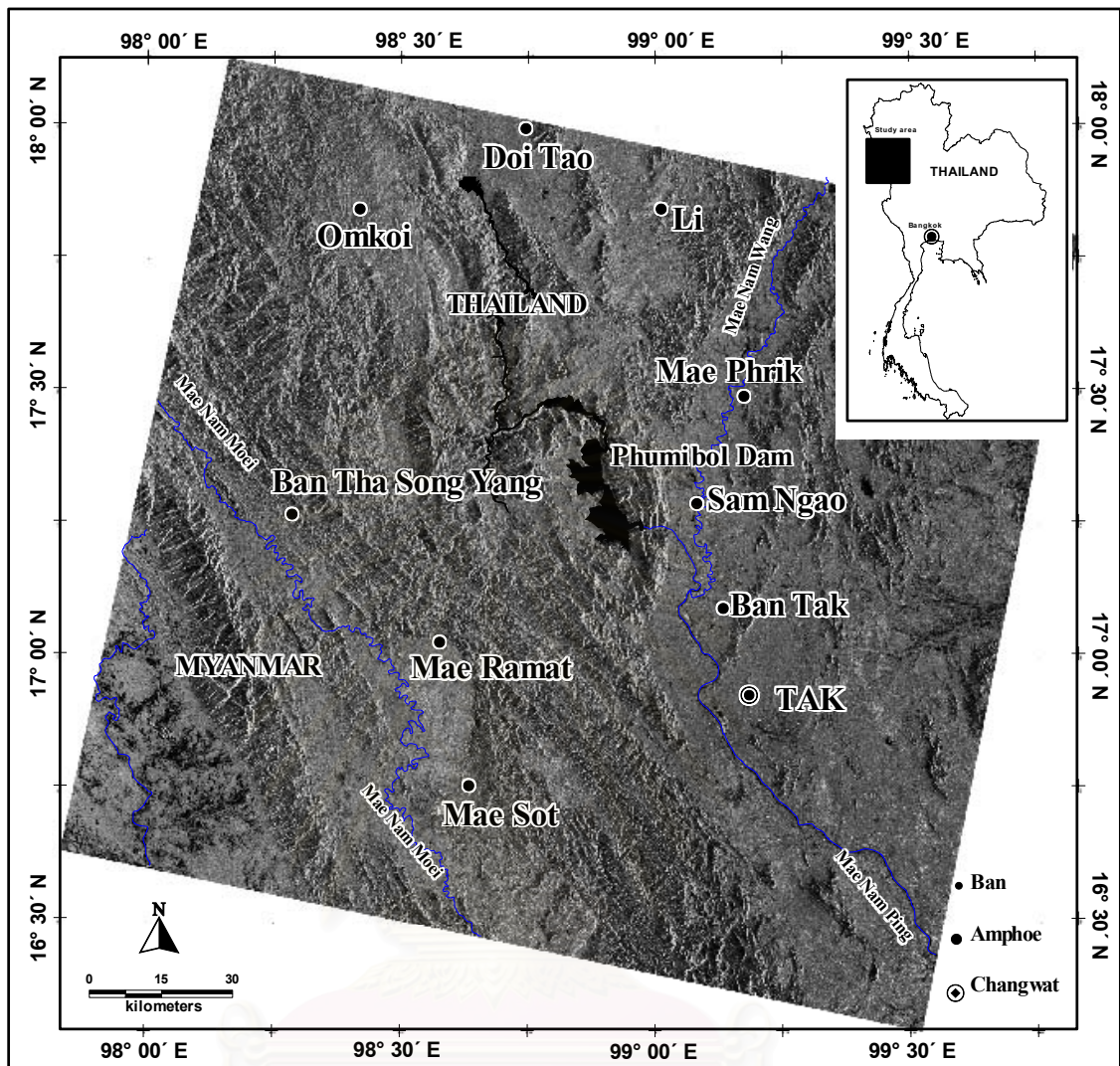


Figure 3.4 Enhanced Radarsat image taken on June 14, 2004 showing physiographic features of the central and southern parts of the study area (Interpreted result is shown in Figure 3.9).

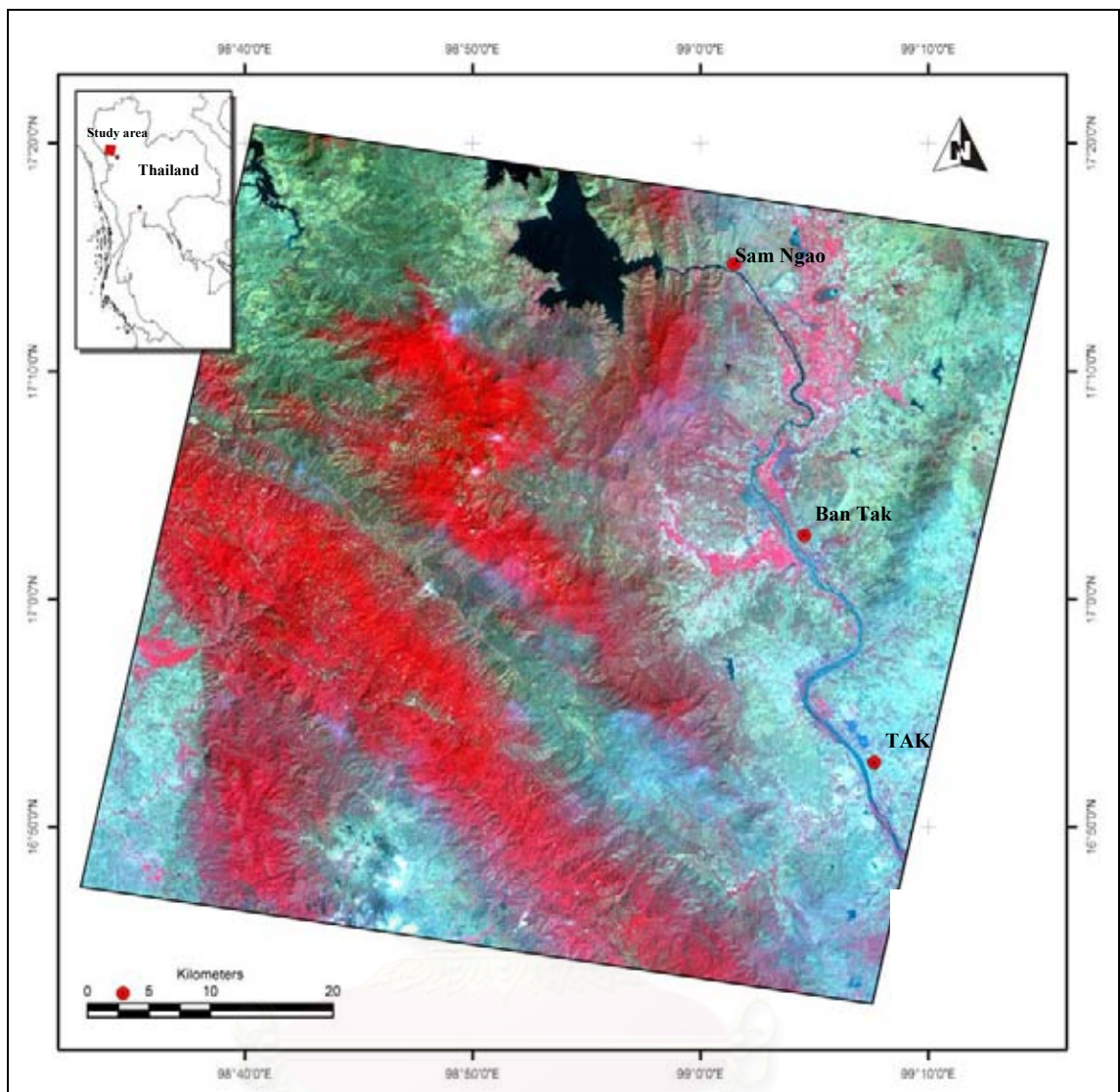


Figure 3.5 Enhanced JERS SAR taken on June 25, 1997 showing physiographic features of the central and southern parts of the study area (Interpreted result is shown in Figure 3.10).

สถาบันวิทยบริการ  
จุฬาลงกรณ์มหาวิทยาลัย

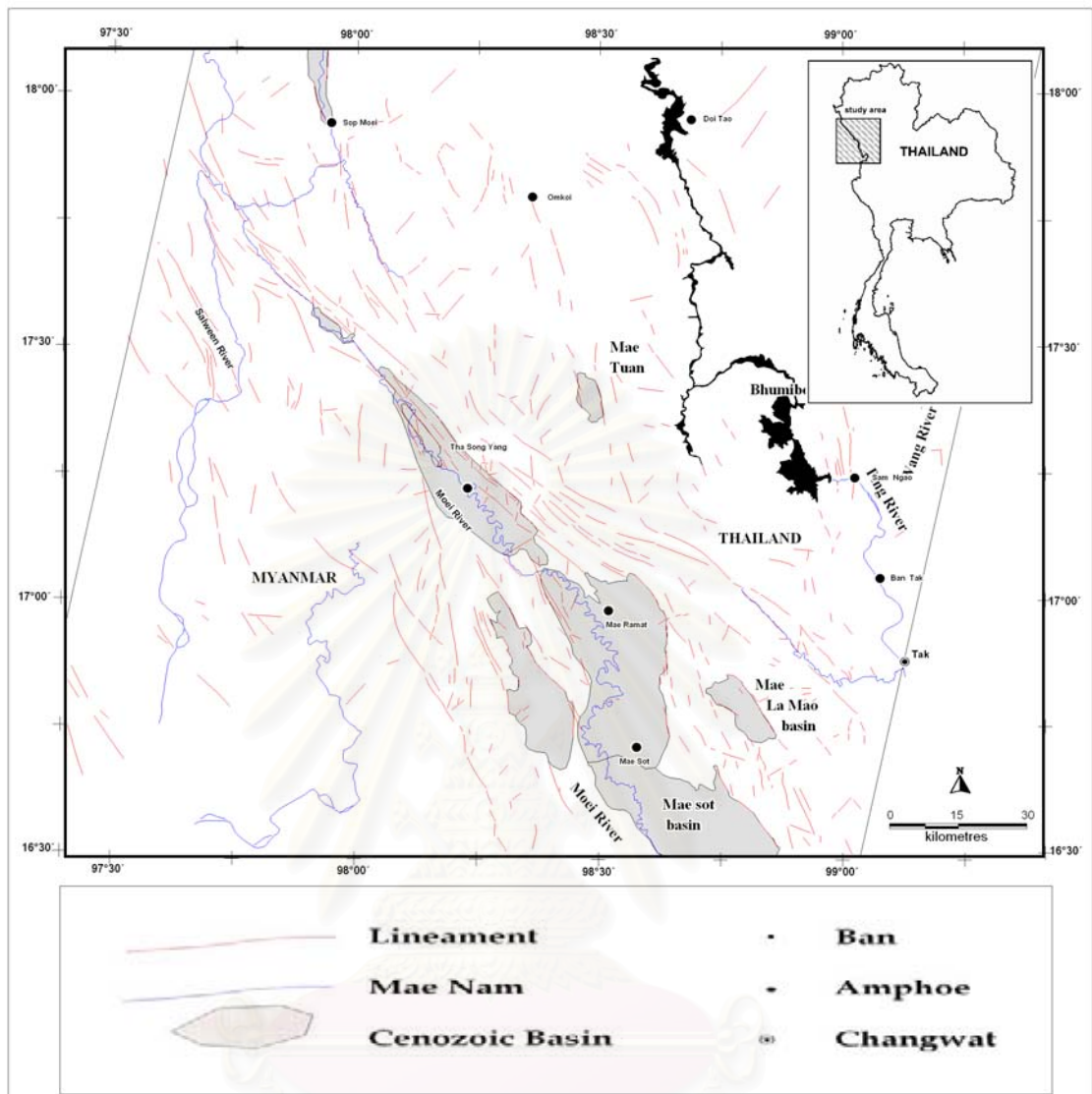


Figure 3.6 Lineaments interpreted using the enhanced Landsat 5 TM image in Figure 3.1 and distribution of Cenozoic basins.

สถาบันวิทยบริการ  
จุฬาลงกรณ์มหาวิทยาลัย

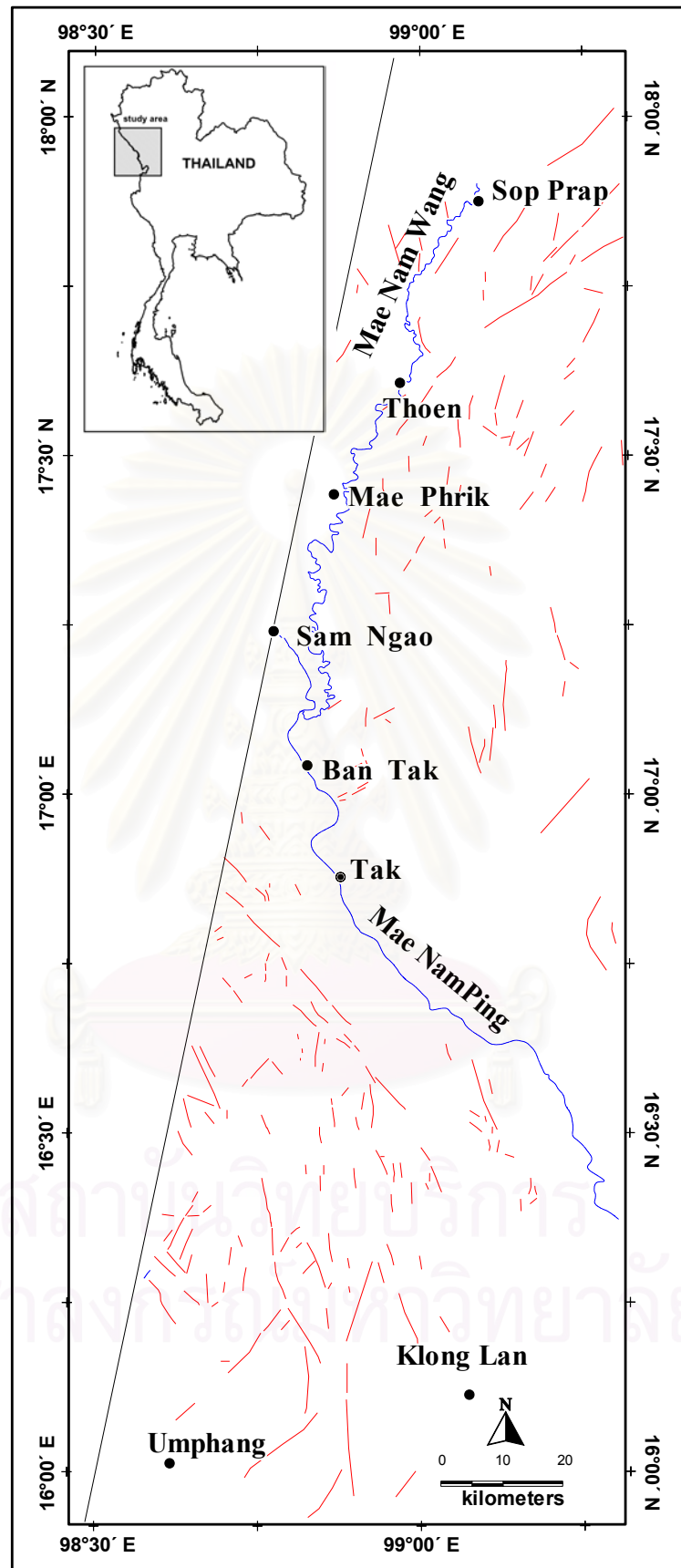


Figure 3.7 Lineaments interpreted using the enhanced Landsat 5 TM image in Figure 3.2.

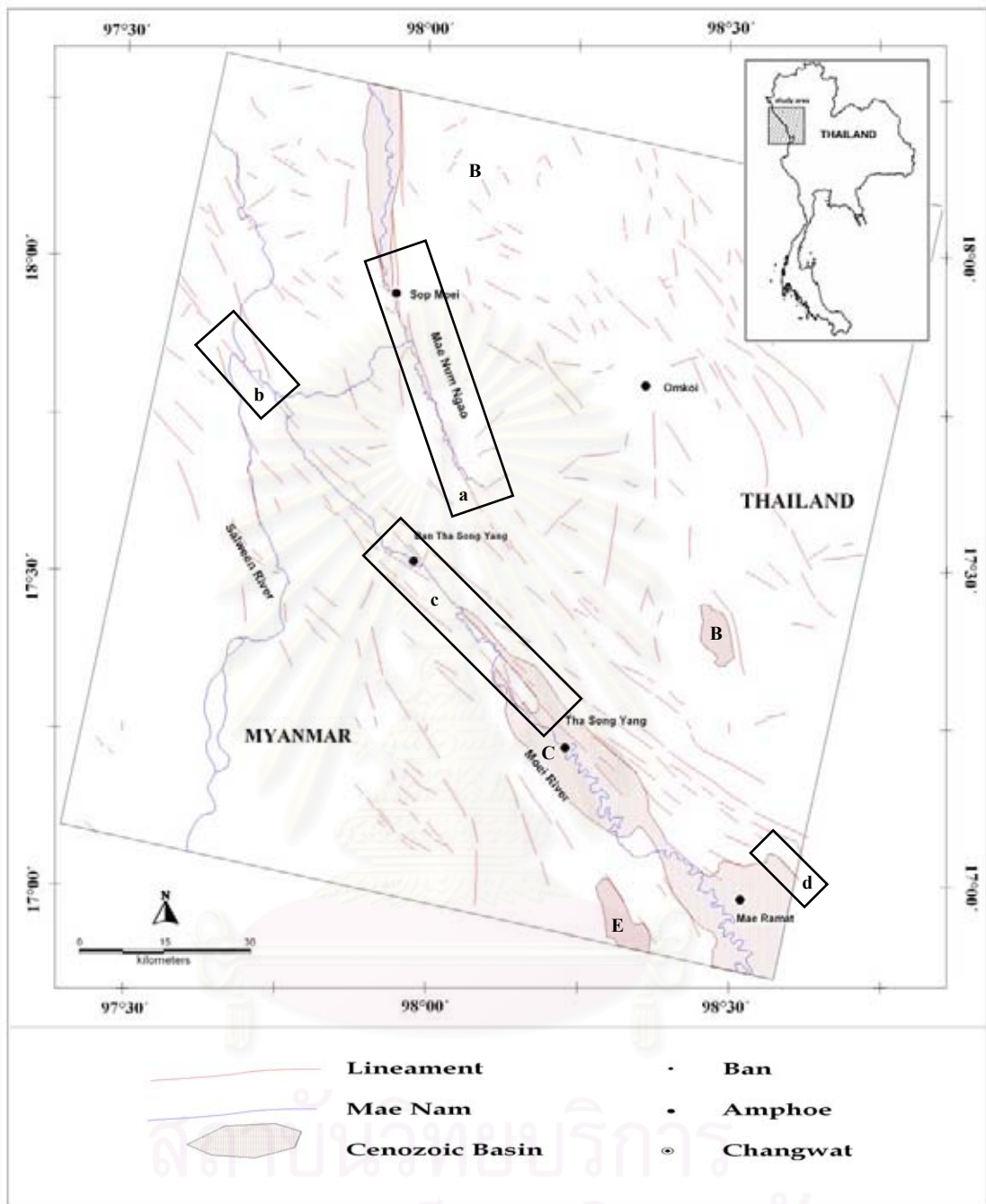


Figure 3.8 Lineament map of the northern area (Mae Ramat–Sop Moei) showing lineament patterns and distribution of Cenozoic basins interpreted using enhanced Radarsat image (from figure 3.3). A = Mae Saraing basin, B = Mae Tun basin, C = Muaywadee1 basin, D = Mae Ramat–Mae Sot basin, E = Muaywadee2 basin.



d and box e in [Figure 3.9](#)). Along the Huai Mae Tho, the lineaments in the northwest-southeast trend were observed. In box f, the lineament is as long as 5 km shown from the area of the Changwat Tak to that of Changwat Khumpang Pet ([Figure 3.9](#)).

### **3.1.3 Result from JERS SAR Image Interpretation**

The interpretation of JERS SAR images for neotectonic evidence along the MPF is used ([Figure 3.10](#)). The results of this technique conform to those of both the Radarsat and the Landsat 5 TM. Three other minor trends of lineaments and faults are in northeast-southwest, east-west, and north-south directions.

## **3.2 Fault Segmentation**

### **3.2.1 General**

Concept of fault segmentation is elucidated by the fact that historical surface rupture triggered by earthquakes along the long faults seldom occurred throughout the entire length, and just only one or two segments became ruptures during large earthquake (McCalpin, 1996). For instance, the San Andreas Fault zone of California was divided into four segments based on difference of historical surface rupture (Allen, 1968). The long fault trace is composed of numerous discrete segments (Segall and Pollard, 1980). The segmentation of fault systems is related to the identification of individual fault segments, based on continuity, character and orientation. It is recommended that a segment can rupture as a unit (Slemmons, 1982). Aki (1984) suggested that the delineation of segments is related to the identification of discontinuities in the fault system. Discontinuity can be divided into two main groups: geometric and inhomogeneous group. Note that this statement has borrowed from seismologists who have used these terms for asperities and barrier. In addition, it is believed that fault may be segmented at a variety of scale that is from a few meters to several tens of kilometers in length (Schwartz, 1989).

All fault segments have their own boundaries. The segment boundary is a portion of a fault where at least two preferable successive rupture zones have ends (Wheeler, 1989). There are several geomorphic features related to fault boundary or termination. For example, releasing bends and steps, restraining bends, branch and cross-cutting structures, and change in sense of slips are commonly observed at segment termination of strike-slip fault (Knuepfer, 1989). For normal and reverse faults, geomorphic features for definition segment endpoints are not clear (McCalpin, 1996).

Since late 1970s, many workers have found that not all faults have historical rupture records along their fault zone. Thus numbers of criteria have been conducted in

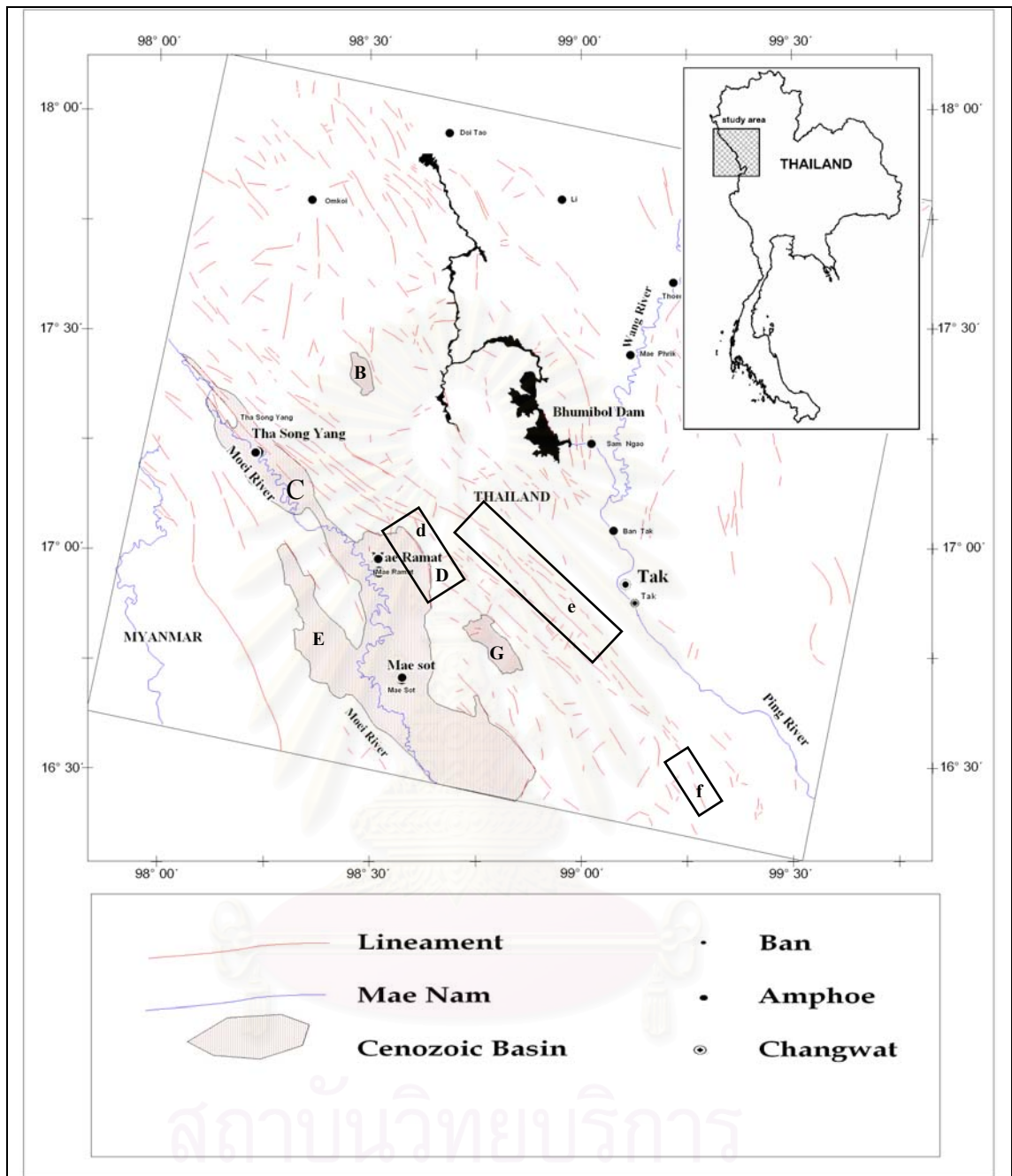


Figure 3.9 Lineament map of the southern area (Mae Sot-Tak) showing lineament patterns and distribution of Cenozoic basins interpreted, using the enhanced Radarsat image (from figure 3.4). C = Muaywadee1 basin, D = Mae Ramat-Mae Sot basin, E = Muaywadee2 basin, G = Mae Lamao basin.

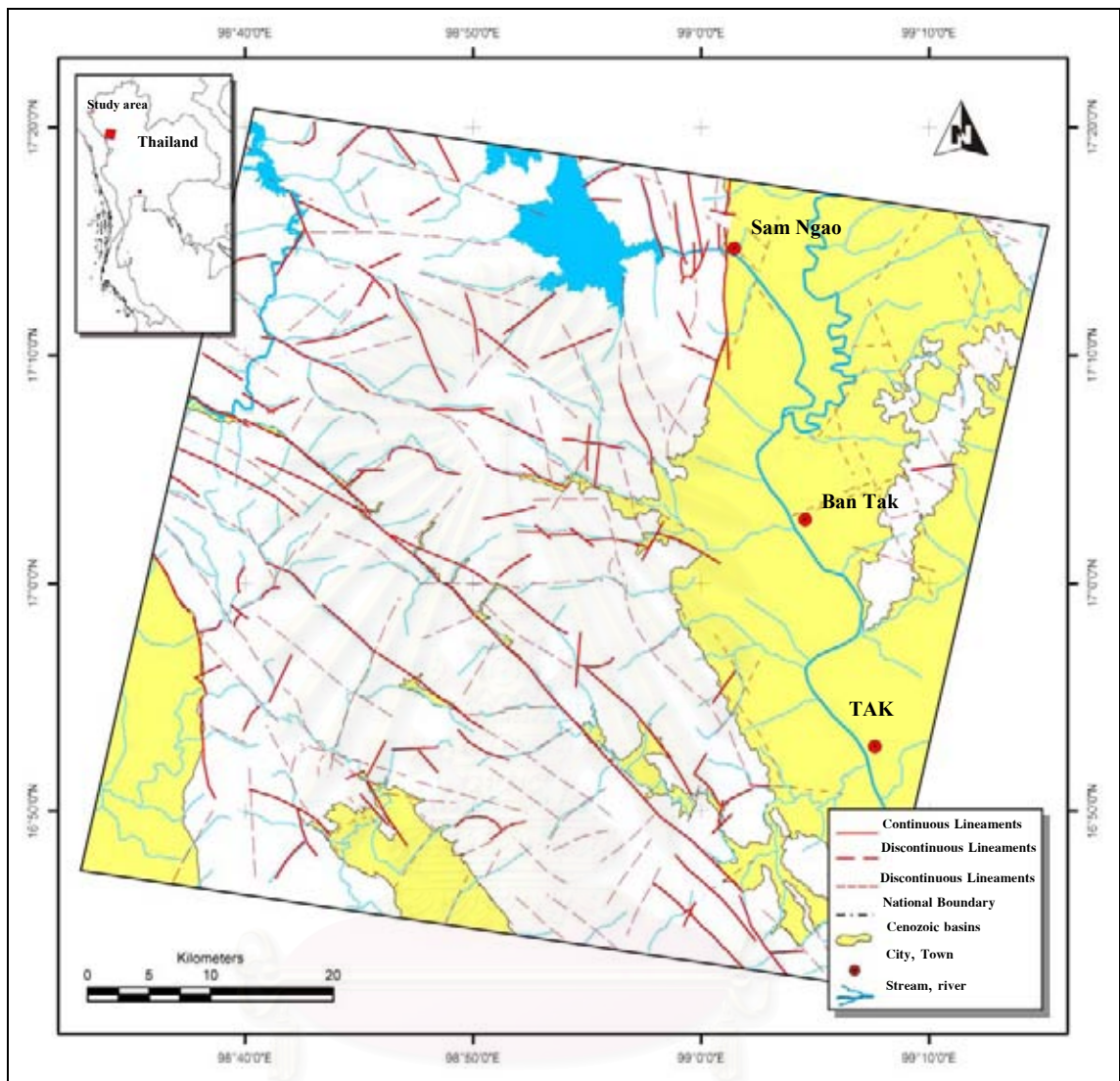


Figure 3.10 Lineaments and distribution of Cenozoic basins in central and southern parts of the study area interpreted using the enhanced JERS SAR image (from Figure 3.5).

จุฬาลงกรณ์มหาวิทยาลัย

order to work on fault segmentation approach such as geometric, structural, geophysical, and geological criteria. McCalpin (1996) had summarized criteria for fault segmentation into five types (Table 3.1). According to new criteria of fault segmentation have arisen, one fault has been segmented by various authors depending upon different criteria. For example, the San Andreas Fault was divided into segments by at least four authors (Table 3.2).

In Thailand, the term “fault segmentation” was first introduced by Fenton et al. (1997) and at least two geologists who show the supporting evidences for fault segmentation, that are – Won-in (1999) and Kosuwan et al. (1999). According to Fenton et al. (1997), two active faults in northern basin and range provinces of Thailand are recognized by fault segmentation, including the Thoen Fault in Changwat Lampang and the Pua Fault in Changwat Nan. Criteria used for segmentation comprise geomorphic feature, structural style, and sense of offset.

Won-in (1999) divided the Three-Pagoda fault in western Thailand into five segments based on structural, geologic, and geometric criteria. Kosuwan et al. (1999) divided the Mae Chan fault zone in Changwat Chiang Rai into four segments based on similar criteria to those of Won-in (1999). According to Udchachon (2002), the study area in the Phare basin, based on remote-sensing, seismicity and field data, at least four fault segments within the Phrae fault system have been discovered, namely, the Southwestern, Western, Southeastern, and Northeastern segments.

### 3.2.2 Results of Fault Segmentation

The advent of satellite-image study is used to assist in delineating the large-scale deformation features and to define the fault segmentation. The latter involves the identification of individual segments that appear to have continuity, character, and orientation. Delineation of segments involves identification of discontinuities in the fault zone. In the present study, four criteria for subdividing discontinuities of faults are applied, including

- (1) earthquake discontinuity, for example, historic rupture, earthquake distribution;
- (2) geometric discontinuity, for example, sense of movement, intersection, segment branch, termination, orientation;
- (3) geologic discontinuity, for instance, those bounded by Quaternary basins and geophysical anomalies; and

Table 3.1 Type of fault segments and the characteristics used to define them (After McCalpin, 1996)

Type of Segment <sup>a</sup>	characteristics used to define the segment <sup>a</sup>	Likelihood of being An earthquake segment <sup>b</sup>
1. Earthquake	Historic rupture limits.	By definition, 100% <sup>c</sup>
2. Behavioral	1) Prehistoric rupture limits defined by multiple, well-dated paleoearthquakes. 2) Segment bonded by changes in slip rates, recurrence intervals, elapsed times, sense of displacement, creeping versus locked behavior, fault complexity.	High  Mod. (26%)
3. Structural	Segment bounded by fault branches, or intersections with other faults, folds, or cross-structures.	Mod.-High (31%)
4. Geologic	1) Bounded by Quaternary basins or volcanic fields. 2) Restricted to a single basement or rheologic terrain. 3) Bounded by geophysical anomalies. 4) Geomorphic indicators such as range-front morphology, crest elevation.	Variable <sup>d</sup> (39%)
5. Geometric	Segments defined by changes in fault orientation, stopovers, separations, or gaps in faulting.	Low-Mod. (18%)

<sup>a</sup> Classification follows the segment boundary types of dePolo et al. (1989, 1991) and Knuepfer (1989).

<sup>b</sup> Percentages = percent of cases where historic ruptures have ended at this type of boundary, as opposed to rupturing through it (Knuepfer, 1989, Table 3).

<sup>c</sup> However, restriction of a single historic rupture to the segment does not mean that all future ruptures will be similarly restricted.

<sup>d</sup> Small number of observations, accuracy questionable (Knuepfer, 1989, Table 3).

Table 3.2 Fault segment lengths proposed for active fault by various authors (After McCalpin, 1996)

Fault name	Type <sup>a</sup>	Number of segments	Total fault length (km)	Mean segment length (km)	Modal segment length (km)	Criteria used for recognition <sup>b</sup>
1. Wasatch fault zone <sup>c</sup>	N	10	343	33	35	B,P,S,G,M
2. NE Basin and Range, >100 km <sup>c</sup>	N	10	-	25	20-25	B,P,S,G,M
3. NE Basin and Range, <100 km <sup>c</sup>	N	20	-	20	10-20	B,P,S,G,M
4. Idaho <sup>d</sup>	N	20	280	22	20-25	B,P,S,G,M
5. North-central Nevada <sup>c</sup>	N	70	-	10	10	M
6. San Andreas <sup>f</sup>	S	4	980	245	15- 175?	B,S,G,M
6. San Andreas <sup>g</sup>	S	7	980	140	300?	B,P,S,M
6. San Andreas <sup>h</sup>	S	784	980	1.2	1	M
6. San Andreas <sup>i</sup>	S	68	980	14	12	M
7. San Jacinto <sup>j</sup>	S	20	250	12	10-15	M
8. Elsinore <sup>k</sup>	S	7	337	48	-	M,P
9. Xianshuihe <sup>l</sup>	S	1	220	220	-	M
10. Transverse Ranges <sup>m</sup>	R	-	-	20-30	-	M
11. Oued Fodda, Algeria <sup>n</sup>	R	3	32	11	11-12	B,P,S,M

<sup>a</sup>N,normal; S,strike-slip; R,reverse.

<sup>b</sup>B,behavioral; p,paleoseismic;  
S,structure; G,geological; M,geometric.

<sup>c</sup>Machette et al. (1992a).

<sup>d</sup>Crone and Haller (1991).

<sup>e</sup>Wallace (1989).

<sup>f</sup>Allen (1968).

<sup>g</sup>Wallace (1970).

<sup>h</sup>Wallace (1973).

<sup>i</sup>Bilham and King (1989).

<sup>j</sup>Sanders (1989).

<sup>k</sup>Rockwell (1989).

<sup>l</sup>Allen et al. (1989).

<sup>l</sup>Allen et al. (1989).

<sup>m</sup>Ziony and Yerkes (1985).

<sup>n</sup>King and Yielding (1983).

(4) structural discontinuity, for example, intersection with other faults, folds, and cross structures, following the recommendation of McCalpin (1996) (see Table 3.1).

Based upon such criteria gathered from interpretation of enhanced image data applied in the current investigation, ten fault segments are recognized. Those are determined, from north to south, as (1) the Sop Moei segment (22 km), (2) the Huai Mae Lo segment (7.5 km), (3) the Ban Tha Song Yang segment (22 km), (4) the Khao Mae Song segment (25 km), (5) the Huai Mae La segment (35 km), (6) the Doi Kala segment (18 km), (7) the Doi Khun Mae Tho segment (21 km), (8) the Doi Luang segment (14 km), (9) the Khao Yao segment (21 km), and (10) the Khlong Phri segment (14 km). (Figure 3.11).

### 3.3 Tectonic Geomorphology

#### 3.3.1 General

In this section, basic concepts of tectonic geomorphology, related to three types of faults; strike-slip, normal, and reverse faults, are briefly explained. The discussion is followed by the methodology and the results of this thesis study.

Accordingly, structure associated with an idealized strike-slip fault model constructed by Christie-Blick and Biddle (1985), suggested that these fault branches should be the component of shear zone, which are synthetic, secondary synthetic, and antithetic shears (Figure 3.12). All of these shear zone features are accommodated in principal displacement zone (PDZ).

According to strike-slip fault zone, a variety of structure and landforms can be originated by simple shear including fractures, folds, normal faults, thrust faults, and reverse faults as illustrated in Figure 3.13 (Christie-Blick and Biddle, 1985). Naturally, within a broad shear zone, different generations of motion have produced various kinds of these structures, all of which can be superimposed and showed array of structural complexity (Sylvester, 1988). In many strike-slip faults, bending fault trace can be observed at overlapping areas among the adjacent blocks. Therefore, fault movement can create both compressive and tensile stresses into the curve of fault segments. For instance, as shown in Figure 3.14, releasing bend and restraining bend can cause pull-apart basins and uplift features related to tension and compression stresses, respectively (Biddle and Christie-Brick, 1985). In many cases, both pull-apart basins and uplift highs may be explained in term of step-over in which two fault segments have end up, and both showing the same sense of movements.

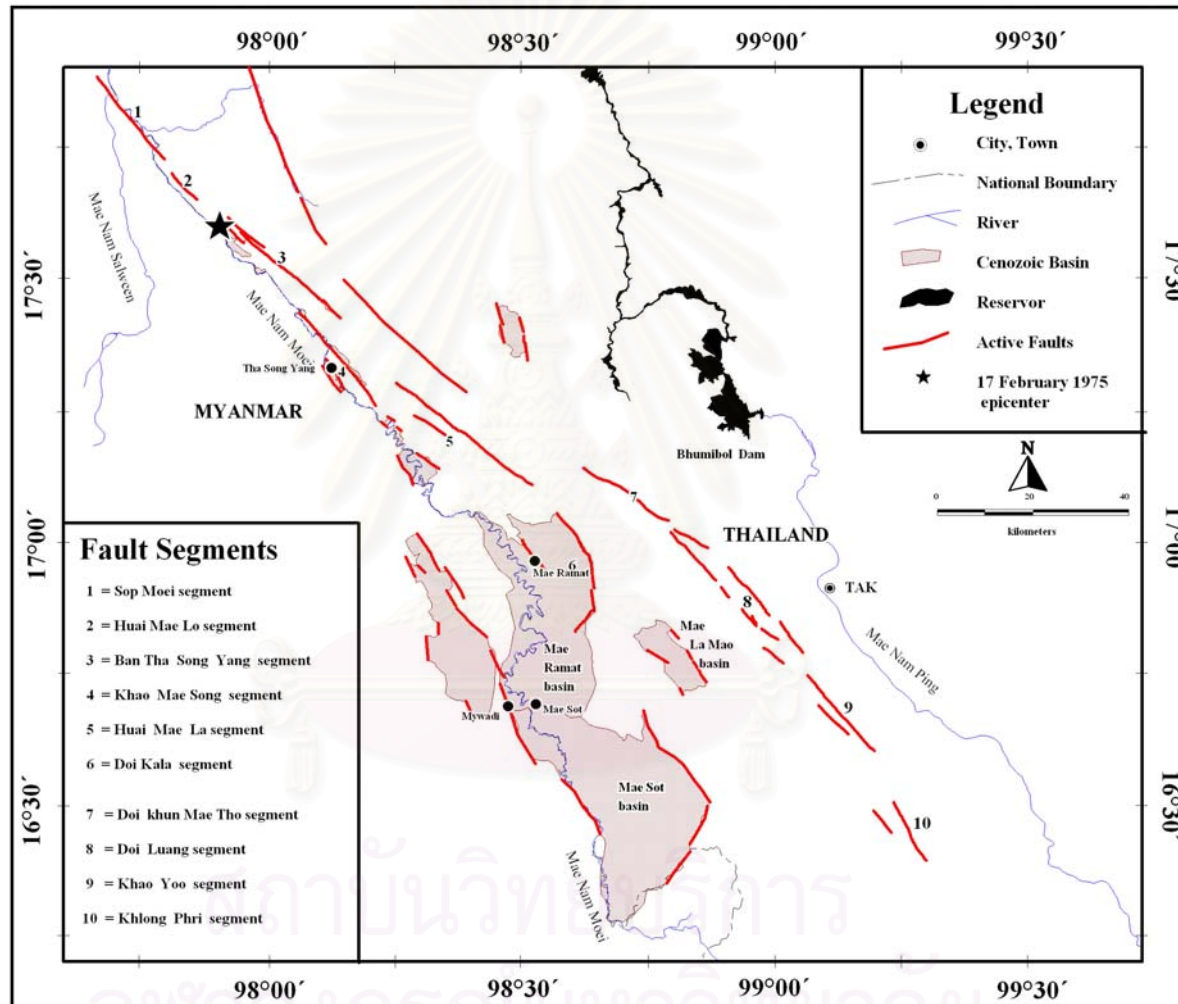


Figure 3.11 Map of the study area displaying locations of the NW-trending Moei-Mae Ping Fault Zone (red line), its major inferred active fault segments, and the 17 February 1975 epicenter.



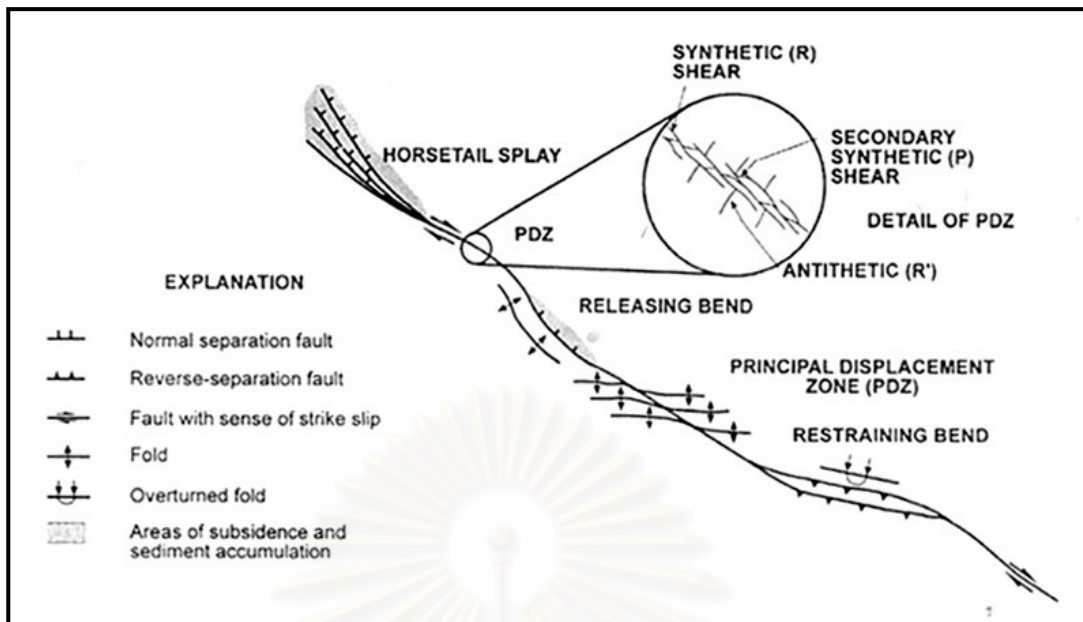


Figure 3.12 Plan view of structure associated with an idealized strike-slip fault (After Christie-Blick and Biddle, 1985).

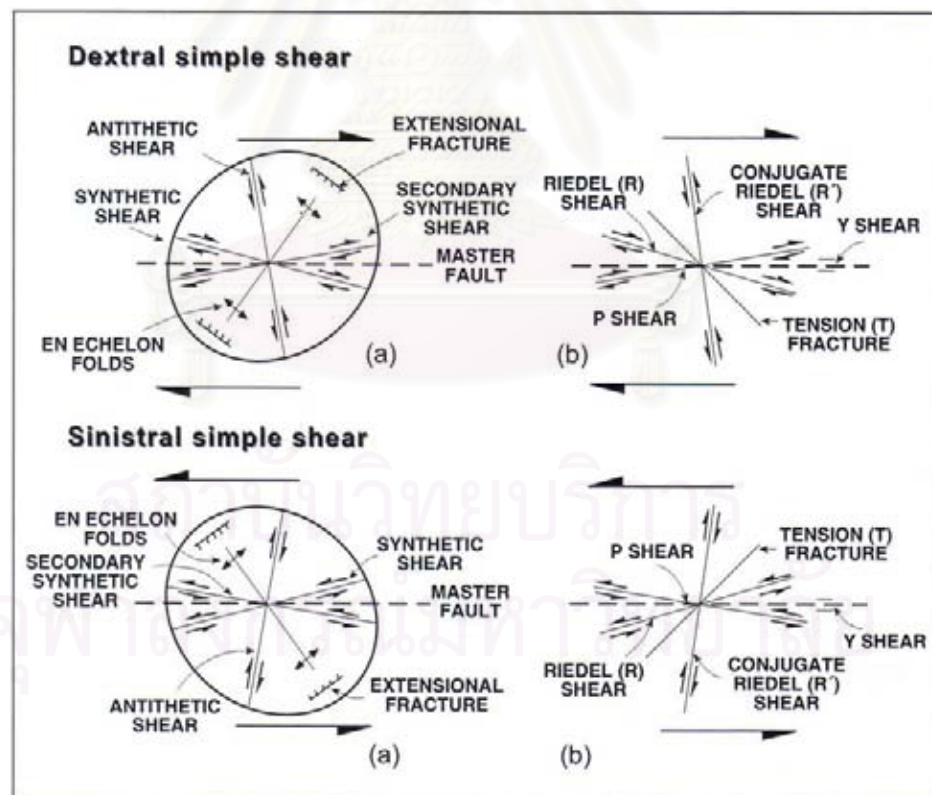


Figure 3.13 Simple shear models associated with strike-slip fault (a) and producing contractional and extensional features (b) (After Christie-Blick and Biddle, 1985).

In conclusion, there are many features of tectonic geomorphology produced by strike slip movement. As shown in [Figure 3.15](#), these features are linear valleys, offset or deflected streams, shutter ridges, sag-ponds, pressure ridges, benches, scarps, and small horsts and garbens (Keller and Pinter, 1996). Noteworthy, fluvial terraces, stream channels, and alluvial fans are typical features used to reconstruct paleoearthquakes offset history (Weldon et al., 1996).

Besides, based on simple shear model illustrating in [Figure 3.13](#), normal fault trace should be formed perpendicular to the direction of maximum elongation and maximum extension stress. [Figure 3.16](#) shows an idealized cross-section of extension tectonic environments. Master fault has bounded the main on the right, accompanied by minor synthetic and antithetic faults. Other structures commonly found in an extension regime are horsts and grabens showing on the left. Depending on tectonic geomorphology on ground surface, typical indicator of normal faulting is a fault scarp (McCalpin, 1996) ([Figure 3.17](#)), which can be developed to form triangular facets when proper condition, such as erosion and repetition of active fault movement has reached ([Figure 3.18](#)). In addition, other evidence of extension environments includes linear-range fronts, escarpments, volcanic flows and cones, rift valleys, and axial rifts of oceanic ridge systems (Keller and Pinter, 1996).

Lastly, tectonic landforms associated with reverse faulting include belt of active folding and faulting, steep mountain fronts, and fault scarps. The elongated axis of these structures is usually found lied perpendicular to the direction of maximum compressive stress axis as show in [figure 3.14](#). The most common geomorphic evidence of compression tectonism in continent is fault scarp (Carver and McCalpin, 1996). Based on historical surface ruptures in Armenia, 1988 earthquake, seven types of thrust fault scarp morphology have been conducted by Phillip et al. (1992) ([Figure 3.19](#)).

Fenton et al. (1997) revealed several tectonic geomorphologies found along seven faults in northern basin and range province of Thailand. These morphologies include linear-range fronts, triangular facets, offset drainages, stream knick points, wine-glass canyons, and scarps. Won-in (1999) mentioned that fault scarps, triangular facets, offset stream channels, shutter ridges, beheaded streams, pressure ridges, fault trace cutting terraces, basin development, parallel ridges, and uplift river gravel deposit are observed along the Three-Pagoda fault zone. Kosuwan et al. (1999) stated that several tectonic geomorphologies, such as offset streams, sag ponds, shutter ridges, and benches, and river terraces on young alluviums/colluviums, were observed along the Mae Chan fault zone.

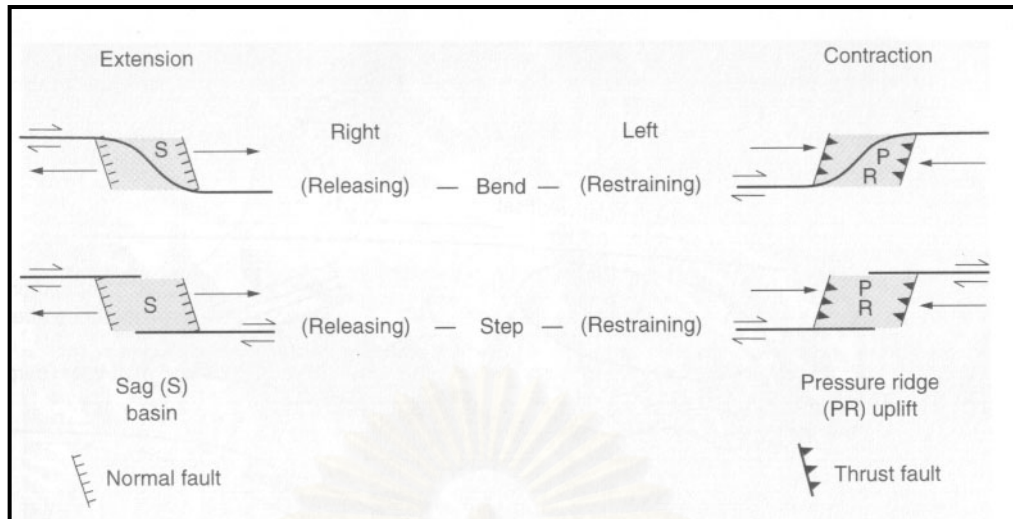


Figure 3.14 Sags and pressure ridges associated with bends and steps along strike-slip faults (After Keller and Pinter, 1996).

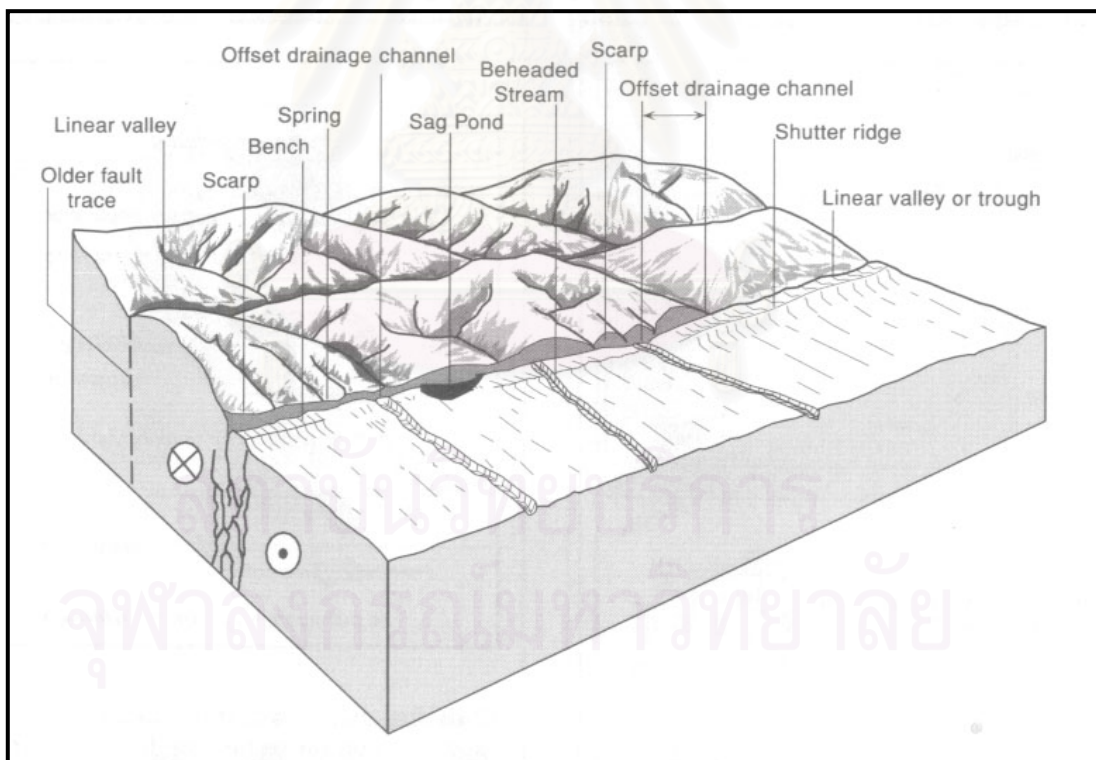


Figure 3.15 Assemblage of landform associated with active tectonic strike-slip faulting (After Burbank and Anderson, 2001).

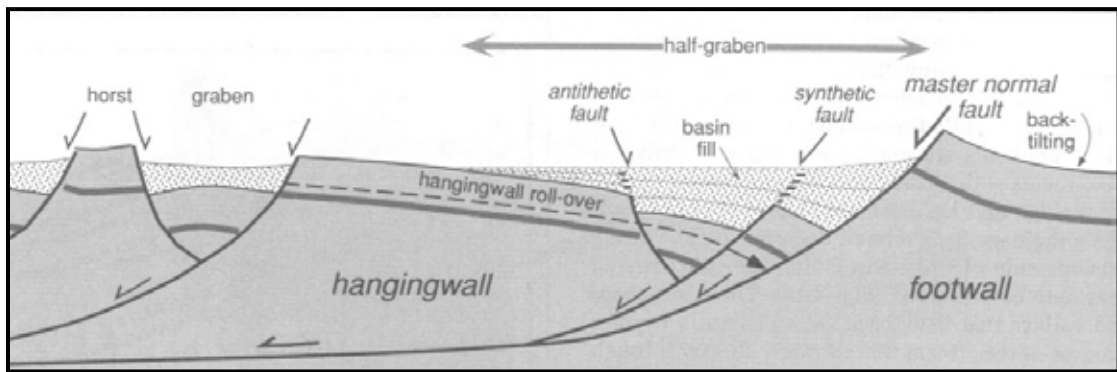


Figure 3.16 Idealized cross-section of extension tectonic environments (After Burbank and Anderson, 2001).

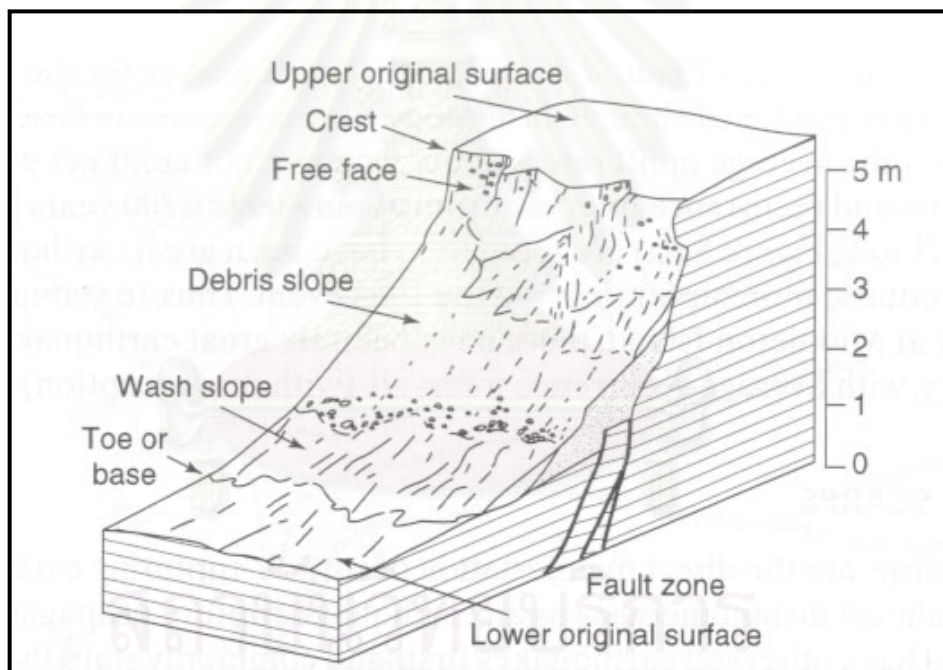


Figure 3.17 Basic slope elements that may be present on a fault scarp (After McCalpin, 1996).

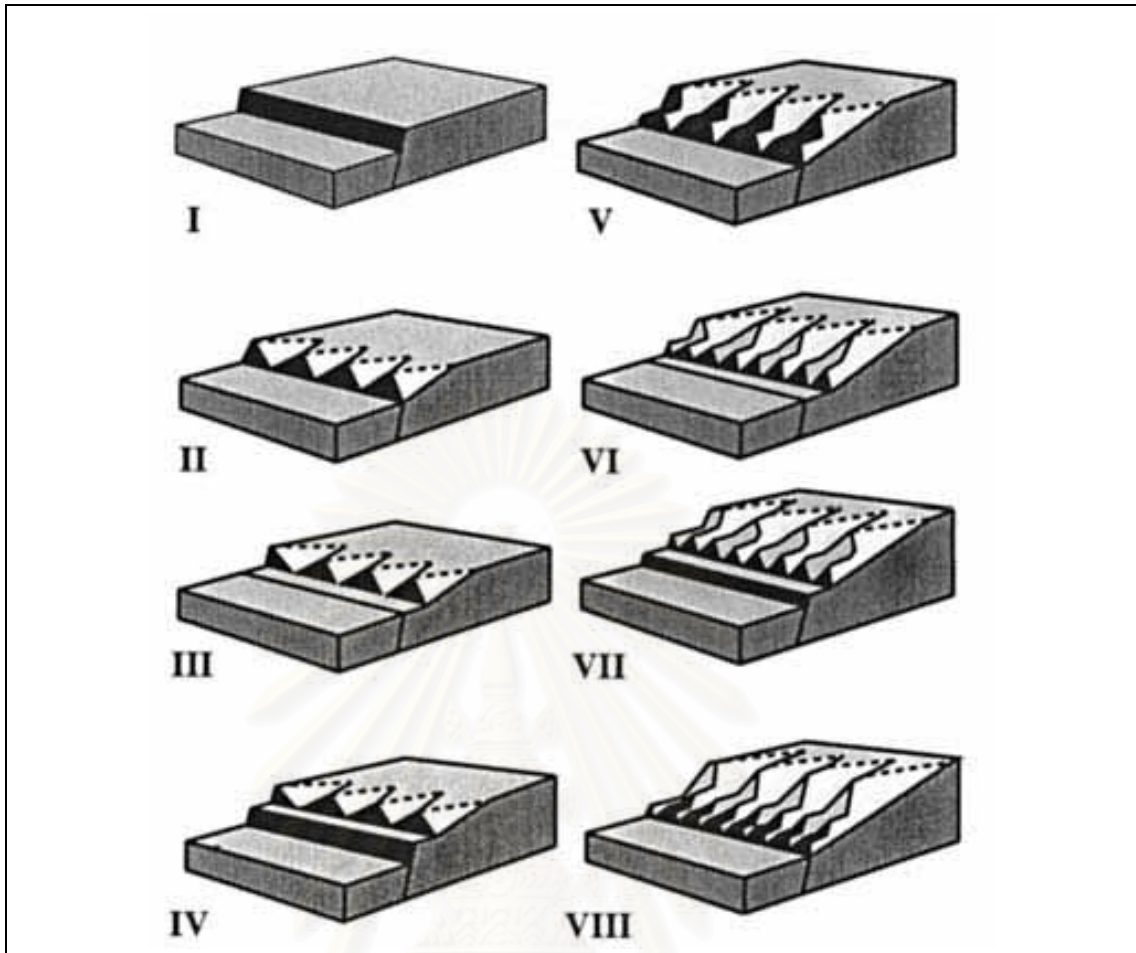


Figure 3.18 Development of triangular facets produced by episodic vertical tectonic movement (After Fenton et al., 1997).

I: Undissected fault scarp.

II: development of faceted spurs by stream cutting across the fault scarp.

III: period of tectonic quiescence with slope retreat, and development of narrow pediment.

IV: renewed fault movement.

V: dissection of the new fault scarp by major streams and streams developed on the faces of the facet spurs developed at stage II.

VI: a new period of tectonic quiescent, with the development of another narrow pediment within the footwall block at the base of the range front.

VII: renewed fault movement.

VIII: dissection of the fault scarp produced at stage

VII resulting in the line of small facet spurs at the base of the range front.

Remnants of narrow pediments (benches) are preserved at the apices of each set of faceted spurs. Progressive slope retreat is accompanied by a decrease in the slope angle of the faceted spurs.

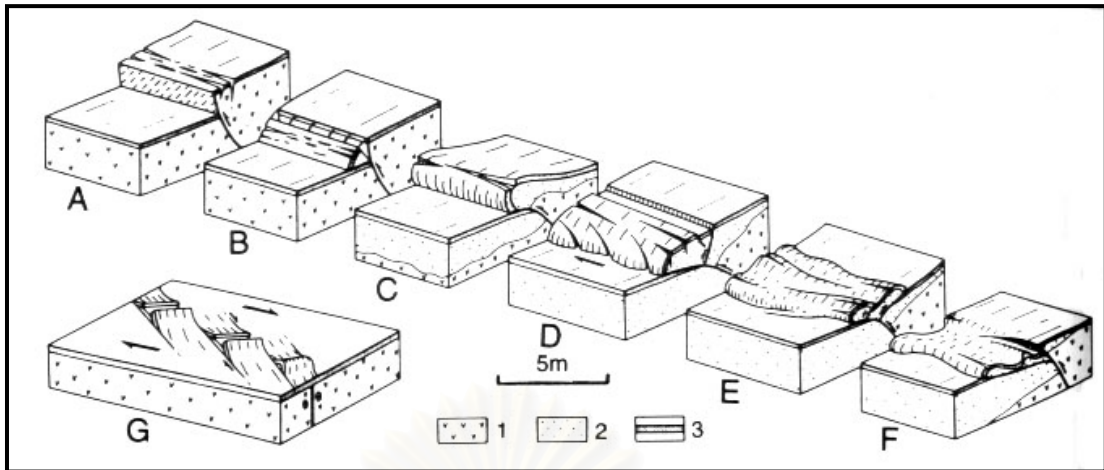


Figure 3.19 Types of reverse fault scarps. (A) Simple reverse (or thrust) scarp. (B) Hanging-wall collapse scarp. (C) Simple pressure ridge. (D) Dextral pressure ridge. (E) Back-thrust pressure ridge. (F) Low-angle ridge. (G) En-echelon pressure ridge. 1, bed rock; 2, soft Quaternary sediments; 3, turf (After Phillip et al., 1992).

สถาบันวิทยบริการ  
จุฬาลงกรณ์มหาวิทยาลัย

### 3.3.2 Results of Tectonic Geomorphological Study

Based on results of lineament analysis by satellite images, several selected areas for aerial photographic investigation are revealed. Regarding the result of air-photo interpretation, at least eight areas are outstanding namely; areas A, B, C, D, E, F, G, and H (Figure 3.20), and significant symbols used for the interpreted maps are shown in Figure 3.21. Two segments are omitted in this study due to they are difficult to access.

#### 3.3.2.1 Area A, Ban Sop Moei, Amphoe Sop Moei, Changwat Mae Hong Son.

The result from aerial-photographic interpretation at the area of Ban Sop Moei along the northwest-southeast trending Sop Moei segment (segment 1) is shown in Figure 3.22. Important tectonic geomorphologic features are sets of triangular facets. The first set consists of six triangular facets which have about 4.5 km average base width, and about 400 m average height from the base with  $60^\circ$  dipping. The second set comprises four triangular facets, of about 1.75 km average base width, and about 180 m average height from the base with  $40^\circ$  dipping. The third set shows seven triangular facets, of about 2.5 km average base width, and average about 220 m height from the base with  $45^\circ$  dipping. However, these facet spurs have their slope angles dip to the northeast direction.

In the western part of Mae Nam Salween, the set of small offset streams indicate right-lateral movements about 150 m, 750 m, and 500 m, respectively, and Huai Bo Kro has its flow direction from southwestward and offset to northwestward before joining the Mae Nam Salween.

The results from aerial photographic interpretation in the Ban Sop Moei area illustrate that the Sop Moei fault segment is nearly continuous and has a length of 25 km, with 16 km lies in Thailand.

#### 3.3.2.2 Area B, Ban Tha Song Yang, Amphoe Tha Song Yang, Changwat Tak.

At the area of Ban Tha Song Yang, aerial-photographic analysis reveals several features of morphotectonic evidences along the 27.5 km long (Figure 3.23), Ban Tha Song Yang fault segment (segment 3). Supporting features include the offset streams, shutter ridges, linear valleys, and fault scarps. The outstanding offset stream observed in this area is the Huai Ma Nok, southeastward of Ban Tha Song Yang. Its flow direction changes from northeastward to southwestward before joining the main Mae Nam Moei. A right-lateral movement caused about 50 m stream shift. A similar situation occurs at the

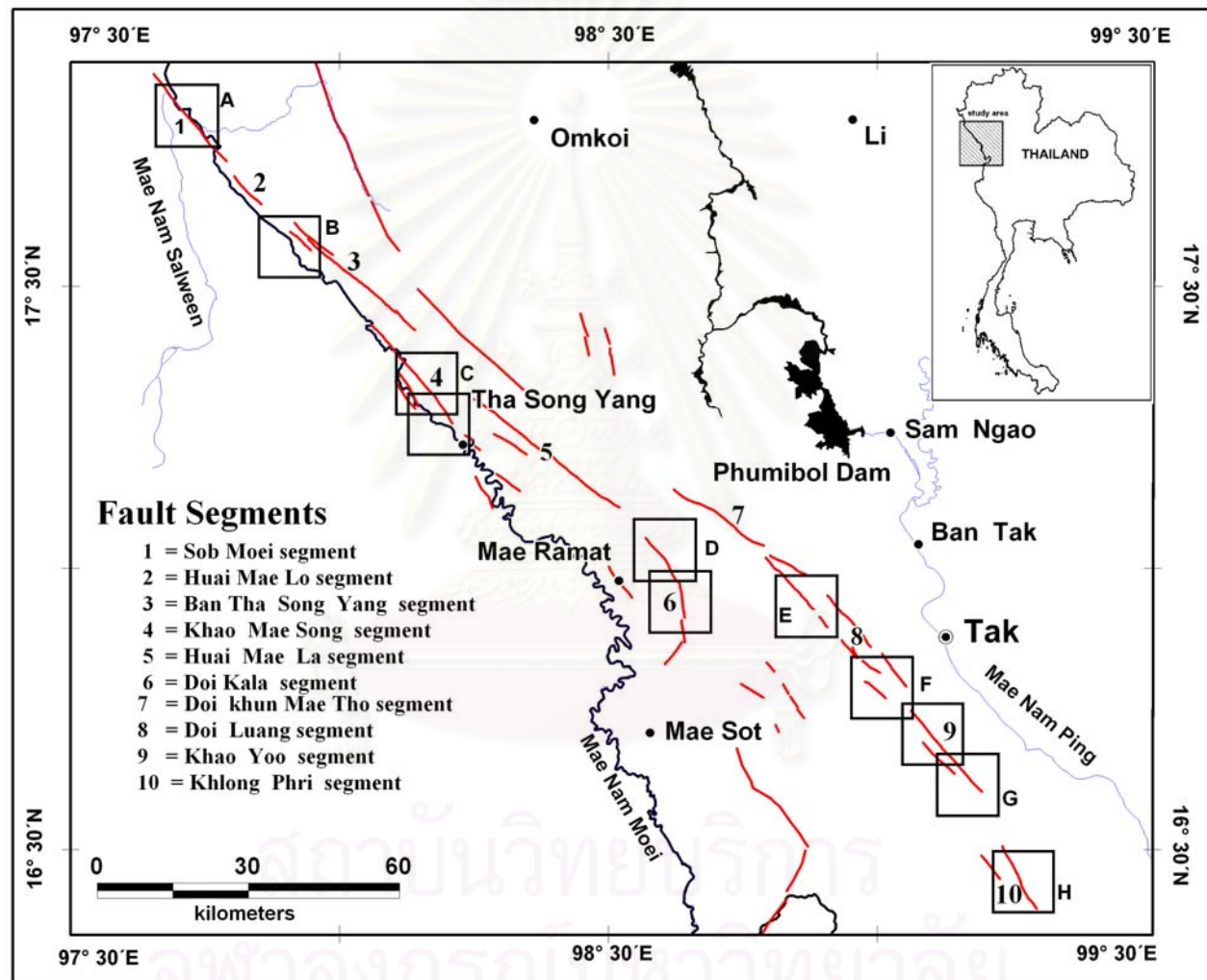


Figure 3.20 Map showing locations of the Moei-Mae Ping Fault Zone (MPFZ, red line) and its major inferred active fault segments. Boxes with numbers indicate selected areas for remote-sensing and aerial photographic interpretations, and detailed paleoseismic studies.



## Symbols

●	<b>Ban</b>
- - -	<b>Boundary</b>
~ ~ ~	<b>Stream, river</b>
⬢	<b>Basin</b>
—	<b>Fault continuity</b>
- - -	<b>Fault discontinuity</b>
◆ ◆ ◆ ◆	<b>Ridge continuity</b>
▲ ▲ ▲ ▲	<b>Ridge discontinuity</b>
┌ ┌ ┌ ┌	<b>Scarp</b>
▲ ▲	<b>Triangular facets</b>
—	<b>Boundary rock unit</b>
T	<b>Triangular facet</b>
S	<b>Fault scarp</b>
R	<b>Shutter ridge</b>
L	<b>Linear valley</b>
O	<b>Offset stream</b>

Figure 3.21 Symbols used as guidelines for descriptions appearing in the interpreted morphotectonic maps (in Figures 3.22-3.32).

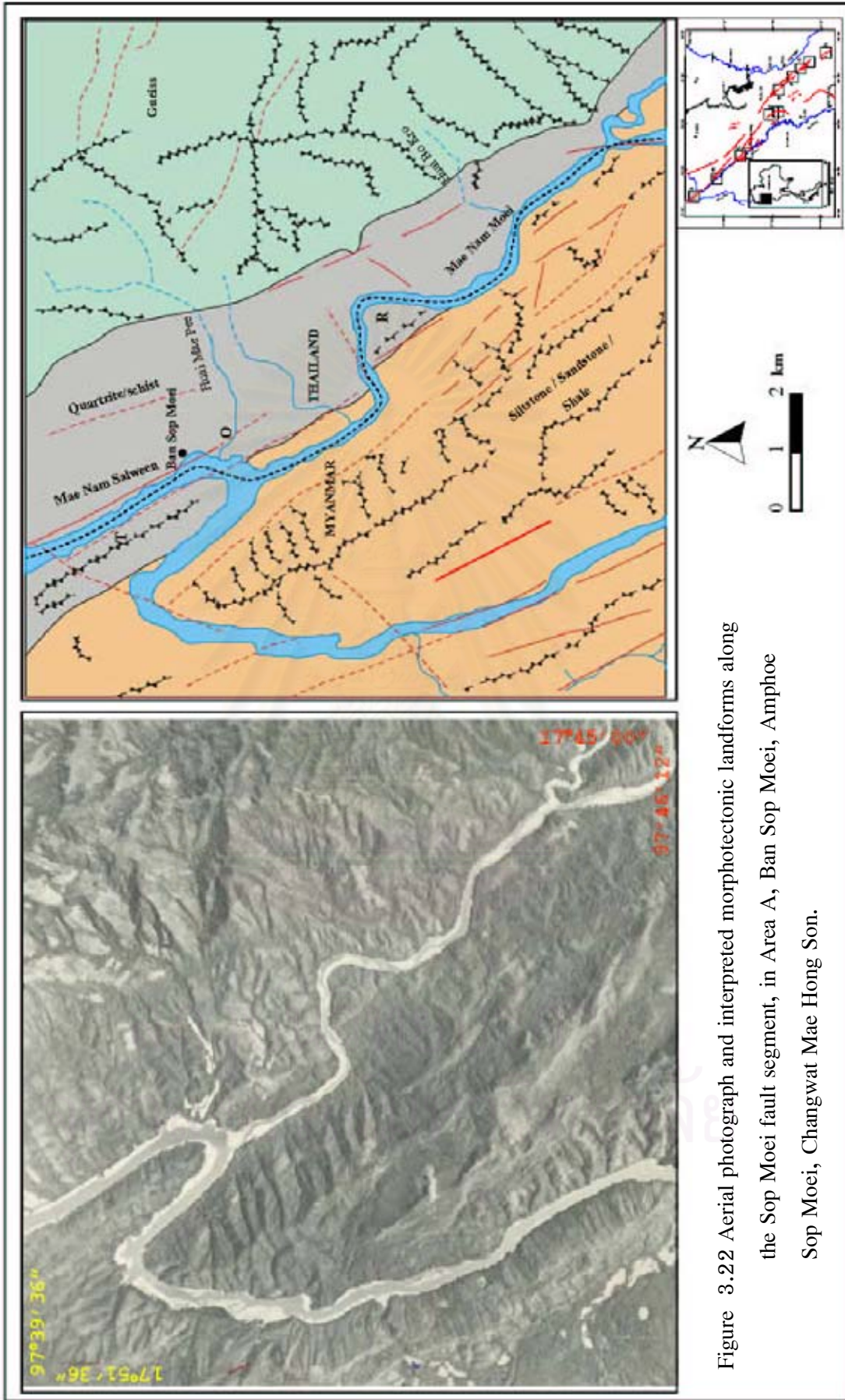


Figure 3.22 Aerial photograph and interpreted morphotectonic landforms along the Sop Moei fault segment, in Area A, Ban Sop Moei, Amphoe Sop Moei, Changwat Mae Hong Son.

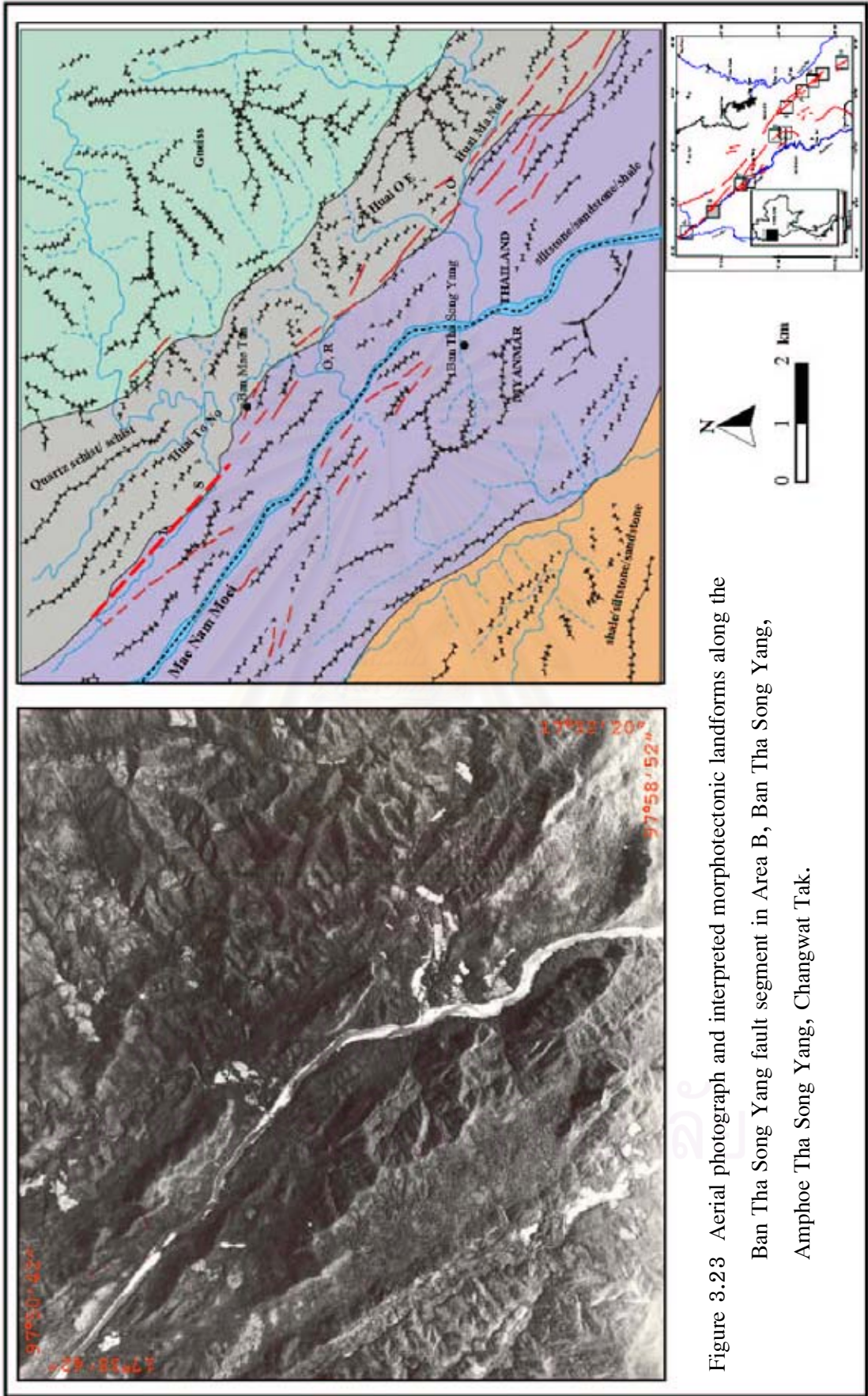


Figure 3.23 Aerial photograph and interpreted morphotectonic landforms along the Ban Tha Song Yang fault segment in Area B, Ban Tha Song Yang, Amphoe Tha Song Yang, Changwat Tak.

Huai To No which its movement probably caused about 500 m stream shift. The occurrence of the northwest–southeast trending shutter ridge of about 200 m average base width and about 65 m height is from the base has been observed (S in Figure 3.23). A fault scarp obviously observed from vertical limestone cliff at Ban Pha Man, and rather continuous. The plane of this fault scarp strikes in the northwest–southeast direction, following the main fault. In some places, the fault planes dip steeply to the northeast. The Nam Mae Tun northwestward of Ban Tha Song Yang and Huai O E at Ban Tha Song Yang occupy the linear valley structure, which is controlled by the northeast–trending fault (L in Figure 3.23).

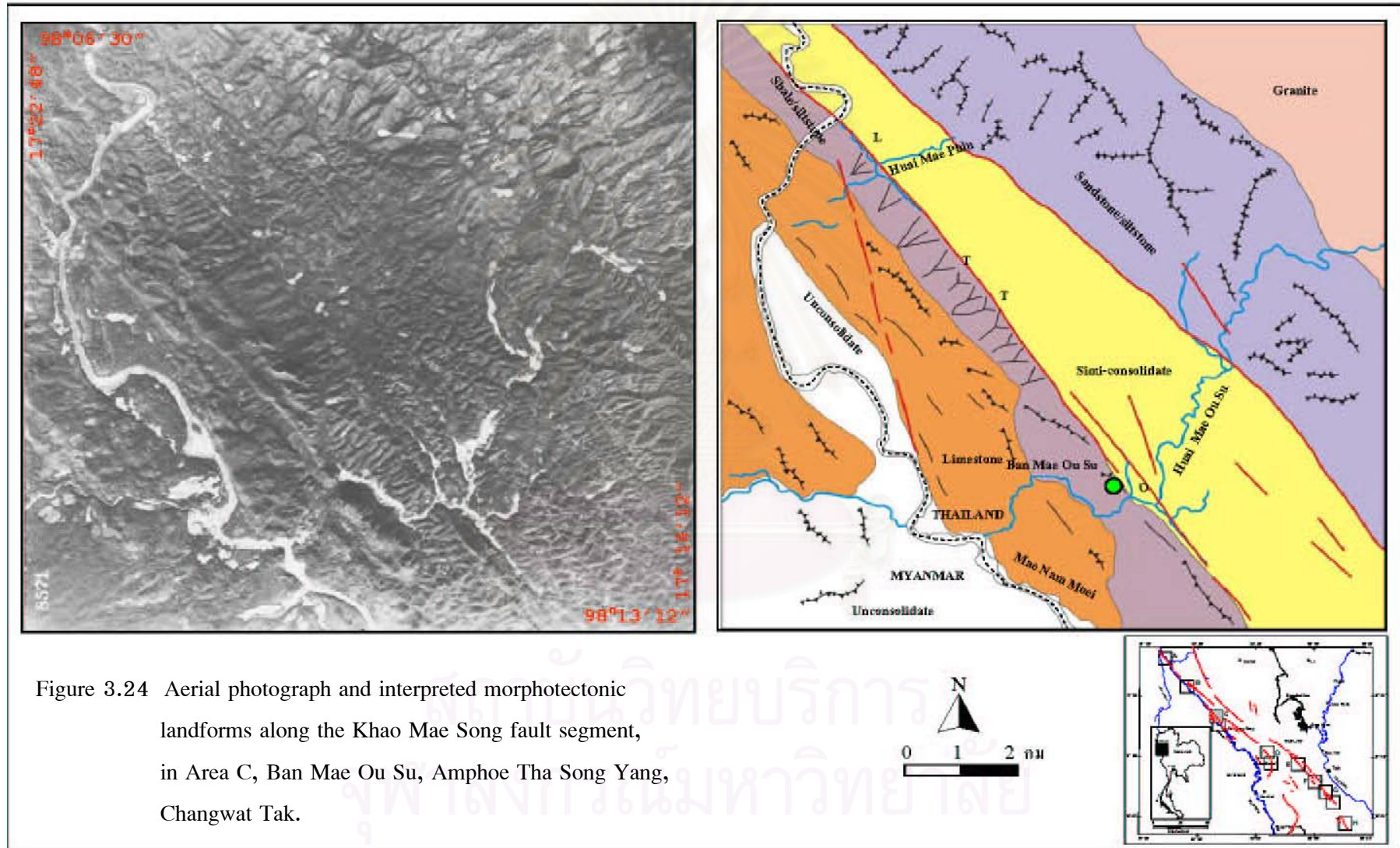
#### **3.3.2.3 Area C, Ban Mae Ou Su, Amphoe Tha Song Yang, Changwat Tak.**

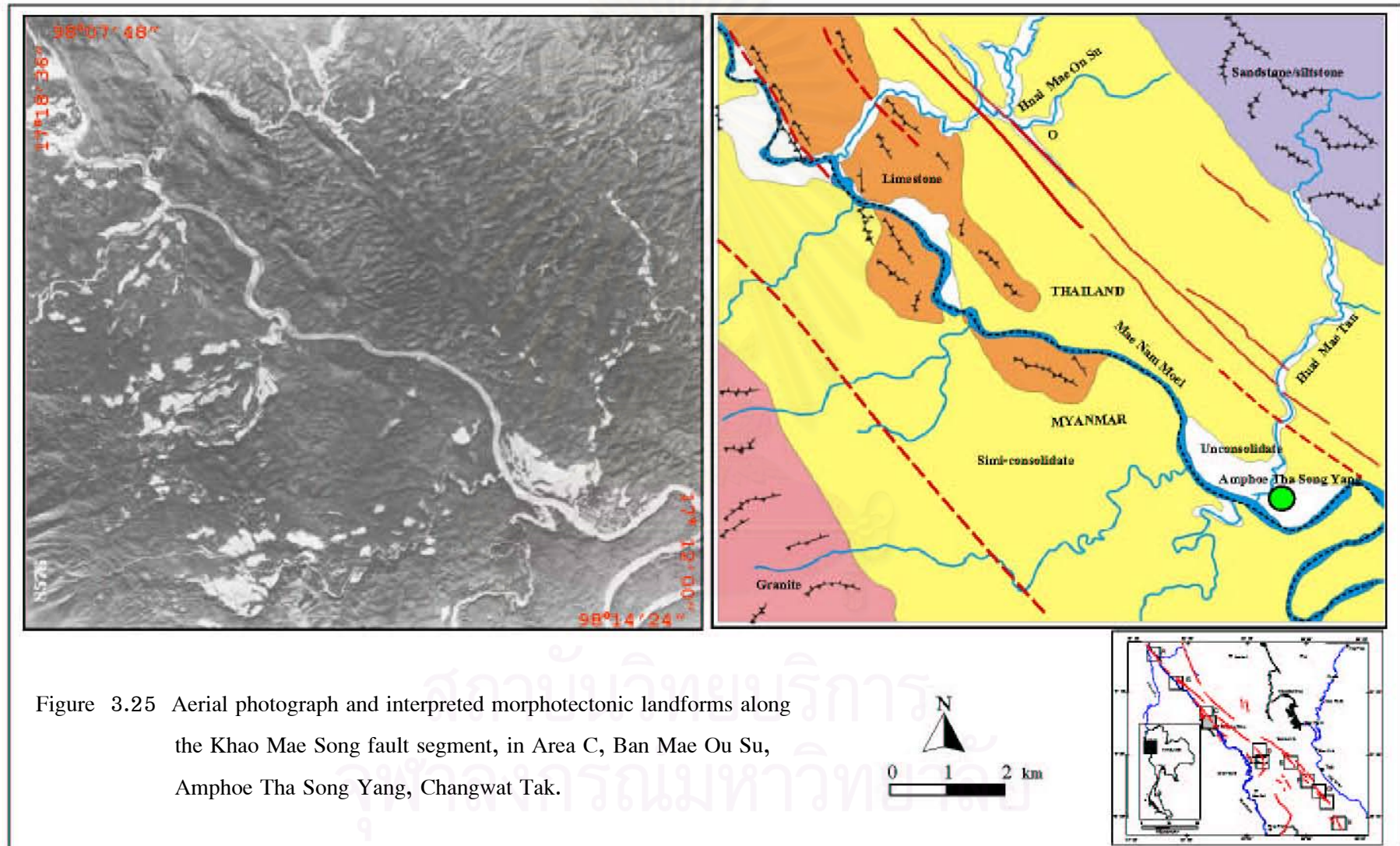
The result from remote–sensing interpretation indicates the major trend of lineaments and faults along the MPFZ in the northwest–southeast direction continuous from Mae Nam Moei (Figure 3.24). The aerial–photographic analysis shows the morphotectonic evidence of offset stream along Huai Mae Phlu and Huai Mae Ou Su offset about 500 m. The set of 11 triangular facets can be delineated. The average base width is about 12.5 km and the average height is about 220 m from the base with  $45^\circ$  faceted spurs dipping to the northeast direction. The linear valley lies in front of these triangular facets. Its trend is parallel to the main fault and directly flows to the Mae Nam Moei at Ban Mae Phlu.

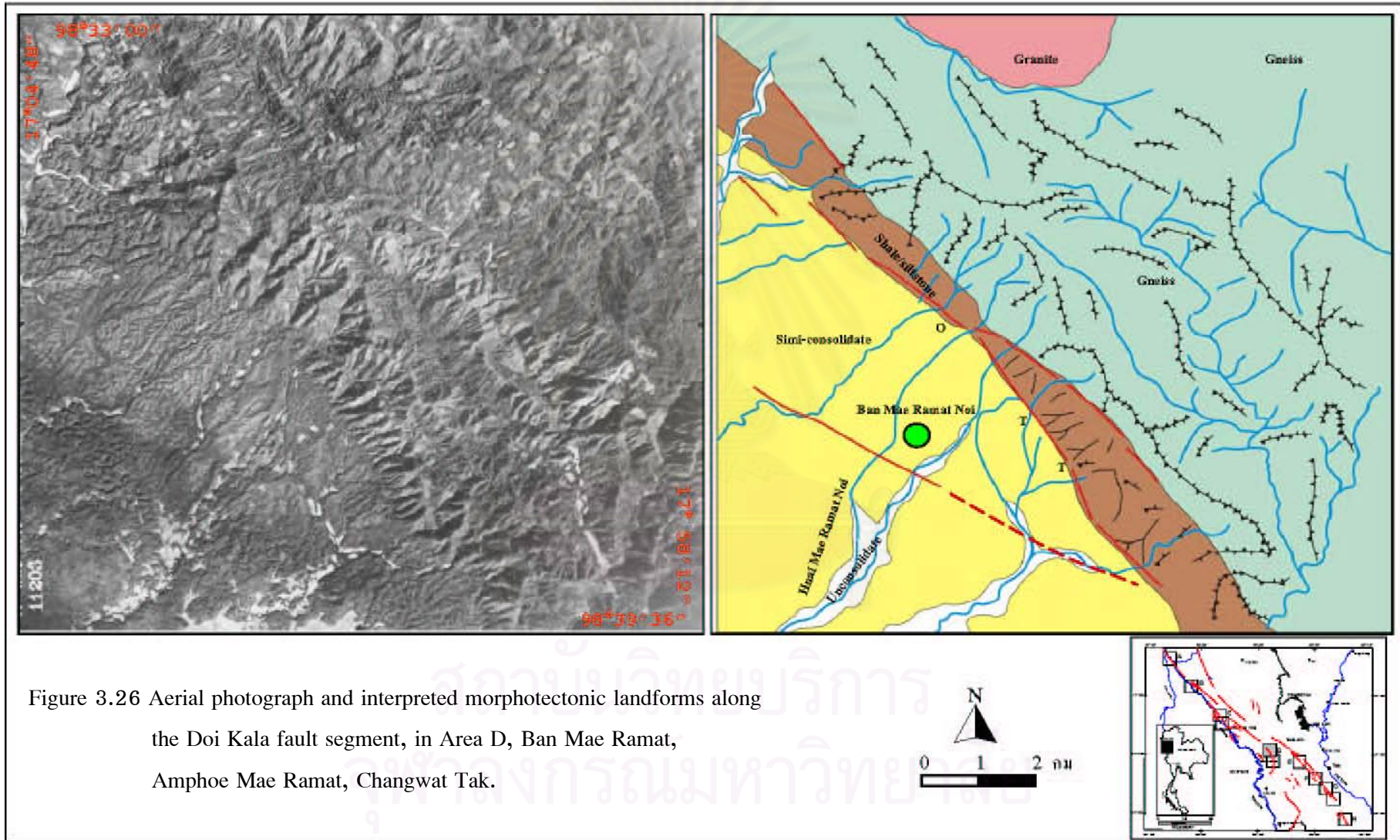
Lying along the middle portion of the aerial–photograph, there exists a northwest–southeast trending fault contact between the Triassic and Quaternary units. At the area of Ban Nong Bua, near the Mae Nam Moei, a trend of Permian Limestone with a length of 9 km acts as the fault scarp, which spur dips to the southwest direction. In the southern part of Ban Mae Ou Su, (Figure 3.25) morphotectonic evidence shows a stream of linear valley characteristic which is parallel to the fault that cut young sediment deposit of Huai Mae Ou Su and Huai Mae Tan. The result from aerial–photographic analysis reveals several features of morphotectonic evidences along the Khao Mae Song fault segment (segment 4), and indicates two fault sub–segments which have the lengths of 25 km and 14 km.

#### **3.3.2.4 Area D, Ban Mae Ramat, Amphoe Mae Ramat, Changwat Tak.**

At the Ban Mae Ramat area in the Mae Ramat Cenozoic basin, the Doi Kala fault segment (segment 6) orients in a similar direction to that of the satellite image, viz. northwest–southeast and north–south (Figures 3.26 and 3.27). Several types of morphotectonic evidences are recognized, such as offset streams, triangular facets, and fault scarps. The Huai Mae Ramat Noi displays the offset of about 100 m with the sinistral







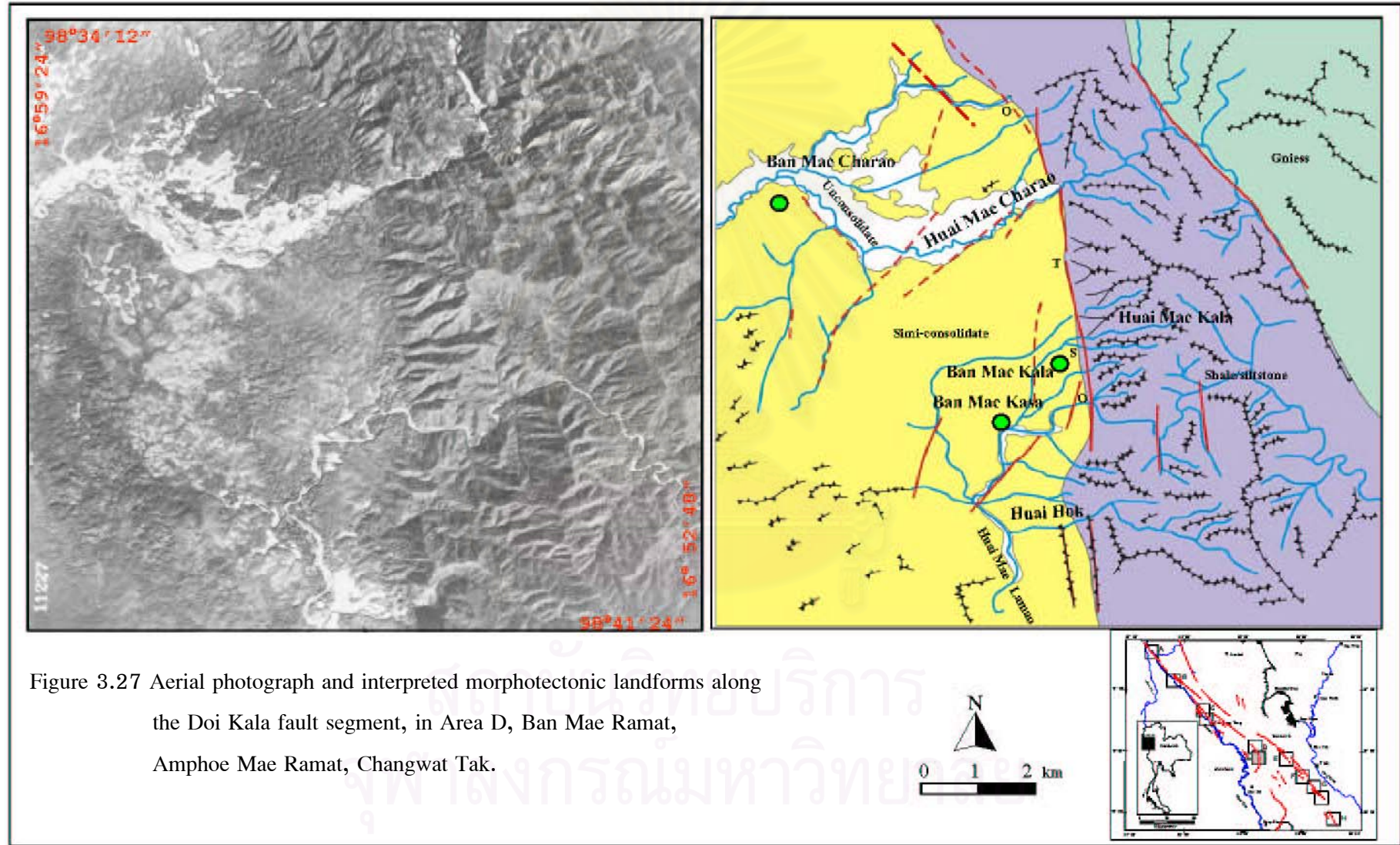


Figure 3.27 Aerial photograph and interpreted morphotectonic landforms along the Doi Kala fault segment, in Area D, Ban Mae Ramat, Amphoe Mae Ramat, Changwat Tak.



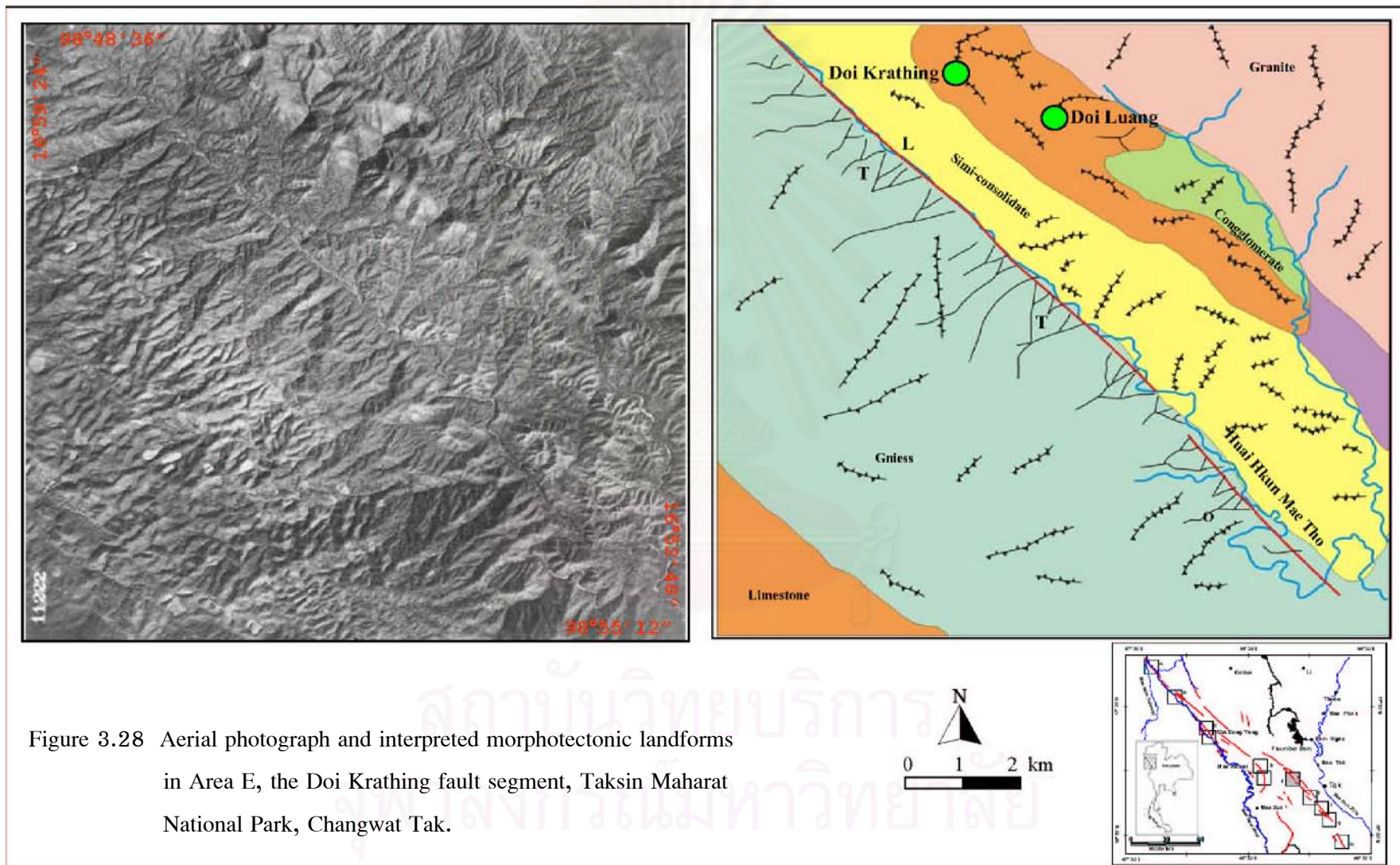
sense of movement, and its flow direction deviates from northeastward to southwestward. At the Huai Mae La Mao, the flow direction changes from the east to west in the Mae Ramat Cenozoic basin and caused about 700 m stream shift. Other small streams, such as the Huai Kala, the Huai Mae Kasa and the Huai Hok, abruptly change their directions from east to west with a right-lateral movement causing the offset of streams (O in Figure 3.26) of about 100 m. Along the fault, a set of triangular facets shows the average base width of about 3 km and the average height of about 140 m from the base. This facet spur dips at high angle to the southwest direction.

The fault of eastward of Mae Ramat Cenozoic basin gives rise to the development of a set of west-dipping triangular facets with the average base width of about 2 km and the average height of 250 m from the base. The fault scarps near Ban Mae Kasa, clearly observed in limestone terrain, particularly are nearly vertical and rather continuous. The fault scarp has a base width of about 2 km and the average height of 500 m. The plane of this fault scarp strikes in a north-south direction, following the main MPFZ. In some places, the fault planes dip very steeply to the west. The Doi Kala fault segment has a length of 23 km.

#### **3.3.2.5 Area E, Doi Krathing, Taksin Maharat National Park, Changwat Tak.**

The Doi Krathing, western past of Tak town-ship, is in the vicinity of MPFZ belonging to the 31 km long Doi Luang fault segment (segment 8). Interpretation by aerial-photographs demonstrates its main traceable northwest-southeast direction similar to that observed in the satellite image. Morphotectonic evidences indicate that the active tectonic morphology includes offset streams, linear valley, and triangular facets (Figures 3.28 and 3.29). Along the northwest-southeast fault, a set of triangular facets about 15.5 km average base width and of about 240 m average height from the base can be recognized. This facet spurs dips to the northeast direction indicating to its normal fault nature. In front of the triangular facets the feature of linear valley of Huai Khun Mae Tho which is parallel to the fault can be identified. In the northern part, a set of triangular facets reveals its landforms of about 10 km average base width and of about 240 m average height from the base. These facets spur dips to the southwest direction indicating its normal fault characteristic.

At the Lan Sang National Park, southern part of Doi Krathing (Figure 3.29), there exists a set of triangular facets showing the average base width of about 10 km and the average height of about 220 m from the base. This facet spurs dip to the northeast



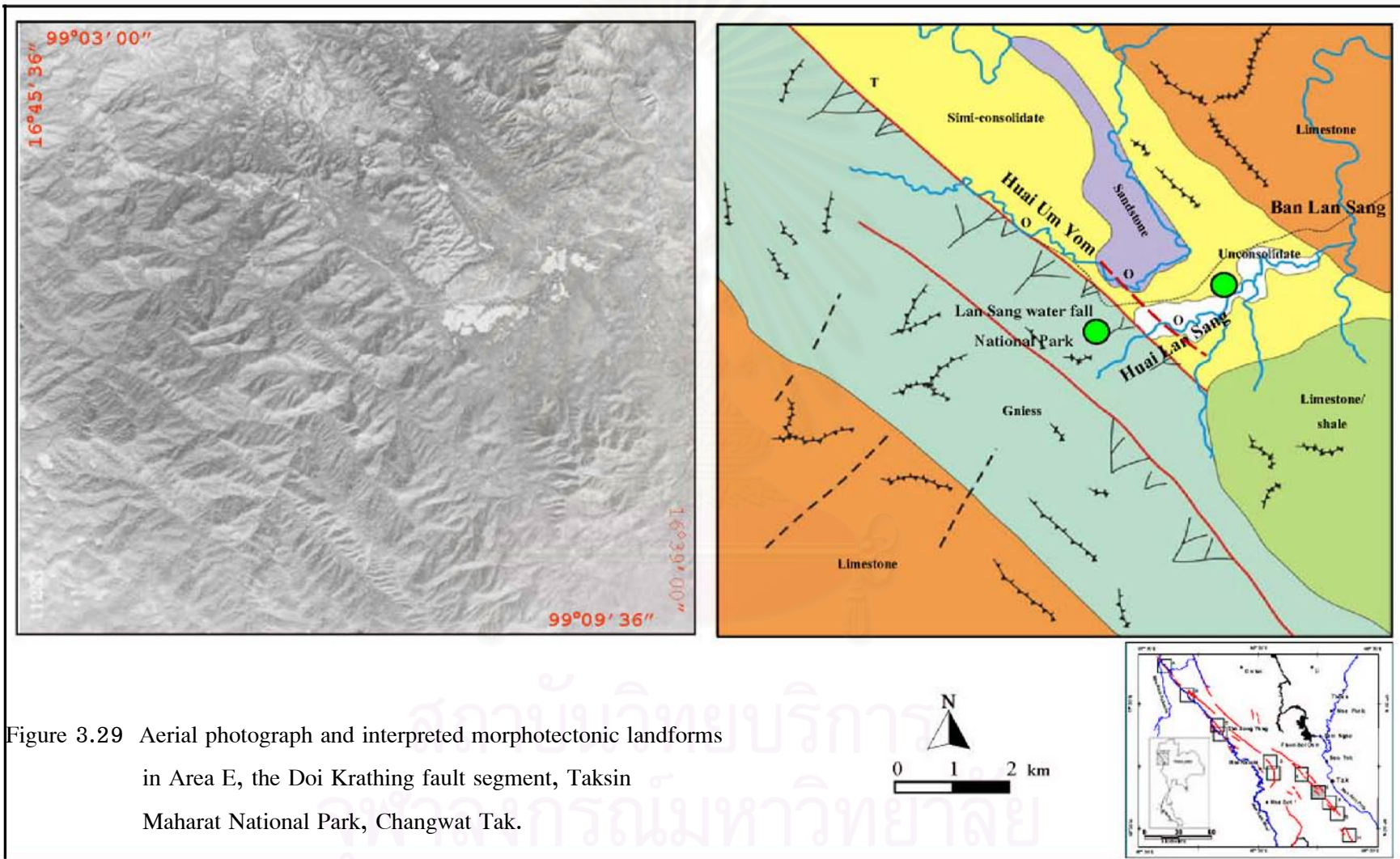


Figure 3.29 Aerial photograph and interpreted morphotectonic landforms in Area E, the Doi Krathing fault segment, Taksin Maharat National Park, Changwat Tak.

direction. The Huai Um Yom displays the offset of about 2,000 m with the right-lateral movement and its course of flowing deviates from southwestward to northeastward and the fault cuts the young sediment deposit of Huai Lan Sang at Ban Lan Sang (Figure 3.29). The morphotectonic landform indicates it as a normal fault with right-lateral movement.

#### **3.3.2.6 Area F, Ban Tha Lay, Tambon Lan Sang, Amphoe Muang, Changwat Tak.**

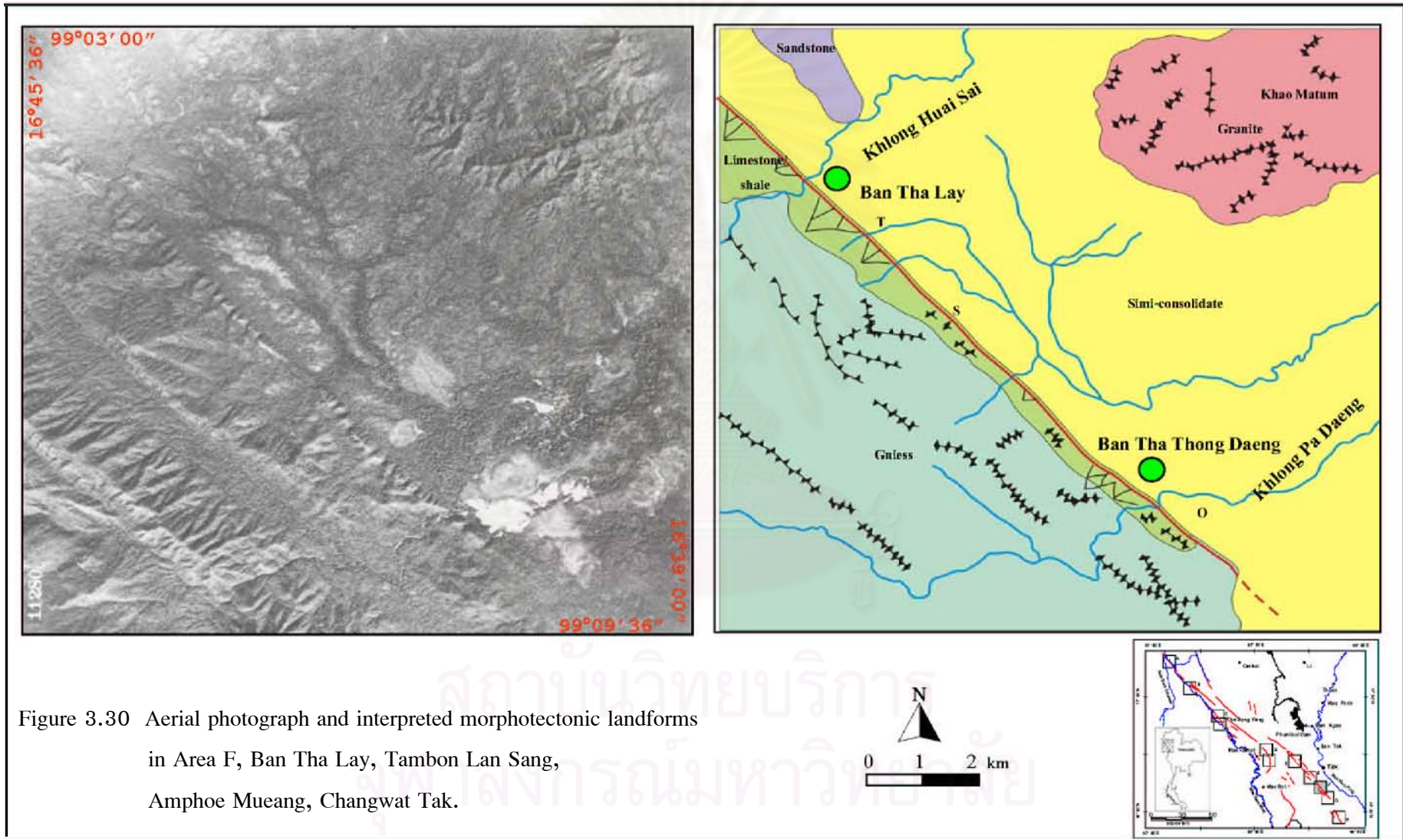
At the Ban Tha Lay area, aerial-photographic analysis reveals several types of morphotectonic evidences along the Khao Yao fault segment (segment 9, Figure 3.30), such as offset streams, triangular facets, and fault scarps. It also has a set of the northeast trending triangular facets with an average base width of about 2 km, an average height of 80 m from the base, with dipping to the northeastward. The tectonic geomorphology indicates a normal fault with right-lateral movement.

#### **3.3.2.7 Area G, Ban Tha Thong Daeng, King Amphoe Na Bot, Changwat Tak.**

At the Ban Tha Thong Daeng area, south of Tak town-ship, is governed by the MPFZ and belonging to the Khao Yao fault segment (segment 9). Interpretation by aerial-photographs demonstrates its main traceable direction similar to that of the satellite image, that is northwest-southeast (Figure 3.31). Morphotectonic evidences, including offset streams, triangular facets, and fault scarps, are observed at Klong Pa Daeng. Its flow direction changes from the southwest to the northeast. This offset is caused by a dextral sense of movement with the total displacement of about 100 m. A set of northeast-dipping triangular facets has the average base width of about 500 m and the average height of 60 m from the base. And set of the hard rock has the average base width of about 750 m and the average height of 100 m from the base. The clearly observed fault scarp close to Ban Na Bot is nearly vertical, nearly continuous and with the fault plane striking in a northwest-southeast direction. In some places, the fault planes dip to the east. The Khao Yao fault segment has a length of 20 km.

#### **3.3.2.8 Area H, Ban Pang Khanun, Amphoe Muang, Changwat Kamphaeng Phet.**

In the area of Ban Pang Khanun, the result from remote-sensing interpretation indicates the major trend of lineaments and faults along the MPFZ in the northwest-southeast direction. There is a northwest-trending fault trace belonging to the Khlong Phri fault segment (segment 10). Along the segment, well-defined morphotectonic evidence,



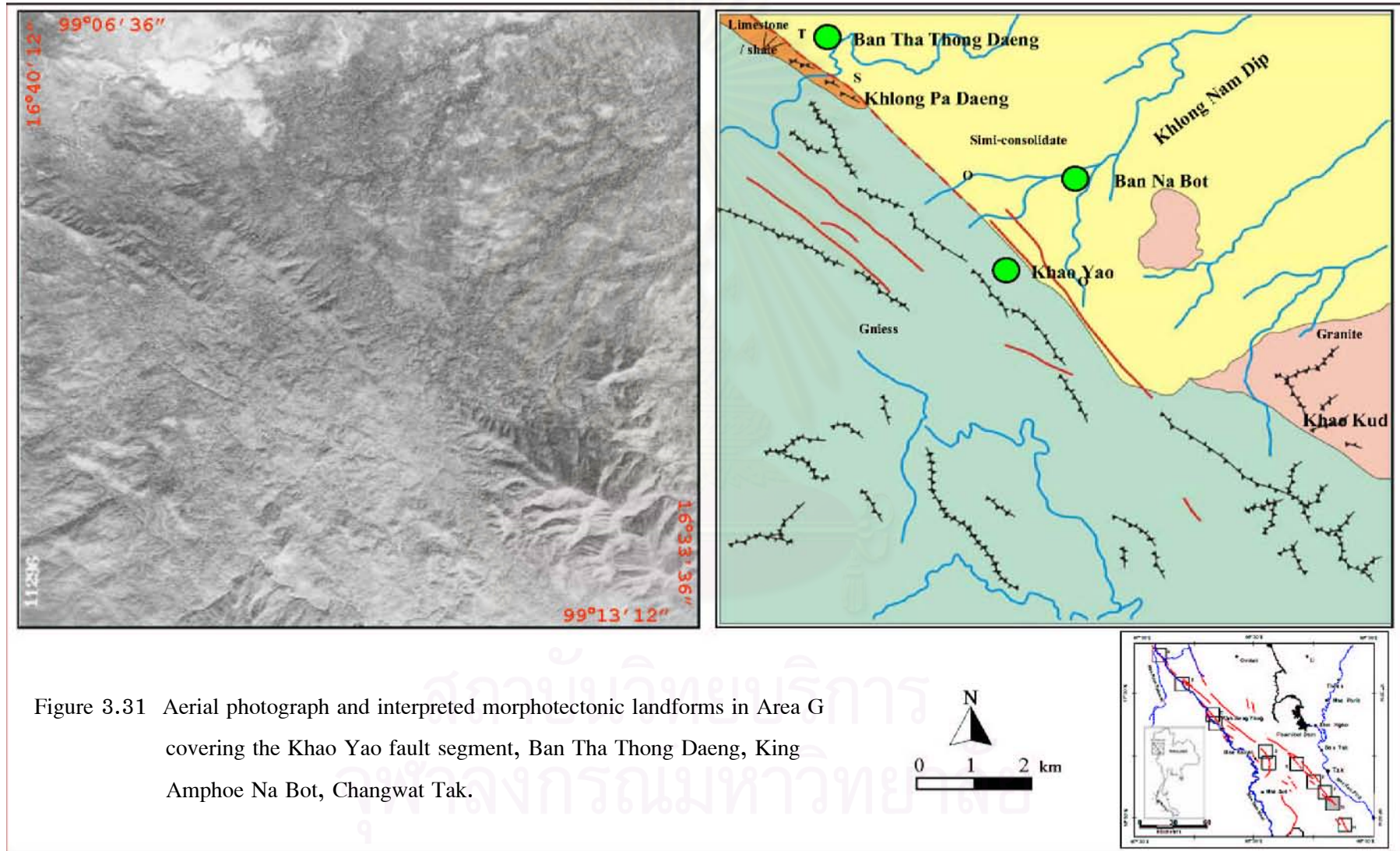
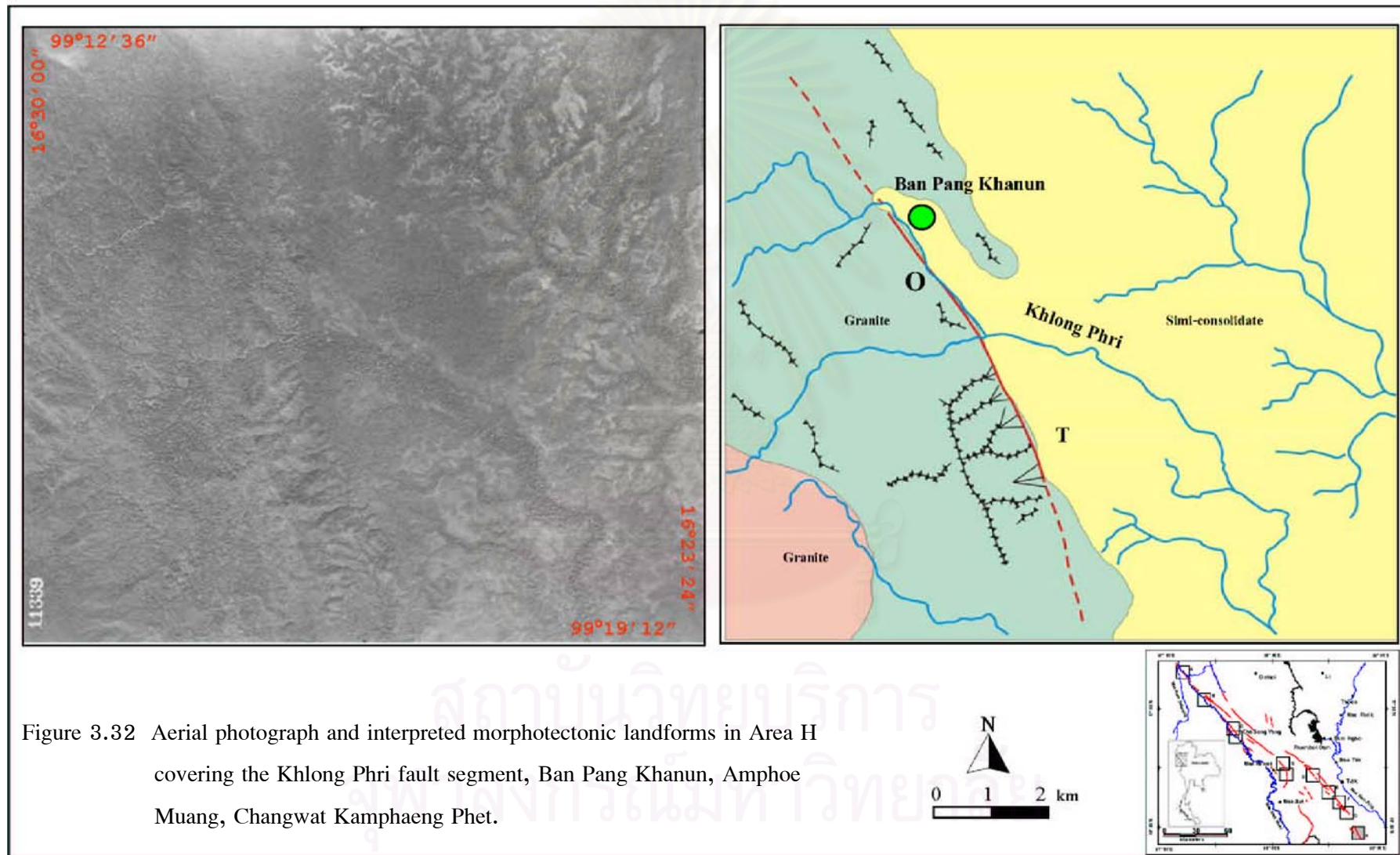


Figure 3.31 Aerial photograph and interpreted morphotectonic landforms in Area G covering the Khao Yao fault segment, Ban Tha Thong Daeng, King Amphoe Na Bot, Changwat Tak.

such as offset streams and a set of triangular facets are delineated (Figure 3.32). The Khlong Phri stream displays an offset of about 100 m by a right-lateral movement along the fault. At the vicinity nearby, it is discovered that there is a set of the northwest trending triangular facets with an average base width of about 400 m and the average height of 100 m from the base, and their faces dip to the northeast direction. The Khlong Phri fault segment has a length of 15 km.



สถาบันวิทยบริการ  
จุฬาลงกรณ์มหาวิทยาลัย





## **CHAPTER IV**

### **FIELD INVESTIGATIONS**

This chapter covers describes mainly the results related to the field exploration. Firstly, it involves the reviews of their general geology of the eight selected areas covering their eight fault segments. Secondly, emphasizes were placed on the field evidences of the morphotectonics features or landforms as investigated or observed in the field along such relevant fault segments. Brief evaluation of the morphotectonic study is also discussed. Lastly, the detailed field survey in the particular area, including the detailed field investigations by trenching traversed across the specific fault segment around Ban Mae Ou Su area were performed.

#### **4.1 Field Evidences of Morphotectonic Features**

In order to clarify and visualize their evidences of morphotectonic features as deduced from the results of remote-sensing interpretation, morphotectonic investigations were conducted. The followings are the descriptions of those evidences.

##### **4.1.1 Area A, Ban Sop Moei, Amphoe Sop Moei, Changwat Mae Hong Son.**

###### **4.1.1.1 General Geology**

Ban Sop Moei Area is situated near the junction of NE-SW trending Mae Nam Moei and NW-SE trending Mae Nam Salween (Figure 4.1). It can be accessed along the Mae Nam Salween from Ban Mae Sam Lap Port to the area in the south with one hour travel. Anyway, the area can also be accessed by temporary roads in dry season.

Based on geological map at scale 1:250,000 Amphoe Li Sheet (Braum et al., 1981) and geological map of Thailand at scale 1:1,000,000 (DMR, 1999), the area is underlain by the succession of Cambrian, Carboniferous, and Quaternary units. The oldest NW-SE striking Cambrian rocks and comprises quartzite, quartz-schist, quartzitic sandstone, and light brown to white marble. The unit is unconformably overlain by the Carboniferous sequence consisting of schist and slaty shale. Attitude of bedding of the Carboniferous formation is similar to the older rocks.

In Mae Nam Moei terrain of Ban Sop Moei, It is composed of the 1.6 Ma to recent age Quaternary deposits of gravel, sand, silt, and clay. It is noted that the unconformity between Carboniferous and Quaternary units is also recognized.

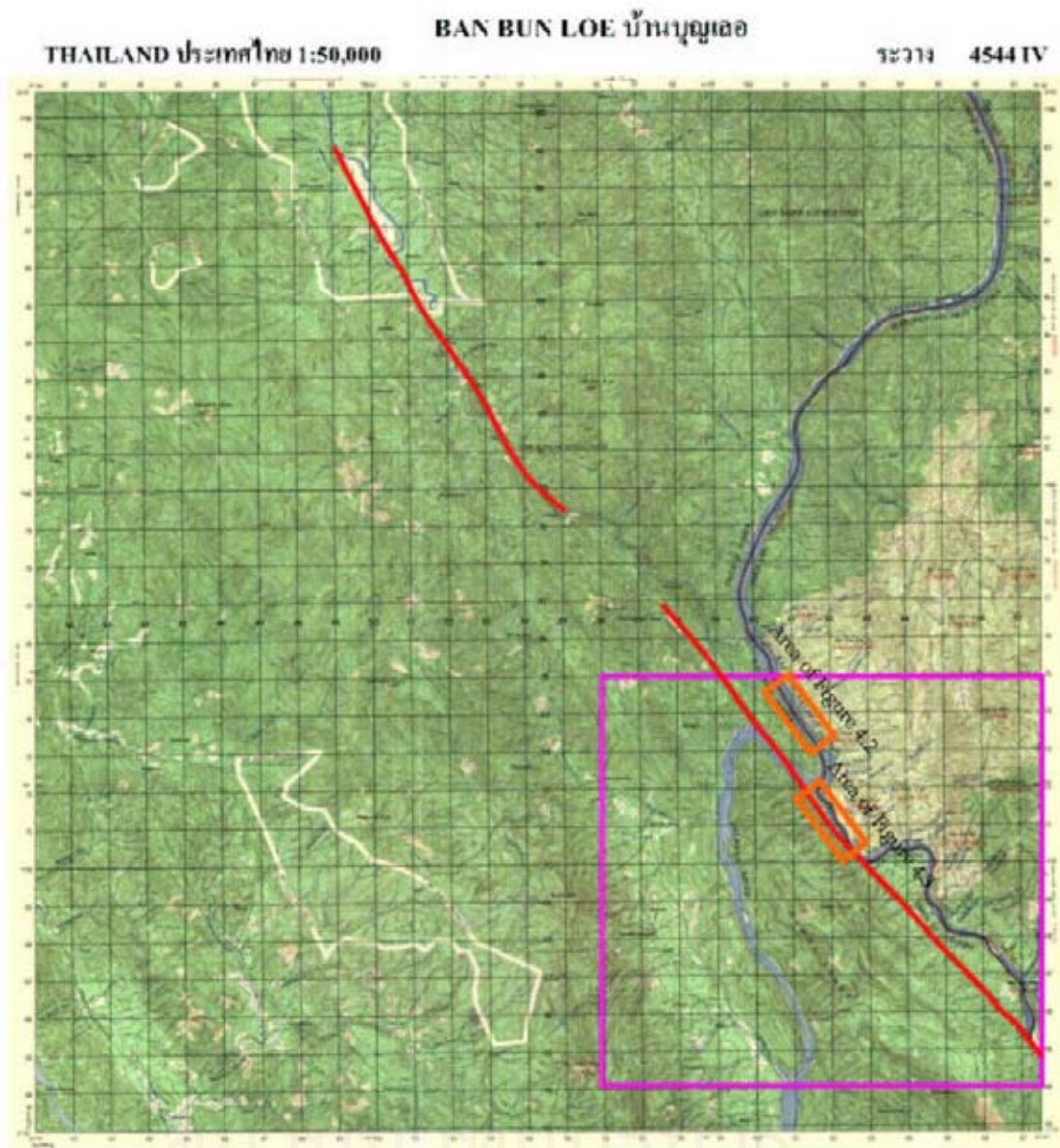


Figure 4.1 Topographic map of Ban Bun Loe, Sheet 4544 IV, showing locations of the Sop Moei fault segment. Note that the b represents the area of aerial photographic interpretation in investigated area A (Royal Thai Survey Department, 1976).

	๔๕๔๓ III	๔๕๔๕ II
	๔๕๔๔ IV	๔๕๔๖ I
		๔๕๔๖ III

#### 4.1.1.2 Field Investigations

The result from aerial-photographic interpretation around Ban Sop Moei area along the northwest-southeast trending Sop Moei fault segment is shown in [Figure 4.1](#). According to the field data from the field investigation, important geomorphologic features and landforms investigated are three sets of triangular facets. The first set shows four triangular facets of about 2.5 km average base width and of about 100 m average height from the base with  $35^\circ$  dipping ([Figure 4.2](#)). These facets of this spur set dips to the southwest direction. The second set reveals seven triangular facets of about 4.0 km average base width and of about 240 m average height from the base with  $60^\circ$  dipping. These facets of the second one spur set dip to the northeast direction ([Figure 4.3](#)). The rest possesses five triangular facets of about 2.5 km average base width and of about 350 m average height from the base with  $60^\circ$  dipping. These facets spur dips to the northeast direction.

In the northern part of Ban Sop Moei, the Huai Mae Pi has its flow direction changes from the northeast to the southwest and flow direction to the Mae Nam Moei. This offset is caused by the dextral movement with the total displacement of about 30 m.

#### 4.1.1.3 Evaluation of Morphotectonic Study

Regarding the result of field investigations and various criteria obtained Area A, it is discovered that the northwest-southeast-trending fault shows a set of triangular facets, dipping at high angles to a northeast direction. It indicates that the surface rupture length of about 16 km is estimated to imply historic earthquake of 6.5 Mw (well and Coppersmith, 1994).

#### 4.1.2 Area B, Ban Tha Song Yang, Amphoe Tha Song Yang, Changwat Tak.

##### 4.1.2.1 General Geology

The study of Ban Ta Song Yang area, northwestward of Amphoe Tha Song Yang, is restricted to the vicinity along the road no.305 (Mae Sot-Tha Song Yang) ([Figure 4.4](#)).

Based on geological map at scale 1:50,000 Ban Tha Song Yang Sheet (Sukvatananont and Assavapatchara, 1991), the area consists of the NW-SE trending Paleozoic, Mesozoic, and Cenozoic successions. The oldest Cambrian rocks comprise quartzite, quartz-schist, quartzitic sandstone, and light brown to white marble. The unit is conformably overlain by limestone, shale, and siltstone of the Ordovician unit. The younger formation of sandstone, siltstone, and shale of the Silurian-Devonian succession



Figure 4.2 A set of triangular facets of the Sop Moei fault segment, and panoramic view of its NE-trending. ( 0361935E/1972014N, 4544 IV)

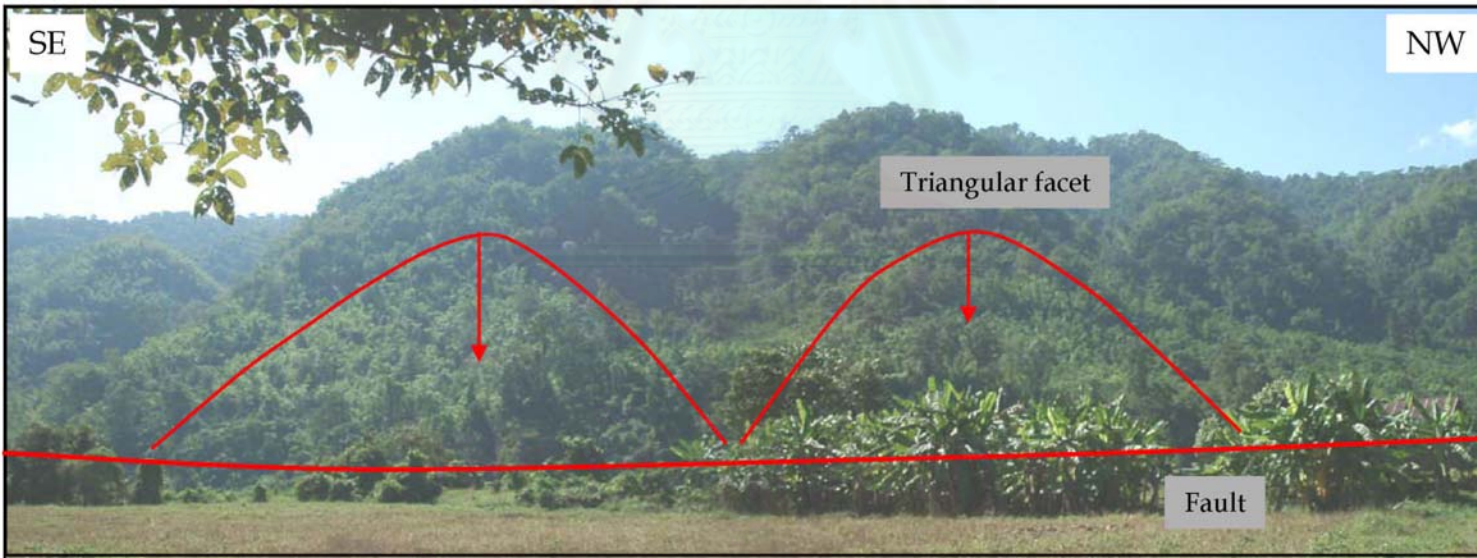


Figure 4.3 A set of triangular facets of the Sop Moei fault segment, and panoramic view of its NE-trending around Ban Sop Moei area, Amphoe Sop Moei, Changwat Mae Hong Son.

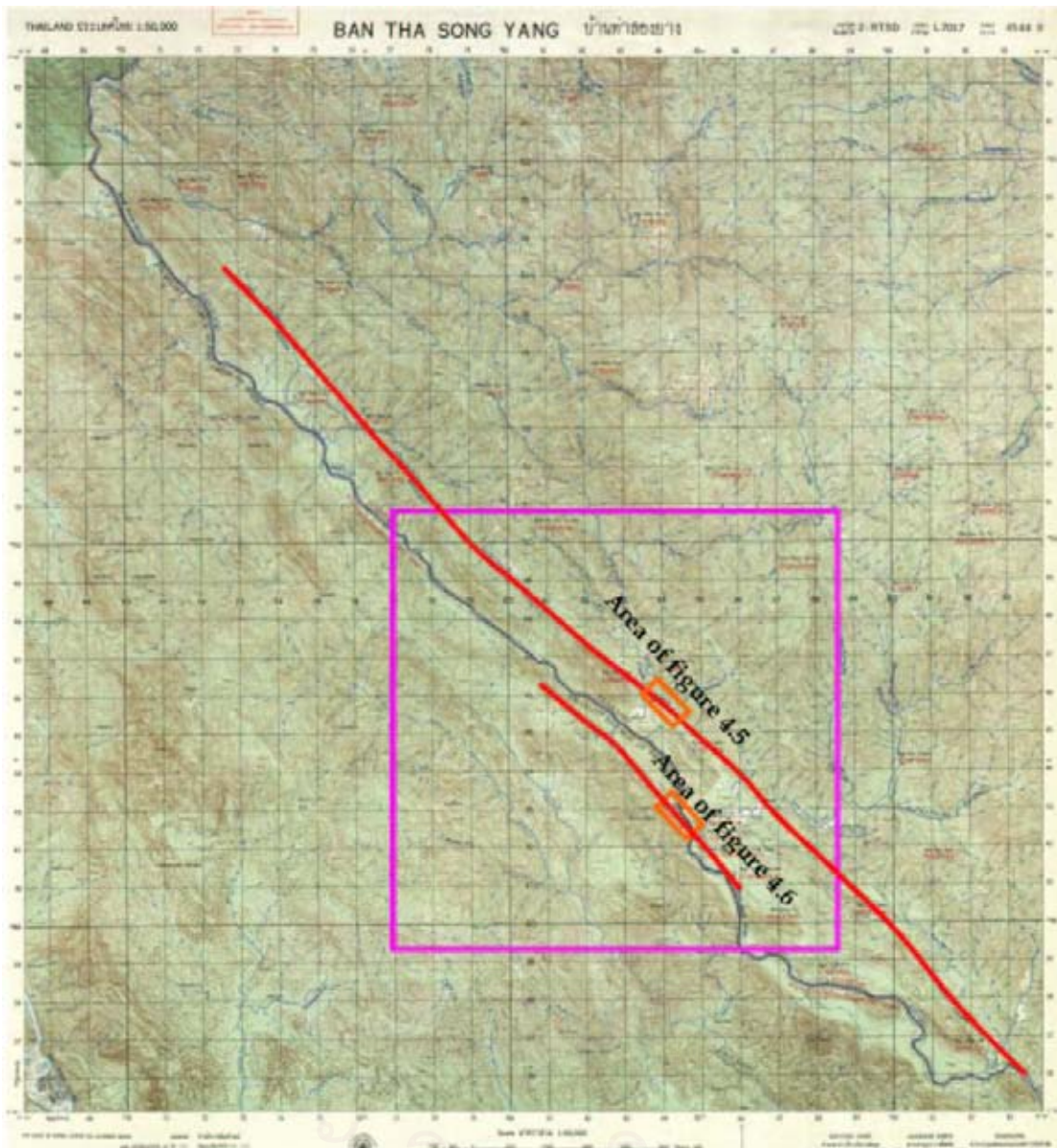


Figure 4.4 Topographic map of Ban Tha Song Yang, Sheet 4544 II, showing locations of the Ban Tha Song Yang fault segment. Note that the box represents the area of aerial photographic interpretation in area B. (Royal Thai Survey Department, 1969)

	4544 I	4544 II
	4544 III	4544 IV
		4544 V

conformably overlies the older unit while it is unconformably underlain by the sandstone, siltstone, shale, and mudstone of Carboniferous–Permian succession.

The Triassic sequence, consists of sandstone, siltstone, shale, and limestone. This succession is unconformably underlain by the Carboniferous–Permian rocks. Ban Tha Song Yang area is situated in the Quaternary sediments which are supplied by Mae Nam Moei. The sequence is composed of gravel, sand, silt, and clay. It is noted that the unconformity between Triassic and Quaternary units is also recognized.

#### **4.1.2.2 Field Investigations**

Field reconnaissance survey in the Ban Tha Song Yang area indicates that the Tha Song Yang fault segment has a continuous length of 27.5 km (Figure 4.4). Additionally, one fault scarp trending in the northwest–southeast direction and the outcrop of shear zone in limestone is recognized. The offset stream observed in this area is the Huai Ma Nok, southeastward of Ban Tha Song Yang. Its flow direction changes from northeastward to southwestward before joining the main Mae Nam Moei (Moei River). A right–lateral movement has caused shifting of the stream for about 50 m. A similar situation occurs at the Huai To No stream which probably has caused the shift of stream for about 500 m. The occurrence of the northwest–southeast trending shutter ridge which has the average base width about 200 m and the height is about 65 m from the base (Figure 4.5). A fault scarp obviously observed in limestone at Ban Pha Man, is almost vertical and rather continuous. The fault scarp strikes in the northwest–southeast direction, following the main fault. In some places, the fault planes dip steeply to the northeast (Figure 4.6). The Nam Mae Tun, northwestward of Ban Tha Song Yang and Huai O E at Ban Tha Song Yang, shows its linear valley feature, which is controlled by the northeast–trending fault.

#### **4.1.2.3 Evaluation of Morphotectonic Study**

Results of field investigation in Area B show several morphotectonic evidences found along the northwest–southeast trending fault, such as offset streams, shutter ridges, linear valleys, and fault scarps indicated right–lateral movement. The surface rupture length of about 27.5 km has deduced to the historic earthquake of 6.75 Mw (well and Coppersmith, 1994).



Figure 4.5 Photograph showing the NE-trending offset stream observed along the Ban Tha Song Yang fault segment (no.3 in Figure 3.11) in Ban Mae Tun area, Amphoe Tha Song Yang, Changwat Tak (view looking at 0384194E/1945584N to NE).

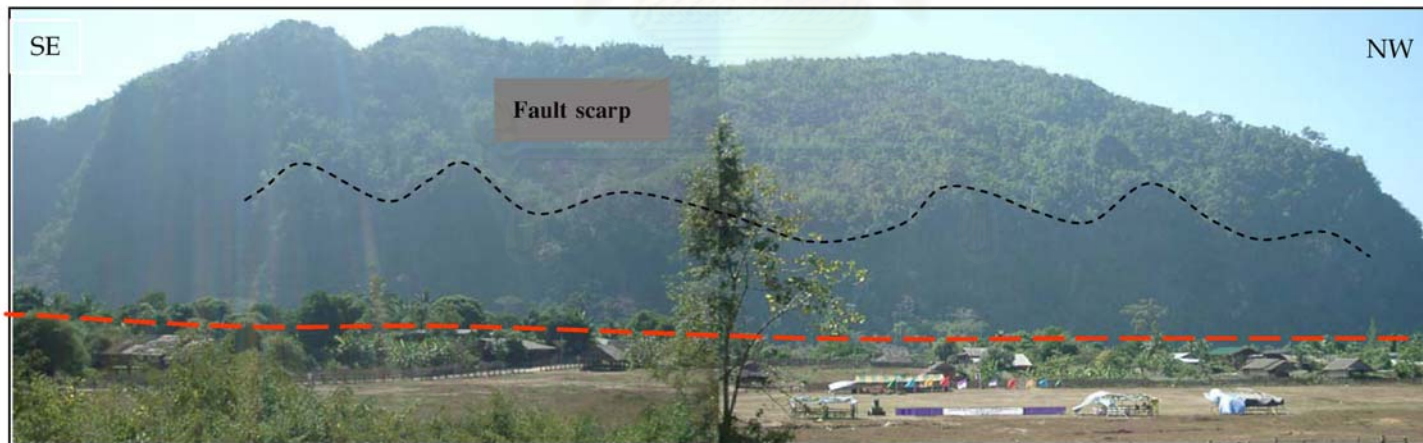


Figure 4.6 Photograph showing the NE-trending fault scarp observed along the Ban Tha Song Yang fault segment (no.3 in Figure 3.11) in Ban Tha Song Yang area, Amphoe Tha Song Yang, Changwat Tak (view looking at 0385685E/1941726N to NE).

### 4.1.3 Area C, Ban Mae Ou Su, Amphoe Tha Song Yang, Changwat Tak.

#### 4.1.3.1 General Geology

The Ban Mae Ou Su area is located near the small valley of Huai Mae Ou Su, 20 km northward from the Amphoe Tha Song Yang (Figure 4.7). Most of hill tribes in the area are generally agriculturists and general service careers.

Based on geological map at scale 1:250,000 (Amphoe Li Sheet), the study area and neighboring consist of Paleozoic, Mesozoic, and Cenozoic successions. The oldest Ordovician sequence is mainly consisted of limestone shale, and siltstone of Ordovician unit. The younger formation, sandstone, siltstone, and shale of Silurian–Devonian succession conformable overlies the older unit and unconformably underlies the sandstone, siltstone, shale, and mudstone of Carboniferous–Permian succession.

The Triassic unit which has been found in the interested area comprises the thick sequence of sandstone, siltstone, shale, and limestone. This succession is underlain unconformably by the Carboniferous–Permian rocks.

The younger unit, Tertiary rocks are composed of semi-consolidated sedimentary rocks with oil shale and peat. The NW–SE elongated–shape basin shape is bounded by NW–SE trending fault contact to the older rocks on both sides.

The recent Quaternary sediments, supplied by the Mae Nam Moei, are deposited in the Amphoe Tha Song Yang. The sequence is composed of gravel, sand, silt, and clay.

#### 4.1.3.2 Field Investigations

The result from field survey indicates the morphotectonic evidence of offset stream along Huai Mae Phlu and Huai Mae Ou Su which offset about 500 m. The set of triangular facets as observed along the highway no. 3199 (Amphoe Tha Song Yang–Ban Tha Song Yang) consists of ten facets. About 15 km of average base width and about 100 m average height from the base with 45° dipping are characterized (Figure 4.8). This facet spurs dip to the northeast direction in front of triangular facets showing linear valley parallel to the main fault and directly flowing down to the Mae Nam Moei at Ban Mae Phlu.

At the Ban Nong Bua area, near the Mae Nam Moei, the fault scarp is presented by the Permian limestone, with spur dips to the southwest direction with a length of 9 km. In the southern part of Ban Mae Ou Su area, (Figures 4.9, 4.10 and 4.11) morphotectonic evidences apparently show a stream course as linear valley feature parallel to fault, offset stream, small shutter ridge, and fault cutting through young sediment deposit of the Huai Mae Ou Su and the Huai Mae Tan. The result from field investigation analysis reveals



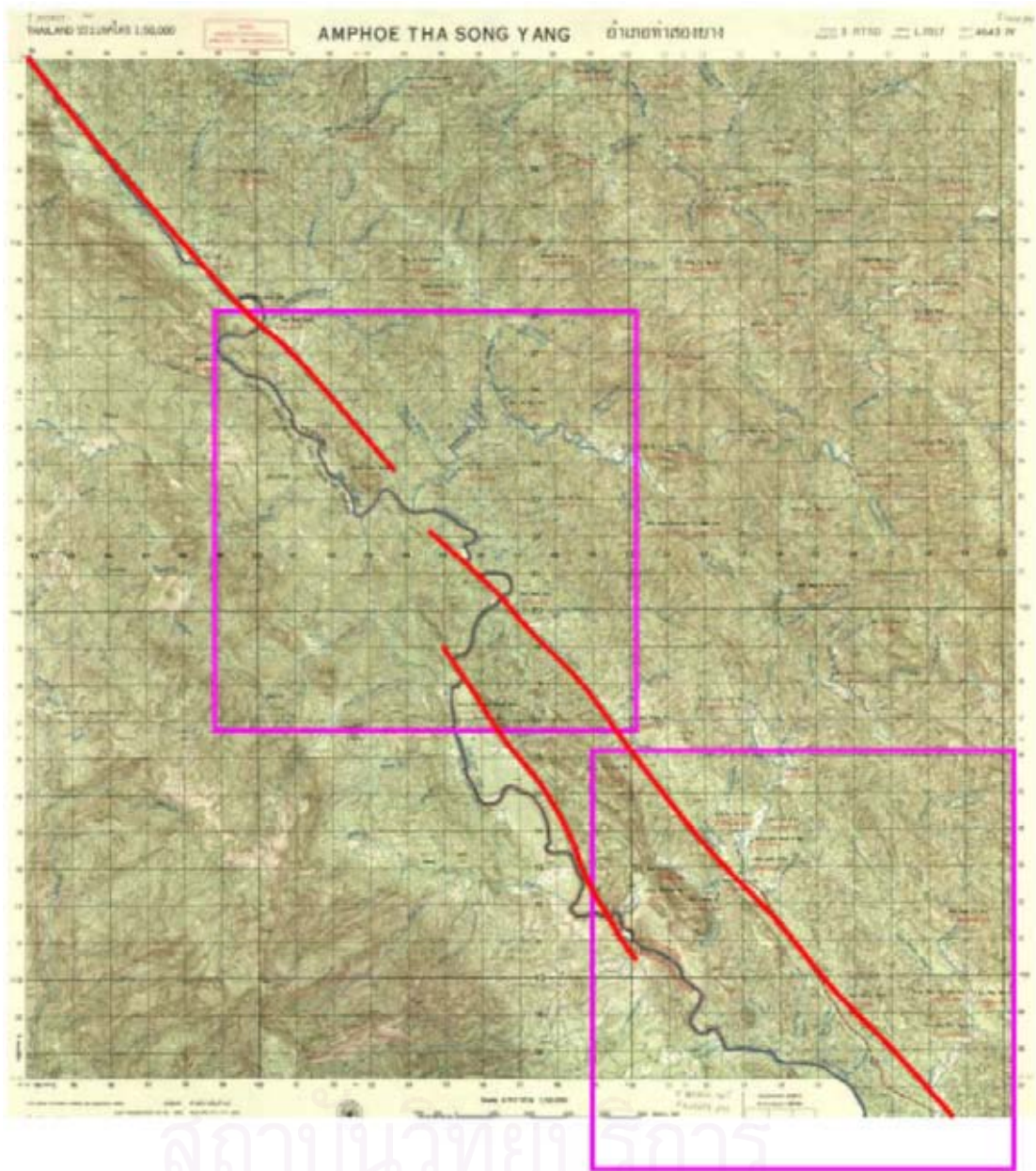


Figure 4.7 Topographic map of Amphoe Tha Song Yang, Sheet 4643 IV, showing location of the Khao Mae Song fault segment. Note that the boxes represent the areas of aerial photographic interpretations in area C (Royal Thai Survey Department, 1969).

4643 III	4643 II
4643 IV	4643 I
	4643 V



Figure 4.8 The faults cutting into Tertiary semi-consolidated sediments observed along Amphoe Mae Ramat–Amphoe Tha Song Yang road, Changwat Tak.



Figure 4.9 Photograph showing the NE-trending triangular facet and bench observed along the Khao Mae Song fault segment (no.4 Figure 3.11), in Amphoe Tha Song Yang area, Changwat Tak.

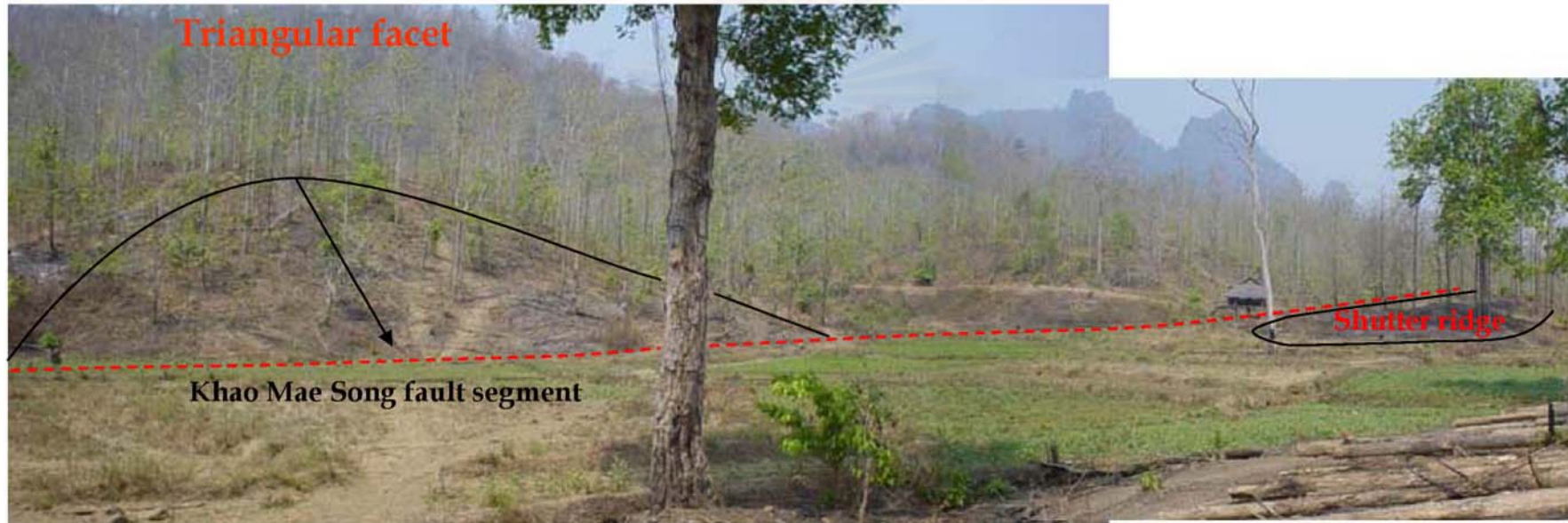


Figure 4.10 Photograph shows the NE trending triangular facet and shutter ridge observed along the Khao Mae Song fault segment (no.4 Figure 3.11) in Ban Mae Ou Su area, Amphoe Tha Song Yang, Changwat Tak (view looking to NW).

Figure 4.11 Photograph shows the NE trending triangular facet observed along the Khao Mae Song fault segment (no.4 Figure 3.11) in Ban Mae Ou Su area, Amphoe Tha Song Yang, Changwat Tak (view looking to SW).

several features of morphotectonic evidences along the Khao Mae Song fault segment, and indicates two fault subsegments having a length of 20 km and 14 km.

#### **4.1.3.3 Evaluation of Morphotectonic Study**

On account of field investigation in Area C, several features of morphotectonic evidences are recognized such as offset streams, shutter ridge, and sets of triangular facets indicating right-lateral movement. The surface rupture length of 20 km resulted from historic earthquake magnitude of 6.6 Mw has characterized (well and Coppersmith, 1994).

#### **4.1.4 Area D, Ban Mae Ramat, Amphoe Mae Ramat, Changwat Tak.**

##### **4.1.4.1 General Geology**

Generally, Ban Mae Ramat area lies in the undulating terrain. Most of the population generally set up their community near the river and most of them are the agriculturists (Figures 4.12 and 4.13). Mae Ka Sa hot spring is the famous tourism attraction of this village.

Based on Geology of Nam Ping Watershed (Boongunpai and Tansathien, 2004), the study area and neighboring area are located in the Tertiary rocks, which are composed of semi-consolidated clastic sedimentary rocks, including oil shale and peat. NW-SE trending fault with gradually change to N-S direction in the east are major structural control boundary of this basin.

##### **4.1.4.2 Field Investigations**

In an area of the Ban Mae Ramat, the Doi Kala fault segment consists of two discontinuous subsegments, one is trending towards northwest with a length of 21 km and the other is trending towards north with a length of 12 km. Field survey indicates a set of large well-preserved triangular facets occurring distinctively in Ordovician limestone. The facet strikes northwest and dips southwest, suggesting the orientation of the main fault. Along the northwest-trending fault subsegment near Ban Yang Pang Chang, there exists a few beheaded stream developed in response to the sudden change of relief and slopes. For the north-trending subsegment, a set of triangular facets has discovered and the northwest-trending fault scarp observed in limestone terrain indicating youthfulness of fault (Figure 4.14). A hot spring is also found nearby indicating the active tectono-magmatism at Ban Mae Kasa (Figure 4.15).

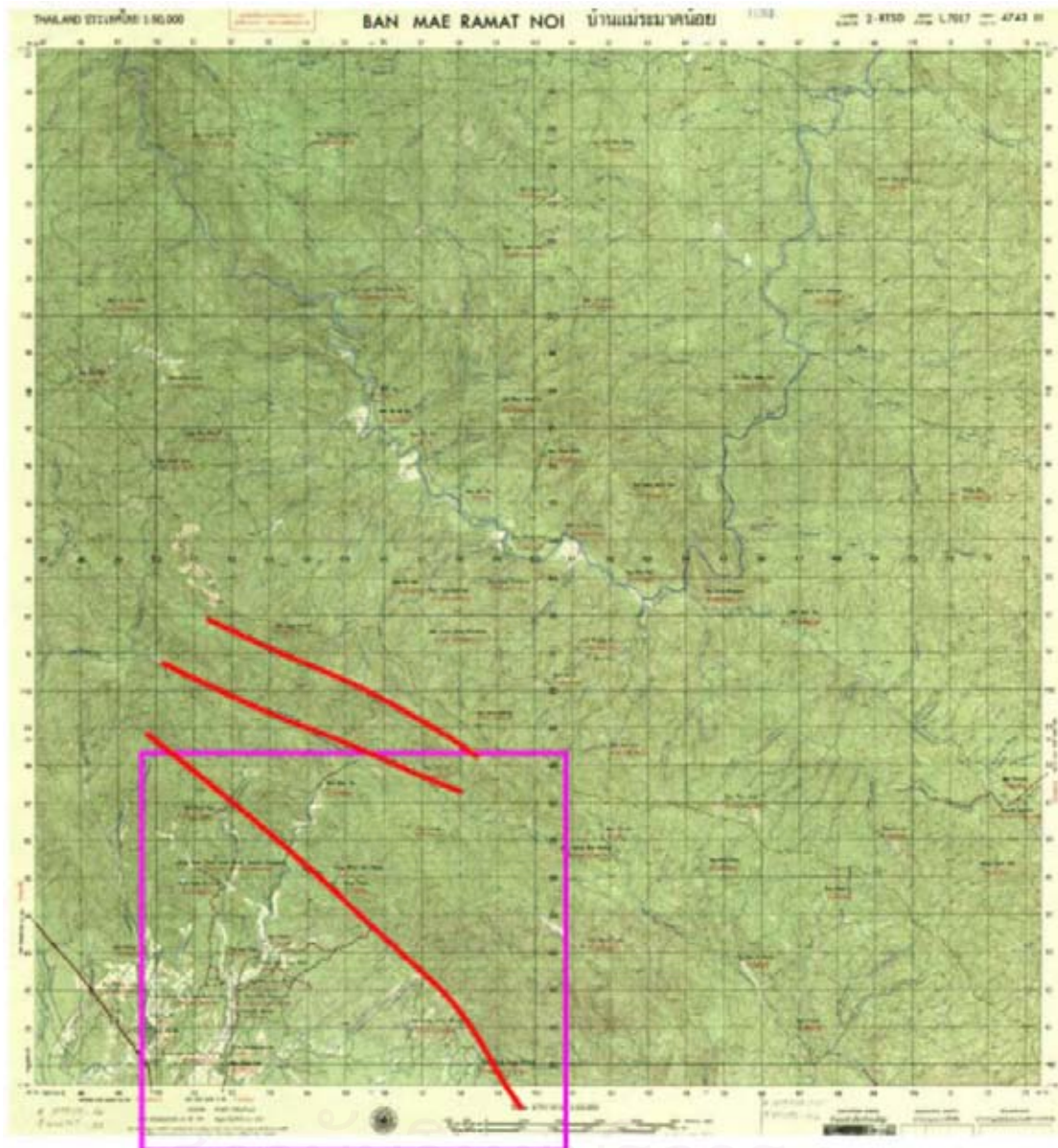


Figure 4.12 Topographic map of Amphoe Mae Ramat Noi, Sheet 4743 III, showing location of the Doi Kala fault segment. Note that the box represents the area of aerial photographic interpretation in area D (Royal Thai Survey Department, 1969).

๔๗๓ I	๔๗๓ II	๔๗๓ III
๔๗๓ IV	๔๗๓ V	๔๗๓ VI
๔๗๓ VII	๔๗๓ VIII	๔๗๓ IX

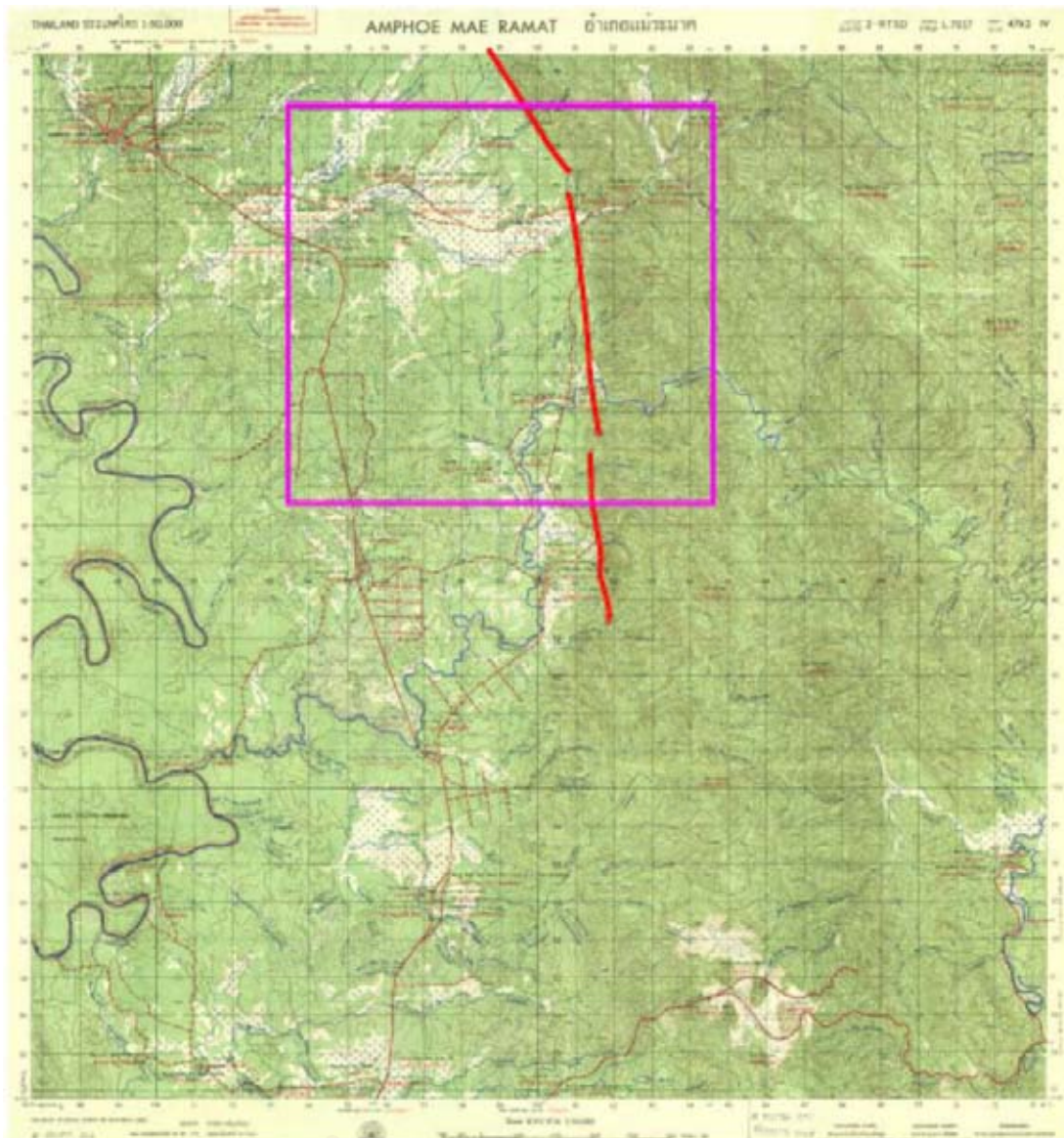


Figure 4.13 Topographic map of Amphoe Mae Ramat, Sheet 4742 IV, showing location of the Doi Kala fault segment. Note that the box represents the area of aerial photographic interpretation in area D (Royal Thai Survey Department, 1979).

๕๕๓ II	๕๖๓ III	๕๖๓ II
๕๕๓ I	๕๖๓ IV	๕๖๓ I
	๕๕๓ III	๕๕๓ II



Figure 4.14 Photograph showing the northern trending facet spurs of Ban Mae Ramat area, Amphoe Mae Ramat, Changwat Tak along the Doi Kala fault segment (no.6 in Figure 3.20).



Figure 4.15 Fault scarp observed at eastern side of limestone mountain, indicating youthfulness of the fault in area D.

#### 4.1.4.3 Evaluation of Morphotectonic Study

In area D, several features of morphotectonic evidence are recognized as results of the field investigation, such as offset streams, triangular facets, and fault scarps. Those indicate right-lateral sense of movement. The surface rupture length of about 21 km, is estimated to generate a historic earthquake magnitude of 6.6 Mw (well and Coppersmith, 1994).

#### 4.1.5 Area E, Doi Krathing, Taksin Maharat National Park, Changwat Tak.

##### 4.1.5.1 General Geology

Some parts of this area are located in both the Taksin Maharat National Park and Lan Sang National Park (Figure 4.16). Four wheel drive car for wood-track is only transportation in this forest. It is noted that the good weather condition and dry season is also necessary to enter the difficult accessible area.

Based on the revised geological map of Nam Ping watershed Project at scale 1:250,000 (DMR, 2003), the study area and neighboring area are consisting of Pre-Cambrian, Triassic, and Tertiary successions, including Triassic granite intrusion. The oldest Pre-Cambrian sequence, NW-SE trending, mainly consist of gneiss, schist, calc-silicate, and marble. The younger, Triassic sequence consists of sandstone, siltstone, shale, and argillaceous limestone.

The youngest unit, Tertiary rocks, restrictly located in undulated terrain, is composed of semi-consolidated sedimentary rocks with oil shale and peat. This succession is unconformably underlain by the Triassic rocks and is fault contact to the Pre-Cambrian succession.

Only the northeastern part of the area E is occupied by the granite pluton.

##### 4.1.5.2 Field Investigations

Regarding the Doi Krathing, locating in the western part of Tak town-ship is in the proximity of the MPFZ, and belonging to the Doi Luang fault segment which possesses its length of 31 km. Morphotectonics indicates the active tectonic morphology includes offset streams, linear valley, and triangular facets. Along the northwest-southeast fault, a set of triangular facets shows the average base width of about 15.5 km and the average height of about 240 m from the base. This facet spur dips to the northeast direction indicates normal fault nature. In front of the triangular facets, the linear valley of Huai Khun Mae Tho which runs parallel to fault has been observed. In the northern part, a set of triangular facets



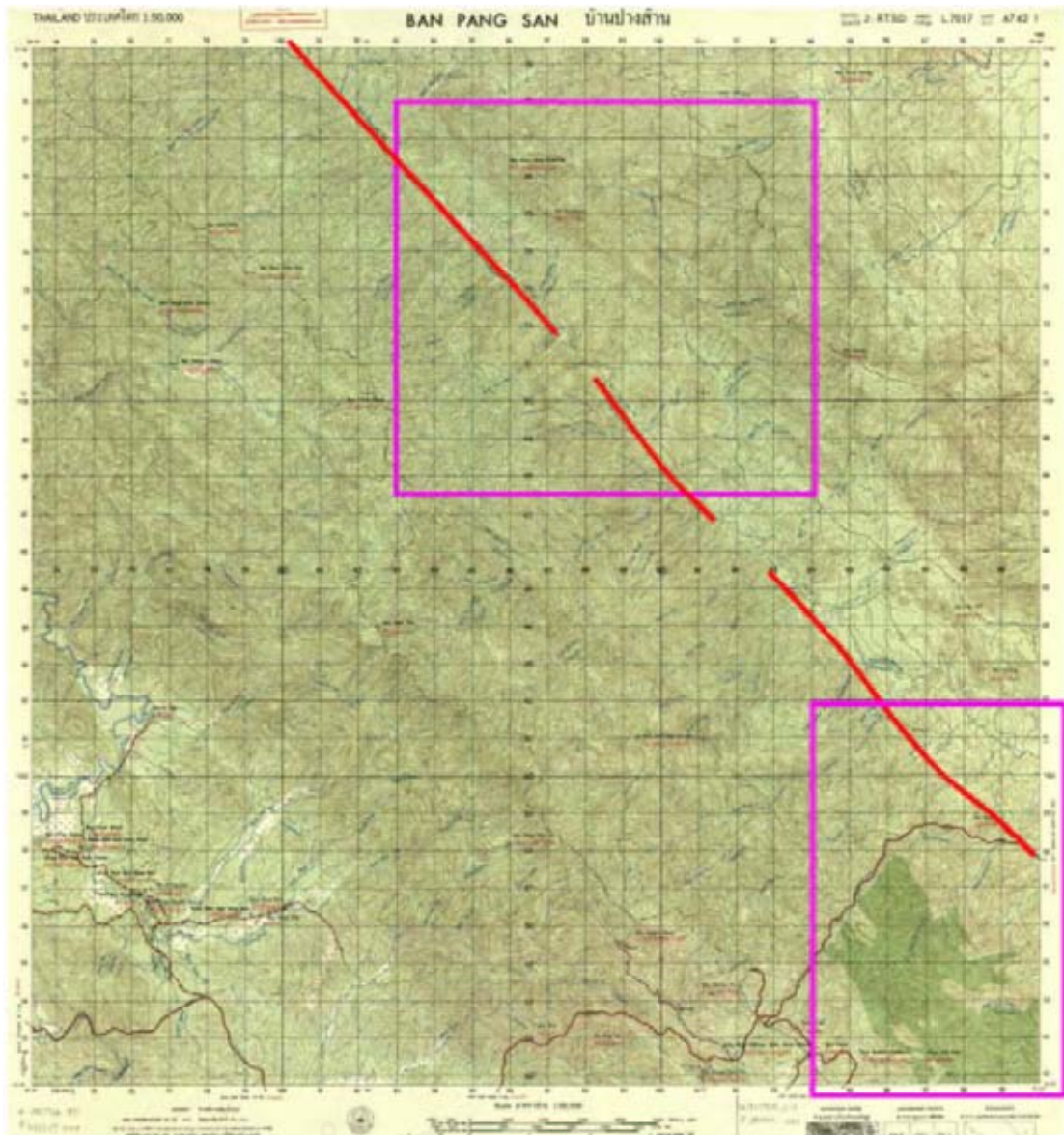


Figure 4.16 Topographic map of Ban Pang San, Sheet 4742 I, showing locations of the Doi Luang fault segment. Note that the boxes represent the areas of aerial photographic interpretations in area E and F (Royal Thai Survey Department, 1995).

4742 III	4742 II	4842 III
4742 IV	4742 I	4842 IV
4742 III	4742 II	4842 III

shows the average base width of about 10 km and the average height of about 240 m from the base. This facet spurs dip to the southwest direction indicates its normal fault characteristic.

At the Lan Sang National Park, southern part of Doi Krathing, there has a set of triangular facets showing the average base width of about 10 km and the average height of about 220 m from the base. This facet spurs dips to the northeast direction. The Huai Um Yom displays the offset of about 2,000 m of the right-lateral sense of movement with its flowing course deviates from southwestward to northeastward, and fault cut through the young sediment deposits of Huai Lan Sang at Ban Lan Sang. The morphotectonic landform indicates that it is normal fault associated with right-lateral sent of movement.

#### **4.1.5.3 Evaluation of Morphotectonic Study**

Result of field investigation in Area E, several morphotectonic evidences of the active faults are offset streams, a linear valley, and a set of triangular facets which indicate right-lateral sent of movement. The facet spur shows dipping to the southwest with normal sense of movement. The surface rupture length of 15.5 km can indicate to its occurrence of historic earthquake magnitude of 6.45 Mw (well and Coppersmith, 1994).

#### **4.1.6 Area F, Ban Tha lay, Tambon Lan Sang, Amphoe Muang, Changwat Tak.**

##### **4.1.6.1 General Geology**

Part of this area, located in the Lan Sang National Park (Figures 4.16 and 4.17), is jungle and highland area. Some part is underlain the flat land using for farm fields.

Base on the investigation, the study area along the Tak-Na Bot route consisted of Pre-Cambrian and Permian successions in the mountainous area and Quaternary deposits in the low land. The oldest Pre-Cambrian sequence, NW-SE trending, mainly consist of gneiss, schist, calc-silicate, and marble. The younger, Permian sequence is composed of limestone, sandstone, and conglomerate. This succession is fault boundaries with the older rocks.

The Tertiary rocks, located over the undulated terrains, are composed of semi-consolidated sedimentary rocks with oil shale and peat. Near the Khlong Pa Dang and Huai Tha Lay, the recent sediments including gravel, sand, and silt are also deposited.

It is noted that the northeastern part of the area the granite pluton with Triassic age is represent.

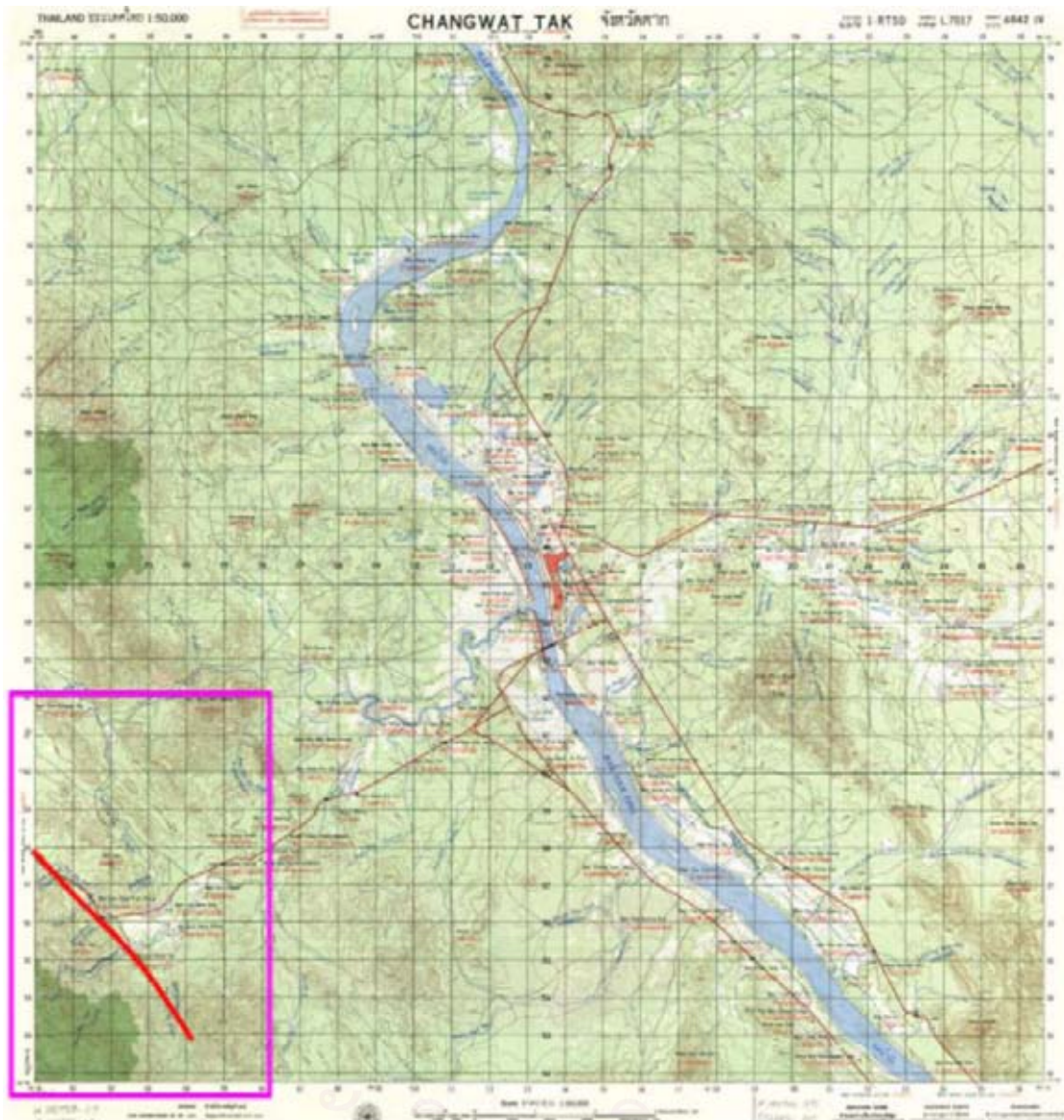


Figure 4.17 Topographic map of Changwat Tak, Sheet 4842 IV, showing locations of the Doi Luang fault segment.

Note that the box represents the areas of aerial photographic interpretations in area F (Royal Thai Survey Department, 1995).

470 II	480 III	490 II
470 I	480 IV	480 I
470 II	480 III	480 II

#### 4.1.6.2 Field Investigations

The field investigation displays several features of morphotectonic evidences along the Khao Yao fault segment having a set of triangular facets. The two facets developed the sets of spurs produced by episodic vertical tectonic movement as illustrated in [Figure 3.18](#) in chapter III. The first set at Ban Huai Bong shows eight facets of about 2.5 km average base width and of about 100 m average height from the base with  $45^\circ$  dipping. These facets spur dips to the northeast direction. The small offset 5–10 meters has been found that indicated right–lateral movement ([Figure 4.18](#)).

The second set, at Ban Tha Lay area, shows four facets and the average base width of about 2.0 km and the average height of about 180 m from the base with  $50^\circ$  dipping. This facet spurs dips to the northeast direction indicating its normal fault nature, such as offset streams, triangular facets, and fault scarps. It also has a set of the northeast trending triangular facets with an average base width of about 2 km, and an average height of 80 m from the base dipping to the northeastward. At the Huai Tha Lay, the fault plane with slickenside of northwest–southeast direction ( $N40^\circ E$ ) was observed. The tectonic geomorphology indicated a normal fault with right–lateral movement.

#### 4.1.6.3 Evaluation of Morphotectonic Study

Result of field investigation in Area F reveals that morphotectonic evidences along the northwest–southeast fault comprise offset streams, triangular facets, and fault scarps that indicate a normal fault with right–lateral movement.

#### 4.1.7 Area G, Ban Tha Thong Daeng, King Amphoe Na Bot, Changwat Tak.

##### 4.1.7.1 General Geology

This area extends continuously from the Area F therefore, its geology is similar to that of the Area F ([Figure 4.19](#)).

Based on the field investigation, the study area along the Tak–Na Bot route consist of Pre–Cambrian and Permian successions in the mountainous area and Quaternary deposits in the low land. The oldest Pre–Cambrian sequence, NW–SE trending, consist mainly of gneiss, schist, calc–silicate, and marble. The younger, Permian sequence, is composed of limestone, sandstone, and conglomerate. This succession is fault boundarie with the older rocks.

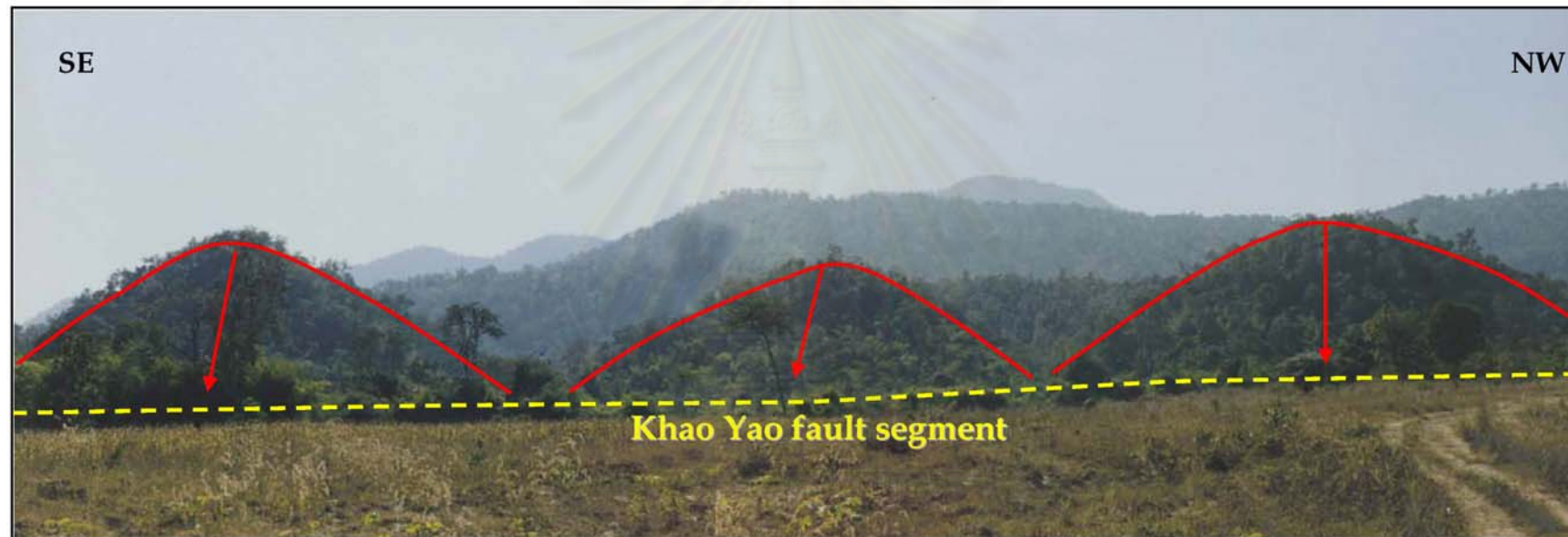


Figure 4.18 Photograph showing the NE trending triangular facets along the Khao Yao fault segment (no.9 in Figure 3.11) in Ban Tha Lay area, Amphoe Muang Tak, Changwat Tak.

สถาบันวิทยบริการ  
จุฬาลงกรณ์มหาวิทยาลัย

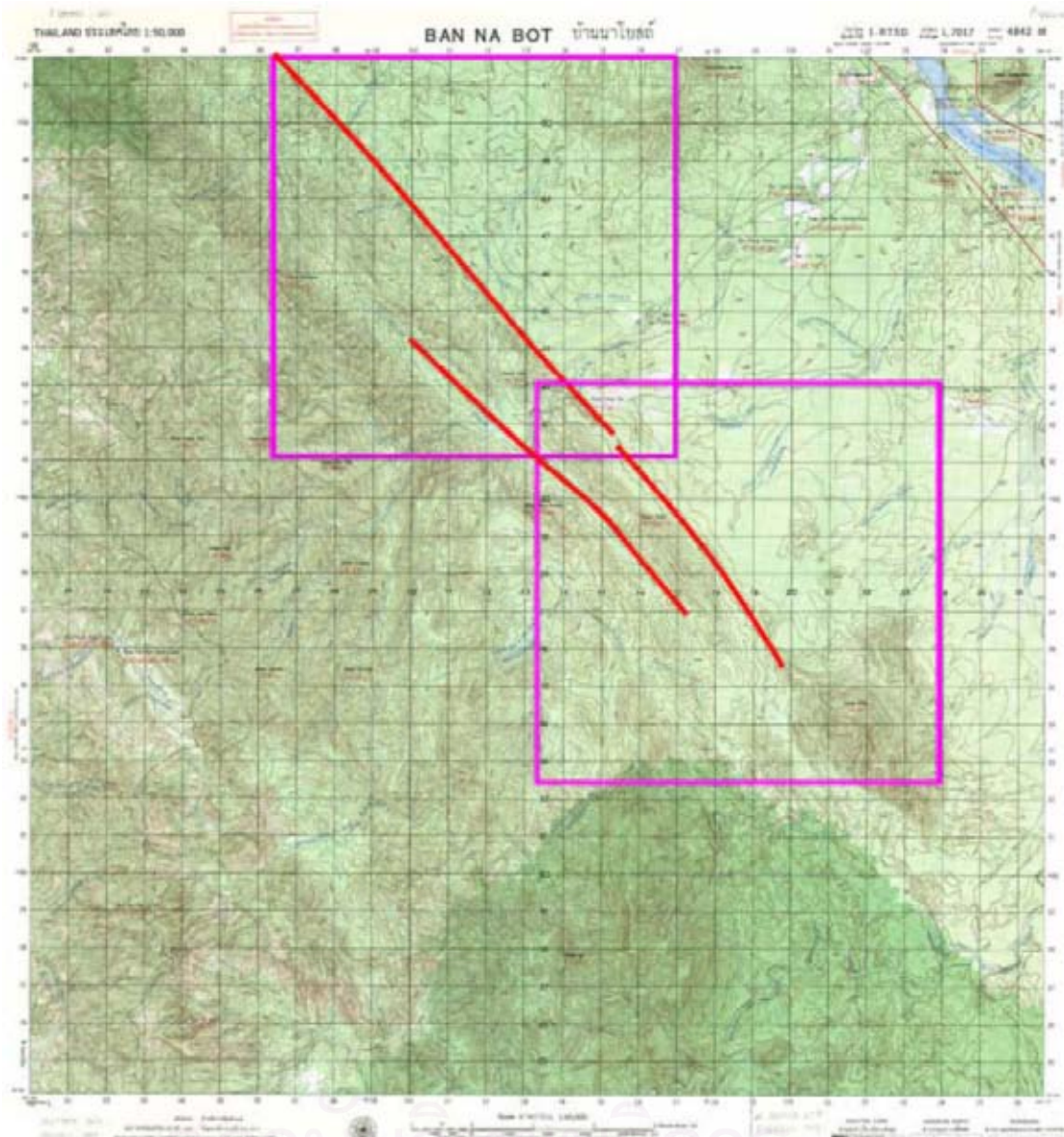


Figure 4.19 Topographic map of Ban Na Bot, Sheet 4842 III, showing locations of the Khao Yao fault segment. Note that the boxes represent the area of aerial photographic interpretation in area G (Royal Thai Survey Department, 1989).

4842 I	4842 II	4842 III
4842 II	4842 III	4842 IV
4842 III	4842 IV	4842 V

The Tertiary rocks, located in undulated terrain, are composed of semi-consolidated sedimentary rocks with oil shale and peat. Near the Khlong Pa Dang and Huai Tha Lay, the recent sediments including gravel, sand, and silt are also deposited.

It is noted that the granite pluton with Triassic age the northeastern part of the area.

#### **4.1.7.2 Field Investigations**

The results from aerial photographic interpretation in the Ban Tha Thong Daeng area illustrates that the Khao Yao fault segment is almost continuous and has a length of 21 km (Figure 4.20). Fault scarps and triangular facets trend towards a northwest-southeast direction. In addition, the triangular facet feature shows sixth facets of about 5.0 km average base width and of about 120 m average height from the base with 40° dipping. It faces to the northeast direction. Field data observed close to Ban Tha Lay reveal the exposures of colluvial deposits, a small shutter ridge, and the left-lateral offset stream. Field observation in the offset stream shows the slickenside plane in northwest-southeast direction (N50° E) with dipping 70°. The Klong Pa Dang has its flow direction that changes from the southwest to the northeast. This offset is caused by a dextral sense of movement with the total displacement of about 100 m.

#### **4.1.7.3 Evaluation of Morphotectonic Study**

Morphotectonic evidences of the active faults as resulted from the field investigation in Area G are offset streams, triangular facets, and fault scarps. They indicated normal with right-lateral movement. The surface rupture can be lineated with the length 20 km corresponding to a historic earthquake magnitude of 6.6 Mw (well and Coppersmith, 1994).

#### **4.1.8 Area H, Ban Pang Khanun, Amphoe Muang, Changwat Kamphaeng Phet.**

##### **4.1.8.1 General Geology**

This study area is in the vicinity Amphoe Muang, Changwat Kamphaeng Phet (Figure 4.21). Part of the area located in the Khong Lan National Park, is forest area and highlands having Thao Doom waterfall as an attractive site. Base on the investigation, the study area consists of Pre-Cambrian in the mountainous area and Quaternary deposits in the low land. The oldest Pre-Cambrian sequence, NW-SE trending, mainly consist of gneiss, schist, calc-silicate, and marble. This succession is fault boundaries with gravel, sand and silt of the recent Quaternary sediments.



Figure 4.20 Photograph showing the NE trending triangular facets along the Khao Yao fault segment (no. 9 in Figure 3.11) in Ban Tha Thong Daeng area, King Amphoe Na Bot, Changwat Tak.

สถาบันวิทยบริการ  
จุฬาลงกรณ์มหาวิทยาลัย



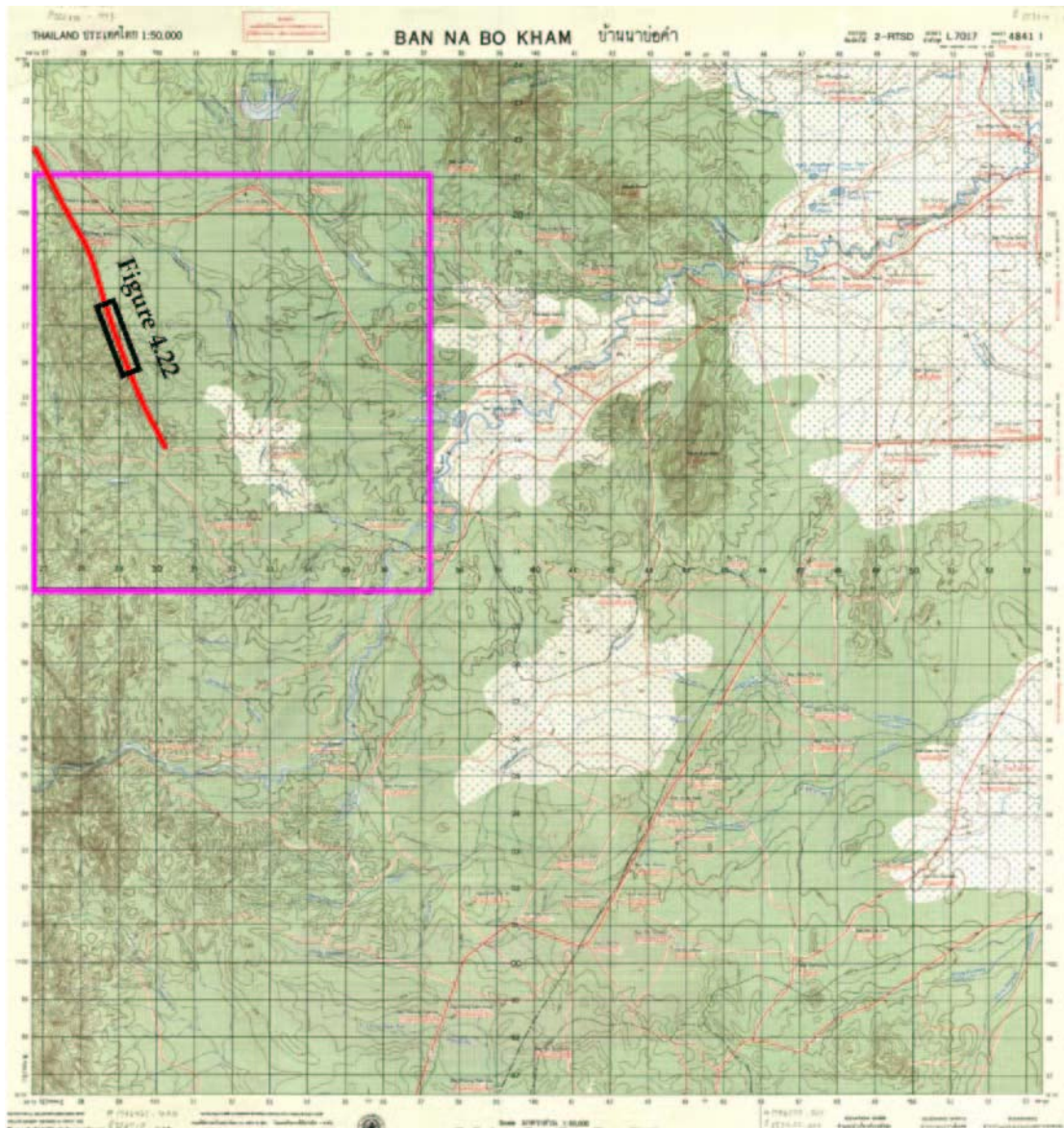


Figure 4.21 Topographic map of Ban Na Bo Kham, Sheet 4841 I, showing locations of the Klong Phri fault segment. Note that the box represents the area of aerial photographic interpretation in area H (Royal Thai Survey Department, 1986).

๔8๔ III	๔8๔ II	๔8๔ III
๔841 IV	๔841 I	๔841 IV
๔8๔ III	๔84 II	๔941 III

It is noted that the Klong Lan National Park office in the northeastern part is also recognized the Triassic granite intrusion.

#### **4.1.8.2 Field Investigations**

The Ban Pang Khanun area, the Klong Phri fault segment processes a continuous length of 15 km. The direction of the main fault trace interpreted by aerial photographs is northwest–southeast. The field reconnaissance survey in the Ban Pang Khanun, reveals that the triangular facets shows ten facets with the average base width about 7.0 km and the average height about 80 m from the base with dipping  $40^\circ$  (Figure 4.22). The triangular facets show their dips to the NE direction, and reveal rather fresh exposures with a small shutter ridge and the right–lateral offset stream.

#### **4.1.8.3 Evaluation of Morphotectonic Study**

Result of the field investigation in Area H, indicate well–defined morphotectonic landforms, including few offset streams and a triangular facet indicated right–lateral movement. The surface rupture length 8.5 km is estimated to represent the historic earthquake magnitude of 6.2 Mw (well and Coppersmith, 1994).

### **4.2 Detailed Field Investigation**

#### **4.2.1 Selection of the Detailed Investigated Area**

In as much as the reliable research needs as much as possible the supporting field evidences relevant to the fault segments concerned, it is prime necessity to study all the fault segment traces. In seeking the specific areas for detailed field investigation, there exist some constraints to access the specified criteria. Therefore, selection of a specific area for this field survey covering eight areas as aforementioned was conducted by compiling relevant supporting information both strength and weakness of each area to bring research to the next step. The most effective and suitable area was chosen for further detailed study. The determination factors are accessibility since the study must use the backhoe for digging field study, lithology, geomorphology, and the ownership and authorization of the proposed area.

Rating formula is shown in table 4.1. Priority of those factors was set based on its importance and relevance to the study. Rating level 3 was set for the most important geologic factor. Those are lithology, and geomorphology. Rating level 2 is the accessibility, and the remaining factors are considered to be rating level 1.



Figure 4.22 Photograph showing the NE trending fault scarp in Ban Pang Khanun, Amphoe Muang, Changwat Kamphaeng Phet along the Klong Phri fault segment (no.10 in Figure 3.11).

สถาบันวิทยบริการ  
จุฬาลงกรณ์มหาวิทยาลัย

Table 4.1 Rating Criteria and Priority for Selection of Detailed Investigation Area (Higher number indicates more weight).

No.	Rating	Criteria	Rating Level
1		<b>Lithology</b>	3
	0	Rock	
	1	Uncosolidated homogenous sediment	
	2	Uncosolidated sediment lying over weathering rock	
	3	Several sediment layers	
2		<b>Geomorphologic evidence</b>	3
	1	One geomorphologic evidence	
	2	Two geomorphologic evidences	
	3	Three geomorphologic evidences	
	4	Four geomorphologic evidences	
3		<b>Accessibility</b>	2
	1	Footpath, trail	
	2	Loose or hard surface, one or more lanes wide or cart track	
	3	Loose light surface, two or more lanes wide	
	4	Hard surface, two or more lanes wide	
4		<b>Ownership of the land and authorization</b>	1
	1	Unauthorized	
	2	Studying in the National Park area must be authorized by National Park, Wildlife and Plant Conservation Department	
	3	Plantation or Forest Reserve	
	4	Private area	

Conclusion of rating formula is shown in [table 4.2](#). Area C and D are the most effective and suitable areas to be considered as the area of study due to their highest score (30) as shown in the table. Area D locates closely to the Mae Kasa hot spring which has been developed to be tourist site. As a result, this area cannot be the area for study. The area C was chosen for further detailed study.

As a consequence, the area selected for detailed field investigation at least can be strongly ascertain to be the represent such the area governing its characteristics of the Moei-Mae Ping Fault Zone for this study.

#### **4.2.2 Result of Detailed Investigation**

Composite investigations were performed basically on the compilation of various available data and information. Based on results of remote-sensing interpretation and an aerial photographic investigation, the morphotectonic evidence of offset stream along Huai Mae Ou Su which offsets about 500 m can be recognized. The set of triangular facets consists of ten facets of about 15 km average base width and of about 100 m average height from the base with  $45^\circ$  dipping (Figure 4.10). This facet spurs dip to the northeast direction. Linear valley paralleling to the main fault along the country road no. 3199 from Amphoe Tha Song Yang to Ban Tha Song Yang occurs in front of the triangular facets. Furthermore, the result from field survey relevant to morphotectonic evidence indicating a stream linear valley paralleling to fault, offset stream, small shutter ridge, and fault cut through the young sediment deposits of Huai Mae Ou Su. With all the results mentioned above, the detailed topographic survey was conducted (Figure 2.23). This method reveals well-defined morphotectonic features, such as triangular facets, shutter ridges, and offset streams. The offset stream displays the right-lateral sense of movement of about 30 m (Figure 2.24). However, based on detailed survey, the offset along the small stream is about 11 meter.

### **4.3 Field Investigation of Ban Mae Ou Su Trench**

#### **4.3.1 Trenching Location**

The study area is located between Amphoe Tha Song Yang and Ban Tha Song Yang at km12+000 along the country road no. 3199. Remote-sensing interpretation shows sharp lineament and geomorphology indicating offset stream, shutter ridge, and triangular facets at grid reference 0411855E 1914246N on 1:50,000 sheet 4536IV (Amphoe Tha Song Yang). The area was located to perform detailed survey scale 1:1,000 and planed to excavate trenches. Two trench sites namely, Ban Mae Ou Su trench no.1

Table 4.2 Rating of Suitability for Selection of the Detailed Field Investigation.

Area	Accessibility	Lithology	Geomorphologic evidence	Ownership of the land and authorization	Suitability for study	Priority
Area A	By boat in dry season only. Loose or hard surface, one or more lanes wide or cart track	Homogenous sediment	offset stream, triangular facet, shutter ridge	Private area	Unsuitable: insecure border area	26
	2*2	3*3	3*3	4		
Area B	Loose light surface, two or more lanes wide. But 4x4 wheel truck that can be accessible all seasons	Uncosolidated sediment lying over weathered rock	linear valley, offset stream, shutter ridge	Private area	Unsuitable: Limestone exposed at the base of a small pit near surfact	25
	2*3	2*3	3*3	4		
Area C	Hard surface, two or more lanes wide can be accessible all seasons	Homogenous sediment	linear valley, offset stream, shutter ridge	Private area	Suitable: a rice field; in the rain season; authorized by the owner	30
	2*4	3*3	3*3	4		

Table 4.2 Rating of Suitability for Selection of the Detailed Field Investigation(continued).

Area D	Hard surface, two or more lanes wide can be accessible all seasons	Homogenous sediment	triangular facet, beheaded stream, shutter ridge	Private area	Unsuitable: located in the area under the authorization of the local government organization	<b>30</b>
	2*4	3*3	3*3	4		
Area E	Loose light surface, two or more lanes wide. But 4x4 wheel truck that can be accessible all seasons	Uncosolidated sediment lying over weathering rock	linear valley, offset stream, triangular facet, shutter ridge	Taksin Maharat National Park	Unsuitable: studying in the National Park area must be authorized by National Park, Wildlife and Plant Conservation Department	<b>24</b>
	2*2	2*3	4*3	2		

Table 4.2 Rating of Suitability for Selection of the Detailed Field Investigation(continued).

Area F	By truck (can be accessible all seasons and then by the nature trail)	Uncosolidated sediment lying over weathered rock	offset stream and triangluar facet	Taksin Maharat National Park	Unsuitable: studying in the National Park area must be authorized by National Park, Wildlife and Plant Conservation Department	14
	2*2	2*3	1*2	2		
Area G	Loose light surface, two or more lanes wide and truck can be accessible all seasons and then by the nature trail	Uncosolidated sediment lying over weathered rock	offset stream and triangluar facet	Lan Sang Waterfall National Park	Unsuitable: studying in the National Park area must be authorized by National Park, Wildlife and Plant Conservation Department	14
	2*2	2*3	1*2	2		



Table 4.2 Rating of Suitability for Selection of the Detailed Field Investigation(continued).

Area H	Loose light surface, two or more lanes wide. But 4x4 wheel truck can be accessible all seasons	Uncosolidated sediment lying over weathered rock	offset stream and triangluar facet	Klong Lan Waterfall National Park	Unsuitable: studying in the National Park area must be authorized by National Park, Wildife and Plant Conservetion Department	15
	2*2	2*3	1*3	2		

(MOS1) and Ban Mae Ou Su trench no.2 (MOS2) (Figures 4.23 and 4.24) were selected for detailed studies of fault and trench logging. The two trenches were excavated in the young sediments deposits traverse across the fault trace perpendicularly, near the offset stream, shutter ridges, and triangular facets.

The techniques, such as trench wall cleaning, curing and brushing, were used to locate and enhance stratigraphic unit, faults, fractures, and features related to faulting in trench. Each trench was grided with 50 cm x 75 cm and logged on graph paper for detail. Detailed logging shows a geologic interpretation of the structural and stratigraphic relations exposed in the trench. After logging, representative samples were collected for age determination of faulting.

#### 4.3.2 Stratigraphic Description

Stratigraphic units from top to bottom of the down thrown block, Ban Mae Ou Su trench no.1 and Ban Mae Ou Su trench no.2 are described in descending order as shown Figures 4.25, 4.26, 4.27 and 4.28 as follows.

Unit A: Pale gray, mainly silty clay. It is the top sediment layer at this wall. It is moderately sorted and rounded with 30 cm thick. It has organic matter.

Unit B: Yellowish brown and gravelly clay. Poorly sorted and moderate asperity. Gravel is subangular-subround. This unit is 30 cm thick.

Unit C: Dark gray, silty clay, well sorted in middle to upper part. It has grave l 5%. Clasts are sandstone, quartz, and limestone varied from 5-7 cm in diameter and subround. It is has organic matter.

Unit D: Stiff clay, light yellowish brown colluviun. It was well sorted, and composed of quartz, sandstone. It has irox-oxide.

Unit E: Dark gray, light gray, yellowish orange, red, poorly sorted. It has highly fractured with irox-oxide fill in fracture.

According to the fault observations, four faults, i.e. F1, F2, F3, and F4, are identified at the southeastern wall of the MOS1 trench (Figures 4.29 and 4.30). The F1 fault from the northeastern end of the wall side cuts the Unit E. The fault strikes N20°W and dips 65° eastward. The F2 and F3 faults also cut the Unit E with strikes of N30°W and N35°W and dip 55° and 25° eastward, respectively, whereas the F4 fault on the northern side of F1 is a synthetic fault and cuts the Unit E, with a strike of S65°W and a dip of 65° westward.

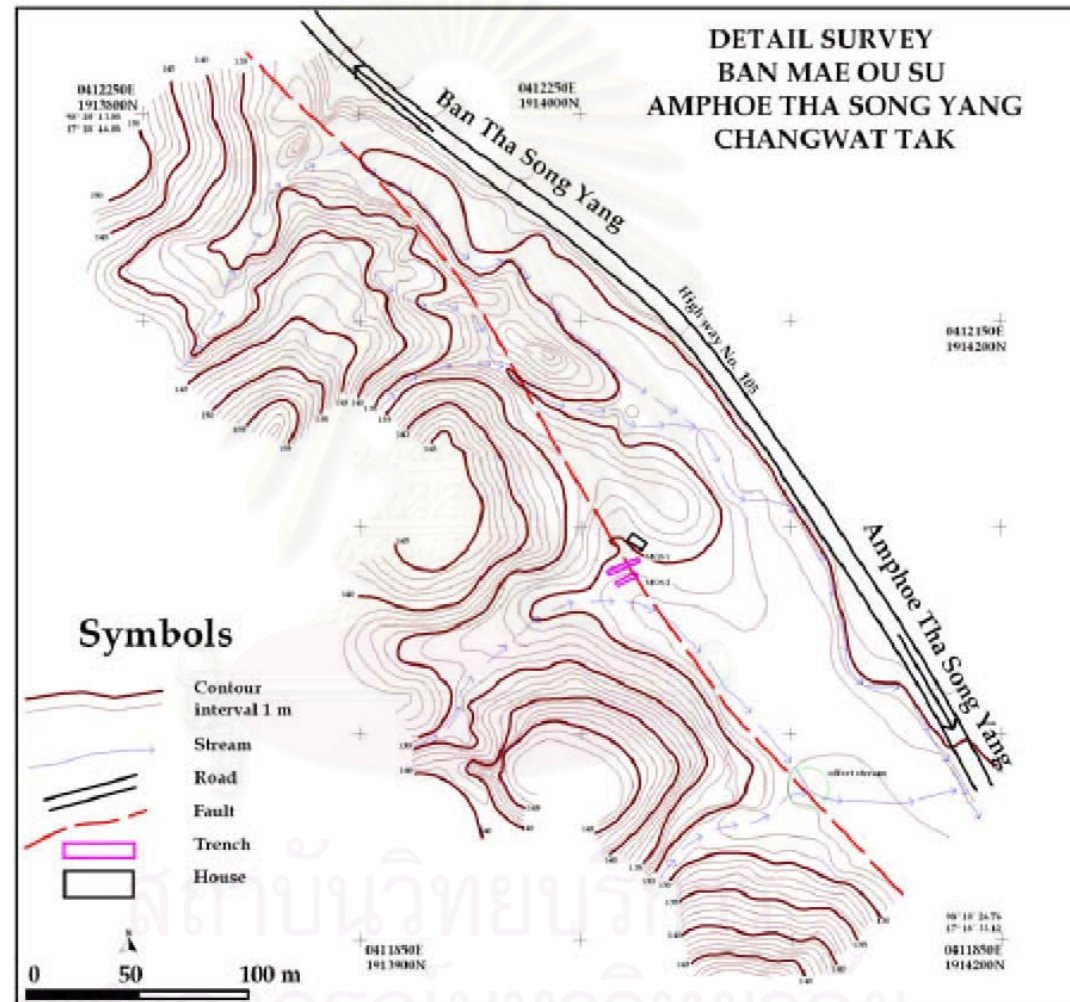


Figure 4.23 Detailed survey map covering offset stream and shutter ridge along the fault segment no.4 (Figure 3.11) of the Ban Mae Ou Su area, Amphoe Tha Song Yang, Changwat Tak.

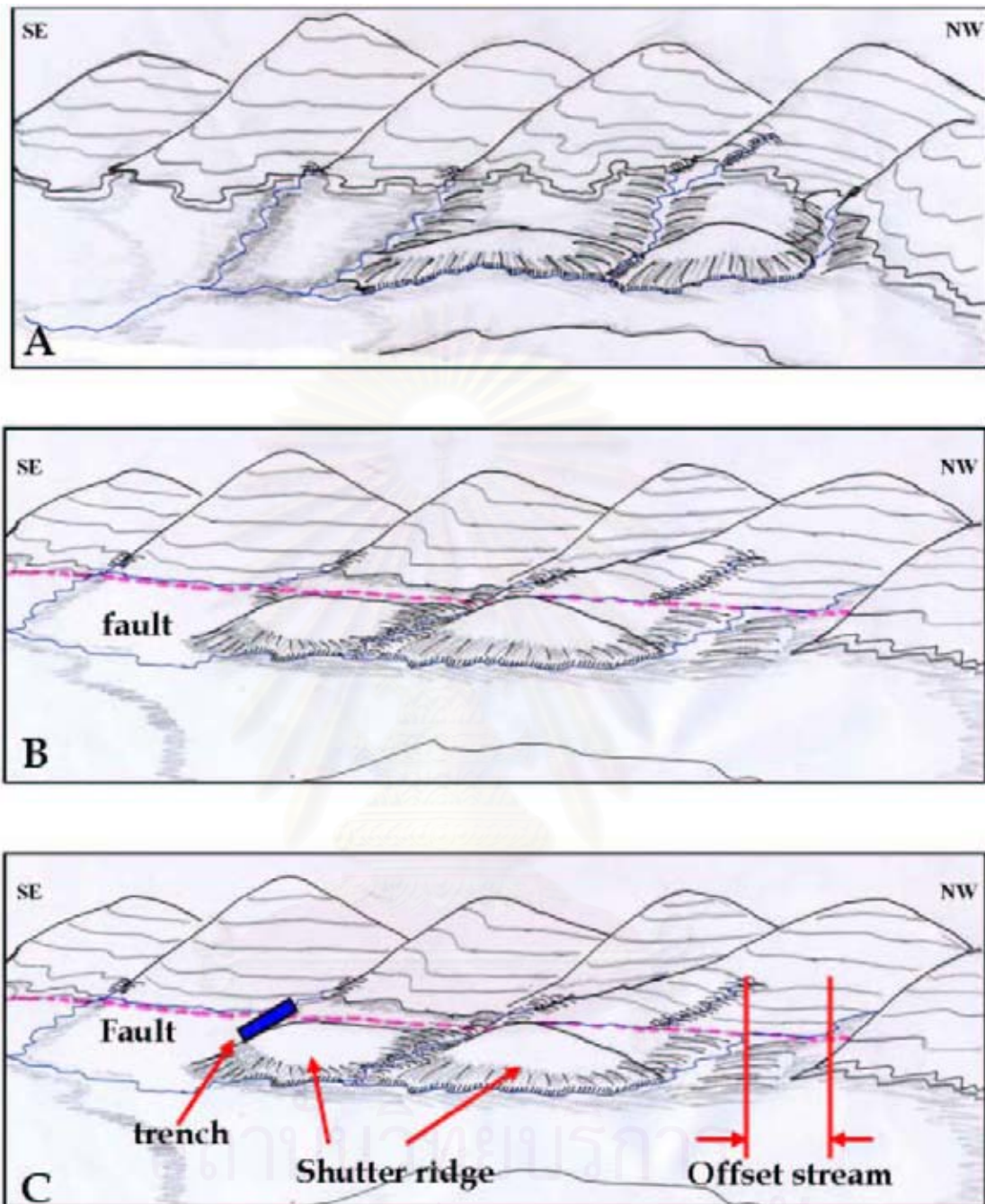
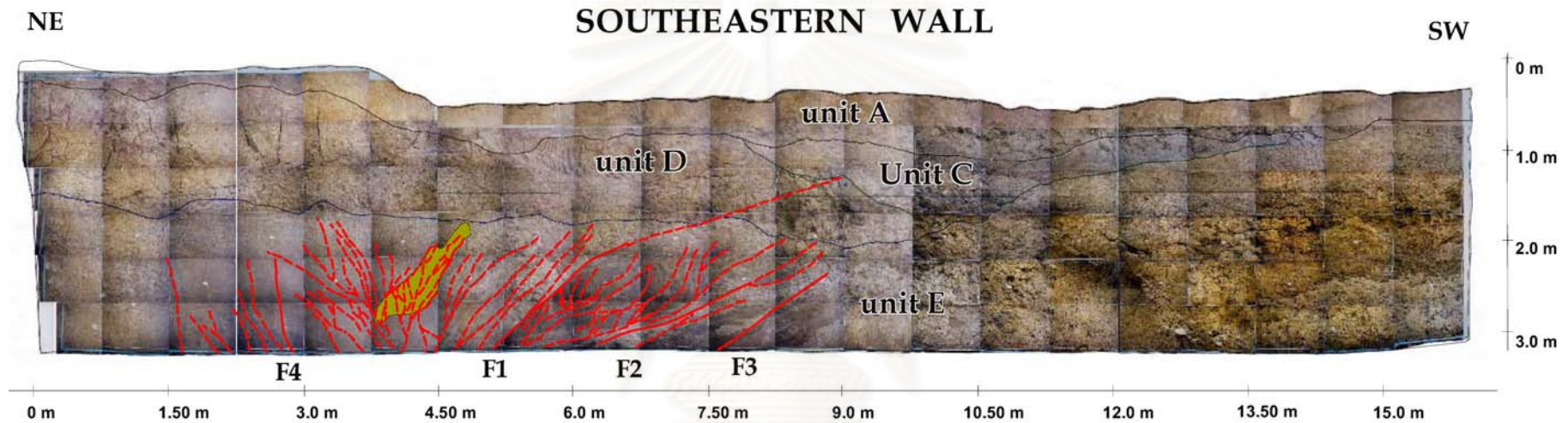


Figure 4.24 Topographic features of area C, Ban Mae Ou Su, Amphoe Tha Song Yang, Changwat Tak. Detailed survey map covering offset stream and shutter ridge of the Ban Mae Ou Su area. Note that in box A is late fault movement, box B is past fault movement, and box C is present fault movement.

## BAN MAE OU SU TRENCH No.1 (MOS1) LOGGING



Unit A : silty clay, pale gray

Unit C : silty clay, dark gray. paleochannel

Unit D : stiff clay, light yellowish brown

Unit E : silty clay, dark gray-black

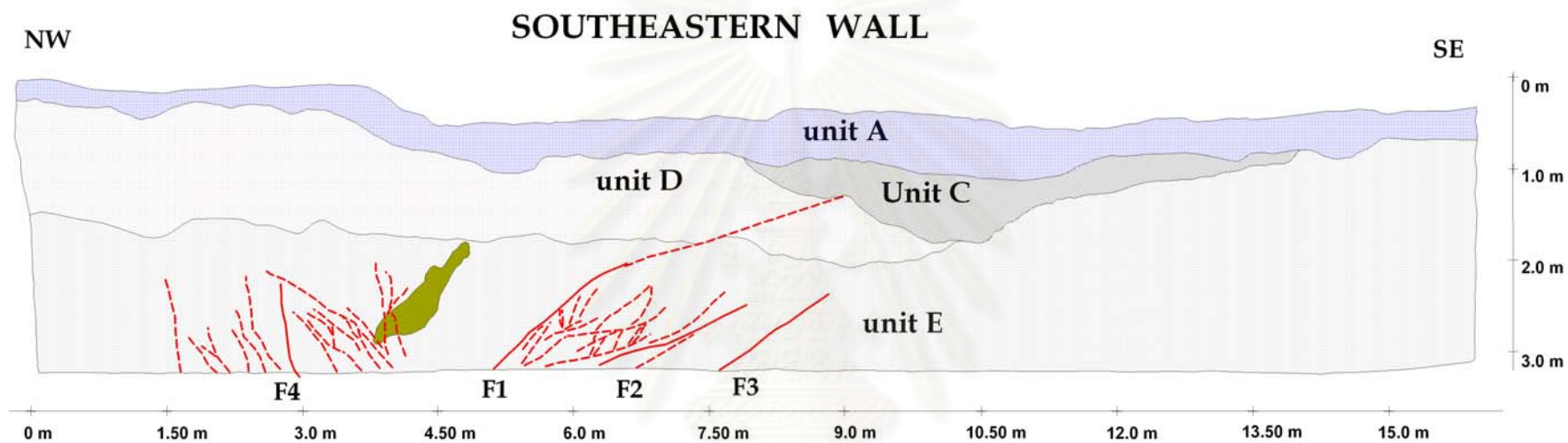
Fault

Fracture

Gravel

Figure 4.25 The southeastern wall of Ban Mae Ou Su Trench No.1 (MOS1) showing principal stratigraphy.

## BAN MAE OU SU TRENCH No.1 (MOS1) LOGGING



**Unit A : silty clay, pale gray.**

**Unit C : silty clay, dark gray; paleochannel.**

**Unit D : stiff clay, light yellowish brown.**

**Unit E : silty clay, dark gray-black.**

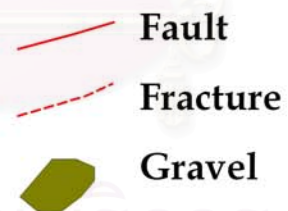


Figure 4.26 Trench-log at the southeastern wall of MOS trench showing principal stratigraphy. Note: Boxes showing the closed-up structures found at SE wall of MSO1 trench (in Figures 4.29 and 4.30).

### BAN MAE OU SU TRENCH No.2 (MOS2) LOGGING

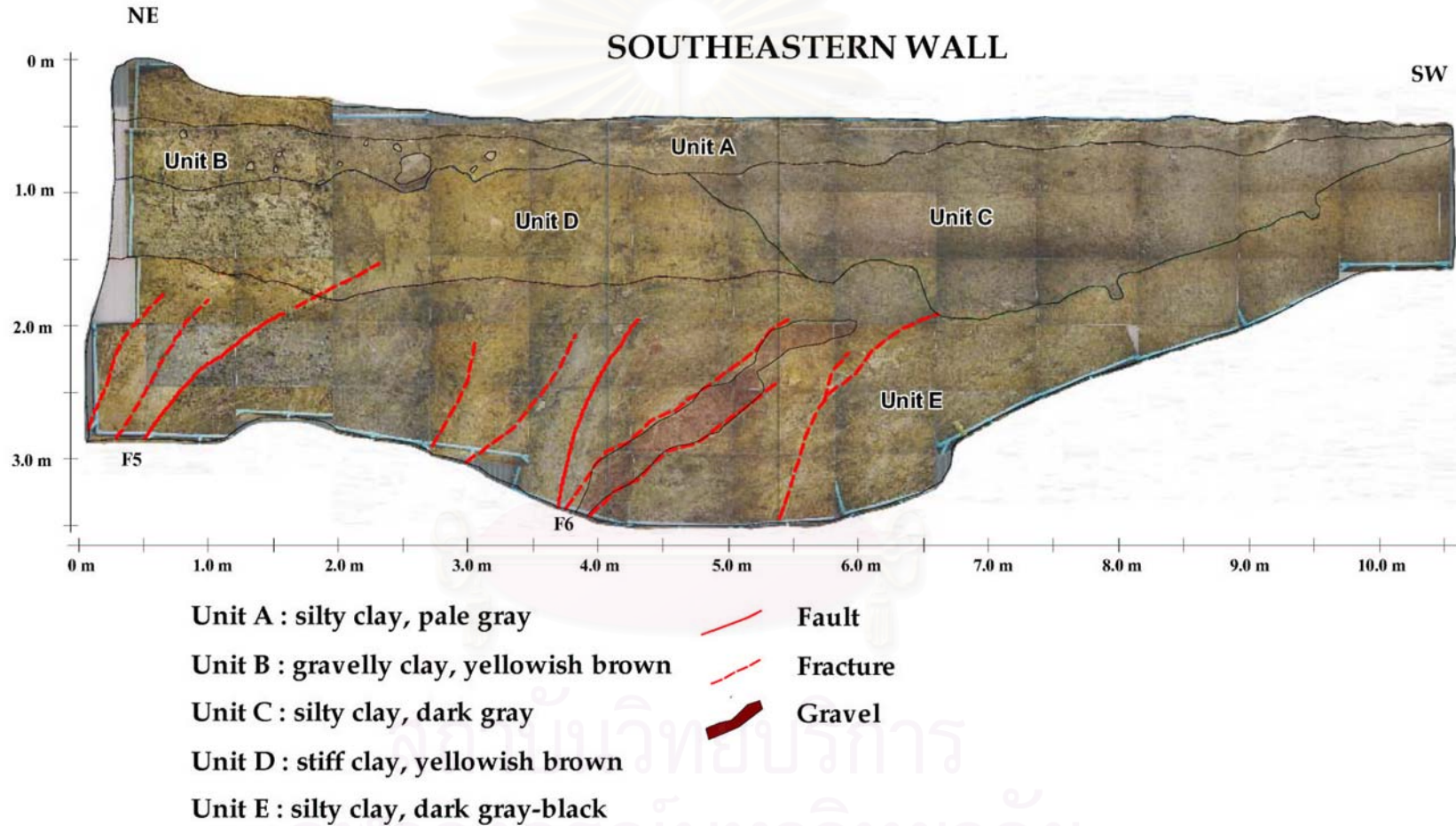


Figure 4.27 The southeastern wall of Ban Mae Ou Su Trench No.2 (MOS2) showing principal stratigraphy.

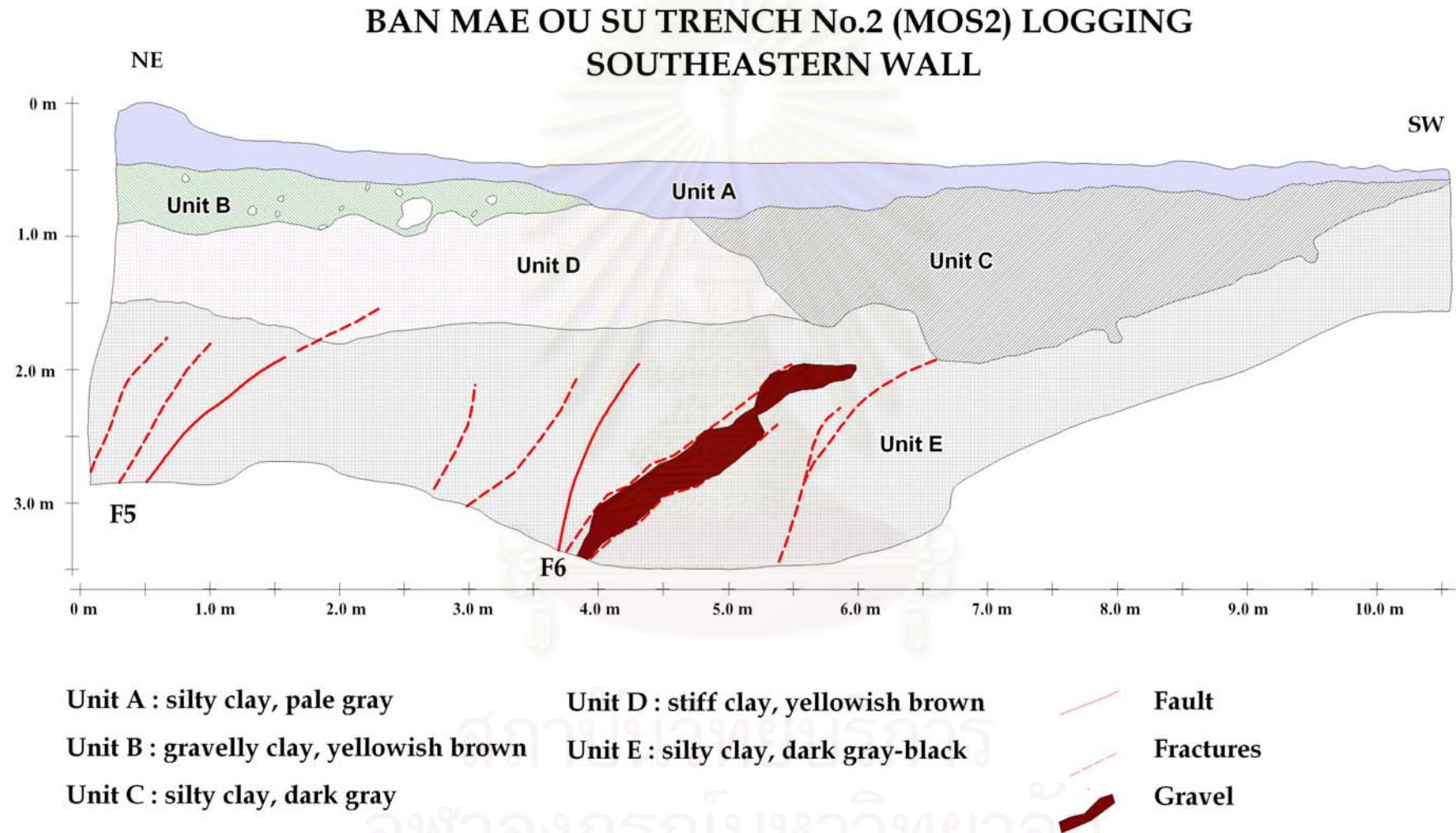


Figure 4.28 Trench-log at the southeastern wall of MOS2 trench showing principal stratigraphy. Note: Boxes showing the closed-up structures found at SE wall of MSO2 trench (in Figures 4.31 and 4.32).



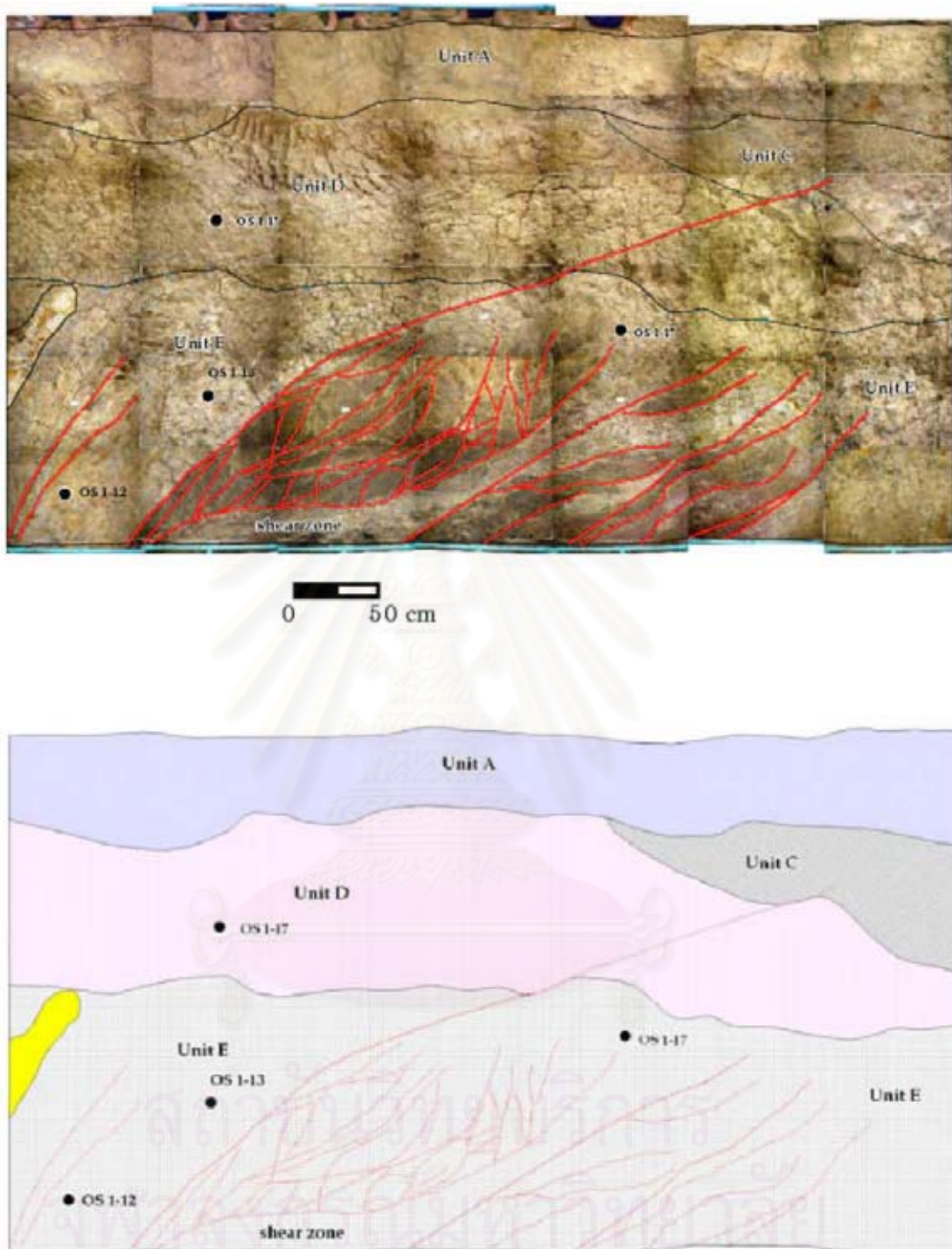


Figure 4.29 Close-up of the southeast wall, MOS1, the fault cuts the Unit E and Unit D.

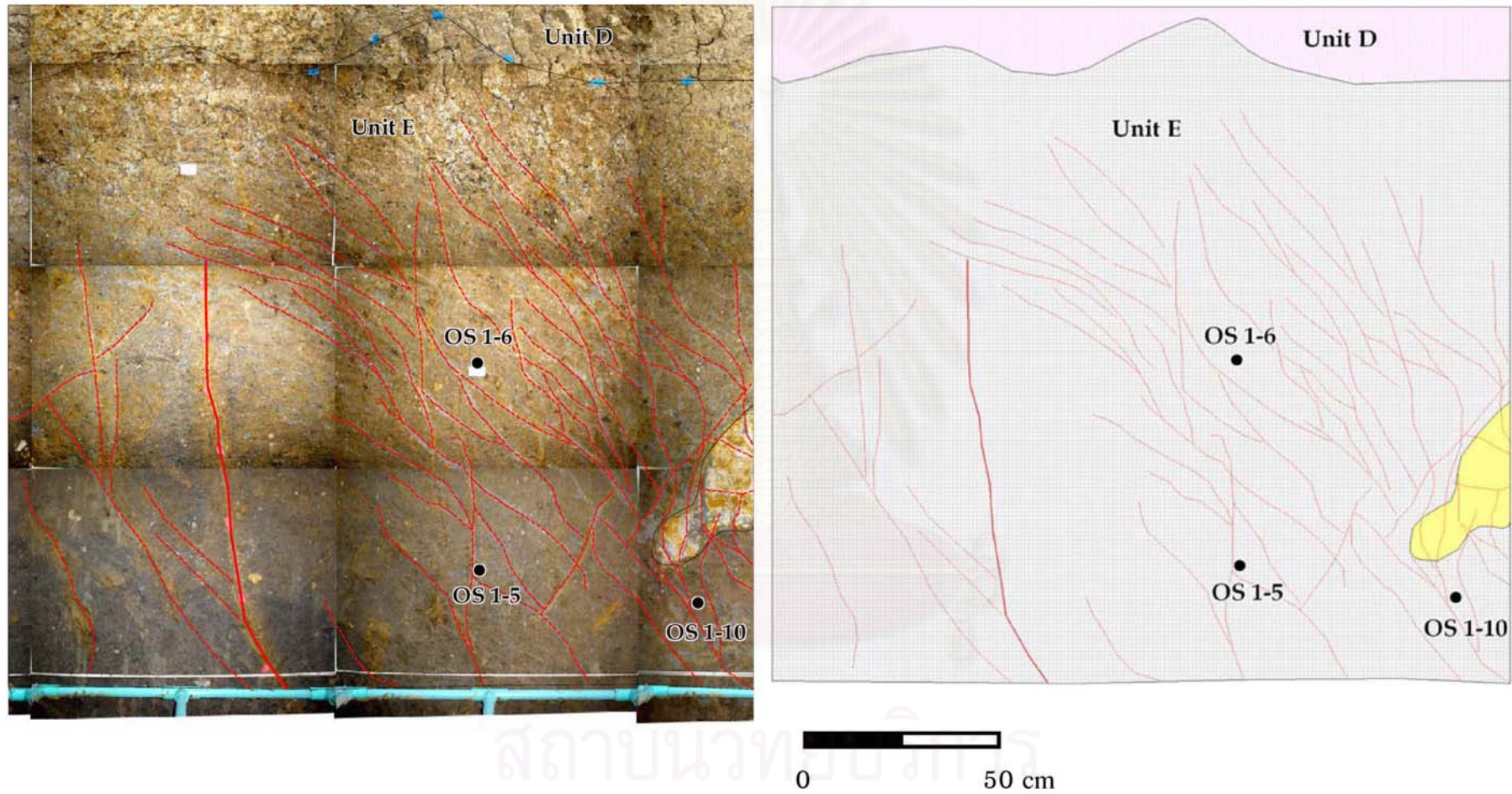


Figure 4.30 Close-up of the southeast wall, MOS1, the fault cuts the Unit E, strike of  $S65^{\circ}W$  and dip of  $80^{\circ}$  westward.

The fault sets, namely as F5 and F6 were observed at the southeastern wall of the MOS2 trench (Figures 4.31 and 4.32). F5 cuts two layers, i.e. units D and E, with a strike of N20°W and a dip of 65° eastward, F5 cuts two layers, units D and E in a reverse sense of movement.

#### **4.3.3 Collected Dating Samples Locations**

##### **4.3.3.1 Ban Mae Ou Su trench no.1**

Thirteen samples were collected in the Ban Mae Ou Su trench no.1 (MOS1) at the southwestern wall for age determination by the Thermoluminescence dating method. Of thirteen samples, three were collected from Unit D, and the rest were collected from Unit E (Figure 4.33).

##### **4.3.3.2 Ban Mae Ou Su trench no.2**

Seven samples were collected in the Ban Mae Ou Su trench no.2 (MOS2) for age determination by the Thermoluminescence dating method. Of seven samples, two were collected from Unit C, and the rest were collected from Unit E. Moreover, two samples were collected from Unit C for age determination by Carbon 14 AMS dating method (Figure 4.34).

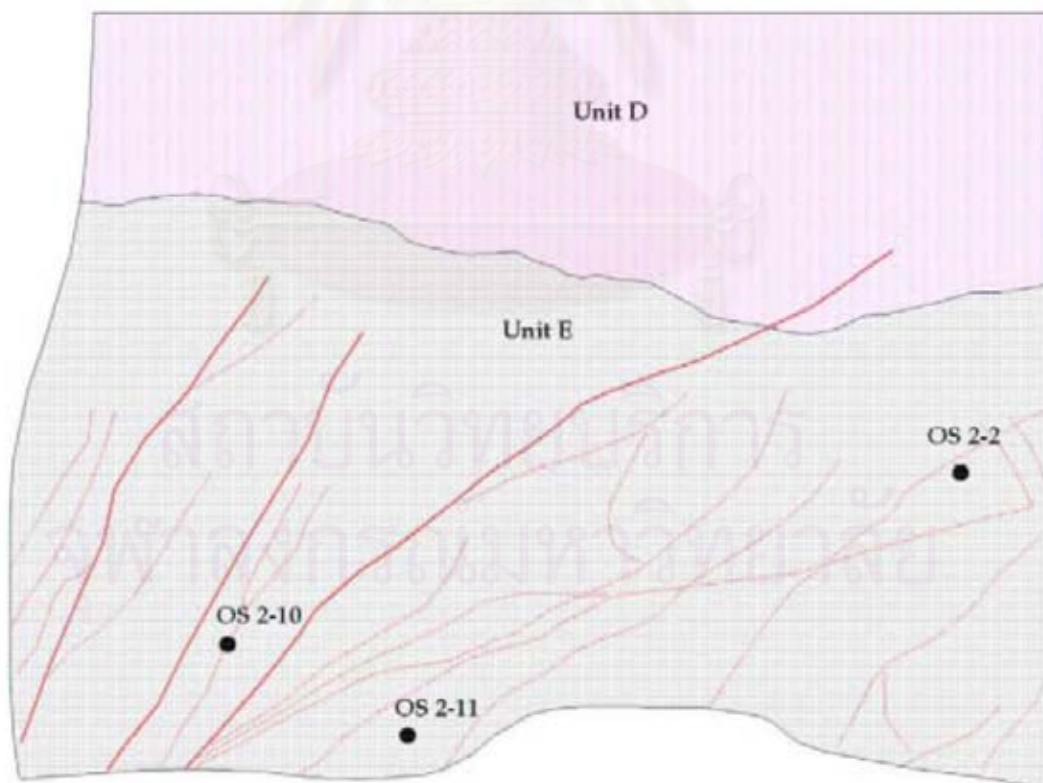
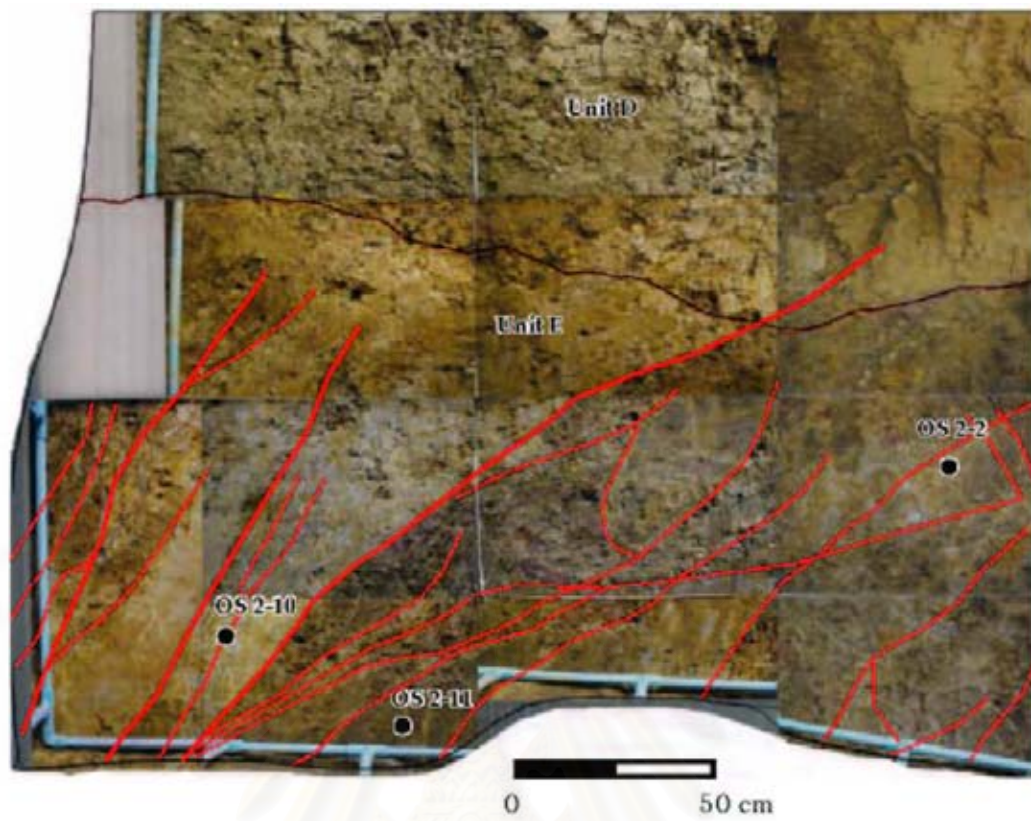


Figure 4.31 Close-up of the southeast wall, MOS2, the fault cuts the Unit E and Unit D.

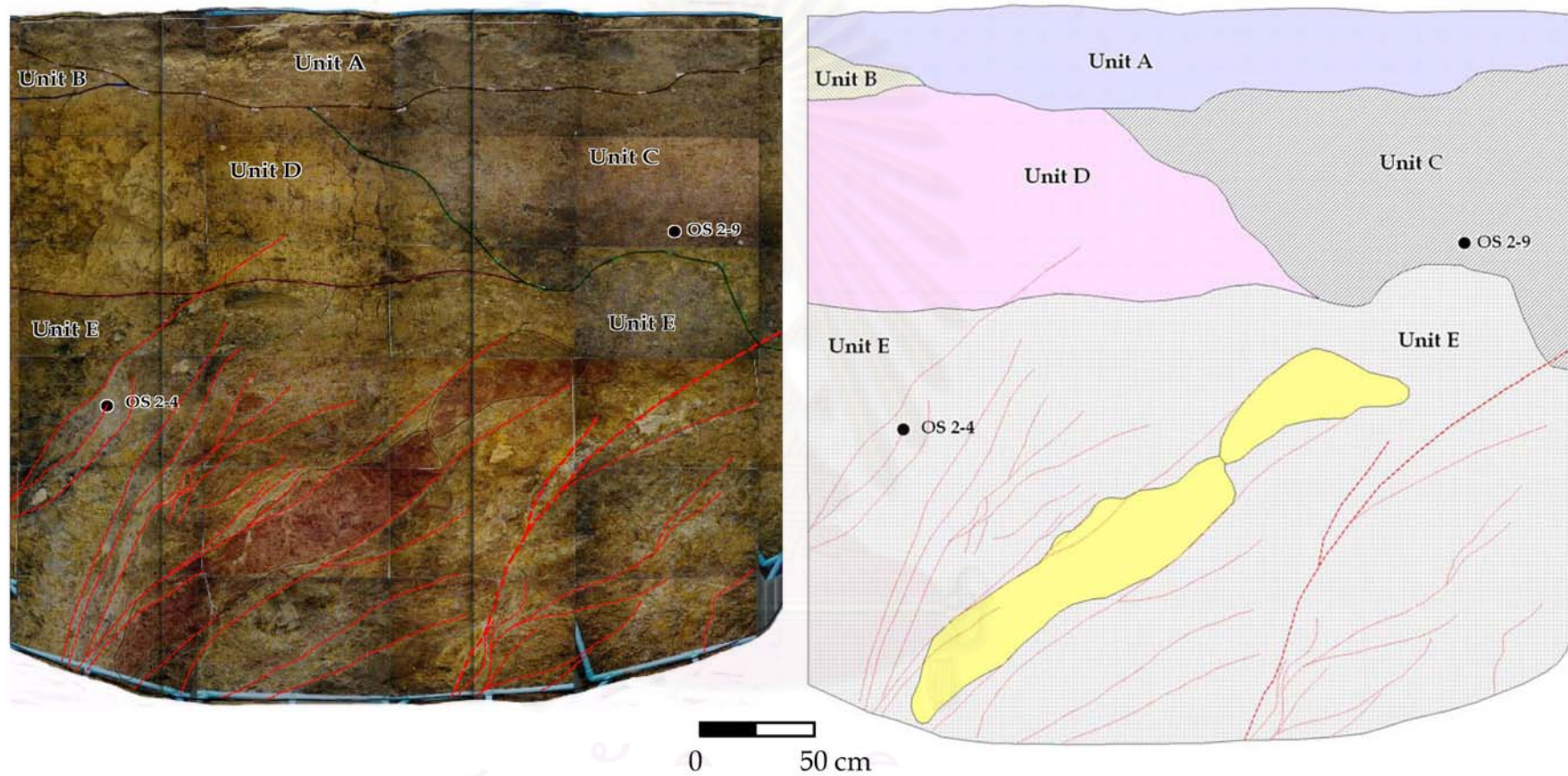


Figure 4.32 Close-up of the southeast wall, MOS2, the fault cuts the Unit E, Unit D, and unit C in the reverse sense of movement.

สถาบันวิทยบริการ  
จุฬาลงกรณ์มหาวิทยาลัย

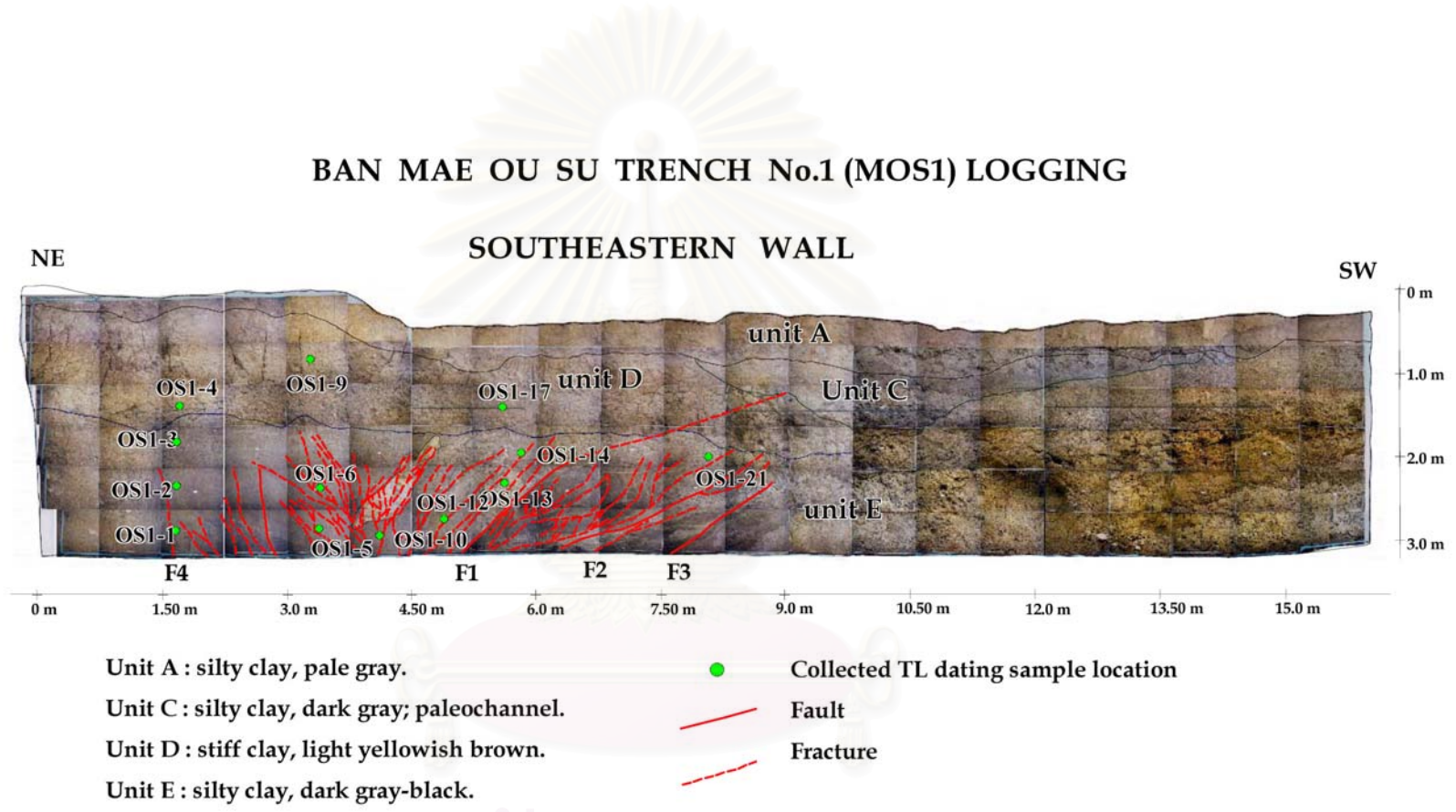


Figure 4.33 The southeastern wall of MOS2 trench and showing locations of collected TL dating samples.

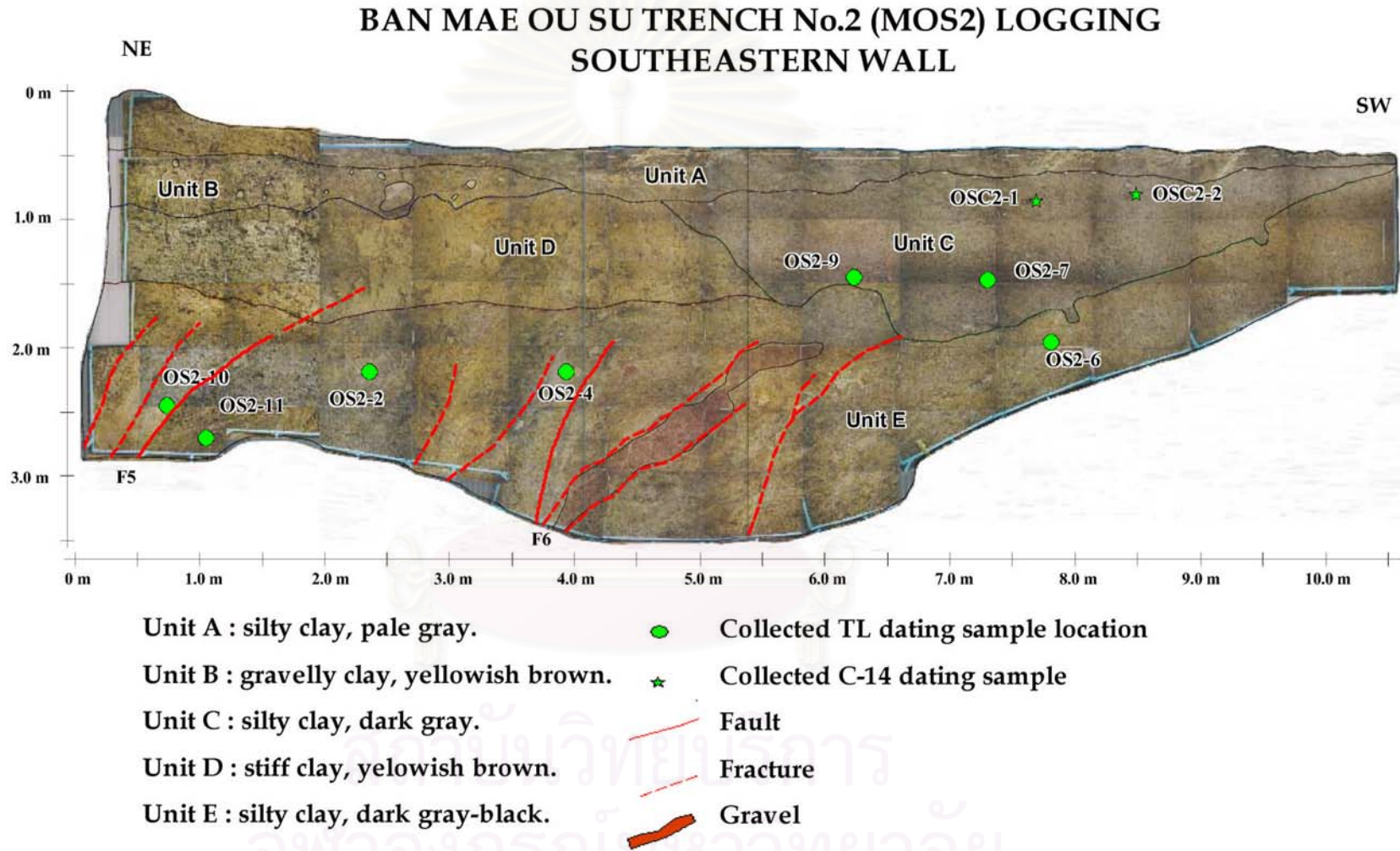


Figure 4.34 The southeastern wall of MOS1 trench showing locations of collected TL and C-14 dating samples.

## CHAPTER V

### THERMOLUMINESCENCE DATING

#### 5.1 Basic Concept

Generally, insulators such as covalence solids and glasses can generate thermoluminescence (TL-dating) signal, but metals cannot. As a result, TL-dating method can be only applied with an insulator crystal. A simple model to review on general background of TL-dating method is based on ionic crystal model, which is simplified as shown in Figure 5.1.

Ionic crystals, for example calcium carbonate and sodium chloride, are composed of lattice of positive and negative ions. In this lattice, it can be defected due to at least three reasons; an impurity atom, a rapid cooling from the molten stage, and damage by nuclear radiation. The defected lattice is presented by lacking of electron from its proper place or electron vacancy, called “electron trap”, leads ionized electrons from vicinity to fill up in this trap hole. In addition, ionized electron is the result of nuclear radiation from earth materials or solar radiation. However, both nuclear radiation and solar radiation have caused much less damages to the lattice structure.

Electrons have been trapped in trap holes lasted until shaken out due to the vibration of crystal lattice. A rapid increase of temperature to high in narrow range leads this vibration to be stronger. In addition, high temperature usually upward of 400°C can evict electrons from deep electron traps to be diffused around the crystal. Note that, because of different crystals, there are different types of traps, and then optimum temperatures to evict electrons in different crystal traps are unique. However, diffused electrons can be directed into two different ways; firstly to be retrapped at different types of defect which is deeper trap, and secondly to be recombined with an ion in lattice which electrons once have previously been evicted.

According to TL-method, since it has mainly concerned only on recombination process, then the process is also reviewed in this section. Anyway, there are two types of recombination process; radiative (i.e., with light emission) or non-radiative. For this method radiative type is interested, which ions or atoms from this recombination process are called luminescence centers and the emitted light is thermoluminescence.

A simplified model of energy level to present thermoluminescence process is illustrated in Figure 5.2.



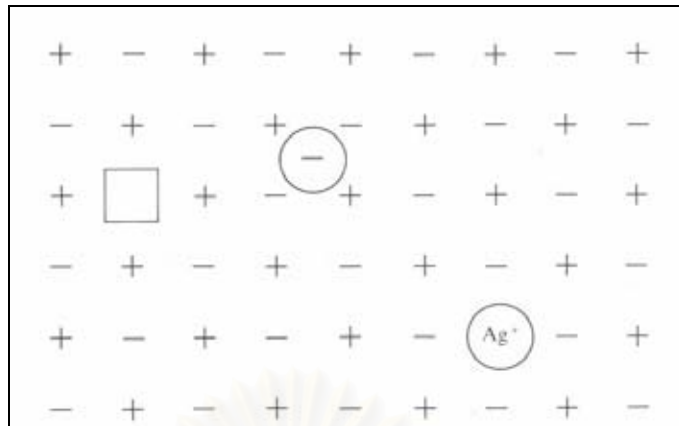


Figure 5.1 A simplified model of lattice structure of an ionic crystal showing three simple types of defect which are negative-ion vacancy on the left, negative-ion interstitial at the center, and substitution impurity center on the bottom right (After Aitken, 1985).

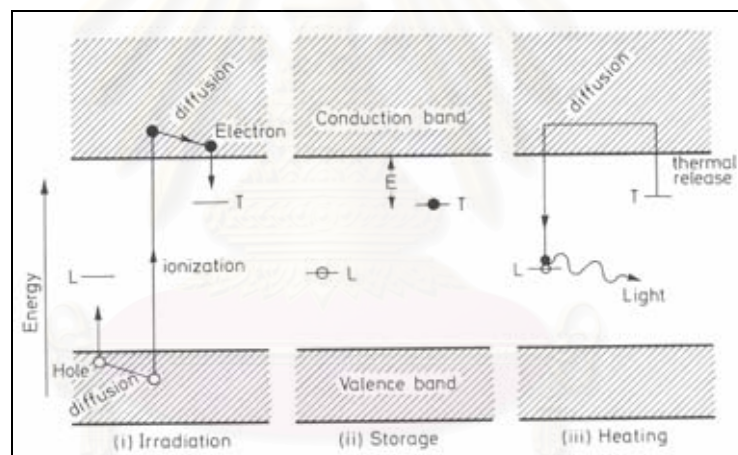


Figure 5.2 Thermoluminescence-process diagram showing energy-level related to three processes; (i) irradiation process, caused by crystal exposed to nuclear radiation, ionized electrons are trapped at hole (T). (ii) Storage stage in which electrons have been trapped, need hole deep enough for electrons (E) during geological time period of sample. (iii) Heating process, at optimum level of temperature, electrons are released and re-combined at luminescence center (L), and then light (TL) is released (After Aitken, 1985).

There are electron traps (T) and center of luminescence (L) located as intermediate between the valence band and the conduction band. The energy (E) is required in an optimum level to shaken out electrons from its deepest hole. In general, when electrons have already shaken out by heating, and recombination is done at the centers of luminescence, light is emitted. However, in some case which recombination has done at non-luminescence center or killer center, there is no emission of light and the energy is represented in the form of heat.

In summary, thermoluminescence process can be concluded in four steps as follows; firstly, ionization of electrons caused by nuclear radiation. Secondly, some of these electrons are trapped in continuous and constant rates lasted until temperature has increased. Thirdly, some of electrons are heated at the optimized temperature level to evict electrons from deep trap hole. Fourthly, some of these electrons are then reach luminescence centers and in case of recombination process has done, light emission from luminescence centers is generated. The amount of emitted light or the number of photon in this stage is depended on the number of trapped electrons, which in turn is the amount of nuclear radiative proportion or paleodose. In addition, dose rate of nuclear radiative applied to environment is called annual dose.

Ultimately, based on TL-process mentioned above, age of quartz-bearing sediments (such as those of this study) can be determined by simple equation 5.1 below;

$$\text{TL-age} = \frac{\text{Paleodose}}{\text{Annual dose}} \dots\dots\dots (5.1)$$

## 5.2 Paleodose and Annual Dose Evaluation

In this section, brief descriptions on paleodose and annual dose evaluation are provided as first and second orders, respectively. Firstly, once sediment sample has been treated to become purified quartz crystals before measurement their quantity of TL-intensity using TL-instrument. The apparatus diagram for TL-measurement is shown in Figure 5.3. However, due to further details of apparatus is out of scope, and then it was not mention herein. The output of TL-intensity from this instrument expresses in the form of grow-curve graph as shown in Figure 5.4 in which X-axis is represented temperature and Y-axis is TL-intensity. Peak of TL-intensity in this curve is used to evaluate paleodose in the next step.

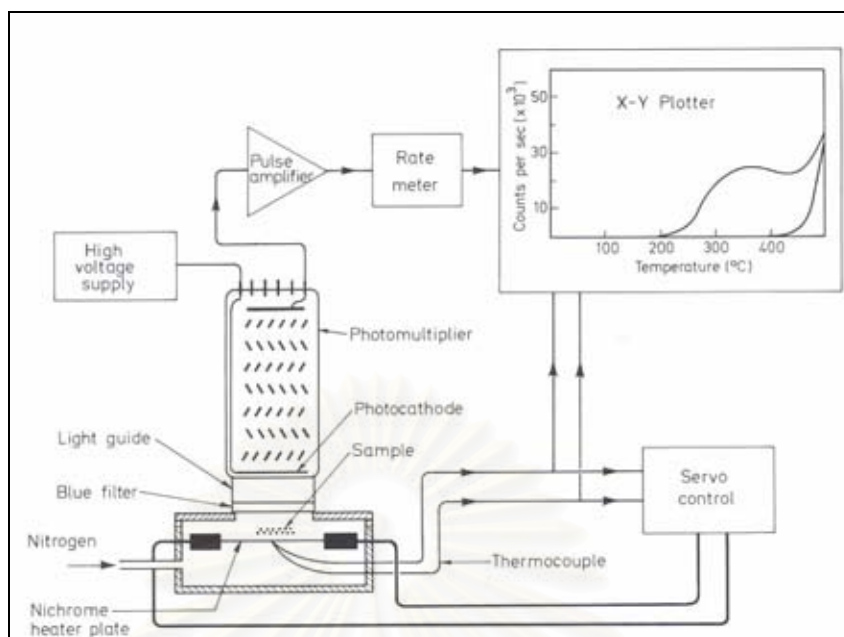


Figure 5.3 Diagram of thermoluminescence instrument (After Aitken, 1985).

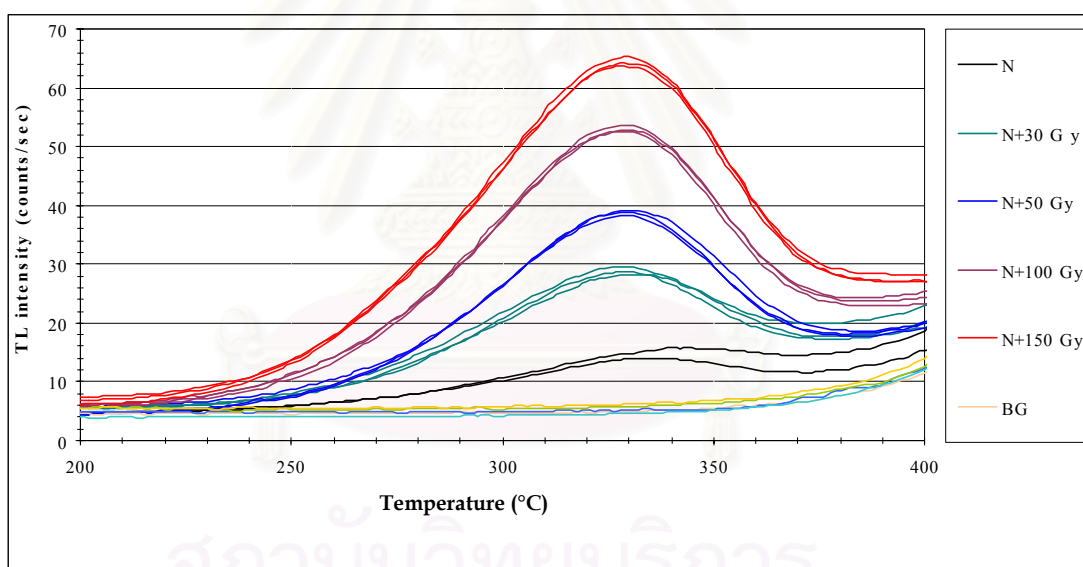


Figure 5.4 A glow curve graph shows relationship between TL intensity versus temperature.

### 5.2.1 Laboratory Analysis

TL laboratory procedure in this study is mainly followed that of Takashima and Honda (1989). The methodology of analysis is composed of 2 main procedures, including paleodose or equivalent dose evaluation and annual dose evaluation (Figure 5.5).

#### 5.2.1.1 Crushing and Sieving

Upon arrival in the laboratory, TL samples normally were dried by 40–50°C baked in the dark room. Water content is also measured for all samples being dated because it is

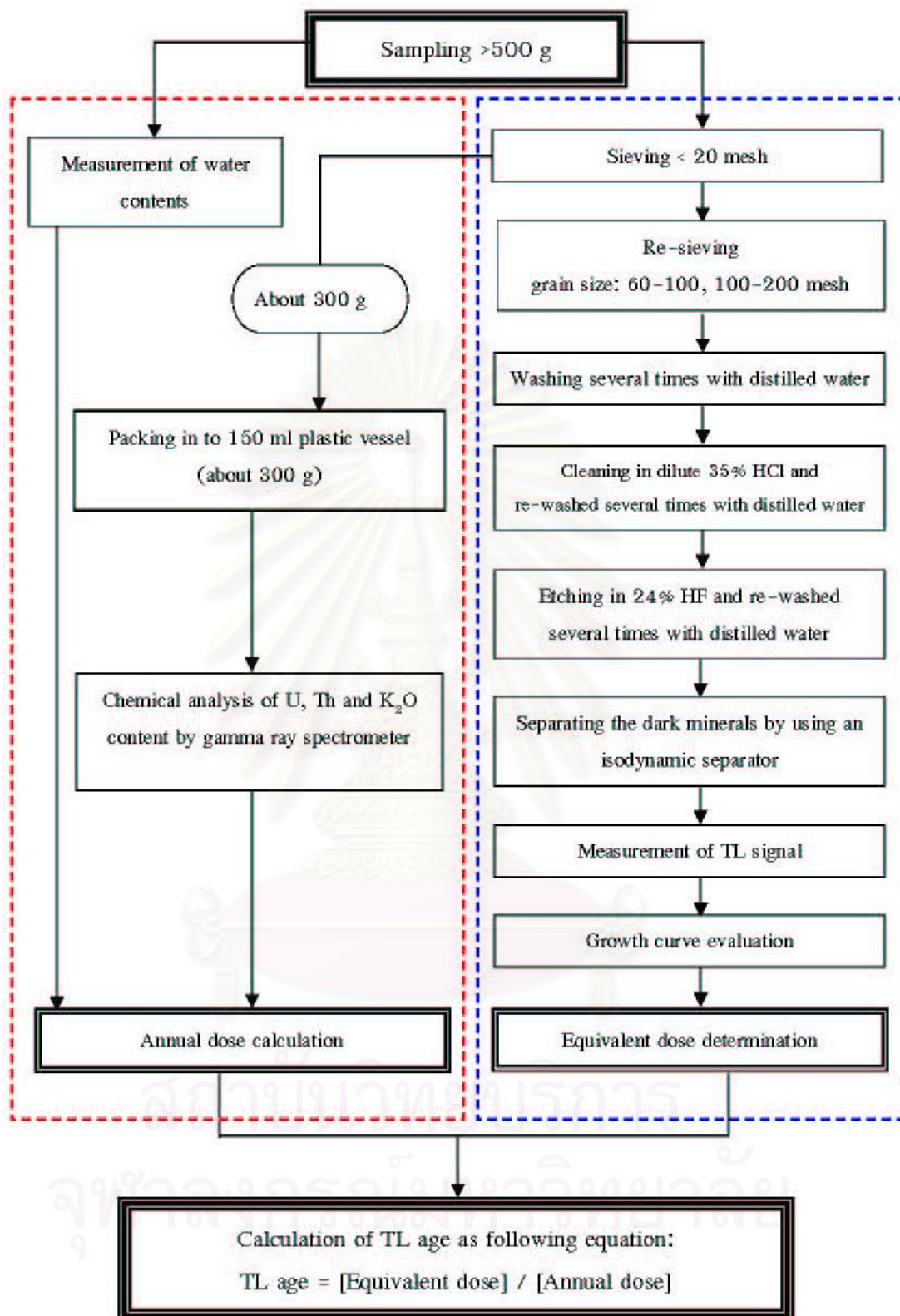


Figure 5.5 Simplified flow chart illustrating laboratory analysis use in this research study. The red dash line is the annual dose procedure and the blue dash line is the equivalent dose procedure (Modified from Takashima and Honda, 1989).

the one significant parameter for annual dose determination. The formula of water content calculation is shown in equation 5.2.

$$\text{Water content} = \frac{(\text{weight of a wet sample} - \text{weight of a dried sample}) \times 100}{\text{weight of a dried sample}} \dots\dots\dots (5.2)$$

After getting dried sample, each sediment sample was shattered by using a rubber-hammer and the material passed through sieves to isolate the grain size fraction in 2 parts. Sediments which grain size pass through 20 mesh ( $<841\mu\text{m}$ ) were collected about 300 g and was separated to keep in plastic containers for annual dose determination. Remnant part from annual dose collection is carefully re-sieved and the material passed through sieves to isolate the grain size fraction between 60–200 mesh. Both of these portions were kept in beakers for purifying quartz grain and equivalent dose determination, respectively. In the annual dose, a sample portion is ready and skips to the measurement step but in both of two portions for equivalent dose determination is necessary to participate in chemical treatment.

#### 5.2.1.2 Paleodose or Equivalent Dose Evaluation

##### A) Chemical Treatment

The main objective of chemical treatment is purification of quartz mineral in TL samples from the method in order to keep off destroying the signal of sample. The detail of chemical treatment is shown below:

- a) Washing the sample by distilled water 10 times for removing some organic materials and clay particles;
- b) Chemically cleansed the sample in dilute 35% HCl at 50–60°C in a period of 15–30 minutes and re-washed several times with distilled water for eliminating carbonates and deep-rooted organic material;
- c) Etching the sample in 24% HF at 50°–60°C for 15–30 minutes and re-washed it several times with distilled water. HF was used to dissolve the plagioclase and outer layer of quartz grains to a depth sufficient for the core remaining to have a negligible component of alpha particle dosage; and
- d) After washing with water and drying in the dark room, the dried sample was then separated to remove out the dark minerals (e.g. zircon, garnet, and metallic minerals) by using an isodynamic separator (Frant's isodynamic magnetrometer)

After finishing sample treatment, it is necessary to check purity of quartz sample by XRD analysis. If the quartz-rich samples contain less than 10% of the other minerals, the samples were supposed to contain pure quartz concentrates. Then the sample was ready for determine equivalent dose in the next step.

### **B) Sample Preparation for Equivalent Dose Measurement**

The pure quartz sample after chemical treatment is subdivided into 3 parts:

- Part 1: Natural quartz sample was used for evaluated natural sensitivities of previously acquired TL signal;
- Part 2: Sample was exposed directly with natural sunlight for 12 hours (Aitken, 1985) to effectively remove all of the previously acquired TL leaving only what is termed as the unbleachable TL signal. This part used for determining residual levels; and
- Part 3: Sample used to find out the characteristic of quartz effective with artificial irradiation that amount of radioactive irradiation (in unit Grey) is known. The gamma ray source for artificial irradiation is a Co<sup>60</sup> from Office of Atomic Energy for Peace (OAEP), Bangkok.

### **C) Equivalent Dose Measurement**

Evaluation of equivalent dose commences with measurement of TL intensities on 3 sample portions: 1) natural sample portion, 2) artificial irradiation sample portion and, 3) residual sample portion (in sediment sample). About 20 mg of sample was filled in aluminum planchettes and placed on a molybdenum heater. The graph shows a relationship between TL intensity and temperature which is called “glow curve” (Aitken, 1985). The term glow curve is given to plot intensities of emitted light versus temperature (Figure 5.5). Calculation of equivalent dose can be done by extrapolating natural signal intensity and residual signal intensity with a growth curve from artificial irradiated signal intensity. The result is assumed to be proportional to the equivalent dose of equation 5.1.

Although the glow curve shown in Figure 5.5 is smooth continuum, it is really composed of stable and unstable signals. This procedure makes by comparing the shape of the natural glow-curve (i.e. the glow-curve observed from a sample which has not received any artificial irradiation in the laboratory) with the artificial glow-curve observed as a result of artificial irradiation.

Thus a constant ratio between natural and artificial glow curves gives an indication that, throughout this plateau region, there has been negligible leakage of electrons over the

centuries that have elapsed since all traps were emptied in the course of the stimulation by ancient environment.

The next step is for the construction of growth curve. This can be done by the increases of TL output with known amounts of additional radiation that induced the sample. The graph showing this relationship is called “growth curve” (Figure 5.6).

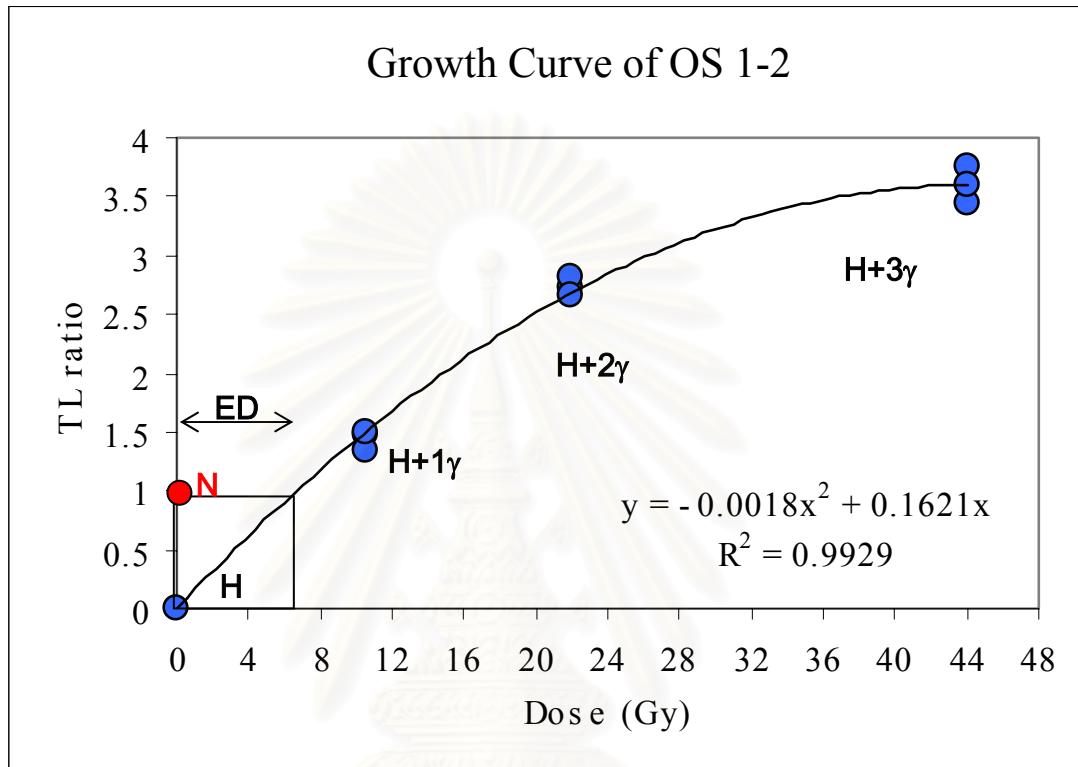


Figure 5.6 Graph showing relationship between TL ratio (artificial glow curves/natural glow curve) versus temperature ( $^{\circ}\text{C}$ ). N is natural signal, H is heated sample at  $320^{\circ}\text{C}$  for 5 hours, and  $\gamma$  is known dosage that irradiated sample.

### 5.2.2 Regeneration Technique

In this technique, the simplest approach to the evaluation of equivalent dose is by the straight-forward procedure of measuring the natural TL intensity from a natural sample (N) and comparing it with the artificial TL intensity from the same sample that know certain dosage (artificial irradiate sample).

In this study, after heating the quartz-extracted at  $320^{\circ}\text{C}$  for 5 hrs, individual samples were liquated for 5 sub-samples (Takashima et al., 1989). For each sub-sample, artificial irradiation was added with the doses of 44, 103, 303, 723, and 1,440 Gy. The values of TL intensity (N/H+ $\gamma$ ) (as shown in Figure 5.6) versus temperature ranges were plotted for each sample and they are shown in Appendix.

The growth curve plot is a graph of TL ratio or TL intensity (as shown in Appendix). It should be noted herein that most graphs of the natural intensity values close to the artificially irradiated liquated (i.e., H+1,440 Gy). Therefore their paleodose can be read after curve fitting for each aliquot (Figure 5.7).

### 5.2.3 Residual Test

In case of sediment sample, evaluation of equivalent dose is complicated by the need to allow for the fact that the equivalent dose is composed of two components: the natural TL signal acquired since deposition and the residual signal that the sample had when it was deposited in the last time.

Many scientists (e.g. Wintle and Huntley, 1980; Tanaka et. al., 1997) proposed several methods to simulate the light source exposures. Samples were exposed to some kinds of light sources. Natural sunlight, UV-ray lamp (365 nm) and xenon lamp were the important illumination sources for bleaching experiments (Won-in, 2003).

In this research study, the naturally bleaching experiment by sunlight requires and depends significantly upon a long sunny day. For the artificial bleaching experiment, it is important to check the minimum of time that can completely bleach samples to the residual level and how much residual level in each sediment sample. The methodology of residual testing starts with bleaching sample and check TL intensity of sample in every 1 hour. Plotting graph showing a relationship between TL intensity and time used for bleaching reveal the minimum time that residual signal begin stable (unbleachable) (Figures 5.8 and 5.9).

### 5.2.4 Plateau Test

According to glow-curve, there are overlapping peaks that may be raised to make misinterpretation of the peak, which is the result of electron emission from deep traps not other shallow traps. Glow-curve peak, which has located in the stable region, is that of interest. The stable region is usually at 300°C or higher where electrons from deep traps are evicted near zero.

The method to recognize the stable region is plateau test as shown in Figure 5.10. There are two glow-curves of natural sample (N) and natural + artificial sample (N+ $\gamma$ ) that had been plotted as solid lines in the same graph. Ratio between N and N+ $\gamma$  is shown as dot line. The plateau of dot line is the stable region. In addition, peaks of both samples have been generated at the same temperature, and N+ $\gamma$  peak is higher than N peak, it means that deep traps are deep enough to contain other electrons.



### 5.2.5 Annual Dose Evaluation

Generally, sediments are exposed continuously to ionizing radiation which originates from their radioactive contents, plus a small fraction from cosmic rays (Aitken, 1985). There are essentially 3 radioactive elements which contribute to the natural dose rate (annual dose) i.e. uranium (U), thorium (Th) and potassium (K). The decay of uranium and thorium results in  $\alpha$ ,  $\beta$  and  $\gamma$  radiation whereas potassium emits  $\beta$  and  $\gamma$  normally, the natural dose rates in most sediment are of the order of mGy/year.

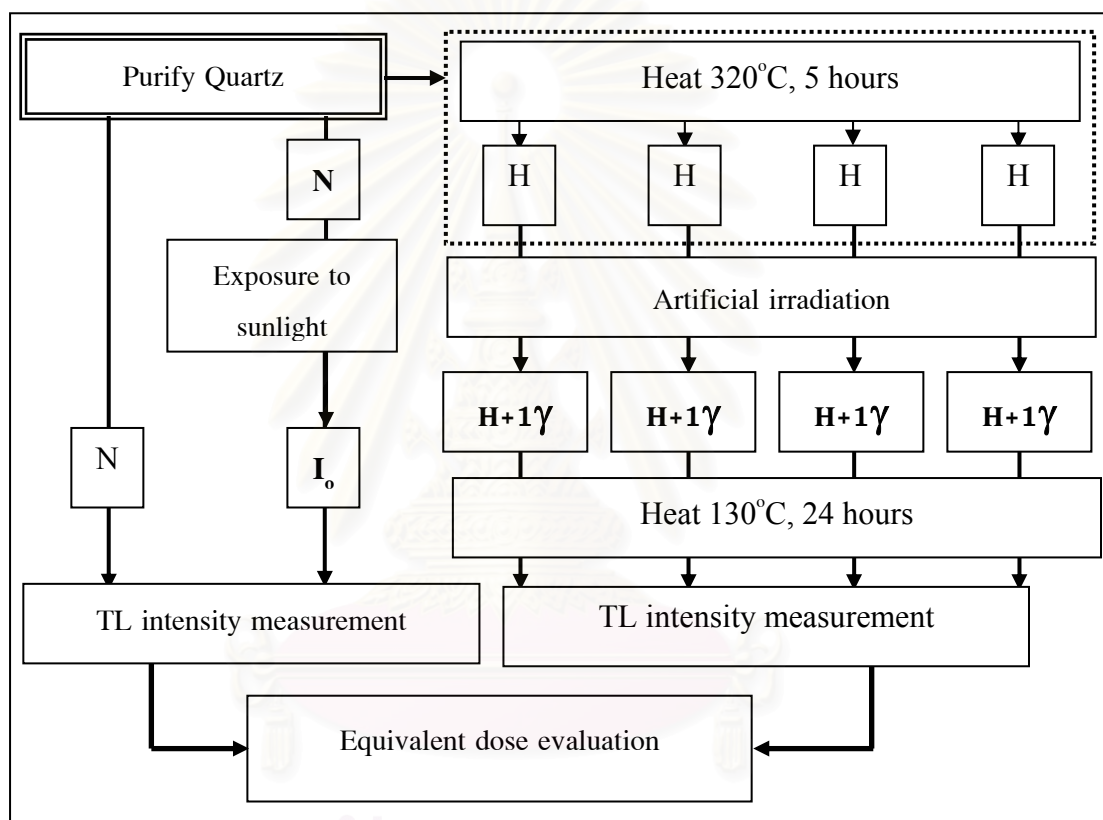


Figure 5.7 Schematic charts of regeneration technique (Takashima et. al., 1989). Note that several portions are used for measurement of the TL intensity; N is natural sample,  $I_o$  is residual intensity from sample, H is 350°C heated sample and  $\gamma$  is known dosage that irradiated sample.

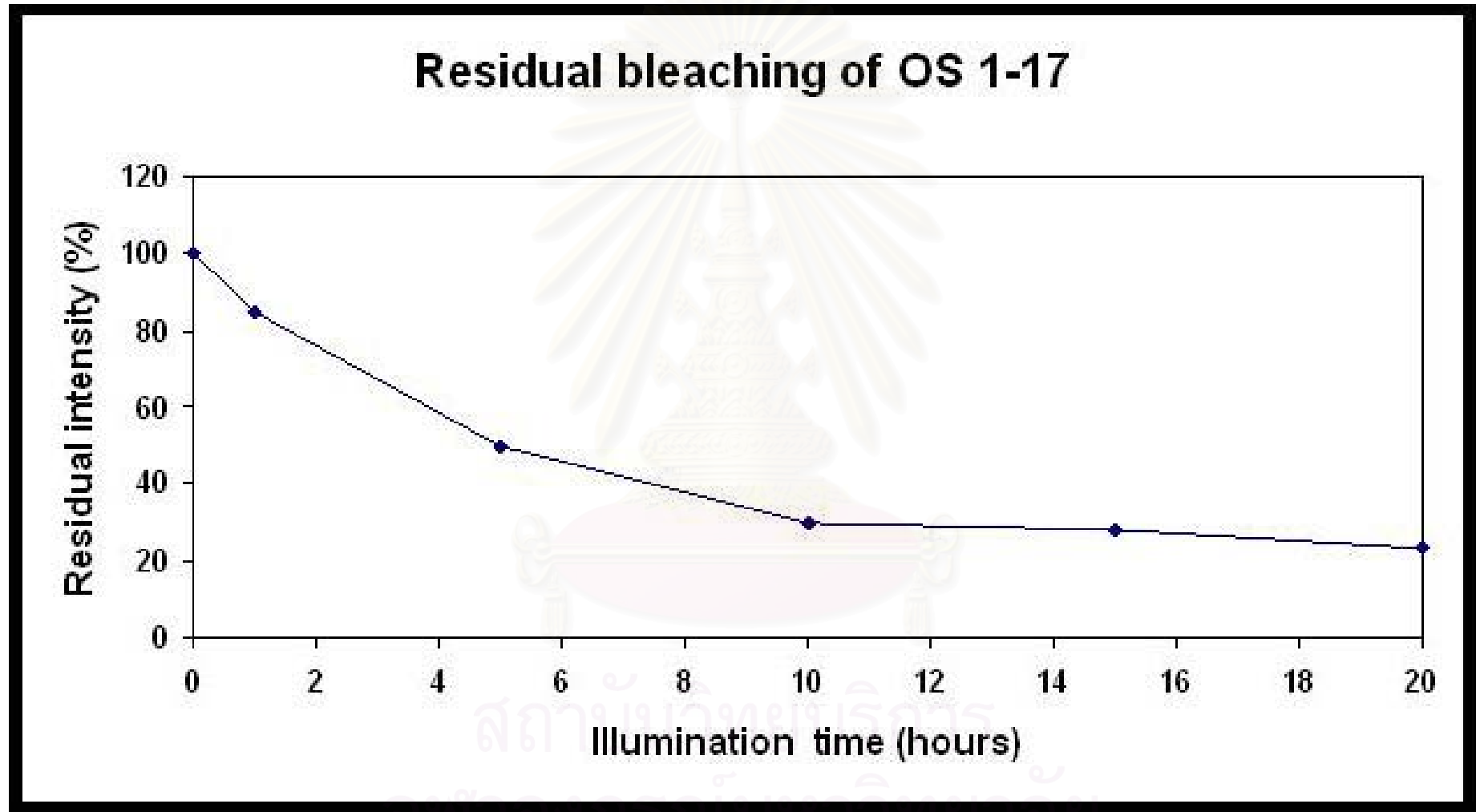


Figure 5.8 Thermoluminescence remaining after bleaching by exposes to sunlight for various time of sample no. OS 1-17

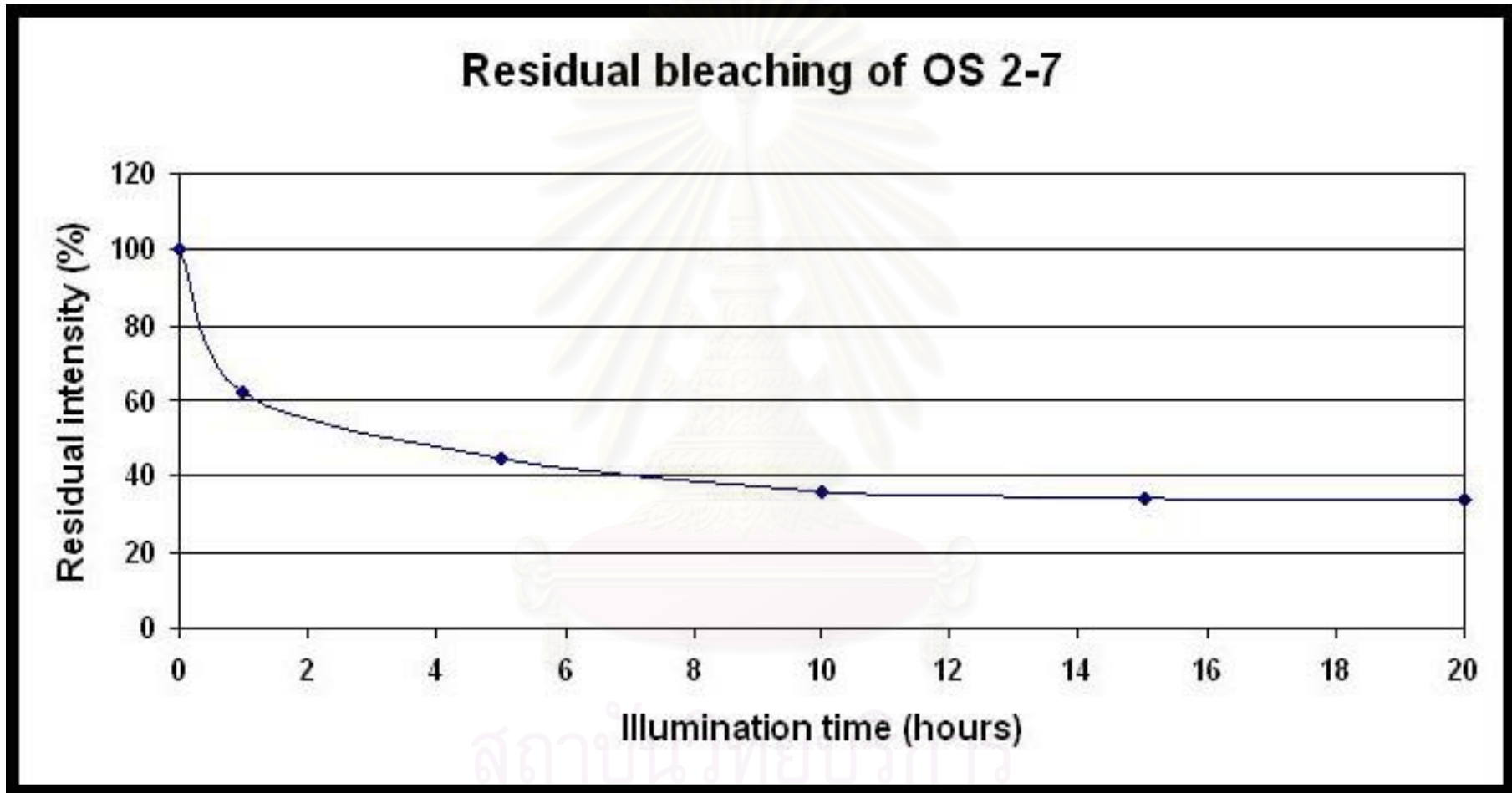


Figure 5.9 Thermoluminescence remaining after bleaching by exposes to sunlight for various time of sample no. OS 2-7

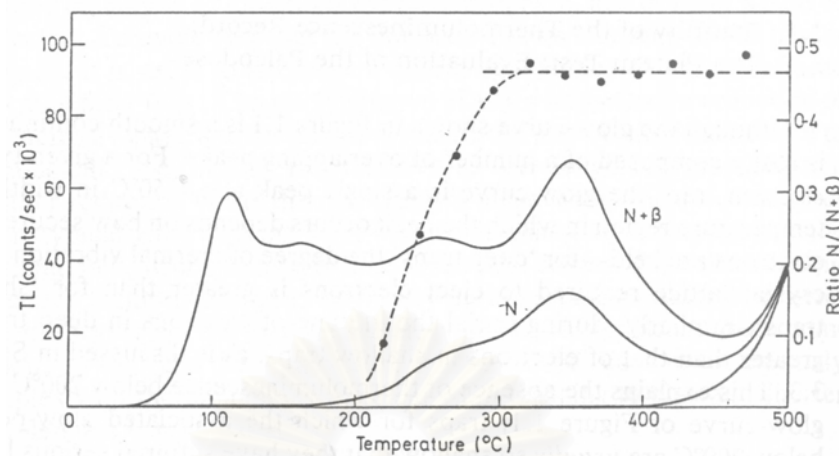


Figure 5.10 Plateau-curve (dashed line) plotted with glow-curves (solid line). Plateau-curve is the ratio of the two glow-curves; N is represented the “natural” glow-curve and  $N+\beta$  is the “natural + artificial” glow-curve (After Aitken, 1985).

For age determination it is necessary to evaluate the natural dose rate accurately. Several components are needed for an accurate annual dose is:

- a. Measurement of U, Th and K contents;
  - b. Calculation of environmental water content in field at time of sample collection;
- and
- c. Cosmic ray component evaluation.

The annual dose to the sample is computed from the concentrations of K, U and Th by the method described by Bell (1979) and Aitken (1985), as shown in equation 5.3.

$$\text{Annual dose} = (\text{AD}) = D_{\alpha} + D_{\beta} + D_{\gamma} + D_c \dots\dots\dots (5.3)$$

Where  $\alpha$  = Alpha irradiation content,

$\beta$  = Beta irradiation content,

$\gamma$  = Gamma irradiation content, and

C = Cosmic ray irradiation content.

#### A) Measurement of Uranium, Thorium, and Potassium Contents

Figure 5.11 shows the schematic preparation and procedure for measurement of U, Th, and K contents by neutron activation analysis (NAA). The estimated standard errors

were less than 10% for U and Th, and less than 3% for K using the fixed count error calculation method (Takashima and Watanabe, 1994).

**B) Annual Dose Calculation**

Annual dose is calculated from chemical data of U, Th, and K contents with the equations proposed by Bell (1979) and Aitken (1985), as shown

$$\begin{aligned}
 AD = & [0.15(2.783U + 0.783Th)/(1+1.50(W/100))] \\
 & +[(0.1148BU + 0.0514BTh \\
 & +0.2492BK)/(1+1.14(W/100))] \\
 & + [(0.1462U + 0.0286Th + 0.8303K)K/(1+1.25(W/100))] \\
 & +0.15 \dots\dots\dots (5.4)
 \end{aligned}$$

- Where
- AD = Annual dose (mGy/year),
  - U = Concentration of uranium in ppm,
  - Th = Concentration of thorium in ppm,
  - K = Concentration of potassium oxide (%),
  - B = Beta coefficient in quartz grains, and
  - W = Water content (%).

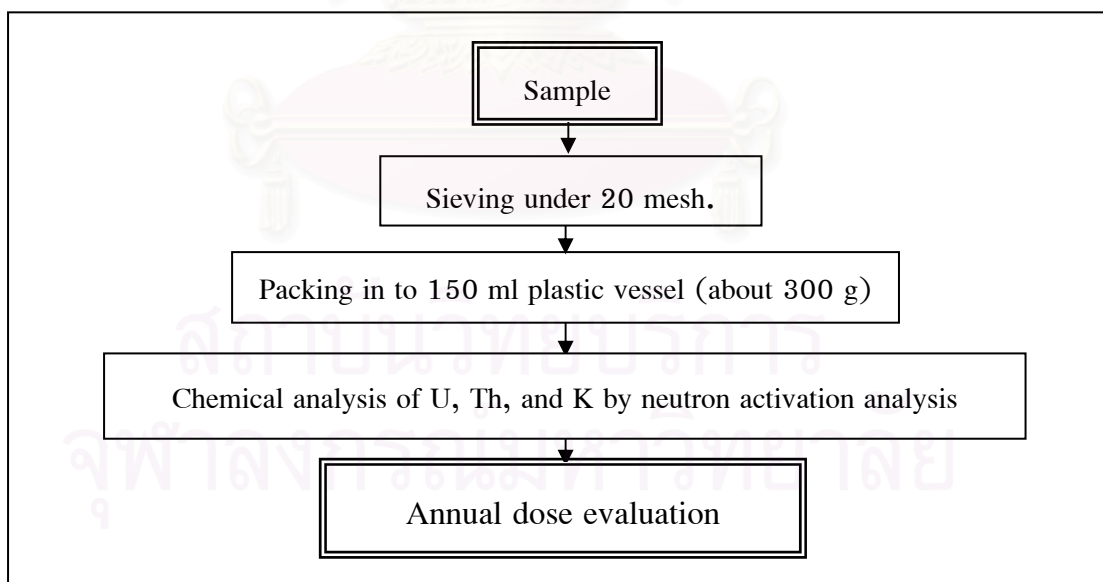


Figure 5.11 Summary of neutron activation analysis (NAA) procedures with sample preparation and annual dose determination.

### 5.2.6 Error Determination

Error in TL-dating result derives mainly from sample preparation and TL measuring apparatus (av. 10%) (Takashima and Honda, 1989), as well as standard deviation (SD) from measured values of ratio  $H+\gamma / N$  on growth curve. So equation for dating errors is described as

$$\text{Error} = \text{Absolute} [(SD_{ED}^2) + (SD_{AD}^2)] \times \text{age} \dots\dots\dots (5.5)$$

Where  $SD_{ED} = \text{Absolute} [(x-x \text{ bar})^2/N]$   
 $SD_{AD} = 10 \%$  (Takashima and Honda, 1989)

### 5.3 Result from Thermoluminescence Dating

A total of 20 fault-related sediment samples were collected from two trenches for determining their ages using the TL-dating method. Summary of the results are shown in Table 5.1. Samples, details, and ages are described below.

Thirteen specimens were sampled and collected from the southeastern wall of MOS1 at the Ban Mae Ou Su area, as shown in Figures 5.12 and 5.13. Ten quartz-enriched sample were selected from the Unit E (dark gray to black silty clay layer), and three samples were selected from Unit D (light to yellowish brown stiff clay)

Sample no.OS1-1 from the bottommost of the Unit E shows good glow curves for both natural and artificially irradiated sample (Appendix A). The plateau test as shown in Appendix B, is the rather stability line at 330°C on ward. The growth curve for sample no. OS1-1 displays the arbitrary TL intensity of a natural sample at 83,000 which is equivalent to the paleodose of 640 Gy, in Appendix C. The sample has the annual dose about 6.42 mGy/yr with the water content of 9.06 %. These TL parameters reveal the TL date of sample no.OS1-1 as 99,800 yr.

Sample no.OS1-2, which is overlying the sample no.OS1-1, displays well-defined glow curves for both natural and artificially irradiated sample (Appendix A). Plots of TL counts per  $(\text{sec} \times 10^3)$  versus individual temperatures illustrate the plateau line at the temperature of 350°C ward. The growth curve graph of the sample also indicates the arbitrary TL intensity of a natural sample at 92,000 giving rise to the paleodose of 375 Gy. The available values yielded the TL date of sample no.OS1-2 to be 66,300 yr.

Sample no.OS1-3 which is overlying the sample no.OS1-2, shows good glow curves for both natural and artificially irradiated sample (Appendix A). The plateau test as shown in Appendix B, is the rather stability line at 370°C on ward. The growth curve for

### BAN MAE OU SU TRENCH No.1 (MOS1) LOGGING

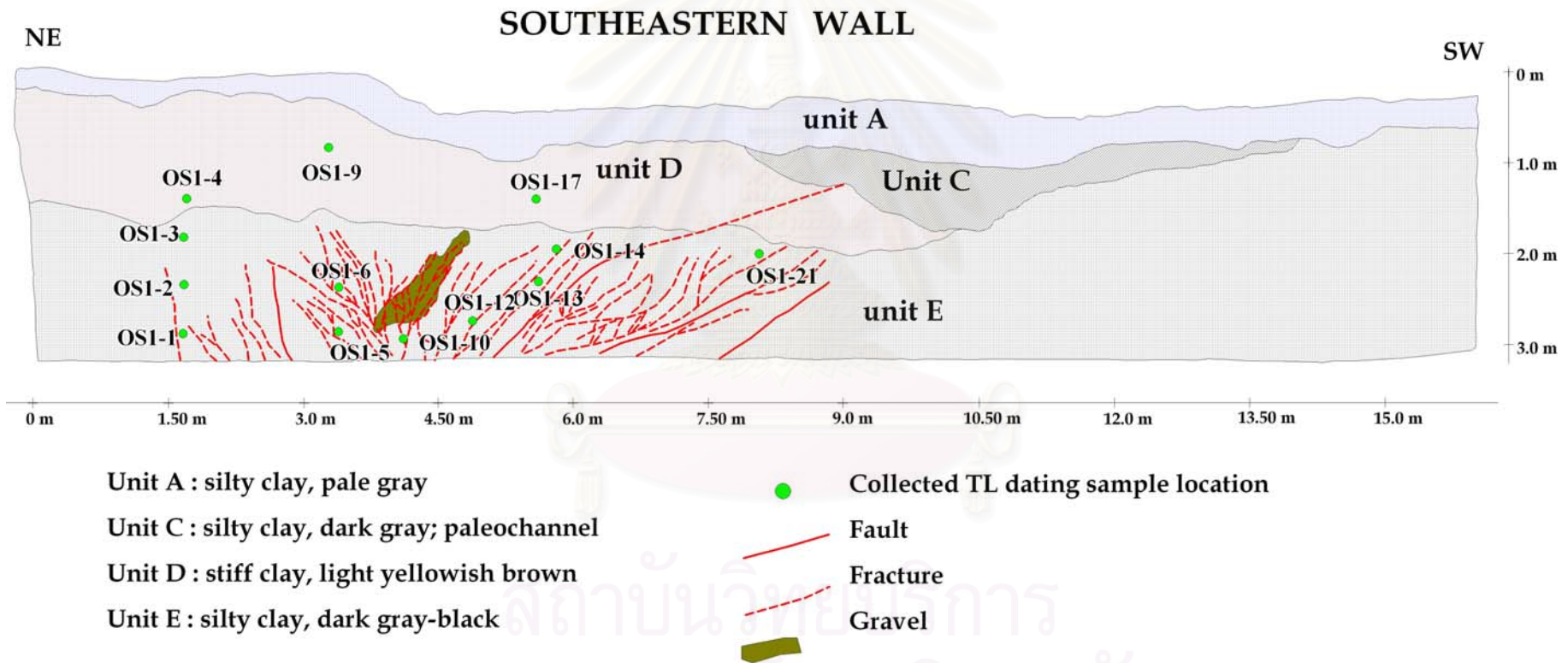


Figure 5.12 Trench-log in the southeastern wall of MOS2 trench and showing principal stratigraphy and locations of TL dating samples.

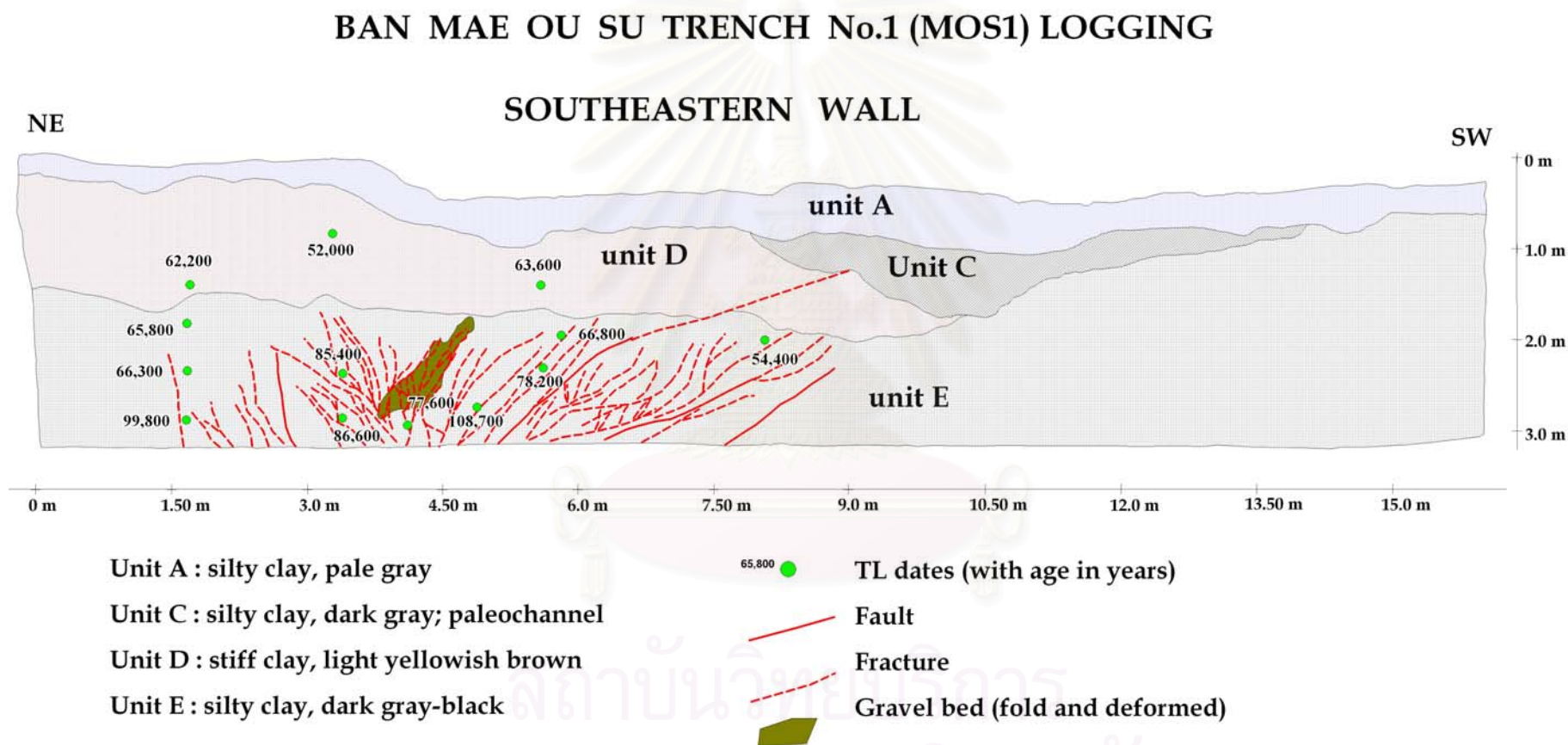


Figure 5.13 Trench-log in the southeastern wall of MOS1 trench and showing principal stratigraphy and thermoluminescence (TL) dates of dating samples.



sample no. OS1-3 displays the arbitrary TL intensity of a natural sample at 100,000 which is equivalent to the paleodose of 343 Gy in Appendix C. The sample has the annual dose about 5.21 mGy/yr with the water content of 6.37 %. These TL parameters reveal the TL date of sample no.OS1-3 as 65,800 yr.

Sample no.OS1-4 from the bottommost of the Unit D shows good glow curves for both natural and artificially irradiated sample (Appendix A). The plateau test as shown in Appendix B, is the rather stability line at 360°C on ward. The growth curve for sample no. OS1-4 displays the arbitrary TL intensity of a natural sample at 55,000 which is equivalent to the paleodose of 380 Gy in Appendix C. The sample has the annual dose about 6.13 mGy/yr with the water content of 4.12 %. These TL parameters reveal the TL date of sample no.OS1-4 as 62,000 yr.

Sample no.OS1-5 from the bottommost of the Unit E shows good glow curves for both natural and artificially irradiated sample (Appendix A). The plateau test as shown in Appendix, is the rather stability line at 340°C on ward. The growth curve for sample no. OS1-5 displays the arbitrary TL intensity of a natural sample at 100,000 which is equivalent to the paleodose of 340 Gy in Appendix. The sample has the annual dose about 6.24 mGy/yr with the water content of 10.05 %. These TL parameters reveal the TL date of sample no.OS1-5 as 86,600 yr.

Sample no.OS1-6 which is overlying the sample no.OS1-5, shows good glow curves for both natural and artificially irradiated sample (Appendix A). The plateau test as shown in Appendix B, is the rather stability line at 360°C on ward. The growth curve for sample no. OS1-6 displays the arbitrary TL intensity of a natural sample at 105,000 which is equivalent to the paleodose of 468 Gy in Appendix C. The sample has the annual dose about 5.48 mGy/yr with the water content of 9.13 %. These TL parameters reveal the TL date of sample no.OS1-6 as 85,400 yr.

Sample no.OS1-9 from the bottommost of the Unit D shows good glow curves for both natural and artificially irradiated sample (Appendix A). The plateau test as shown in Appendix B, is the rather stability line at 350°C on ward. The growth curve for sample no. OS1-9 displays the arbitrary TL intensity of a natural sample at 48,000 which is equivalent to the paleodose of 380 Gy in Appendix C. The sample has the annual dose about 7.32 mGy/yr with the water content of 5.14 %. These TL parameters reveal the TL date of sample no.OS1-9 as 52,000 yr.

Sample no.OS1-10 from the bottommost of the Unit E shows good glow curves for both natural and artificially irradiated sample (Appendix A). The plateau test as shown

in Appendix B, is the rather stability line at 370°C on ward. The growth curve for sample no. OS1-10 displays the arbitrary TL intensity of a natural sample at 70,000 which is equivalent to the paleodose of 400 Gy in Appendix C. The sample has the annual dose about 5.17 mGy/yr with the water content of 9.87 %. These TL parameters reveal the TL date of sample no.OS1-10 as 77,600 yr.

Sample no.OS1-12 which is overlying the sample no.OS1-10, shows good glow curves for both natural and artificially irradiated sample (Appendix A). The plateau test as shown in Appendix B, is the rather stability line at 350°C on ward. The growth curve for sample no. OS1-12 displays the arbitrary TL intensity of a natural sample at 45,000 which is equivalent to the paleodose of 640 Gy in Appendix C. The sample has the annual dose about 5.89 mGy/yr with the water content of 7.30 %. These TL parameters reveal the TL date of sample no.OS1-12 as 108,700 yr.

Sample no.OS1-13 from the steepest a part of the Unit E shows good glow curves for both natural and artificially irradiated sample (Appendix A). The plateau test as shown in Appendix B, in the rather stability line at 360°C on ward. The growth curve for sample no. OS1-13 displays the arbitrary TL intensity of a natural sample at 80,000 which is equivalent to the paleodose of 487 Gy in Appendix C. The sample has the annual dose about 6.24 mGy/yr with the water content of 6.96 %. These TL parameters reveal the TL date of sample no.OS1-13 as 78,200 yr.

Sample no.OS1-14 from the central part of the Unit E shows good glow curves for both natural and artificially irradiated sample (Appendix A). The plateau test as shown in Appendix B, is the rather stability line at 355°C on ward. The growth curve for sample no. OS1-14 displays the arbitrary TL intensity of a natural sample at 56,000 which is equivalent to the paleodose of 360 Gy in Appendix C. The sample has the annual dose about 5.41 mGy/yr with the water content of 9.42 %. These TL parameters reveal the TL date of sample no.OS1-14 as 66,800 yr.

Sample no.OS1-17 from the bottommost of the Unit D shows good glow curves for both natural and artificially irradiated sample (Appendix A). The plateau test as shown in Appendix B, is the rather stability line at 360°C on ward. The growth curve for sample no. OS1-17 displays the arbitrary TL intensity of a natural sample at 60,000 which is equivalent to the paleodose of 417 Gy in Appendix C. The sample has the annual dose about 6.57 mGy/yr with the water content of 6.55 %. These TL parameters reveal the TL date of sample no.OS1-17 as 63,600 yr.

Sample no.OS1-21 from the steepest a part of the Unit E shows good glow curves for both natural and artificially irradiated sample (Appendix A). The plateau test as shown in Appendix B, is the rather stability line at 360°C on ward. The growth curve for sample no. OS1-21 displays the arbitrary TL intensity of a natural sample at 68,000 which is equivalent to the paleodose of 378 Gy in Appendix C. The sample has the annual dose about 6.89 mGy/yr with the water content of 12.02 %. These TL parameters reveal the TL date of sample no.OS1-21 as 54,400 yr.

The other seven samples were collected from the southeastern wall of the MOS2 from Ban Mae Ou Su. As shown in Figures 5.14 and 5.15, five samples were collected from the Unit E (dark grey to black silty clay, the oldest layer in the trench), and two samples were selected from Unit C (the dark grey silty clay layer).

Sample no.OS2-2 from the bottommost of the Unit D shows good glow curves for both natural and artificially irradiated sample (Appendix A). The plateau test as shown in Appendix B, is the rather stability line at 260°C on ward. The growth curve for sample no. OS2-2 displays the arbitrary TL intensity of a natural sample at 550 which is equivalent to the paleodose of 455 Gy in Appendix C. The sample has the annual dose about 5.73 mGy/yr with the water content of 7.43 %. These TL parameters reveal the TL date of sample no.OS2-2 as 59,600 yr.

Sample no.OS2-4 from the bottommost of the Unit D shows good glow curves for both natural and artificially irradiated sample (Appendix A). The plateau test as shown in Appendix B, is the rather stability line at 270°C on ward. The growth curve for sample no. OS2-4 displays the arbitrary TL intensity of a natural sample at 600 which is equivalent to the paleodose of 330 Gy in Appendix C. The sample has the annual dose about 5.36 mGy/yr with the water content of 9.79 %. These TL parameters reveal the TL date of sample no.OS2-4 as 60,900 yr.

Sample no.OS2-6 from the bottommost of the Unit D shows good glow curves for both natural and artificially irradiated sample (Appendix A). The plateau test as shown in Appendix B, is the rather stability line at 260°C on ward. The growth curve for sample no. OS2-6 displays the arbitrary TL intensity of a natural sample at 530 which is equivalent to the paleodose of 500 Gy in Appendix C. The sample has the annual dose about 5.88 mGy/yr with the water content of 10.29 %. These TL parameters reveal the TL date of sample no.OS2-6 as 86,000 yr.

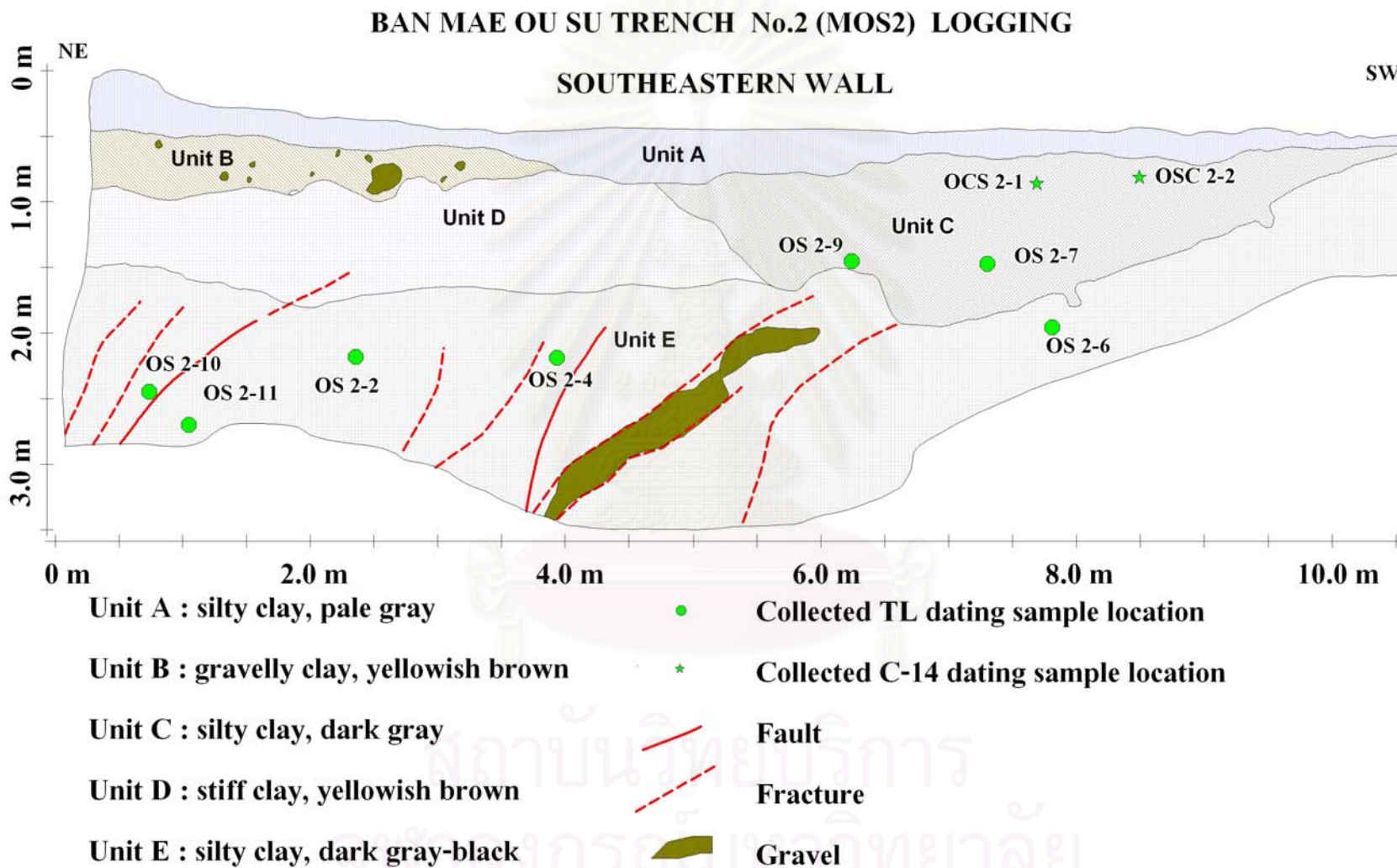


Figure 5.14 Trench-log in the southeastern wall of MOS2 trench and showing principal stratigraphy and location of TL and C-14 dating samples.

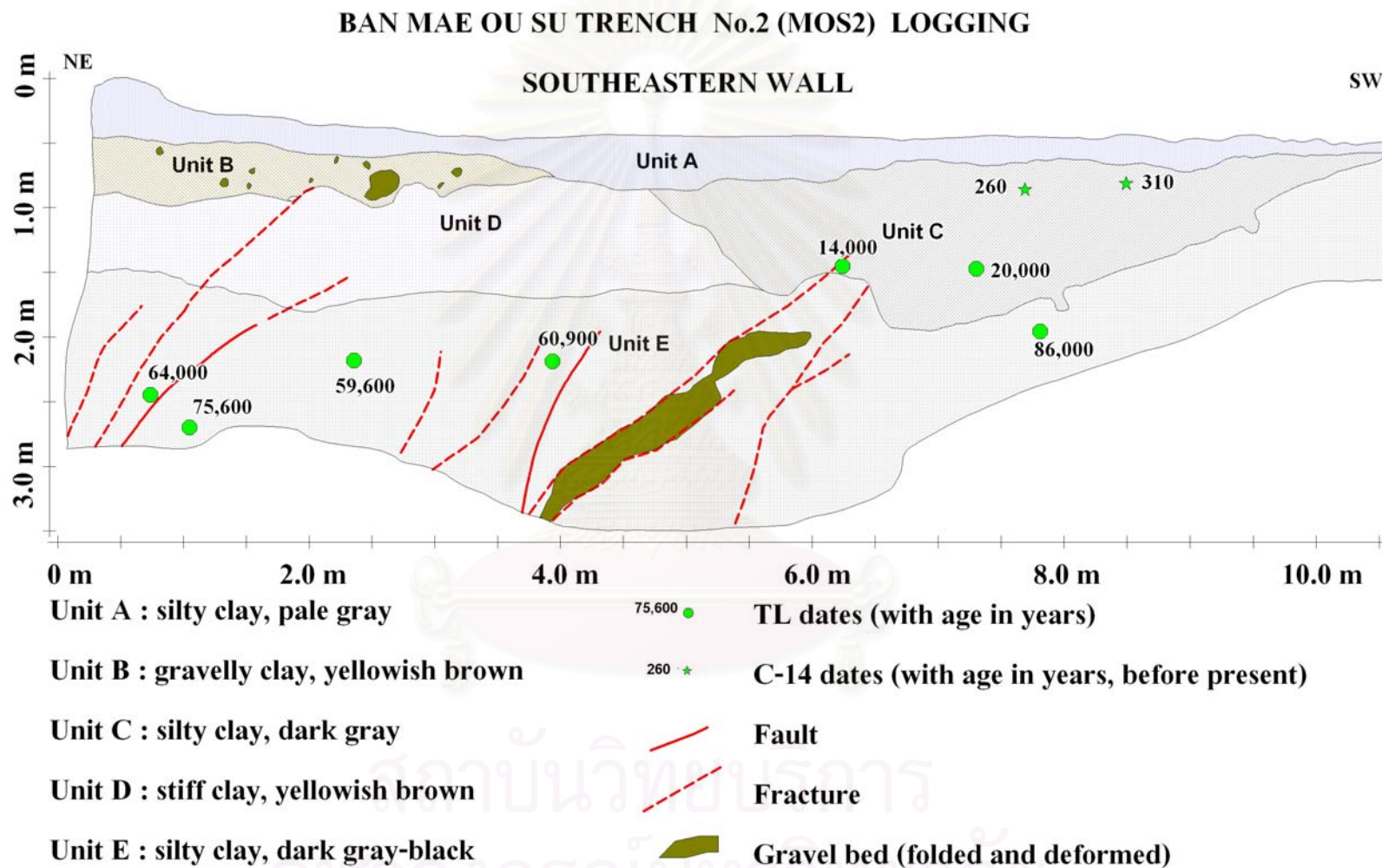


Figure 5.15 Trench-log in the southeastern wall of MOS2 trench and showing principal stratigraphy and thermoluminescence (TL) and C-14 AMS dates of dating samples.

Sample no.OS2-7 from the bottommost of the Unit D shows good glow curves for both natural and artificially irradiated sample (Appendix A). The plateau test as shown in Appendix B, is the rather stability line at 260°C on ward. The growth curve for sample no. OS2-7 displays the arbitrary TL intensity of a natural sample at 130 which is equivalent to the paleodose of 100 Gy in Appendix C. The sample has the annual dose about 5.14 mGy/yr with the water content of 11.73 %. These TL parameters reveal the TL date of sample no.OS2-7 as 20,000 yr.

Sample no.OS2-9 from the bottommost of the Unit D shows good glow curves for both natural and artificially irradiated sample (Appendix A). The plateau test as shown in Appendix B, is the rather stability line at 270°C on ward. The growth curve for sample no. OS2-9 displays the arbitrary TL intensity of a natural sample at 90 which is equivalent to the paleodose of 70 Gy in Appendix C. The sample has the annual dose about 4.89 mGy/yr with the water content of 11.06 %. These TL parameters reveal the TL date of sample no.OS2-9 as 14,000 yr.

Sample no.OS2-10 from the bottommost of the Unit D shows good glow curves for both natural and artificially irradiated sample (Appendix A). The plateau test as shown in Appendix B, is the rather stability line at 280°C on ward. The growth curve for sample no. OS2-10 displays the arbitrary TL intensity of a natural sample at 520 which is equivalent to the paleodose of 380 Gy in Appendix C. The sample has the annual dose about 5.92 mGy/yr with the water content of 7.30 %. These TL parameters reveal the TL date of sample no.OS2-10 as 64,000 yr.

Sample no.OS2-11 from the bottommost of the Unit D shows good glow curves for both natural and artificially irradiated sample (Appendix A). The plateau test as shown in Appendix B, is the rather stability line at 260°C on ward. The growth curve for sample no. OS2-11 displays the arbitrary TL intensity of a natural sample at 410 which is equivalent to the paleodose of 410 Gy in Appendix C. The sample has the annual dose about 5.43 mGy/yr with the water content of 10.84 %. These TL parameters reveal the TL date of sample no.OS2-11 as 75,600 yr.

However, it is worth to be noted that their two results of radiocarbon datings by accelerator mass spectrometers (AMS). Their two results as determined from two collected samples in unit C of Ban Mae Ou Su trench No.2 (MOS2) are of  $260 \pm 40$  years BP and  $310 \pm 40$  years BP. Their calibrations of radiocarbon age to calendar years are present in Appendix D.

Table 5.1 Summarization of TL-dating results.

Sample No.	U (ppm)	Th (ppm)	K (%)	Water Content (%)	Annual Dose (mGy/yr.)	Paleodose (Gy)	TL Age (year)
OS1-1	2.63	14.08	2.54	9.06	6.42	640	99,800 ± 2600
OS1-2	2.37	12.25	2.23	9.17	5.66	375	66,300 ± 3,300
OS1-3	2.32	10.64	1.88	6.37	5.21	343	65,800 ± 3,000
OS1-4	2.9	12.33	1.99	4.12	6.13	380	62,200 ± 2,500
OS1-5	3.27	13.43	2.13	10.05	6.24	540	86,600 ± 4,400
OS1-6	2.52	11.88	2	9.13	5.48	468	85,400 ± 3,900
OS1-9	3.04	16.06	2.52	5.14	7.32	380	52,000 ± 2,100
OS1-10	1.92	11.76	2.12	9.87	5.17	400	77,600 ± 3,900
OS1-12	2.19	14.5	2.03	7.30	5.89	640	108,700 ± 3,500
OS1-13	2.73	14.84	1.96	6.96	6.24	487	78,200 ± 2,800
OS1-14	2.67	12.06	1.81	9.42	5.41	360	66,800 ± 2,750
OS1-17	3.00	14.46	2.18	6.55	6.57	417	63,600 ± 2,800
OS1-21	3.51	16.04	2.38	12.02	6.89	490	71,200 ± 2,800
OS2-2	2.79	12.18	1.92	7.43	5.73	455	59,600 ± 2,000
OS2-4	2.55	13.18	1.64	9.79	5.36	330	60,900 ± 900
OS2-6	2.92	14.61	1.75	10.29	5.88	500	86,000 ± 2,200
OS2-7	3.37	11.81	1.25	11.73	5.14	100	20,000 ± 500
OS2-9	2.92	11.37	1.3	11.06	4.89	70	14,000 ± 400
OS2-10	2.27	14.52	2.01	7.30	5.92	380	64,000 ± 2,100
OS2-11	2.46	12.02	2.08	10.84	5.43	410	75,600 ± 2,500

จุฬาลงกรณ์มหาวิทยาลัย

## CHAPTER VI

### DISCUSSION

In this chapter, emphasis is placed on the discussion relating to the interpretation of the result explained in chapter V. The discussion is divided into three parts: characteristics of the studied fault, slip rates and paleoearthquake magnitudes, and neotectonic evolution of the study area.

#### 6.1 Characteristics of the Studied Fault

Chuaviroj (1991) stated that the Mae Ping Fault Zone (MPFZ) is the NW-trending major fault zone which includes several active and inactive associated faults, such as the Moei-Uthai Thani Fault (Nutalaya et al., 1985), the Lan Sang-Wang Chao Fault Zone (Bunopas, 1981), the Mae Ping Fault (Polachan and Sattayarak, 1989). It is the strike-slip fault with the length of 750 km. Due to the remote-sensing and paleoseismic trenching informations of this study reveal that the MPFZ is the strike-slip fault with the dip angles varying from 40° to 70°. It consists of ten fault segments. The studied faults show both senses of movement-viz. sinistral and dextral, the former is, however, less common in term of geomorphic evidences. The right lateral movement is found at the Amphoe Tha Song Yang of Khao Mae Song fault segment, whereas the left lateral movements are found at the Huai Mae Tun and Huai Ma Nok, which belong to the Ban Tha Song Yang segment. Meanwhile, the left lateral movement is found at the Huai Mae Tan, which belongs to Khao Mae Song fault segment. The results indicate that the MPFZ also show its vertical movement in both normal and reverse senses. The earthquake with the magnitude of 5.6 was reported to have occurred in 1975 at the Huai Mae Lo fault segment with the recorded dextral displacement and some reverse movement. Thitipattanakul (2005) recently applied the Ground Penetrating Radar (GPR) and remote-sensing results to characterize the MPFZ in Ban Mae Ou Su area. He found that the studied fault cut through Quaternary sedimentary layers in the right lateral movement with a few vertical components (Figures 6.1 and 6.2).

Hinthong (1997) and Charusiri et al. (2001) reported the TL ages of the MPFZ from Quaternary sediment layers and fault gouge materials. They concluded, based on the dating results, that there are four earthquake events happened along the Ban Tha Song Yang, and Huai Mae Lo segments. These events were taken place during 0.16, 0.21, 0.37, and 1.17 Ma ago. However, their results seem to be much older than the current



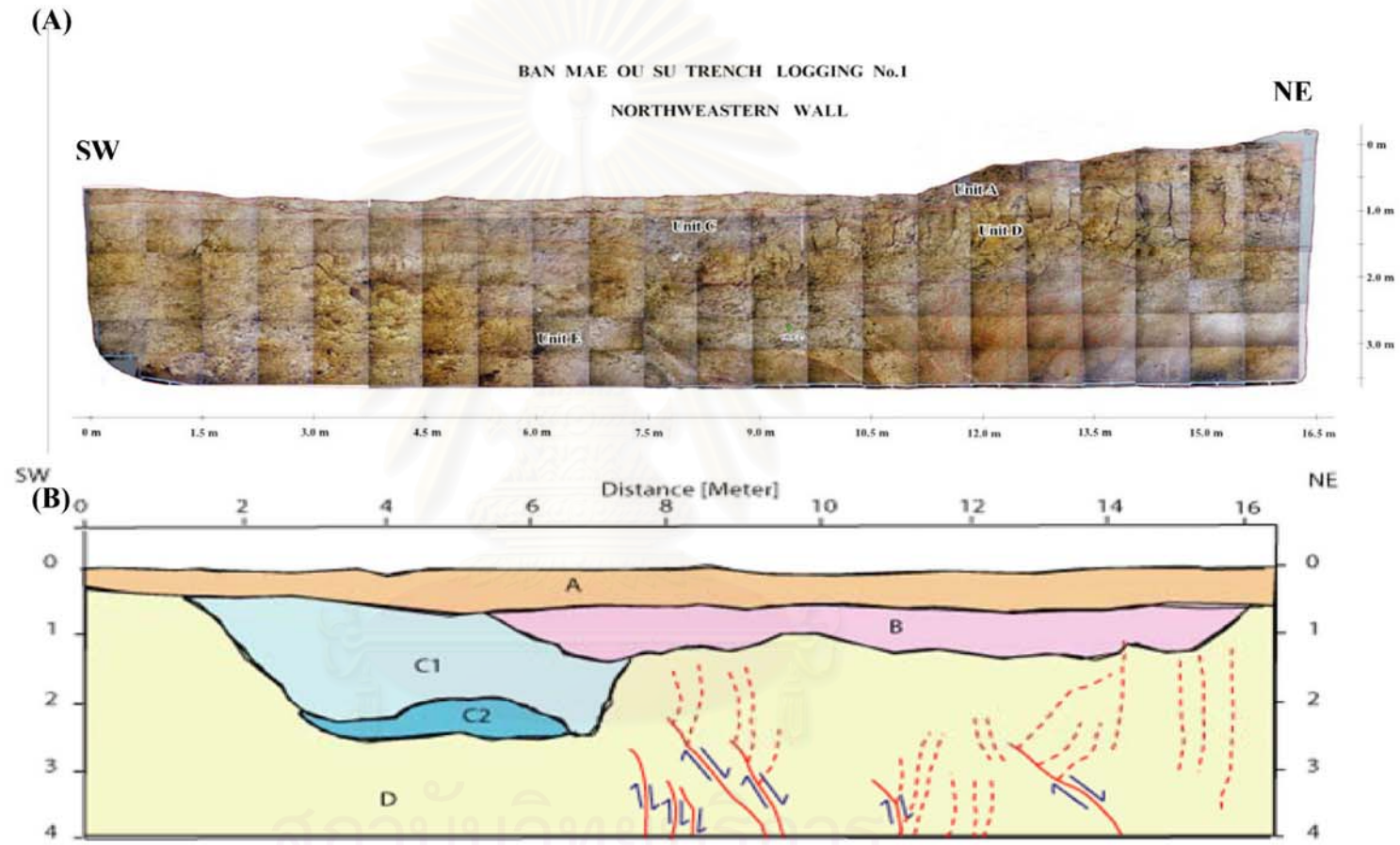


Figure 6.1 The comparison from 2 type data, (A) the trenching MOS1 logging (B) the GPR interpretation profile from the first line survey (After Thitipattanakul 2005).

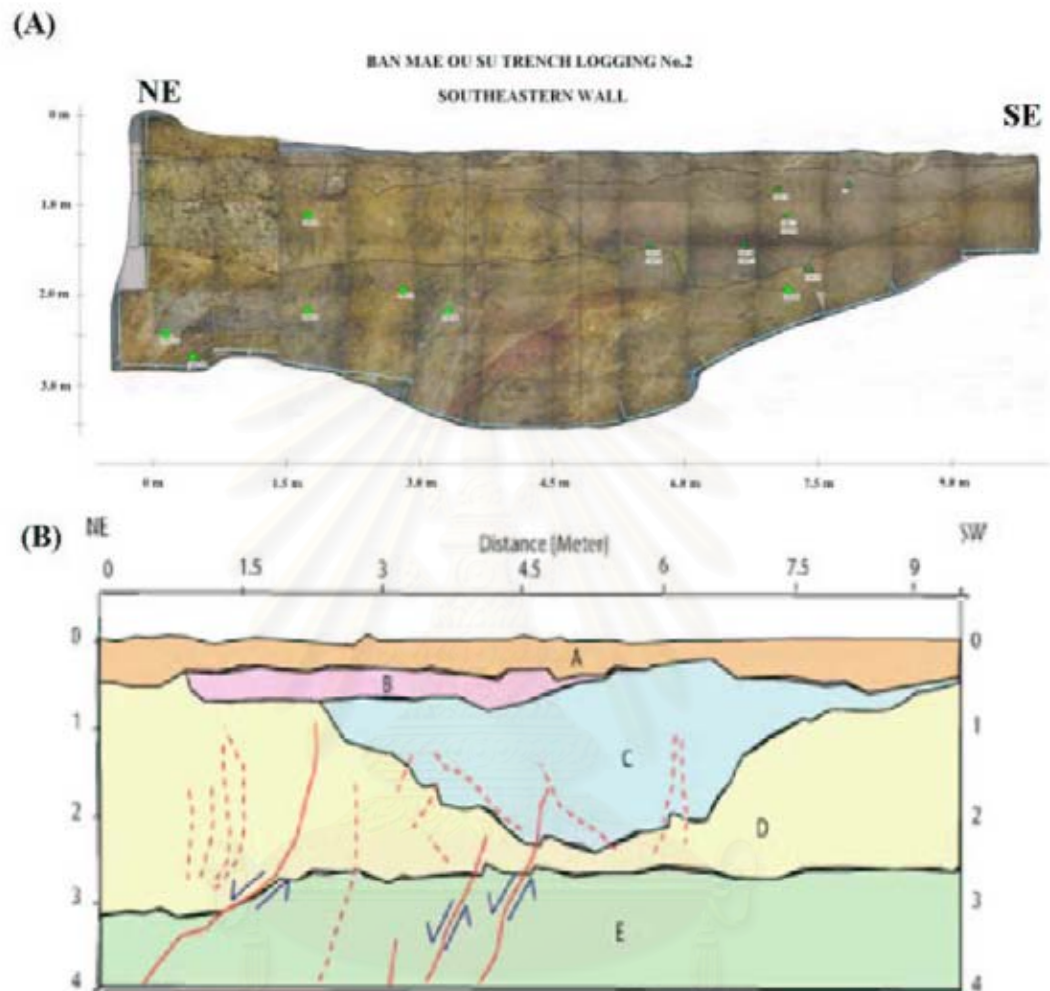


Figure 6.2 The comparison from 2 type data, (A) the trenching MOS1 logging (B) the GPR interpretation profile from the first line survey (After Thitipattanakul 2005)

results. In this study, the TL dating result from the Khao Mae Song fault segment, point to three paleo-earthquake events, viz 85,000, 65,000, and 15,000 yr-old events. In terms of geology and seismology, if we take the entire earthquake events into account, it is likely that only the Khao Mae Song is active whereas the Ban Tha Song Yang and Huai Mae Lo segments are potentially active faults, following the definition of Hinthong (1997). But if it is based on the definition of Charusiri et al., (2001), it is quite likely that all the studied fault segments are active. Once data on epicentral distribution are overlain onto the fault map (Figure 6.3) it is certain that all segments are regarded as active. This is because several epicenters are located proximately at the interpreted fault traces.

## 6.2 Slip Rate and Paleoseismicity Magnitude

Well and Coppersmith (1994) reported the positive correlation between surface rupture length (SRL) and magnitude ( $M_w$ ) for worldwide (216 historic) earthquakes of all slip type (Figure 6.4). Table 6.1 shows the results of paleoseismicity magnitudes of the MPFZ in Tak area as applied to one of the concepts of Well and Coppersmith (1994)'s equations which are related to regression relationships. In this study the following equations are applied for paleoseismicity magnitude estimation. They are shown in equations 6.1 and 6.2

$$M = 5.08 + 1.16 \log (\text{SRL}) \dots\dots\dots (6.1)$$

$$M = 6.93 + 0.82 \log (\text{AD}) \dots\dots\dots (6.2)$$

When

$M$  = moment magnitude ( $M_w$ );

SRL = surface rupture length; and

AD = average displacement.

The surface rupture lengths are deduced from measurements based upon both field and remote-sensing data. The average displacements (AD) are from the average of the stream offset and are estimated from geodetic surveys and remote-sensing information.

As stated in chapter III, there are about ten fault segments in the study area. In order to receive reliable results, the present study preferably applied only the equation using surface rupture length (SRL). Followings are the paleoseismicity magnitude calculated from such equation.

- (1) Sop Moei segment has surface rupture length (SRL) of about 22 km, it reveals estimated magnitudes of 6.63 on the Richter scale.

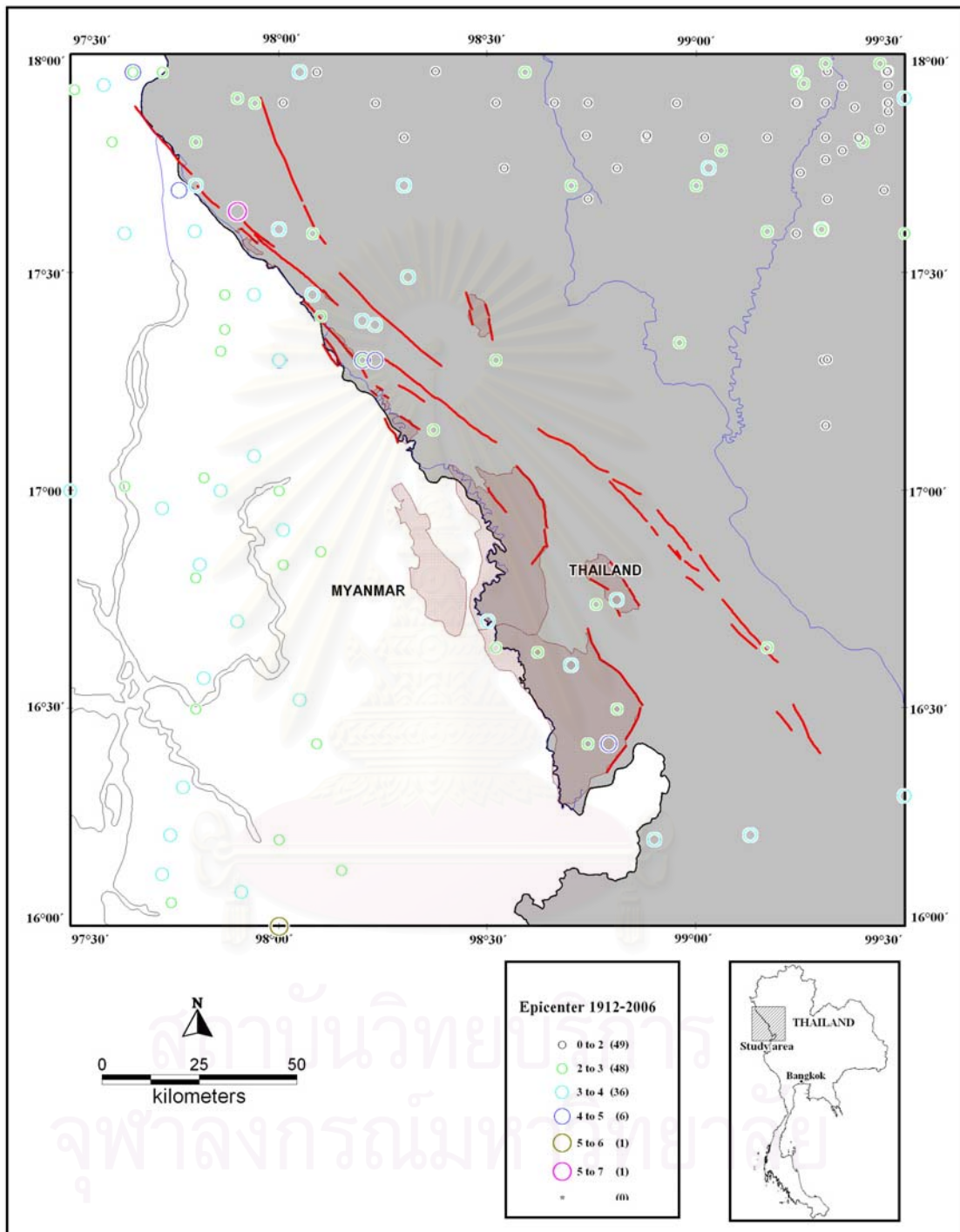


Figure 6.3 Map of Tak and adjacent areas showing epicentral distribution from 1912 to 2006 (Data from Nutalaya et al., 1985; Thai Meteorological Department, 2002; and [http://neic.usgs.gov/neis/epic/epic\\_global.html](http://neic.usgs.gov/neis/epic/epic_global.html)).

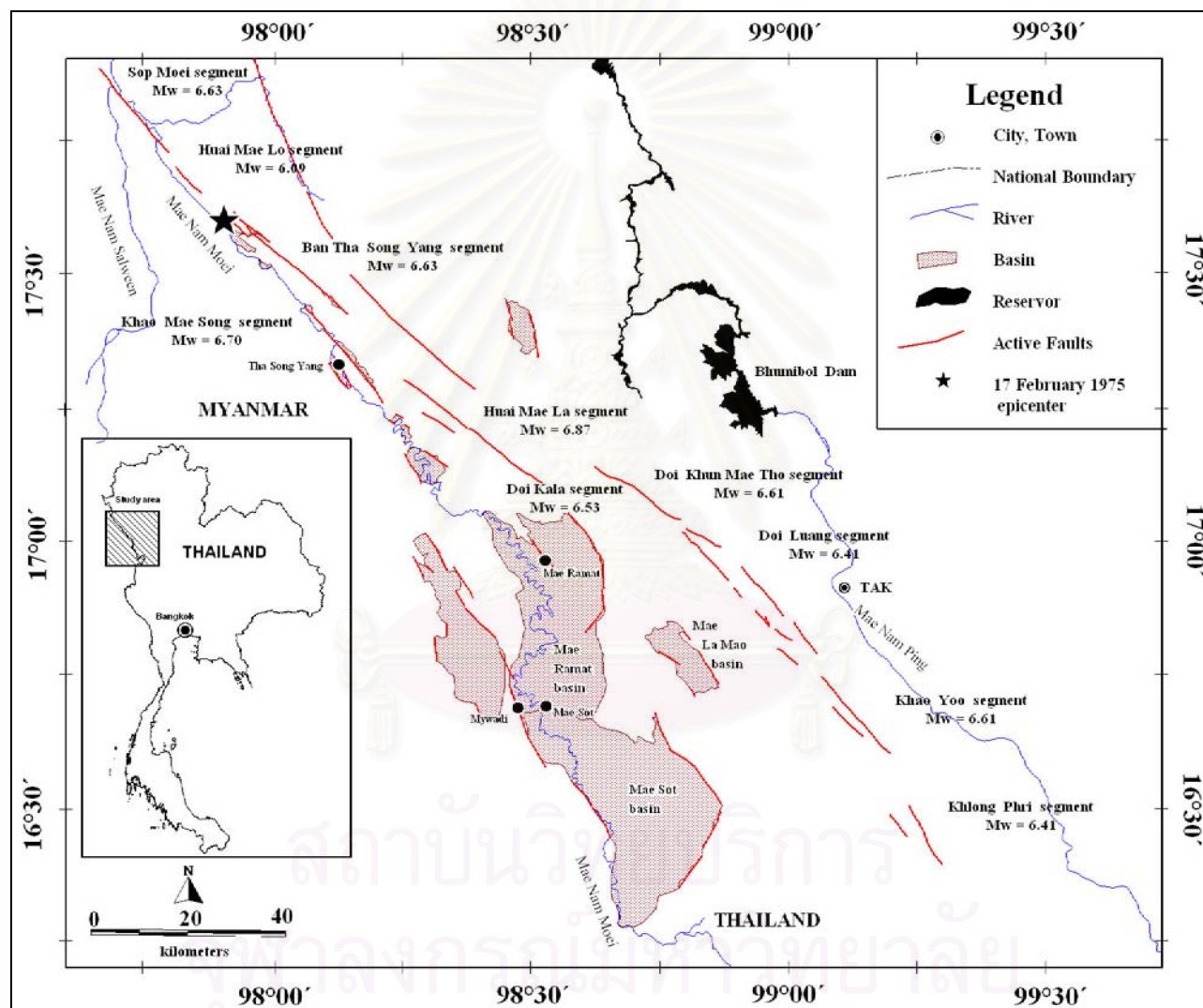


Figure 6.4 Map showing fault segments and their paleoearthquake magnitudes of the Moei-Mae Ping Fault Zone.

(2) Huai Mae Lo segment has surface rupture length (SRL) of about 7.5 km, it reveals estimated magnitudes of 6.09 on the Richter scale.

(3) Ban Tha Song Yang segment has surface rupture length (SRL) of about 22 km, it reveals estimated magnitudes of 6.63 on the Richter scale.

(4) Khao Mae Song segment has surface rupture length (SRL) of about 25 km, it reveals estimated magnitudes of 6.70 on the Richter scale.

(5) Huai Mae La segment has surface rupture length (SRL) of about 35 km, it reveals estimated magnitudes of 6.87 on the Richter scale.

(6) Doi Kala segment has surface rupture length (SRL) of about 18 km, it reveals estimated magnitudes of 6.53 on the Richter scale, respectively.

(7) Doi Khun Mae Tho segment has surface rupture length (SRL) of about 21 km, it reveals estimated magnitudes of 6.61 on the Richter scale.

(8) Doi Luang segment has surface rupture length (SRL) of about 14 km, it reveals estimated magnitudes of 6.41 on the Richter scale, respectively.

(9) Khao Yao segment has surface rupture length (SRL) of about 21 km, it reveals magnitudes of 6.61 on the Richter scale.

(10) Khlong Phri segment has surface rupture length (SRL) of about 14 km, it reveals estimated magnitudes of 6.41 on the Richter scale.

Table 6.1 and Figure 6.4 summarize the individual paleoearthquake magnitudes that are considered to have occurred for each fault segment. In an estimation of slip rate, it is important to know the ages of sedimentary units which were cut by active faults. It is also essential to determine ages of paleoearthquake faulting. As shown in Figures 5.13 and 5.15, the TL ages of units E and D in Ban Mae Ou Su trenches nos.1 and 2 are about 100,000 yrs and 65,000 yrs, respectively. Unit E in trench no.1 was cut by two faults; the older one (F1) of about 85,000 yrs, and the younger one (F2) of about 65,000 yrs. Unit C which is about 20,000 yrs-old, was cut by the younger fault (F3) with the movement of about 15,000 yrs. It is likely that the slip rate is estimated for the Khao Mae Song segment if the displacement along the Huai Mae Ou Su is about 11 meters. However, at present, it is difficult to visualize, whether or not the 11 meters offset movement along the F2 or F3. Thus, two assumptions are required. The first assumption is that such offset was triggered by F2 movement and the other assumption is the offset was significantly governed by F2 movement.

Table 6.1 paleoearthquake magnitudes of the MPFZ in Tak area, estimation from Well and Coppersmith (1994).

No.	Fault Segment	surface rupture length (SRL, km)	moment magnitude (Mw)
1	Sop Moei	22	6.63
2	Huai Mae Lo	7.5	6.09
3	Ban Tha Song Yang	22	6.63
4	Khao Mae Song	25	6.70
5	Huai Mae La	35	6.87
6	Doi Kala	18	6.53
7	Doi Khun Mae Tho	21	6.61
8	Doi Luang	14	6.41
9	Khao Yao	21	6.61
10	Khong Phri	14	6.41

The offset by F3 faulting was also observed in Unit C in Ban Mae Ou Su trench no.2. Therefore, the slip rate is inferred to be ca. 0.73 mm/yr (11,000 mm/15,000yr). Because Unit D is also cross cut by the F2, and then the slip rate is considered to be ca. 0.17 mm/yr (11,000/65,000 yr).

If one applied the F1 movement with the total offset of about 30 meters at Ban Mae Ou Su, then the slip rate is estimated ca. 0.35 mm/yr (30,000 mm/85,000 yr). This value is in the previously estimated range.

In conclusion, the Khao Mae Song fault has the slip rate varying from 0.17 mm/yr to 0.73 mm/yr.

### 6.3 The Linkage of Neotectonic Evolution

The result of field, trench-log, and remote-sensing data reveal the essential right lateral sense of movement. Additionally, the result of focal mechanism of 1975 earthquake (Nutalaya et al., 1985) in the study area conforms very well with the current result. Moreover, there is no doubt that the Moei-Mae Ping Fault Zone is still active till present as studied by Nutalaya et al. (1985). It implies that the maximum compression stress is in the north-south direction in order for the fault to show the E-dextral sense. However, this NW-trending fault may have occurred long times ago (Charusiri et al., 2002) and noted that this fault may have been formed since Late Triassic-Early Jurassic, with the opposite sense of movement, viz. sinistral movement. Reactivation of the fault may have taken place by the collision of western Burma block with Shan-Thai block. This reactivation also triggered the similar left lateral movement along the Moei-Mae Ping Fault Zone as shown by the displacement of Oligocene-Miocene (30 Ma) metamorphic core complex (Morley, 2002) of about 60 km (Tapponier et al., 1986). If one takes into account these figures, then one can calculate the long-term slip-rate to be up to 2 mm/yr. However, it has been disputed if all the left-lateral displacement is of Tertiary or not (Morley, 2002). Collision of Western Burma with Shan-Thai block may have also been a considerable amount of the left-lateral movement (Charusiri et al., 2002; Cooper et al., 1989; and Tapponier et al., 1986). The long-termed slip-rate can be computed, based on the ca. 85-95 km offset of Triassic granites in western Thailand (from Samoeng-Mae Sariang area to Ban Rai-U Thai Thani area), as approximately of 1.41-1.58 mm/yr. Based on the overall result, it is estimated that the approximate long-termed slip rate is  $1.5 \pm 0.08$  mm/yr (Figure 6.5).

As noted by Charusiri et al. (2002) (see also Figure 6.6) the change in tectonic styles may have occurred as Indian continental block was collided with Asia in the northward direction. Then the movement in a left lateral sense may have become the right



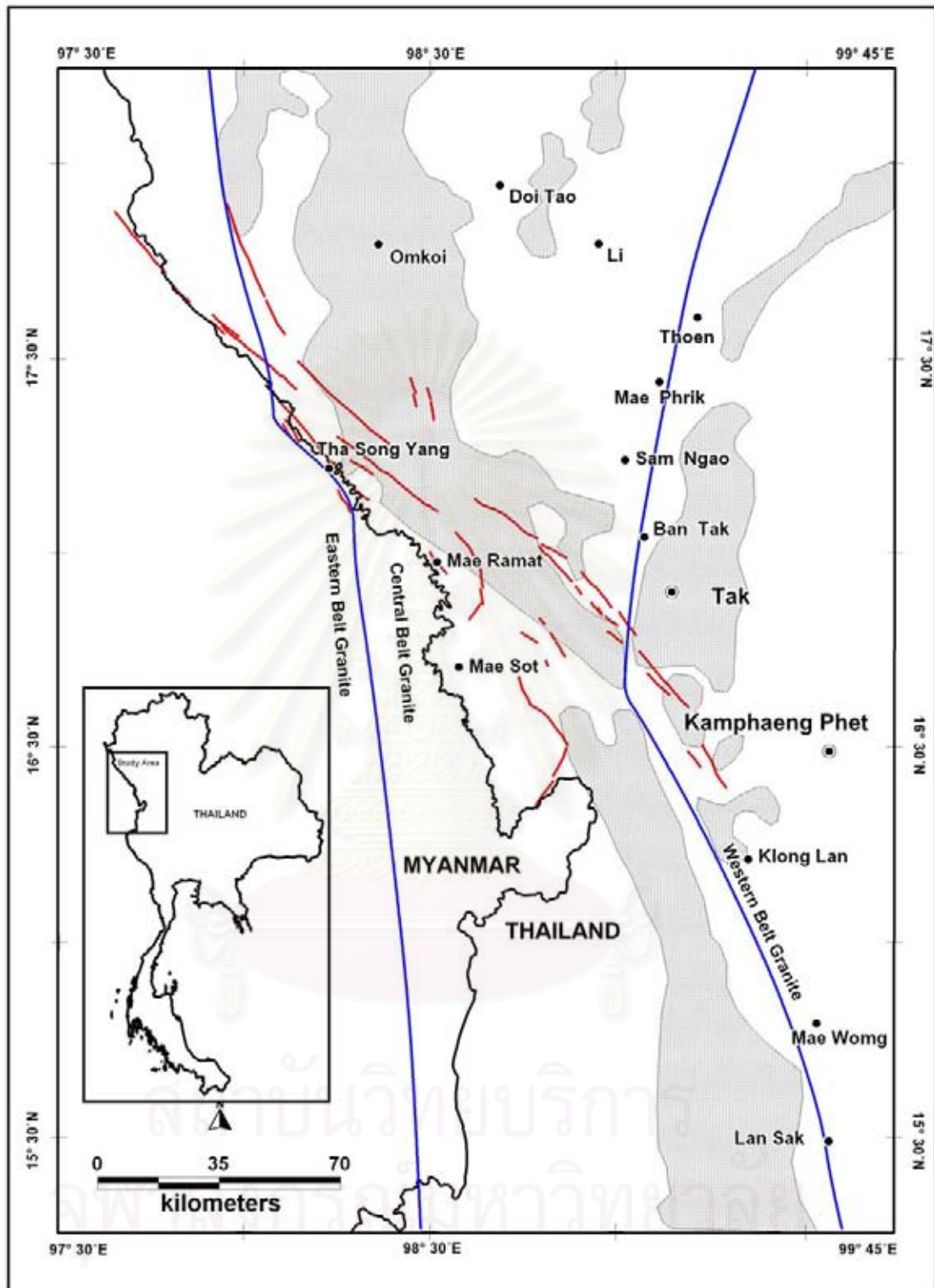


Figure 6.5 Simplified distribution granite map of Northwestern Thailand, and offset of Triassic granites (Modified after DMR, 1999).

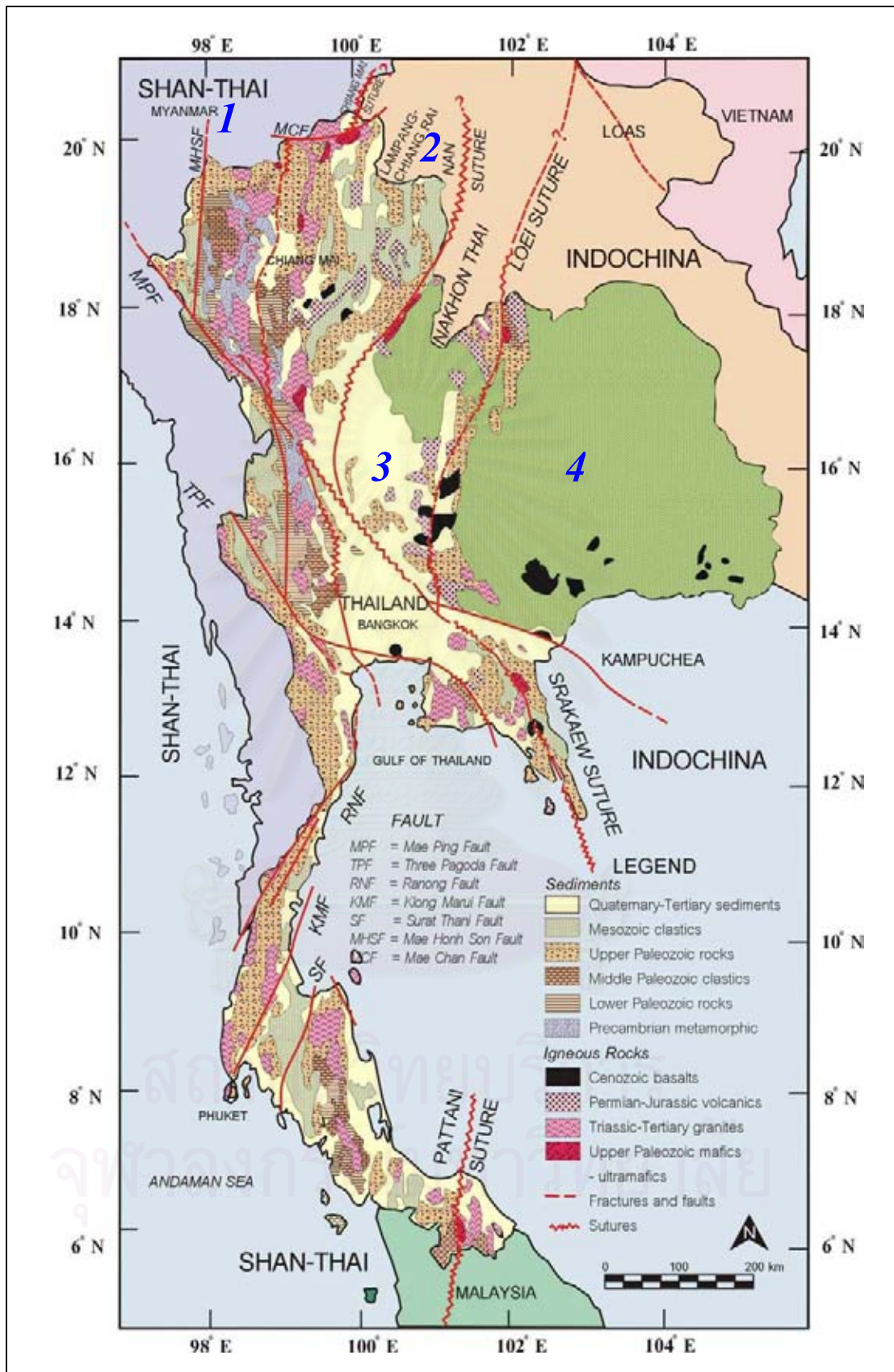


Figure 6.6 Map of Thailand showing the tectonic units, 1 = Shan-Thai plate 2 = Lampang-Chiang Rai plate, 3 = and Nakhon Thai plate, 4 = Indochina plate (After Charusiri et al., 2002).

lateral movement along the Moei–Mae Ping Fault Zone. It probably required a long period of time to change the direction. This perhaps suggests that the basins may have formed in response to Late Eocene–Late Oligocene escape tectonics along the NW–trending Moei–Mae Ping Fault Zone. Compression tectonics became essential and as a result of crustal thickening with the Shan–Thai block. Some Tertiary inversion relevant to such collision tectonics occurs as far east as the Khorat Plateau (Morley, 2002). It is considered that under left–lateral motion, the study region would be a compressively restraining bend; hence a sedimentary basin would not form. Consequently, it is inferred, based on the result of remotely–sensed data, which subsequent dextral motion occurred in order to create an extensional basin at a dilationally releasing bend.

Three major N–trending sedimentary basins are recognized (as shown in Figure 6.7) along the studied Moei–Mae Ping Fault Zone (1) Mae Tuen in the north, (2) Mae Ramat–Mae Sot in the south–central, and (3) Mae Lamao in the east. Uttamo et al. (2001) classified these N–trending Cenozoic basins as belonging to the pull–apart basin type. However, it takes into account the fact that the opening of the basin requires extension stress regime in the east–west direction by the movement along the NW–trending fault. The basins are governed and developed along the releasing bends at the tip of the large–scale strike slip faults (Elder et al., 2000; Storli et al., 2001) whereas there exists some places along the fault at which the restraining bends occur. The locations of the trend are favoured for the restraining bends (or a principal displacement zone) when several sets of reverse faults are encountered. To the south the small–to large–scale basins are recognized at the transtensional splay zone. The studied NW–trending fault displays a releasing offset at the fault tip (Woodcock and Fischer, 1986; Sylvester, 1986; and Storli et al., 2001). Further northwards, this studied fault continues and perhaps terminates at the Shan Boundary Fault in eastern Myanmar.

It is considered herein that the major NW–trending Moei–Mae Ping Fault Zone is an essentially principal displacement zone while the normal faults at the tip of the fault represent the basin–boundary faults of a transtensional splay zone of the strike slip system. This interpretation is similar to simple shear model of Sylvester (1986) (Figure 6.8). The splay faults form at the ends of R shears and curve towards parallelism with the extension fractures. Therefore, R shear is mainly a strike–slip fault stem in the central part of the deformation zone and is significantly a normal fault system at its extremities (Sylvester, 1988). Uttamo et al. (2003) recognized eight basins identified as fault–tip basins in northern Thailand. There include Li, Phrae, Thoen, Chiang Rai, Chiang Khong, Pai, and Wiang Haeng Basins. It is also inferred that the basins in the study region are also classified

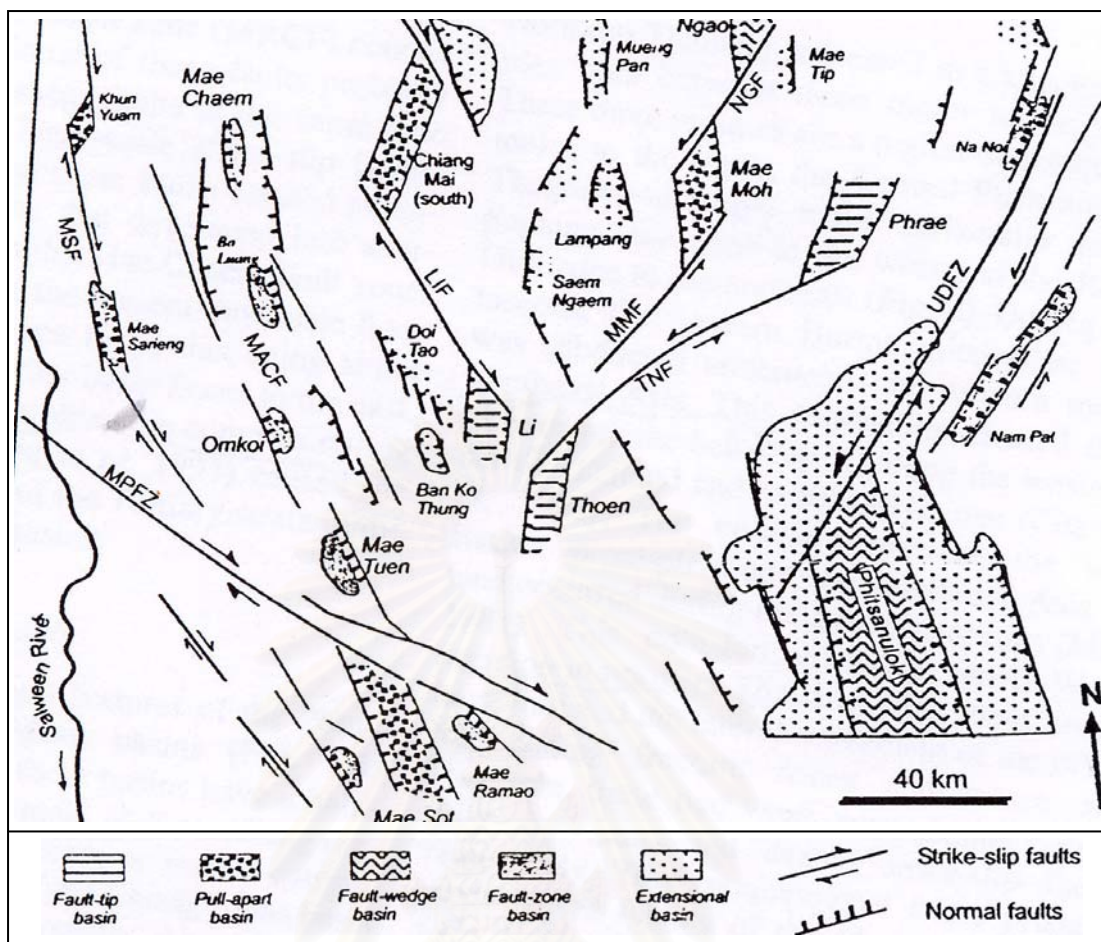


Figure 6.7 A simplified tectonic model of Tertiary basin formation in the study area

(Modified after Uttamo et al., 2003).

สถาบันวิทยบริการ  
จุฬาลงกรณ์มหาวิทยาลัย

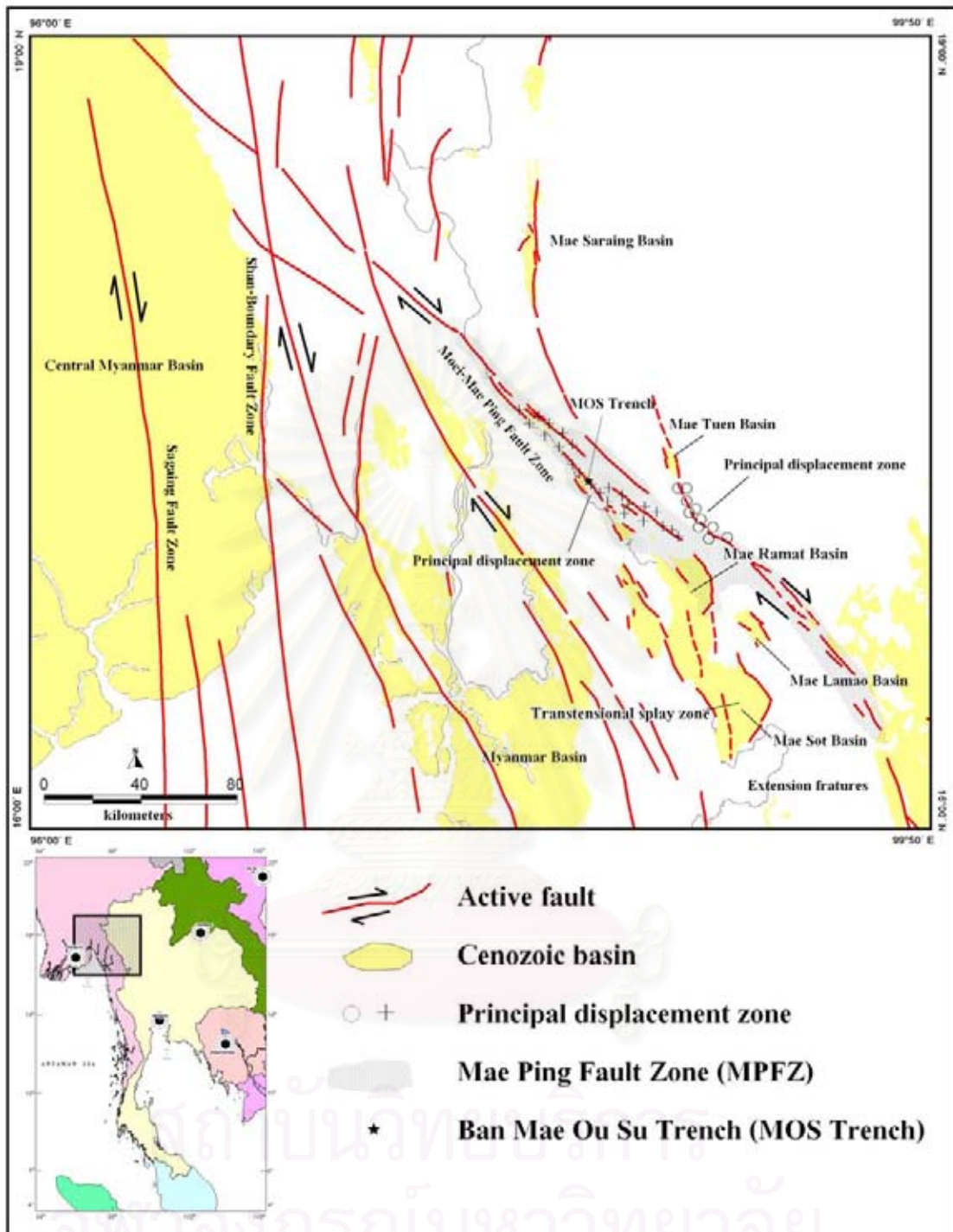


Figure 6.8 Interpretation map showing the dextral movement along the NW-trending of Moei-Mae Ping Fault Zone and the development of fault-tip or fault-bend (This study and modified from Uttamo et al., 2003 and Morley, 2002)

as fault-tip basins, and they are not interpreted as pull-apart basins as mentioned by Uttamo et al. (2003)

In conclusion, it is considered that the NW-trending Moei-Mae Ping Fault Zone which is active at present controls the development of the Cenozoic basins by the dextral movement along the fault plane.



สถาบันวิทยบริการ  
จุฬาลงกรณ์มหาวิทยาลัย

## CHAPTER VII

### CONCLUSIONS

Based on the results of remote-sensing analysis (Landsat 5 TM, Radarsat, JERS SAR, and aerial photograph) integrated with ground-truth investigation, detailed topographic survey as well as those of TL-dating and Carbon-14 AMS of fault-related sediments, and neotectonics of the Moei Mae Ping Fault Zone in Changwat Tak, northwestern Thailand, the conclusions can be drawn as the followings;

1) MPFZ is the northwest-trending, 230 km-long fault extending from easternmost Myanmar to northwestern Thailand, and perhaps to central Thailand and Tonle Sap in Cambodia.

2) Lineaments belong to the MPFZ orientated in the northwest-southeast, northeast-southwest, north-south, and east-west directions. The major trends of lineaments are the northwest-southeast directions and are regarded as a major fault zone.

3) MPFZ can be divided, based on discontinuity criteria, from north to south in to ten fault segments, viz. the Sop Moei segment (22 km), the Huai Mae Lo segment (7.5 km), the Ban Tha Song Yang segment (22 km), the Khao Mae Song segment (25 km), the Huai Mae La segment (35 km), the Doi Kala segment (18 km), the Doi Khun Mae Tho segment (21 km), the Doi Luang segment (14 km), the Khao Yao segment (21 km), and the Khlong Phri segment (14 km). All segments more or less align in a northwest-southeast direction, but Doi Kala segment is in an almost north-south direction.

4) Significant and well-defined types of morphotectonic evidences are triangular facets, fault scarps, beheaded streams, offset streams, shutter ridges, and linear valleys. They are discovered along the MPFZ, particularly where bed rock connects with the roughly northwest-trending Cenozoic basins.

5) Estimation from the surface rupture length of about 25 km, the Khao Mae Song segment indicates that an earthquake may have occurred in this area with the maximum magnitude of  $M_w$  6.70. The fault show the right-lateral sense of movement at present with the slip rate of this fault segment is about 0.17–0.73 mm/yr

6) Three major earthquakes with the paleoearthquake of about 7 on the Richter scale occurred about 80,000, 65,000, and 15,000 years ago.

7) The fault also displays a sinistral lateral movement prior to Oligocene with a slip rate of about 1.5 mm/yr (Charusiri et al., 2002; Cooper et al., 1989; Tapponier et al., (1986); and Morley, 2002).

8) Dextral movement along the studied fault is responsible for the development of the Tertiary extensional, fault-tip basin.



สถาบันวิทยบริการ  
จุฬาลงกรณ์มหาวิทยาลัย



## REFERENCES

- Abbott, P. L. 2004. Natural Disasters. 4 th ed. New York: The McGraw-Hall, 460pp.
- Aitken, A. J. 1985. Thermoluminescence Dating. New York: Academic Press, 351pp.
- Aki, K. 1984. Asperities of Barrier on an Earthquake Fault and Strong Motion Prediction. Jour. Geophys. Res., v.98: 5681-5698.
- Albee, A. L. and Smith, J. L. 1966. Earthquake Characteristics and Fault Activity in Southern California. Engineering Geology in Southern California. Association of Engineering Geologists. Glendale, California. Los. Angeles Section Special Publication: 9-34.
- Allen, C. R. Armand, F. Richter, C. F. and Nordquist, J. M. 1965. Relationship between Seismicity and Geologic Structure in the Southern California Region. Bulletin of the Seismological Society of America; v. 55; no.4: 753-797.
- Allen, C. R. 1986. Seismological and Paleoseismological Techniques of Research in Active Tectonics. In: Wallace, R. E. ed. In: Active Tectonics: Studies in Geophysics. Natl. Acad. Press. Washington, DC: 148-154.
- Barr, S. M. and MacDonald, A. S. 1987. Nan River Suture Zone, Northern Thailand. Geology, v.15: 907-910.
- Bell, W. T. 1979. Thermoluminescence dating: Radiation dose-rate data. Archaeometry, v.21: 243-245.
- Benson, A. M. Little, T. A. Van Dissen, R. J. Hill, N. and Townsend, D. B. 2001. Late Quaternary Paleoseismic History and Surface Rupture Characteristic of the Eastern Awatere Strike-Slip Fault, New Zealand. GSA Bull., v.113. no.8: 1079-1091.
- Biddle, K. T. and Christie-Blick, N. 1985. Glossary-Strike-Slip Deformation, Basin Formation, and Sedimentation. In: Biddle, K. T., and Christie-Blick, N. eds. Strike-Slip Deformation, Basin Formation and Sedimentation. Spec. Pub. Soc. Econ. Paleont. Miner. Tulsa, 37: 375-385.
- Bolt, B. A. 1999. Earthquakes. 4 th ed. New York: W. H. Freeman and Company, 366pp.

- Boongunpai, N. and Tansathien, W. 2004. Geology of Nam Ping Watershed Project. Report No.1/2004. sheet Moulmein (NE47-14), sheet Phitsanulok (NE47-15), sheet Nakhon Sawan (ND47-3), scale 1:250,000. Department of Mineral Resources. Geological Survey Bureau: 87pp.
- Bott, J. Wong, I. Prachuab, S. Wechbunthung, B. Hinthong, C. and Sarapirome, S. 1997. Contemporary seismicity in northern Thailand and its tectonic implications. In: Proceedings of the International Conference on Stratigraphy and Tectonic Evolution of Southeast Asia and the South Pacific, Bangkok, Department of Mineral Resources, August: 453-464.
- Braun, E. V. Hahn, L. and Maronde, H. D. 1981. Geologic Map of Northern Thailand 1:250,000: Sheet (Amphoe Li), Federal Institute for Geosciences and Natural Resources.
- Bunopas, S. 1976. On the Stratigraphic Successions in Thailand-A Preliminary Summary. Journal of Geological Society of Thailand, v.2. no.1-2: 31-58.
- Bunopas, S. 1981. Paleogeographic History of Western Thailand and Adjacent part of Southeast Asia. A plate tectonic interpretation. Ph.D Thesis. Victoria University of Wellington: 810pp.
- Bunopas, S. 1994. The Regional Stratigraphic, Paleogeographic and Tectonic Events of Thailand and Continental Southeast Asia. In: Angsuwathana, P., Wongwanich, T., Tansathien, W., Wongsomsak, S., and Tulyatid, J. eds. In: Proceedings of the International Symposium on Stratigraphic Correlation of Southeast Asia, Bangkok, Thailand: 2-24.
- Burbank, D. W. and Anderson, R. S. 2001. Tectonic Geomorphology. USA: Blackwell Science, 288pp.
- Carver, G. A. and McCalpin, J. P. 1996. Paleoseismology of Compression Tectonic Environment. In: McCalpin, J. P. ed. Paleoseismology, New York: Academic Press, 183-270.
- Charusiri, P. Charusiri, B. Pongsapich, W. and Suwanwerakamtorn, R. 1994. Application of Enhanced Satellite-Borne Images to the Relationships between Fractures and Mineralization in the Nam Mae Moei-Nam Mae Ping Area, Northern Thailand. Natural Resources Research. Oxford University Press, v.3 No.1: 46-49.

- Charusiri, P. Daorerk, V. and Supajanya, T. 1996. Applications of Remote-Sensing Techniques to Geological Structures Related to Earthquakes and Earthquake-Prone Areas in Thailand and Neighbouring Areas. A Preliminary Study. Journal of Scientific Research. Chulalongkorn University, Vol. 21. No.1: 14-38.
- Charusiri, P. Kosuwan, S. Fenton, C. H. Tahashima, T. Won-in, K. and Udchachon, M. 2001. Thailand Active Fault Zones and Earthquake Analysis: A Preliminary Synthesis. Jour. Asia Earth Sci. (submitted for publication).
- Charusiri, P. Daorerk, V. Choowoing, M. Archibald, D. Hisada, K. and Ampaiwan T. 2002. Geotectonic Evolution of Thailand: A New Synthesis. Journal of the Geological Society of Thailand: 1-20.
- Charusiri, P. Daorerk, V. Warnichai P. Choowoing, M. Nutthee, R. Won-in, K. Surakotra, S. Singmuang, R. Jampangern, K. and Chusuthisakun, K. 2004. Executive Summary Report Preliminary Study of Active Fault on the Salaween Power Plant Project. Department of Geology, Faculty of Science, Chulalongkorn University submitted to Department of Mineral Resources. Ministry of Natural Resources and Environment. Bangkok: 38pp.
- Chauviroj, S. 1991. Geotectonic of Thailand. Department of Mineral Resources. Bangkok: 58pp (in Thai).
- Christie-Blick, N. and Biddle, K. T. 1985. Deformation and Basin Deformation along Strike-Slip Fault. In: Biddle, K. T., and Christie-Blick, N. eds. Strike-Slip Deformation, Basin Formation, and Sedimentation, Society of Economic Paleontologists and Mineralogists, Spec. Pub. 37: 1-34.
- Cluff, L. S. and Bolt, B. A. 1969. Risk from Earthquake in the Modern Urban Environment with Special Emphasis on the San Francisco Bay Area, Urban Environmental Geology in the San Francisco Bay Region. In Association Engineering Geologist Sacramento, California: San Francisco Section Special Public: 25-64.
- Cooper, M. A. Herbert, R. and Hill, G. S. 1989. The Structural Evolution of Triassic Intermontane Basins in Northeastern Thailand. In: International Symposium on Intermontane Basins: Geology and Resources Chiang Mai University: 231-240.
- Daly, M. C. Cooper, M. A. Wilson, I. Smith, D. G. and Hooper, B. G. D. 1991. Cenozoic Plate Tectonics and Basin Evolution in Indonesia. Marine and Petroleum Geology. 8: 2-21.

- DeBari, S. M. Igneous Petrology. Department of Geology Western Washington University. From [www.ac.wvu.edu/~debari/406/lec1.html](http://www.ac.wvu.edu/~debari/406/lec1.html) (2007, January 10).
- Department of Highways. Highway Map of Thailand. Information Technology Division. From <http://map-project.doh.go.th/ZoomRaster.asp?Region=3&Zoom=1> (2007, January 10).
- Department of Mineral Resources. 1999. Geologic Map of Thailand 1: 1,000,000, Department of Mineral Resources. Bangkok (with English explanation).
- Department of Mineral Resources. 2003. Executive Summary Report of Geology Map of Nam Ping Watershed Project. Department of Mineral Resources. Geological Survey Bureau. Bangkok: 24pp (in Thai).
- DePolo, C. M. Clark, D. G. Slemmons, D. B. and Aymand, W. H. 1989. Historical Basin and Range Province surface faulting and fault segmentation. Schwartz D. P. and Sibson, R. H. eds., :In Fault Segmentation and Controls of Rupture Initiation and Termination. U.S. Geol. Surv. Open File Rep, 89-315: 131-162.
- DePolo, C. M. Clark, D. G. Slemmons, D. B. and Ramelli, A. R. 1991. Historical surface faulting in the Basin and Range Province, Western North America: implications for fault segmentation. Jour. Structure Geol, 13: 123-136.
- Dewey, J. F. Cande, S. and Pitman, W. 1989. Tectonic Evolution of the India/Eurasia Collision Zone. Eclogae Geologicae Helvetica, 82: 717-734.
- Elder, C. Uttamo, W. Nichols, G. Chantraprasert, S. Srisuwon, P. and Al-Barwani, B. 2000. Tertiary Strike-slip basin Formation in an Extruded Continental Wedge, Northern Thailand. In: The Symposium on the Intracontinental Effects of the Indo-Eurasian Collision. The Geoscience 2000 Meeting. Manchester, UK.
- Fenton, C. H. Charusiri, P. Hinthong, C. Lumjuan, A. and Mangkonkarn, B. 1997. Late Quaternary faulting in northern Thailand. In: Proceedings of the International Conference on Stratigraphy and Tectonic Evolution of Southeast Asia and the South Pacific, Bangkok, Department of Mineral Resources, August: 436-452.
- Fenton, C. H. Charusiri, P. and Wood, S. H. 2003. Recent Paleoseismic Investigations in Northern and Western Thailand, Annals of Geophysics: 957-981.
- Forman, S. L. Nelson, A. R. and McCalpin, J. P. 1991. Thermoluminescence Dating of Faulting-Scarp-Derived Colluvium: Deciphering the Timing of Paleearthquake

- on the Weber Segment of the Wasatch Fault Zone, North Central Utah. Journal of Geophysical Research, 96: 595-605.
- Hall, R. 1996. Reconstructing Cenozoic SE Asia. In: Hall, R. and Blundell, D. eds., Tectonic Evolution of Southeast Asia. Geological Society of London Special Publication No. 106: 153-184.
- Hinthong, C. 1991. Role of tectonic setting in earthquake event in Thailand. In ASEAM-EC Workshop on Geology and Geophysics. Jakarta, Indonesia: 1-37.
- Hinthong, C. Siribhakdi, K. Yaemniyon, N. Klaipongpun, S. and Chittrakarn, P. 1992. Study on geology, Earthquake, and Mineral Resources of the Nam Yuam River Basin Project, Thailand. prepared on behalf of EGAT-DMR joint study program under the work No.6 (Study of active fault in Thailand) of the sub-committee of the nation committee on earthquake: 104pp.
- Hinthong, C. 1995. The Study of Active Faults in Thailand. In: Proceedings of the Technical Conference on the Progression and Vision of Mineral Resources Development, Department of Mineral Resources, Bangkok: 129-140.
- Hinthong, C. 1997. The Study of Active Faults in Thailand. Report of EANHMP. An Approach to Natural Hazards in the Eastern Asia: 17-22.
- Hobbs, W. H. 1972. Earth Features and Their Meaning. New York: Macmillan, 506pp.
- Hongjatsee, U. 1999. Major fault and seismic hazard in northern, Thailand. Master's Thesis. Department of Geology, Faculty of Science, Chiang Mai University: 128pp.
- Huchon, P. LePichon, X. and Rangin, C. 1994. Indochina Peninsula and the collision of India and Eurasia. Geology, 22: 27-30.
- Hutchinson, C. S. 1989. Geological evolution of south-east Asia. New York: Oxford university Press, 368pp.
- International Atomic Energy Agency. 1988. Code on the Safety of Nuclear Power Plants: Siting, Code 50-C-S. IAEA. Vienna.
- International Atomic Energy Agency. 1992. Code on the Safety of Nuclear Research Reactors: Design, Safety Series No.35-S1. IAEA. Vienna.

- Keller, E. A. and Pinter, N. 1996. Active tectonics: Earthquake, uplift, and landscape, New Jersey: Prentice-Hall, 338pp.
- Kious, W. J. and Tilling, R. I. The Dynamic Earth: The Story of Plate Tectonics (online edition). From <http://dept.kent.edu/geology/ehlab/tectonics/tectonics.htm> (2007, January 10).
- Klaipongpan, S. Chakramanont, V. Pinrode, J. and Chittrakarn, S. 1991. Geological and Seismicity Evaluation of Srinakarin Dam, In: Proceedings of the Second International Conference on Recent Advances in Geotechnical Engineering and Soil Dynamics: 1357-1363.
- Knuepfer, P. L. K. 1989. Implications of the Characteristics of End-Points of Historical Surface Fault Ruptures for the Nature of Fault Segmentation. In: Schwartz, D. P. and Sibson, R. H. eds., Fault Segmentation and Controls of Rupture Initiation and Termination, U.S. Geological Surv. Open File Rep.89-315: 193-228.
- Kosuwan, S. Saithong, P. Lumjuan, A. Takashima, I. and Charusiri, P. 1999. Preliminary Results of Studies on the Mae Ai Segment of the Mae Chan Fault Zone, Chiang Mai Northern Thailand. The CCOP Meeting on Exodynamic Geohazards in East and Southeast Asia. July 14-16, Pattaya, CCOP: 1-8.
- Lacassin, R. Maluski, P. Leloup, P. H. Tapponnier, P. Hinthong, C. Siribhakdi, K. Chuavithit, S. and Charoenpravat, S. 1997. Tertiary Diachronic Extrusion and Deformation of western Indochina: Structural and  $^{40}\text{Ar}/^{39}\text{Ar}$  evidence from NW Thailand. Journal of Geophysical Research, 102: 10013-10037.
- Lee, T. Y. and Lawver, L. A. 1995. Cenozoic plate reconstructions of Southeast Asia. Tectonophysics, 251: 85-138.
- Le Dain, A. Y. Tapponnier, A. L. and Molnar, P. 1984. Active Faulting and Tectonics of Burma and Surrounding Regions. Journal of Geophysical Research, 89: 453-372.
- MaCalpin, J. P. 1996. Paleoseismology, California: Academic press, 588pp.
- Matthews, S. J. Fraser, A. J. Lowe, S. Todd, S. P. and Peel, F. J. 1997. Structure, Stratigraphy and Petroleum Geology of the SE Nam Con Son Basin, Offshore Vietnam. In: Fraser, A. Matthews, S. Murphy, R. eds., Petroleum Geology of Southeast Asia. Geol. Soc. London, Spec. Publ., vol. 126: 89-106.

- McKenzie, D. 1972. Active Tectonics of the Mediterranean Region. Royal Astron. Soc. Geophys. Jour., v.30: 109–185.
- Michael, P. Introduction to the Lithosphere, University of British Columbia Okanagan Canada. Online from <http://www.physicalgeography.net/fundamental/images/lithosphere.gif> (2007, February 22).
- Molnar, P. and Deng, Q. 1984. Faulting Associated with Large Earthquake and the Average Rate of Deformation in Central and Eastern Asia. Journal of Geophysical Research, v.89: 6203–6227.
- Molnar, P. and Tapponnier, P. 1975. Cenozoic tectonics of Asia: effects of a continental collision. Science, 280: 419–426.
- Molnar, P. and Tapponnier, P. 1977. Relation of the Tectonics of Eastern China to the India–Eurasia Collision; Application of Slip–Line Field Theory to large–scale Continental Tectonics. Geology, (Boulder) 5 (4): 212–216.
- Morley, C. K. Woganan, N, Sankumarn, N. Hoon, T. B. Alief, A. and Simmons, M. 2001. Late Oligocene–Recent Stress Evolution in Rift Basins of Northern and Central Thailand Implications for Escape Tectonics. Tectonophysics, Vol.334: 115–150.
- Morner, N. 1990. Neotectonics and Structural Geology; General Introduction. Bull. Int. Quat. Ass. Neotect. Comm: 13–87.
- Muir W. R. and Mallard, D. J. 1992. When is a Fault Extinct? Jour. Geol. Soc. Lond, 149: 251–255.
- Ni, J. and York, J. E. 1978. Late Cenozoic Tectonics of the Tibetan Plateau. J. Geophys. Res., 83: 5377–5384.
- Nutalaya, P. and Sodsri, S. 1983. Earthquake Data of Thailand and Adjacent Areas, Geological Society of Thailand: 109pp.
- Nutalaya, P. Sodsri, S. and Arnold, E. P. 1985. Series on Seismology–Volume II–Thailand. In: Arnold, E. P ed., Southeast Asia Association of Seismology and Earthquake Engineering: 402pp.
- Nutthee, R. 2002. Young Fault Movements along the Southern Segment of Sri Sawat Fault, Amphoe Sri Sawat, Changwat Kanchanaburi, Master’s Thesis. Department of Geology, Graduate School, Chulalongkorn University: 205pp.

- Nutthee, R. Charusiri, P. Tahashima, I. and Kosuwan, S. 2005. Paleo-Earthquake along the Southern Segment of the Sri-Sawat Fault, Kanchanaburi, Western Thailand: Morphotectonic and TL-dating Evidence. In: Proceedings of the International Conference on Geology, Geotechnology and Mineral Resources of INDOCHINA, November 28-30, 2005, Kkon Kaen, Thailand: 542-554.
- Obruchev, V. A. 1948. Osnovnyje Certy Kinetiki I Plastiki Neotectoniki, Izv. Akad. Nauk SSSR Ser. Geol.5(in Russian).
- O' Leary, D. W. Fridman, J. D. and Pohn, H. A. 1976. Lineament, Linear, Lineation: Some Proposed New Standards for Old Terms. Bull. Geol.soc.Am, 87: 1463-1469.
- O' Leary, D. W. and Simson, S. L. 1977. Remote Sensing Application to Tectonism and Seismicity in the Northern Part of the Mississippi Embayment. Geophysics, v.42 no.3: 542-548.
- Packham, G. 1996. Cenozoic SE Asia: reconstructing its aggregation and reorganization. In: Hall R., and Blundell, D. J. eds., Tectonic Evolution of Southeast Asia. Geol. Soc. London Spec. Publ, 106:123-152.
- Park, R. G. and Jaroszewski, W. 1994. Craton Tectonics, Stress and Seismicity. In: Hancock, P. L. ed., Continental Deformation. Oxford: Pergomon Press, 200-222.
- Phillip, H. Pogozhin, E. Cisternas, A. Bousquet, J. C. Borison, B. and Karakhanian, A. 1992. The Armenian Earthquake of 1988 December7; Faulting and Folding, Neotectonics and Paleoseismicity. Geophys. Jour. Int, 110: 141-158.
- Polachan, S. 1988. The Geological Evolution of the Mergui Basin, SE Andaman Sea, Thailand. PhD thesis. Royal Holloway and Bedford New College, Univesity of London: 218pp.
- Polachan, S. and Satayarak, N. 1989. Strike-Slip Tectonics and the Development of Tertiary Basins in Thailand. In: Proceedings of the International Symposium on Intermountain Basin, Geology and Resources, 30 Jan-2 Feb 1989, Chiang Mai, Thailand: 243-253.
- Rangin, C. Jolivet, L. and Pubellier, M. 1990. A Simple Model for the Tectonic Evolution of Southeast Asia and Indonesia Region for the past 43 m.y. Bulletin de la Société géologique de France, 8 VI: 889-905.



- Rangin, C. Maw, W. Lwin, S. Naing, W. Mouret, C. Bertrand, G. and Anonymous. 1999. Cenozoic Pull-Apart Basins in Central Myanmar; of the Path Trace of India along the Western Margin of Sundaland. In: European Union of Geosciences Conference; EUG 10. Strasbourg, France: 59pp.
- Rhodes, B. P. Perez, R. Lamjuan, A. and Kosuwan, S. 2002. Kinematics of the Mae Kuang Fault, Northern Thailand Basin and Range Province. The Symposium on Geology of Thailand. August 2002, Bangkok Thailand: 298-308.
- Rhodes, B. P. Perez, R. Lamjuan, A. and Kosuwan, S. 2004. Kinematics and tectonic implications of the Mae Kuang Fault, northern Thailand. Journal of Asian Earth Sciences, 24: 79-89.
- Royal Thai Survey Department. 1969. Topographic Map of Thailand Scale 1;50,000, edition 2-RTSD, Series L 7017, Sheet 4544 II Ban Tha Song Yang. Bangkok, Thailand: Royal Thai Survey Department.
- Royal Thai Survey Department. 1969. Topographic Map of Thailand Scale 1;50,000, edition 3-RTSD, Series L 7017, Sheet 4643 IV Amphoe Tha Song Yang. Bangkok, Thailand: Royal Thai Survey Department.
- Royal Thai Survey Department. 1969. Topographic Map of Thailand Scale 1;50,000, edition 2-RTSD, Series L 7017, Sheet 4743 III Ban Mae Ramat Noi. Bangkok, Thailand: Royal Thai Survey Department.
- Royal Thai Survey Department. 1976. Topographic Map of Thailand Scale 1;50,000, edition 2-RTSD, Series L 7017, Sheet 4544 IV Ban Bun Loe. Bangkok, Thailand: Royal Thai Survey Department.
- Royal Thai Survey Department. 1979. Topographic Map of Thailand Scale 1;50,000, edition 2-RTSD, Series L 7017, Sheet 4643 IV Amphoe Mae Ramat. Bangkok, Thailand: Royal Thai Survey Department.
- Royal Thai Survey Department. 1986. Topographic Map of Thailand Scale 1;50,000, edition 2-RTSD, Series L 7017, Sheet 4841 I Ban Na Bo Kham. Bangkok, Thailand: Royal Thai Survey Department.
- Royal Thai Survey Department. 1989. Topographic Map of Thailand Scale 1;50,000, edition 1-RTSD, Series L 7017, Sheet 4842 III Ban Na Bot. Bangkok, Thailand: Royal Thai Survey Department.

- Royal Thai Survey Department. 1995. Topographic Map of Thailand Scale 1;50,000, edition 2-RTSD, Series L 7017, Sheet 4742 I Ban Pang San. Bangkok, Thailand: Royal Thai Survey Department.
- Royal Thai Survey Department. 1995. Topographic Map of Thailand Scale 1;50,000, edition 1-RTSD, Series L 7017, Sheet 4842 IV Changwat Tak. Bangkok, Thailand: Royal Thai Survey Department.
- Saithong, P. 1998. Preliminarily Studied Geomorphology along the Mae Ping Fault. Special Project. Bachelor of science, Department of Geotechnology, Faculty of Tecnology, Khon Khon University: 59pp.
- Sarapirome, S. and Khundee, S. 1994. Preliminary study on Neotectonics in the Mae Hong Son-Khun Yuam Valley. Geological Survey Division, Department of Mineral Resources: 1-13.
- Schwartz, D. P. and Sibson, R. H. 1989. Introduction to Workshop on Fault Segmentation and Controls of Rupture Initiation and Termination. In: Schwartz, D. P. and Sibson, R. H. eds., Fault Segmentation and Controls of Rupture Initiation and Termination. U.S. Geological Survey, Open-File Report: 89-315.
- Segall, D. and Pollard, D. D. 1980. Mechanics of Discontinuous Faults. J. Geophys. Res., 85: 4337-4350.
- Sengor, A. M. C. and Hsu, K. J. 1984. The Cimmerides of Eastern Asia, History of the Eastern End of the Paleo-Tethys. Memoire de Ia societe geologique de France, 147: 139-167.
- Siribhakdi, K. 1986. Seismicity of Thailand and Periphery, Geological Survey Division, Department of Mineral Resources Bangkok. In: Panitan Lukleunaprasit et al. eds., Proceedings of the 1 st Workshop on Earthquake Engineering and Hazard Mitigation. Bangkok, November 1986, Chulaongkorn University: 151-158.
- Slemmons, D. B. 1982. Determination of Design Earthquake Magnitudes for Microzonation. 3<sup>rd</sup> International Earthquake Microzonation Conference Proceedings: 119-130.
- Slemmons, D. B. 1991. Introduction in the Geology of North America. In: Slemmon, D.B. Engdahl, E.R. Zoback, M.D. and Blackwell, D.D. eds., The Geology of North America. Decade Map Vol. 1, Neotectonics of North America. Geological Society of America, Boulder, Colorado: 1-20.

- Solonenko, V. P. 1973. Paleoseimogeology. Izv. Acad. Sci. USSR.Phys. Solid Earth, 9: 3-16 (in Russian).
- Srisuwan, P. 2002. Structural and Sedimentological Evolution of the Phrae Basin, Northern, Thailand. PhD. thesis. Department of Geology, Royal Holloway, University of London: 502pp.
- Stewart, I. S. and Hancock, P. L. 1994. Neotectonics. In: Hancock, P. L. Continental Deformation: 370 -409
- Storli, F. Marin, R. S. Faccenna, C. and Sainz, A. C. 2001. Role of the backstop-to-cover thickness ratio on vengeance partitioning in experimental thrust wedges. Terra Nova, 13(6): 413-417.
- Strandberg, C. H. 1967. Aerial Discovery Manual. New York: John Wiley & Son.
- Strogen, D. M. 1994. The Chiang Muan Basin, a Tertiary Sedimentary Basin of Northern Thailand. PhD. Thesis. Department of Geology, Royal Holloway and Bedford New College, Univesity of London: 417pp.
- Sukvatananont, P. and Assavapatchara, S. 1991. Geological Map of Ban Tha Song Yang, scale 1:50,000. Geological Survey Division, Department of Mineral Resources.
- Sylvester, A. G. 1988. Strike-Slip Faults. Geol. Soc. Am. Bull., 100: 1666-1703.
- Takashima, I. Charusiri, P. Kosuwan, S. and Won-In, K. 1999. TL-age Dating Results on the Mae Chan Segment of the Mae Chan fault, Northern Thailand. In: constraints for Quaternary faulting Proceedings and Abstracts of the International Workshop GPA'99; Tectonics, Geodynamics and Natural Hazards in West Pacific-Asia. Department of Geology and Minerals of Vietnam: 275-286 .
- Takashima, I. and Honda, S. 1989. Comparison between K-Ar and TL Dating Results of Pyroclastic Flow Deposits in the Aizutajima Area, Northeast Japan. Journal of Geological Society, 95: 807-816.
- Takashima, I. and Walanabe, K. 1994. Thermoluminescence Age Determination of Lava Flows/Domes and Collapsed Materials at Unzen Volcano, SW Japan. Bulletin of the Volcanological Society of Japan, 39: 1-12.
- Tanaka, K. Hataya, R. Spooner, N. A. Questiaux, D. G. Saito, Y. and Hashimoto, T. 1997. Dating of Marine Terrace Sediments by ESR, TL and OSL Methods and their Applicabilities. Quaternary Science Reviews, 16: 257-264.

- Tapponnier, P. Peltzer, G. Armijo, R. Le Dain, A. and Coobbold, P. 1982. Propagating Extrusion Tectonics in Asia: New insights from simple experiments with plasticine. Geology, v. 10: 611–616.
- Tapponnier, P. Peltzer, G. and Armijo, R. 1986. On the Mechanics of Collision between India and Asia. In: Coward, M. P., and Ries, A. C. eds., Collision Tectonics. Journal of the Geological Society of London. Special Publication, V.19: 115–157.
- Tapponnier, P. and Molnar, P. 1977. Active Faulting and Tectonics in China. Jour. Geophys. Res, 82: 3425–3459.
- Thailand Meteorological Department. 2002. Earthquake Information Catalogue. Report of Thailand Meteorological Department. Bangkok (digital files and unpublished).
- Thiramongkol, N. 1986. Neotectonism and Rate of Uplift in the Eastern Margin of the Lower Central Plain of Thailand. In: Thiramongkol N. ed., Proceedings of the Workshop on Economic Geology Tectonics, Sedimentary Processes and Environment of Quaternary of SE Asia. Had Yai, IGCP: 35–44,
- Thitipattanakul, T. Saithong, P. Yoeyodsang, S. Kosuwan, S. Charusiri, P. and Pananont, P. 2004. Ground Penetration Radar Investigations along the Mae Ping Fault Zone, Ban Mae Ou Su, Tak Province, Northwestern Thailand. In: Proceeding of the International Conference on Applied Geophysical. Chiang Mai 2004 (abstracts).
- Tulyatid, J. 1997. Application of airborne Geophysical Data to the Study of Cenozoic Basins in Central Thailand. PhD. Thesis. School of Earth Science, The University of Leeds: 325pp.
- Udachachon, M. 2002. Neotectonics of the Southeastern Segment of the Phrae Fault System, Phrae Basin, Northern Thailand. Master's Thesis. Department of Geology, Faculty of Science, Chulalongkorn University: 231pp.
- Udachachon, M. Charusiri, P. Daorerk, V. Won-in, K. and Takashima, I. 2005. Paleoseismic Studies along the Southeastern portion of the Phrae Basin, Northern Thailand. In: Proceedings of the International Conference on Geology, Geotechnology and Mineral Resources of INDOCHINA. November 28–30, 2005. Kkon Kaen, Thailand: 511–516.

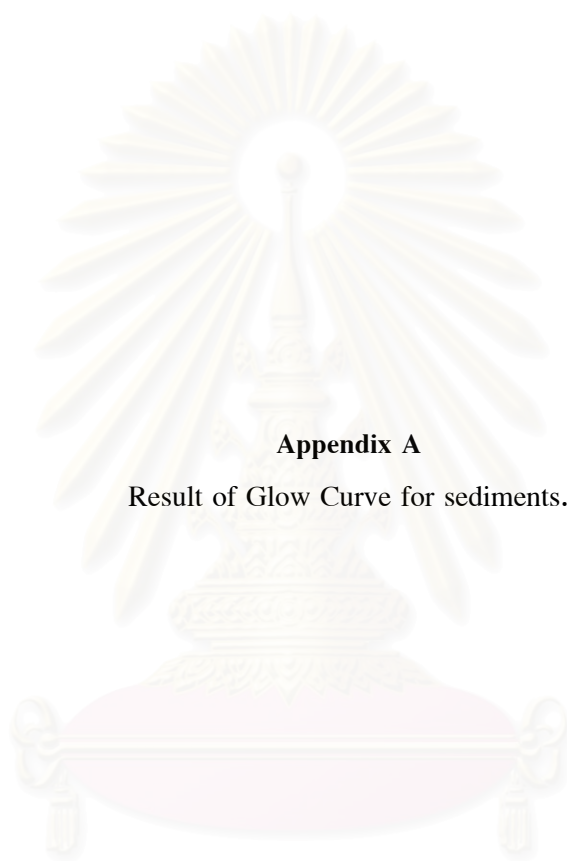
- U.S. Committee on Large Dams. 1998. Neotectonics and Dam, Guidelines and Case Histories. Updated guidelines for selecting parameters for dam projects, 96pp.
- U.S. Geological Survey National Earthquake Information Center. Earthquake Data Base. NEIC: Earthquake Search Results from [http://neic.usgs.gov / neis/ epic/ epic\\_global.html](http://neic.usgs.gov/neis/epic/epic_global.html) (2006, November 22).
- U.S. Nuclear Regulatory Commission. 1982. Appendix A: Seismic and geologic siting criteria for nuclear power plants. Code of Fed. Regul. 10. Chap. 1, Part 100. 1 September, 1982: 549-559.
- Uttamo, W. Elders, C. and Nichols, G. 2003. Relationships between Cenozoic Strike-slip fault and Basin Opening in Northern Thailand. In Storch, F. Holdsworth, R. E. and Salvini, F. eds., Strike-Slip Deformation Belts. Geological Society of London. Special Publications, 210: 89-108.
- Wallace, R. E. 1980. Active fault, Paleoseismology, and Earthquake Hazards. Proceedings of the Seventh World Conference on Earthquake Engineering. Istanbul, Turkey. v.1: 115-122.
- Wallace, R. E. 1981. Active Fault, Paleoseismology and Earthquake Hazard in Western United States. In: Simpson, D.W. and Richards, P. G. eds., Earthquake Prediction: An International Review. Washington, DC. Maurice Ewing Ser, 4; 209-216.
- Wallace, R. E. 1986. Active Tectonics. Washington: National Academic Press, 266pp.
- Wallace, R. E. 1990. The San Andreas Fault System, California. U.S. Geol. Surv. Prof. Pap, 1515: 283pp.
- Weldon, R. J. McCalpin, J. P. and Rockwell, T. K. 1996. Paleoseismology of Strike-Slip Tectonic Environments. In: McCalpin, J. P. ed. Paleoseismology, New York: Acad. Press, 271-329.
- Wells, D. L. and Coppersmith, K. J. 1994. New Empirical Relationships among Magnitude, Rupture Width, Rupture Area, and Surface Displacement. In: Bulletin of the Seismological Society of America. V.84: 974-1002.
- Wesnousky, S. G. Scholz C. H. Shimazaki, K. and Matsuda, T. 1984. Integration of Geological and Seismological data for the Analysis of Seismic Hazard; a Case Study of Japan. Bull Seismol. Soc. Am, 74: 687-708.

- Wheeler, R. L. 1989. Persistent Segment Boundaries on Basin-Range Normal Faults. In: Stewart D. P. and Sibson, R. H. eds., Fault Segmentation and Controls of Rupture Initiation and Termination. U.S. Geol. Surv., Open File Rep. 89-135: 432-444.
- Willis, B. 1923. A Fault Map of California. Bulletin of the Seismological Society of America, 13: 1-12.
- Wintle, A. G. and Huntley, D. J. 1980. Thermoluminescence Dating of Ocean Sediments. Canadian. Journal of Earth Sciences, 17: 348-360.
- Won-in, K. 1999. Neotectonic evidences along the Three Pagoda Fault Zone, Changwat Kanchanaburi. Master's Thesis. Department of Geology, Faculty of Science, Chulalongkorn University, 188pp.
- Won-in, K. 2003. Quaternary Geology of the Phrae Basin, Northern Thailand and Application of Thermoluminescence Technique for Quaternary Chronology. PhD. Thesis. Graduate School of Mining and Engineering, Akita University: 200pp.
- Woodcock, N. H. and Fischer, M. 1986. Strike-slip duplexing. J. Struct. Geol., 8: 725-735.
- Wood, H. O. 1915. California Earthquake, A Synthetic Study of Recorded Shocks. Bulletin of the Seismological Society of America, v.6: 54-196.
- Woodward Clyde Federal Services. 1996. Seismic hazards evaluation, Environmental Impact Assessment: Geological Aspect, Kaeng Sua Ten Dam Project Changwat Phrae. unpublished report prepared by GMT Corporation and other for the Department of Mineral Resources.
- Western States Seismic Policy Council. 1997. Active Fault Definition for the Basin and Range Province. WSSPC Policy Recommendation 97-1 White Paper. May 22, 1997., San Francisco, CA: 3pp.



APPENDICES

สถาบันวิทยบริการ  
จุฬาลงกรณ์มหาวิทยาลัย

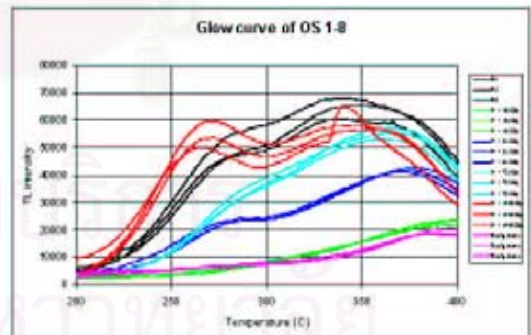
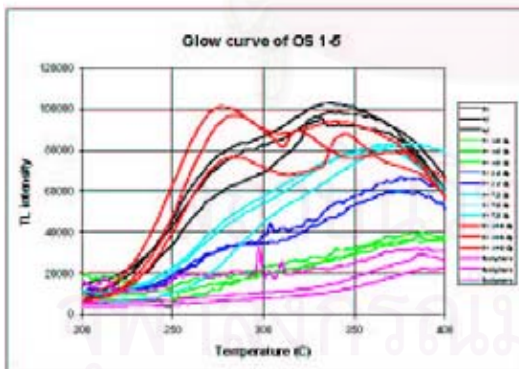
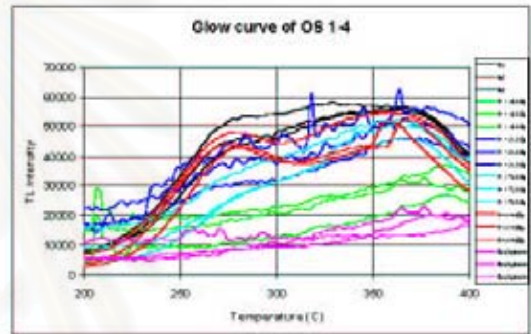
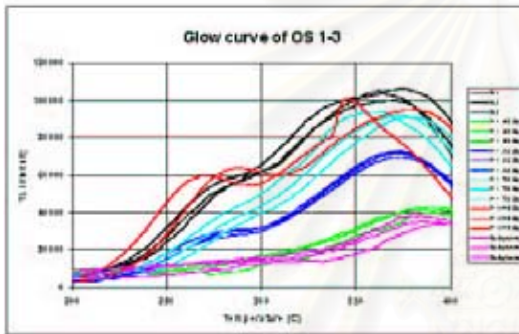
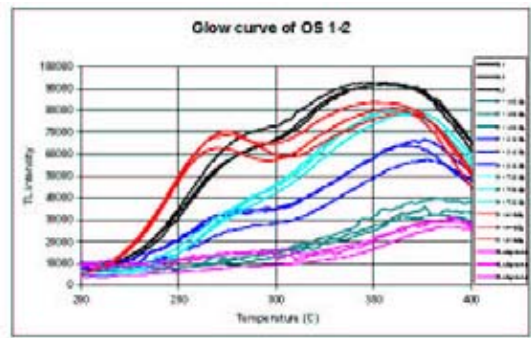
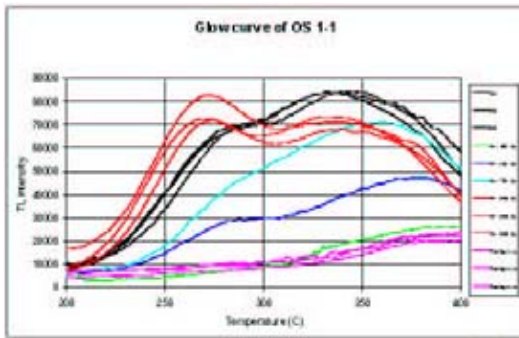


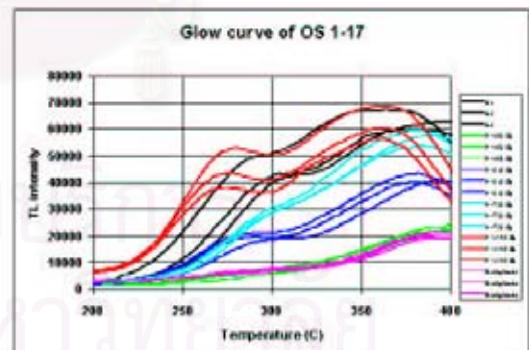
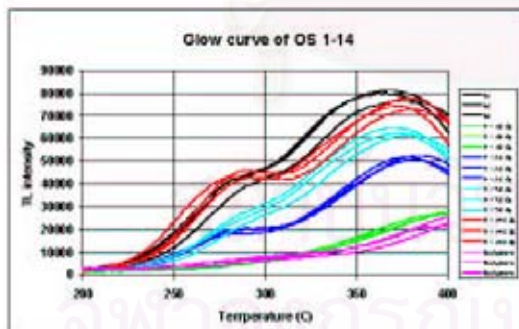
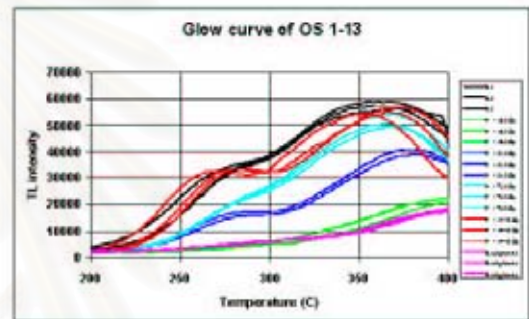
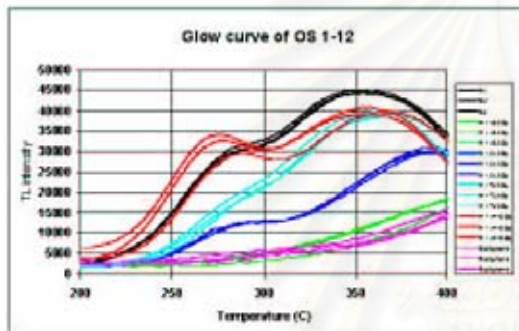
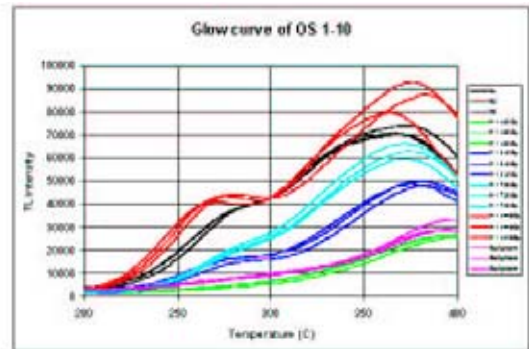
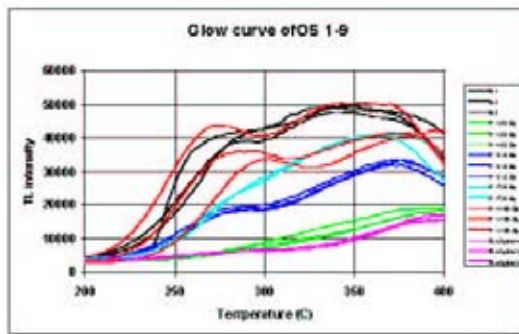
**Appendix A**

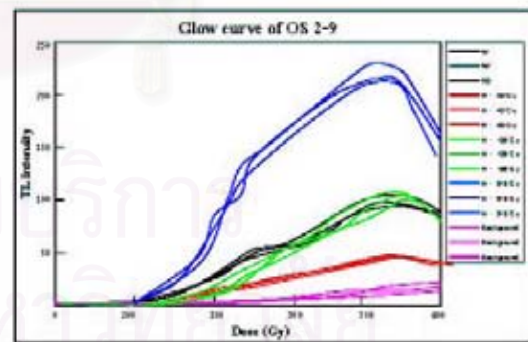
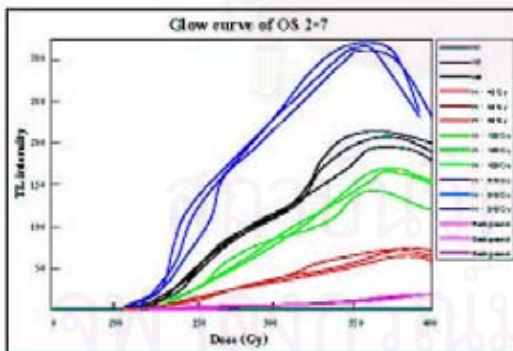
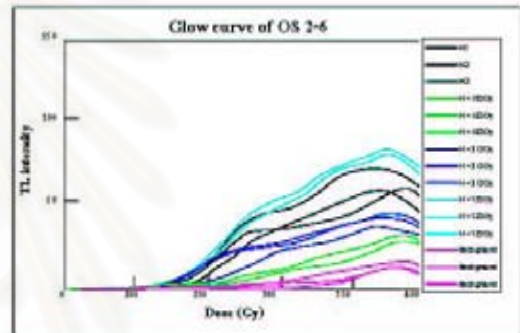
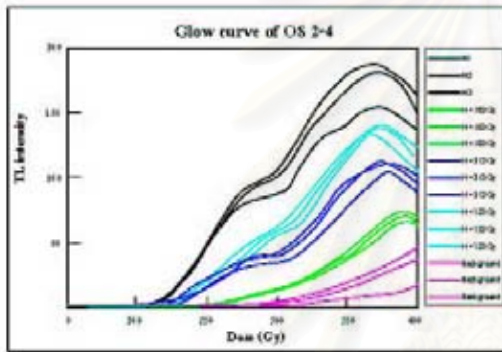
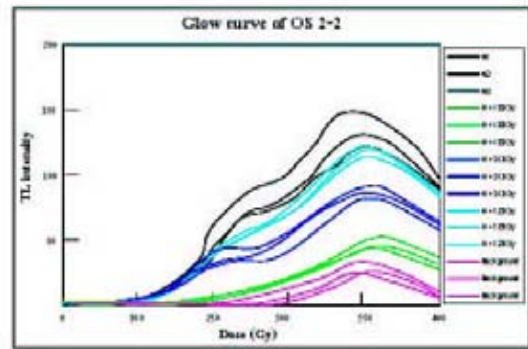
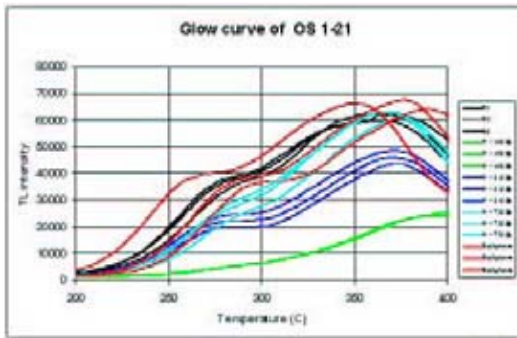
Result of Glow Curve for sediments.

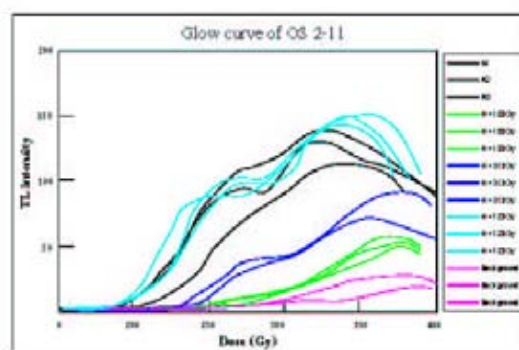
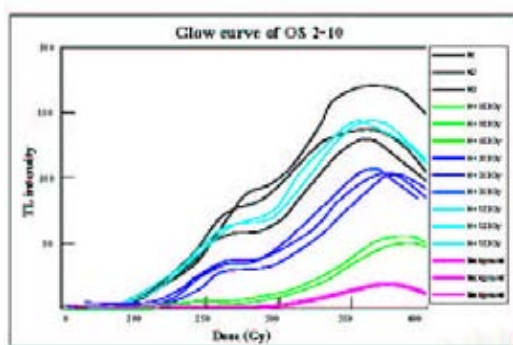
สถาบันวิทยบริการ  
จุฬาลงกรณ์มหาวิทยาลัย



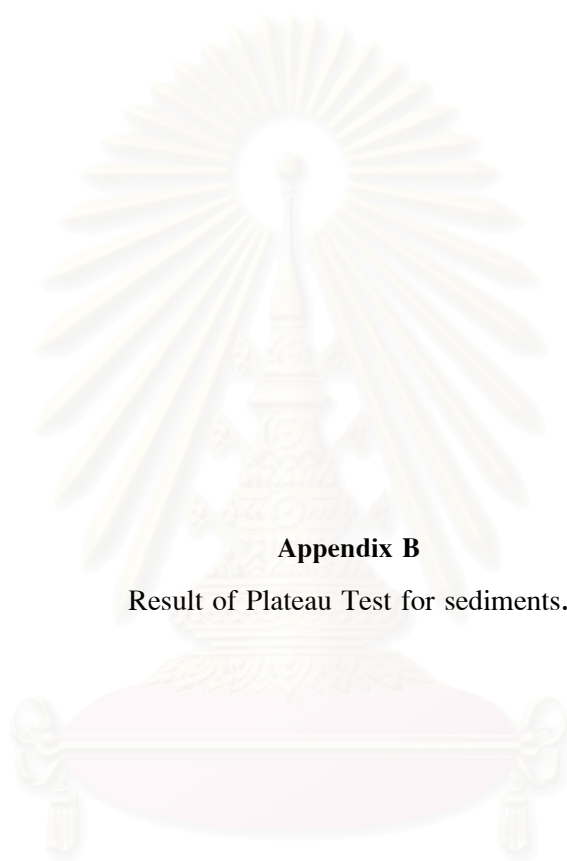








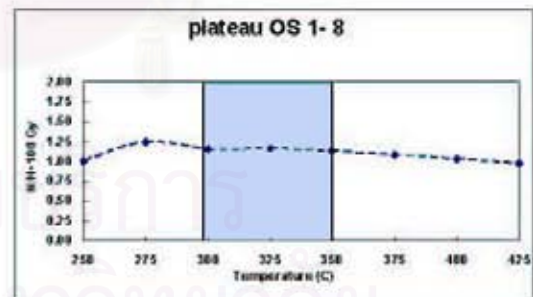
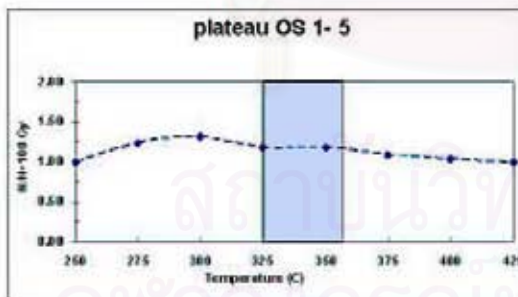
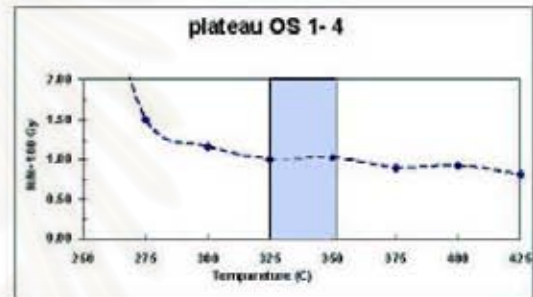
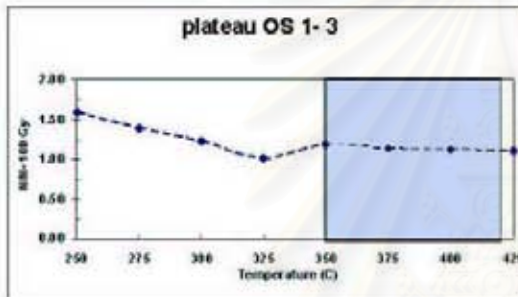
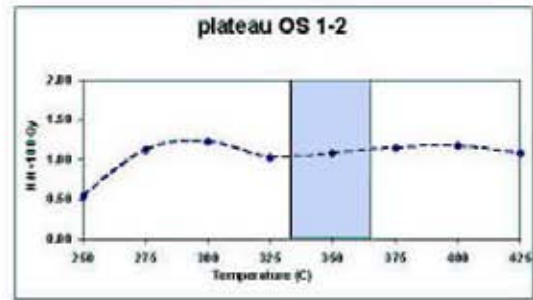
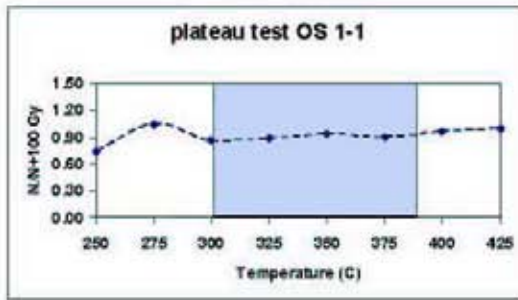
สถาบันวิทยบริการ  
จุฬาลงกรณ์มหาวิทยาลัย

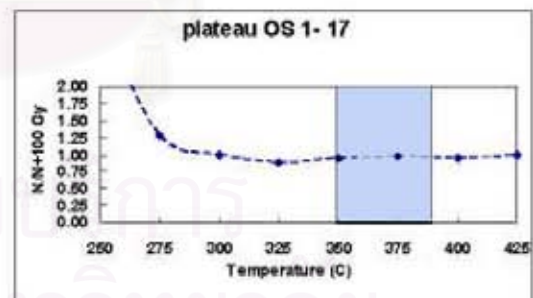
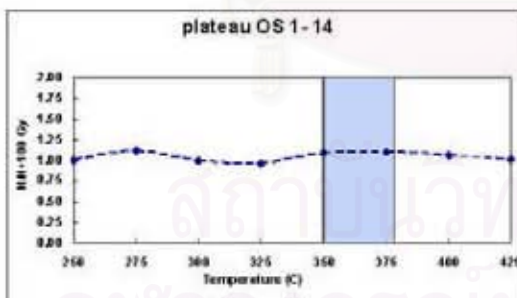
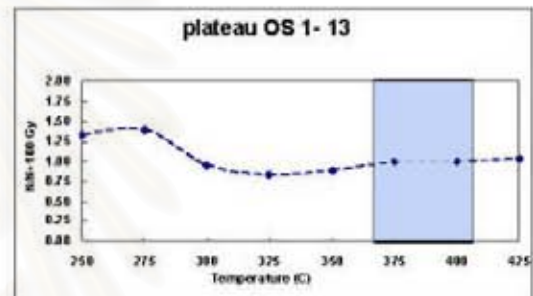
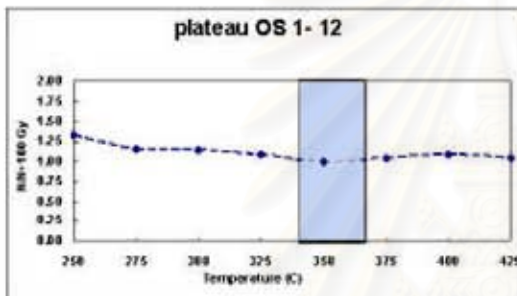
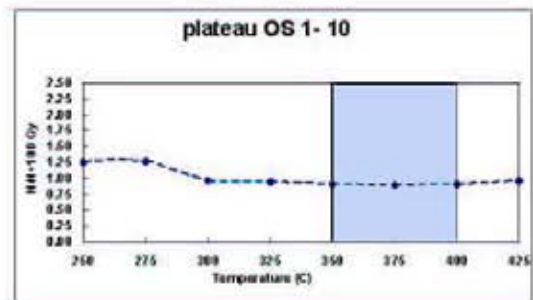
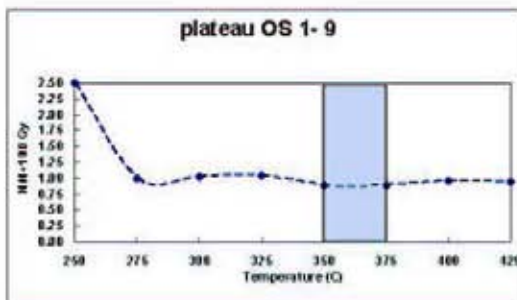


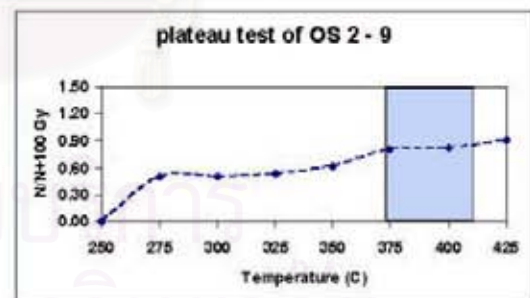
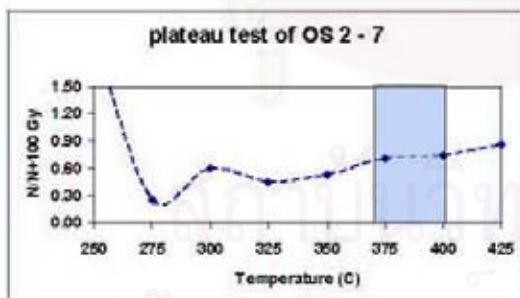
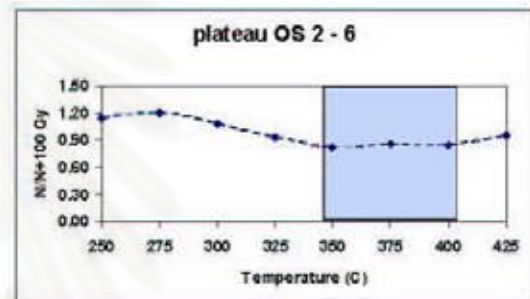
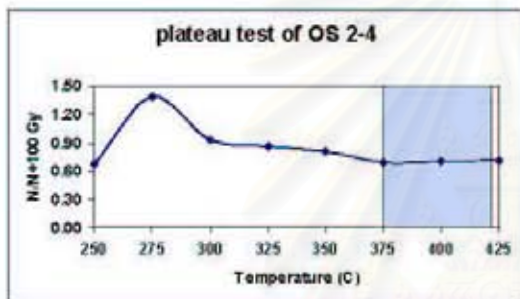
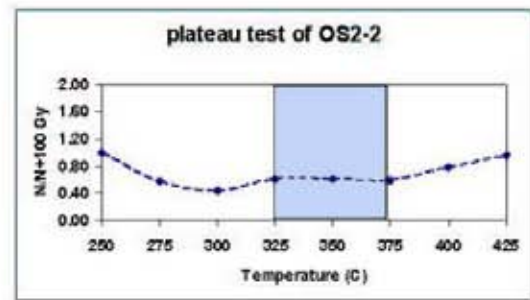
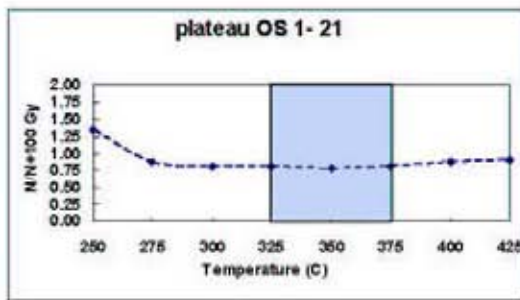
**Appendix B**

Result of Plateau Test for sediments.

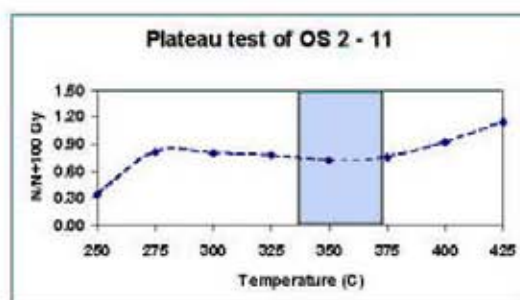
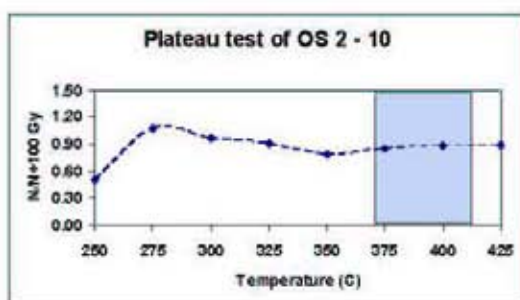
สถาบันวิทยบริการ  
จุฬาลงกรณ์มหาวิทยาลัย



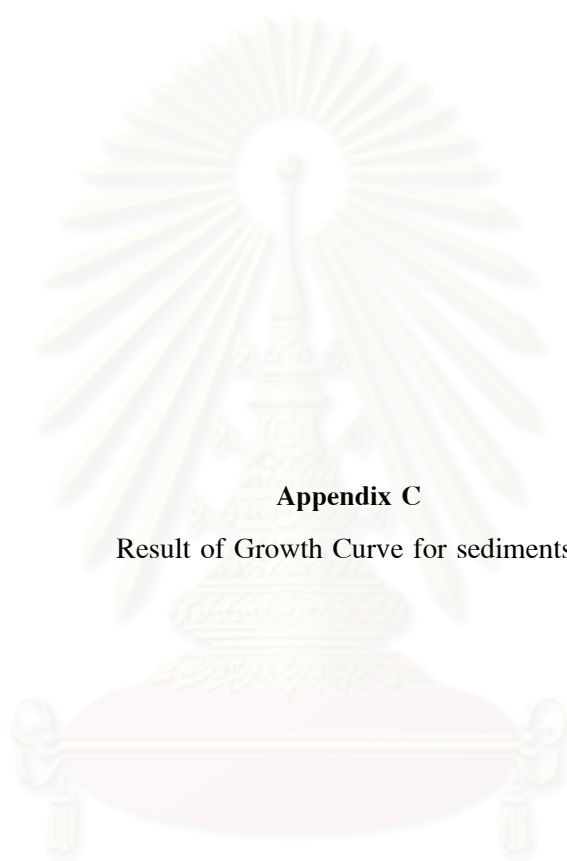








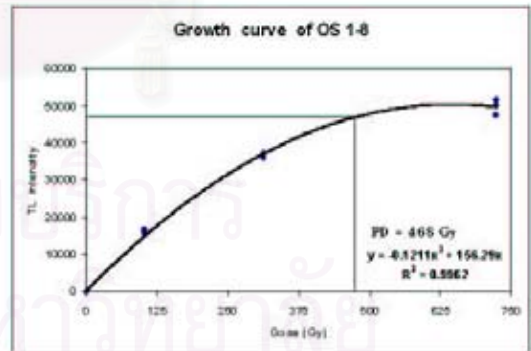
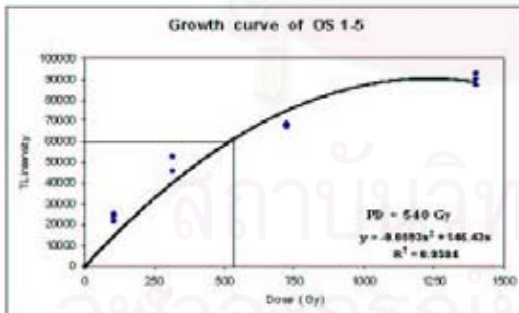
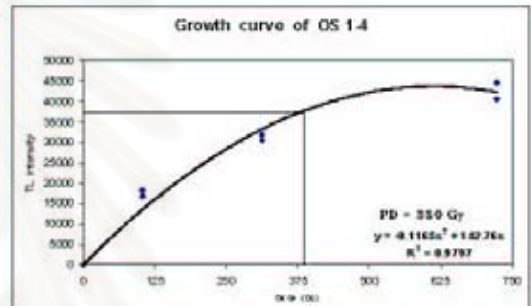
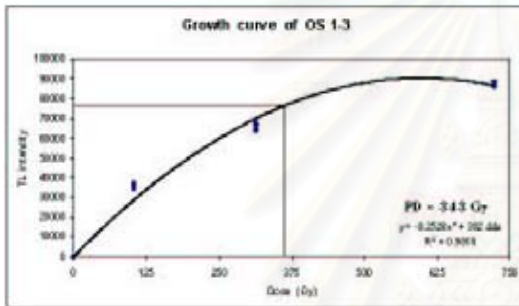
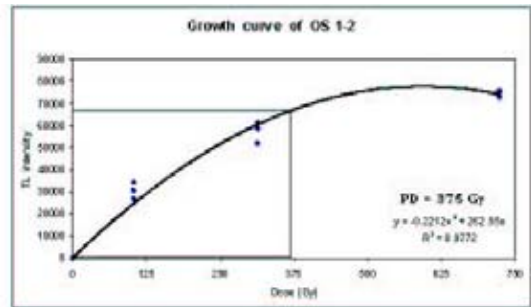
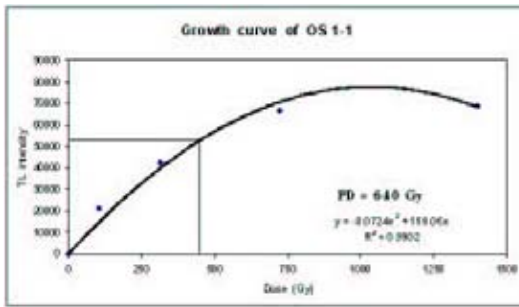
สถาบันวิทยบริการ  
จุฬาลงกรณ์มหาวิทยาลัย

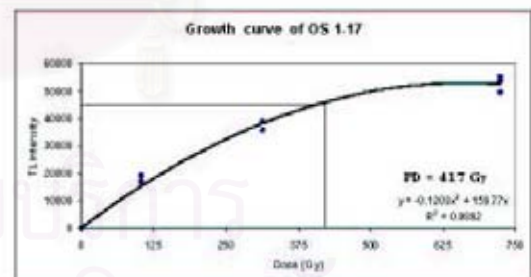
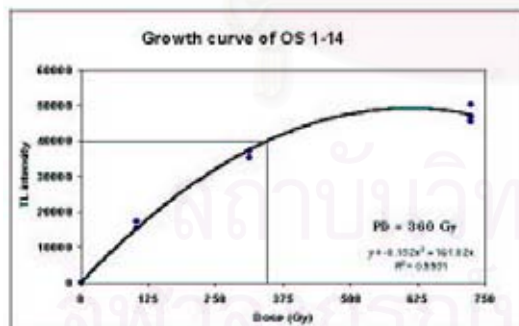
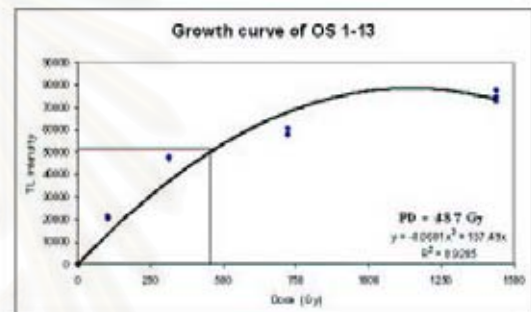
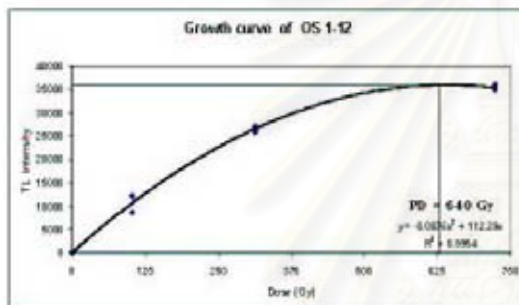
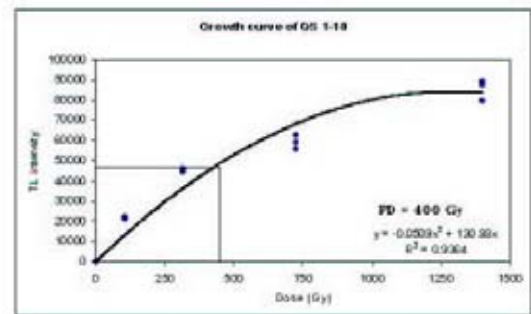
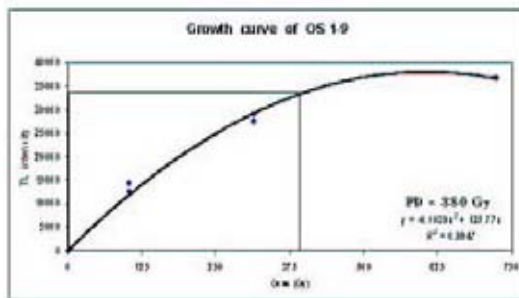


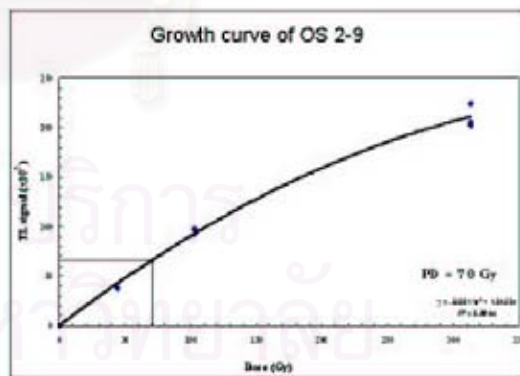
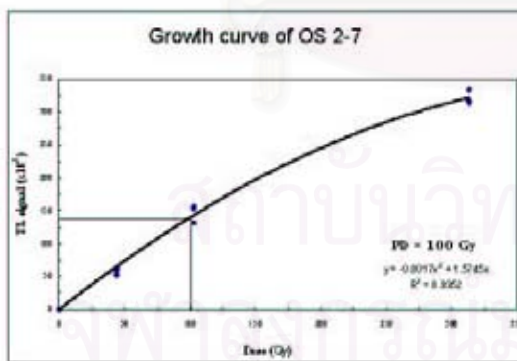
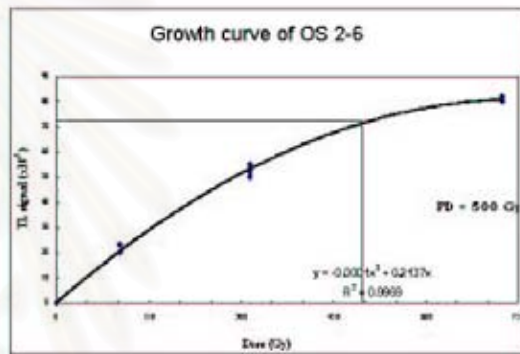
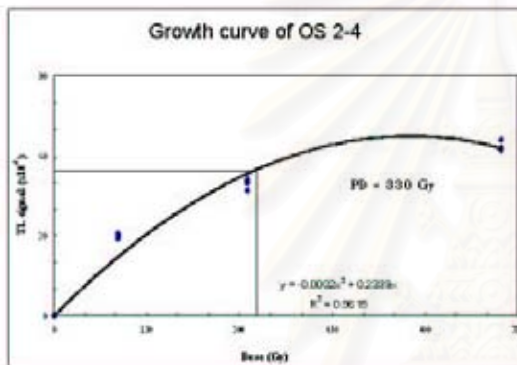
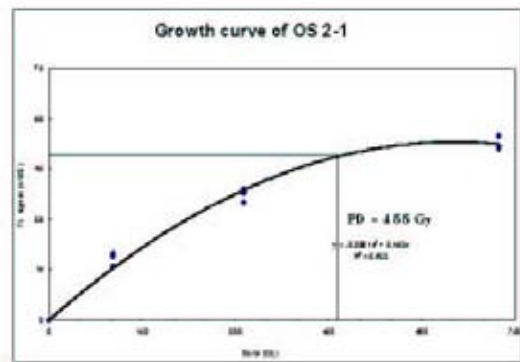
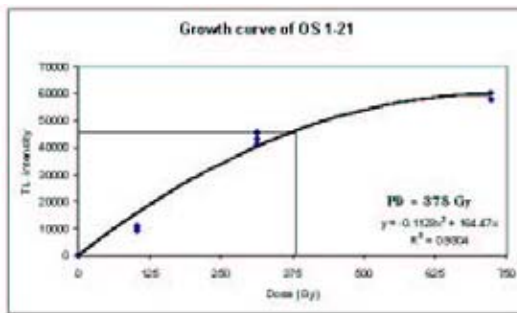
### Appendix C

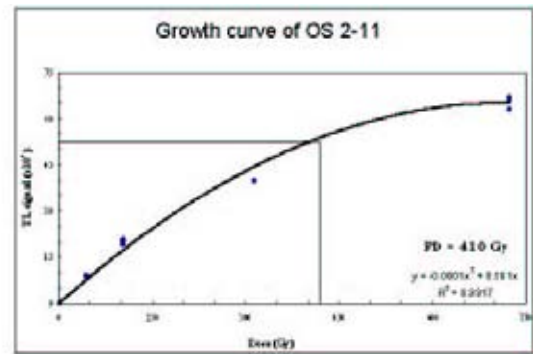
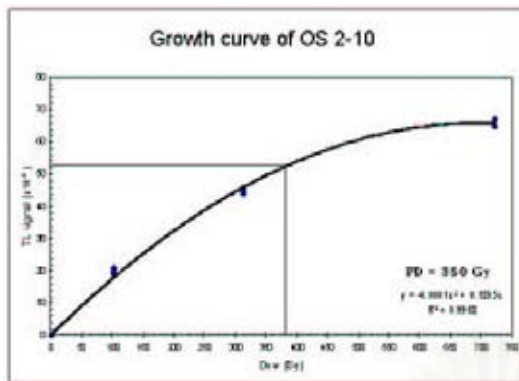
Result of Growth Curve for sediments.

สถาบันวิทยบริการ  
จุฬาลงกรณ์มหาวิทยาลัย

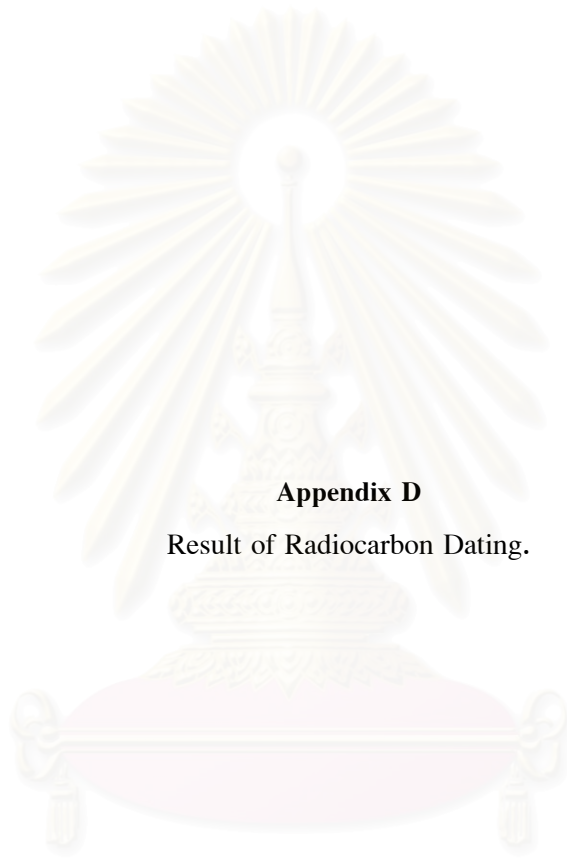








สถาบันวิทยบริการ  
จุฬาลงกรณ์มหาวิทยาลัย



**Appendix D**  
Result of Radiocarbon Dating.

สถาบันวิทยบริการ  
จุฬาลงกรณ์มหาวิทยาลัย

## CALIBRATION OF RADIOCARBON AGE TO CALENDAR YEARS

(Variables: C13/C12=-27;lab,mult=1)

Laboratory number: Beta-205734

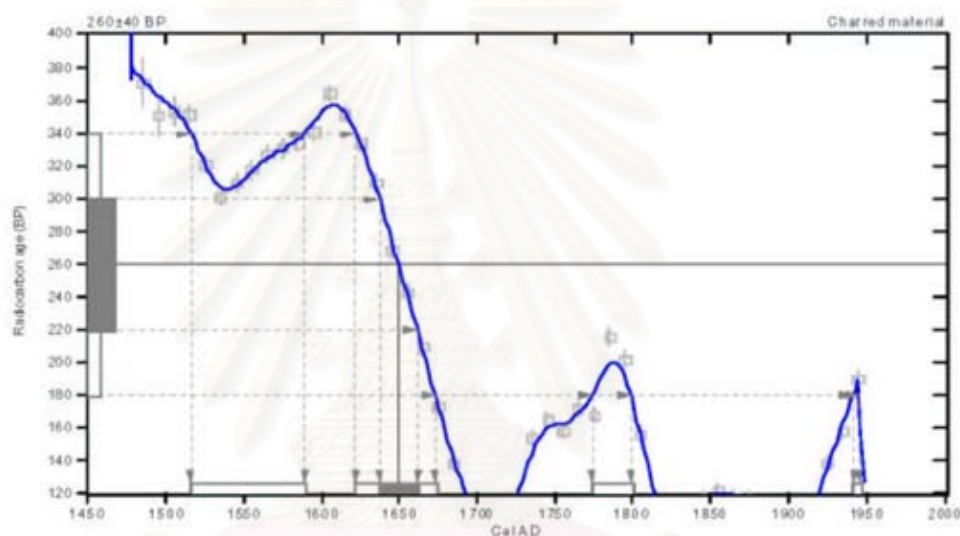
Conventional radiocarbon age:  $260 \pm 40$  BP

2 Sigma calibrated results: Cal AD 1520 to 1590 (Cal BP 430 to 360) and  
Cal AD 1620 to 1670 (Cal BP 330 to 280) and  
Cal AD 1770 to 1800 (Cal BP 180 to 150) and  
Cal AD 1940 to 1950 (Cal BP 10 to 0)

Intercept data

Intercept of radiocarbon age  
with calibration curve: Cal AD 1650 (Cal BP 300)

1 Sigma calibrated result: Cal AD 1640 to 1660 (Cal BP 310 to 290)



### References:

- Database used  
INTCAL98  
Calibration Database  
Editorial Comment  
Stuiver, M., van der Plicht, H., 1998, Radiocarbon 40(3), pxi-xiii  
INTCAL98 Radiocarbon Age Calibration  
Stuiver, M., et al., 1998, Radiocarbon 40(3), p1041-1083  
Mathematics  
A Simplified Approach to Calibrating C14 Dates  
Talma, A. S., Vogel, J. C., 1991, Radiocarbon 33(2), p317-322

**Beta Analytic Radiocarbon Dating Laboratory**

4993 N.W. 74th Court, Miami, Florida 33153 • Tel: (305)667-3167 • Fax: (305)661-0964 • E-Mail: beta@radiocarbon.com

จุฬาลงกรณ์มหาวิทยาลัย



## CALIBRATION OF RADIOCARBON AGE TO CALENDAR YEARS

(Variables: C13/C12=-25.7;lab. mult=1)

Laboratory number: Beta-205735

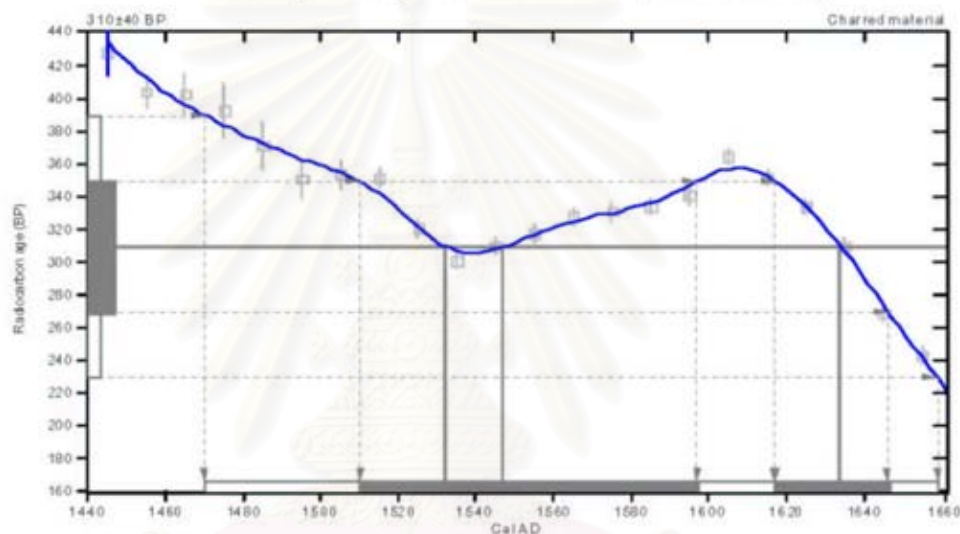
Conventional radiocarbon age: 310±40 BP

2 Sigma calibrated result: Cal AD 1470 to 1660 (Cal BP 480 to 290)  
(95% probability)

Intercept data

Intercepts of radiocarbon age  
with calibration curve: Cal AD 1530 (Cal BP 420) and  
Cal AD 1550 (Cal BP 400) and  
Cal AD 1630 (Cal BP 320)

1 Sigma calibrated results: Cal AD 1510 to 1600 (Cal BP 440 to 350) and  
Cal AD 1620 to 1650 (Cal BP 330 to 300)



### References:

- Database used*  
INTCAL98  
*Calibration Database*  
*Editorial Comment*  
Stuiver, M., van der Plicht, H., 1998, Radiocarbon 40(3), pxi-xiii  
*INTCAL98 Radiocarbon Age Calibration*  
Stuiver, M., et. al., 1998, Radiocarbon 40(3), p1041-1083  
*Mathematics*  
*A Simplified Approach to Calibrating C14 Dates*  
Talma, A. S., Vogel, J. C., 1991, Radiocarbon 33(2), p317-322

**Beta Analytic Radiocarbon Dating Laboratory**

4993 E.W. 74th Court, Miami, Florida 33153 • Tel: (305)667-3167 • Fax: (305)661-0904 • E-Mail: beta@radiocarbon.com

จุฬาลงกรณ์มหาวิทยาลัย

## BIOGRAPHY

Mr. Preecha Saithong was born on November 22, 1975 in Ubonratchathani, Thailand. He graduated high school from Benchama Maharat School, Ubonratchathani, in 1994. In 1998 he received a B.Sc. degree in Geotechnology from the Department of Geotechnology, Faculty of Technology, Khon Kaen University, Thailand. After his graduation, he started to work in 1998 as a government official at the Environmental Geology Section, Geological Division, and Department of Mineral Resources (DMR). In 2002, he has moved to work in the different section, the Geohazard Section, Environmental Geology Division, Department of Mineral Resources (DMR), and is still employed until this present time. In 2003 he enrolled as a graduate student of Geology program at Graduate School, Chulalongkorn University, Bangkok, Thailand.



สถาบันวิทยบริการ  
จุฬาลงกรณ์มหาวิทยาลัย